CATALYTIC HYDROCRACKING AND CHARACTERISATION OF HEAVY HYDROCARBON LIQUIDS

Marcos G. Millán-Agorio

Department of Chemical Engineering

Imperial College London

University of London

A thesis submitted for the degree of Doctor of Philosophy of the University of London and the Diploma of Imperial College

August 2005



ABSTRACT

Catalytic hydrocracking is a potential process route for upgrading heavy hydrocarbons derived from coal and petroleum into more valuable products such as transport fuels. This potential has been reinforced in view of recent increases in oil prices. In addition, more demanding environmental regulations regarding the disposal of heavy residues, the decline in light oil reserves and production and the increase in the reserves of heavy oil discovered have contributed to make hydrocracking more attractive. However, it still presents technical challenges due to the large consumption of expensive hydrogen and the quick deactivation of the catalysts employed, which are an obstacle to its widespread industrial application.

The present study has two main thrusts, the testing of new hydrocracking catalysts and the development of analytical tools for the characterisation of heavy hydrocarbons. The use of pillared clays as hydrocracking catalysts has been explored in this work. Some of the pillared clays tested exhibited high activities, comparable to that of a commercial $NiMo/Al_2O_3$ used as reference, towards the hydrocracking of a coal extract. Pillared clays also showed resistance to deactivation by coke deposition, maintaining their activity despite a large amount of carbonaceous material deposited on the catalyst surface, which produced an almost complete loss of surface area. Fresh and used catalysts have been analysed by scanning electron microscopy and X-ray microanalysis. Preferential deposition on the catalyst support rather than on active sites and the dynamic exchange of material adsorbed on the catalyst with the solution are thought to contribute to the persistent activity of these catalysts.

The characterisation of heavy hydrocarbons plays a key role in the evaluation of hydrocracking catalysts and it is also relevant to several other processes involving coal and petroleum utilisation. Matrix-assisted laser desorption/ionisation mass spectrometry (MALDI-MS) has been studied in this work as a technique suitable to generate molecular mass distributions of heavy hydrocarbons. Much attention has been dedicated to the development of MALDI-TOF MS and laser desorption (LD) MS as techniques to apply in order to obtain reliable molecular mass distributions of these materials. As size exclusion chromatography (SEC) has been widely applied to the analysis of hydrocracking products, special attention has been devoted to validate the SEC calibration based on polymers by MALDI-MS and LD-MS. The pyridine insoluble fraction of a coal tar pitch showed bimodal distributions by both SEC and

MALDI-MS. A good correlation has been observed between these two techniques up to molecular weights of 10,000 Da.

ACKNOWLEDGEMENTS

I am grateful to my supervisors Profs Rafael Kandiyoti and Denis Dugwell and Dr Alan Herod for their support, encouragement and help, past, present and future.

The collaboration of our partners in the present project, Elma Gyftopoulou and Prof Tony Bridgwater from Aston University and Dr Joe Hriljac from the University of Birmingham, in the supply and characterisation of the pillared clay catalysts is gratefully acknowledged.

I am grateful to the P4 Group for access to the MALDI-MS facilities.

I would also like to thank Carolina Galmes, for her support, friendship and help -not least dealing with the formatting of this text; Trevor Morgan for his friendship and his valuable collaboration with the analytical techniques; Ashleigh Cousins, for her friendship and helpful advice; Cristina Adell, Cecilia Hinojosa, Dr Barbara Apicella, Mahtab Berouzi, and Dr Fatma Karaca for their help with sample analyses; everyone in the group, who made it a great place for studying during these years and my parents and the rest of my family for their permanent support over the distance.

TABLE OF CONTENTS

ABSTRACT **2**

1 INTRODUCTION **17**

1.1 COAL LIQUEFACTION 17

1.2 UPGRADING HEAVY OIL FRACTIONS 18

1.3 OBJECTIVES OF THE PRESENT STUDY 19

1.4 THE STRUCTURE OF THIS THESIS 20

2 BACKGROUND **22**

2.1 PROCESSES IN HYDROCRACKING OF COAL AND OIL-DERIVED LIQUIDS 22

2.1.1 Coal liquefaction 22

2.1.2 Hydrocracking in the petroleum industry 23

2.2 CATALYSTS AND CATALYST DEACTIVATION 25

2.2.1 Hydroprocessing Catalysts 25

2.2.2 Catalyst deactivation by coke deposition 27

2.2.3 Effect of catalyst properties in coke deposition 27

2.2.4 Effect of feed composition on coke deposition 30

2.2.5 Effect of hydroprocessing conditions on coke deposition 31

2.2.6 Effect of reaction time on the carbonaceous deposits. 31

2.3 MOLECULAR MASS DISTRIBUTIONS IN COAL AND OIL DERIVED SAMPLES 34

2.3.1 Size Exclusion Chromatography 34

2.3.2 Mass Spectroscopy 37

2.3.3 UV-Fluorescence Spectroscopy 39

2.3.4 Other techniques 40

3 EXPERIMENTAL **43**

3.1 HYDROCRACKING EXPERIMENTS 43

3.1.1 Micro-bomb Reactor 43

3.1.2 Procedure 44

3.2 ANALYTICAL TECHNIQUES 48

3.2.1 Gas Chromatography 48
3.2.2 Size Exclusion Chromatography 48
3.2.3 Thermogravimetric Analysis – ">450°C" fraction 50
3.2.4 Thermogravimetric analysis - Carbonaceous deposition on the catalyst 51
3.2.5 UV Fluorescence Spectroscopy 52
3.2.6 Surface area measurements 52
3.3 FRACTIONATION TECHNIQUES 52

4 MODIFICATIONS TO THE EXPERIMENTAL PROCEDURE FOR HYDROCRACKING EXPERIMENTS 54

4.1 THE USE OF NO SOLVENT IN HYDROCRACKING EXPERIMENTS 54
4.1.1 Hydrocracking experiments with solvent 55
4.1.2 Hydrocracking experiments without solvent 57
4.2 THE USE OF COATED CATALYST 58
4.3 CHANGES TO THE DRYING METHOD 61
4.4 CHANGES TO THE BOILING POINT DETERMINATION METHOD 62
4.5 SEC ON THE ">450°C" FRACTION OF THE POINT OF AYR EXTRACT 64

5 EFFECT OF REACTION TIME ON EXTENT OF HYDROCRACKING USING A COATED NIMO CATALYST 67

5.1 INTRODUCTION 67
5.2 EXPERIMENTAL 70
5.2.1 Hydrocracking experiments 70
5.2.2 Precoating of catalyst with carbon deposit 70
5.3 RESULTS 70
5.3.1 Conversions 70
5.3.2 Size Exclusion Chromatography 72
5.3.3 UV-Fluorescence Spectrometry 74
5.3.4 Surface Area Measurements 75
5.4 DISCUSSION 76
5.5 CONCLUSIONS 78

6 PILLARED CLAYS AS HYDROCRACKING CATALYSTS: TESTS WITH FRESH CATALYSTS 80

6.1 INTRODUCTION 80
6.2 EXPERIMENTAL 85
6.3 RESULTS AND DISCUSSION 86
6.3.1 Evaluation of Cr montmorillonites 86
6.3.2 Evaluation of Sn laponites 92
6.3.3 Evaluation of other catalysts 96
6.4 CONCLUSIONS 98

7 PILLARED CLAYS AS HYDROCRACKING CATALYSTS: TESTS WITH REUSED CATALYSTS 100

7.1 INTRODUCTION 100
7.2 EXPERIMENTAL 100
7.3 RESULTS AND DISCUSSION 101
7.3.1 Evaluation of the Cr montmorillonites 101
7.3.2 Evaluation of the Sn laponites 106
7.3.3 Evaluation of other catalysts 109
7.4 CONCLUSIONS 112

8 CATALYST CHARACTERISATION 114

8.1 INTRODUCTION 114
8.2 EXPERIMENTAL 114
8.2.1 Surface area measurements 114
8.2.2 Scanning electron microscopy and X-ray microanalysis 114
8.3 RESULTS AND DISCUSSION 115
8.3.1 Surface area measurements 115
8.3.2 Scanning Electron Microscopy and X-ray microanalysis. 118
8.4 CONCLUSIONS 124

9 HYDROCRACKING OF OTHER FEEDS: A VACUUM RESIDUE AND THE PYRIDINE INSOLUBLE FRACTION OF A COAL TAR PITCH 126

9.1 HYDROCRACKING OF THE PYRIDINE INSOLUBLE FRACTION OF A COAL TAR PITCH 126
9.1.1 Introduction 126
9.1.2 Experimental 127
9.1.3 Results and Discussion 127

9.1.4 Conclusions 132
9.2 HYDROCRACKING OF A PETROLEUM VACUUM RESIDUE 132
9.2.1 Introduction 132
9.2.2 Experimental 133
9.2.3 Results and Discussion 134
9.2.4 Conclusions 136

10 CHARACTERISATION OF COAL DERIVED SAMPLES BY LASER DESORPTION AND MALDI-TOF MS 137

10.1 INTRODUCTION 137
10.1.1 The fundamentals of MALDI-TOF 137
10.1.2 Applications of MALDI-TOF to heavy hydrocarbons 139
10.2 EXPERIMENTAL 141
10.3 RESULTS AND DISCUSSION 146
10.3.1 Analysis of polystyrene standards 146
10.3.2 Analysis of size exclusion chromatography fractions 147
10.3.3 Analysis of solvent solubility fractions 150
10.4 CONCLUSIONS 158

11 CONCLUSIONS AND RECOMMENDATIONS FOR FUTURE WORK 159

11.1 CONCLUSIONS 159
11.2 RECOMMENDATIONS FOR FUTURE WORK 160

12 REFERENCES 162

APPENDIX I: LIST OF PUBLICATIONS RELATED TO THE PRESENT WORK 174

TABLE OF FIGURES

Figure 2.1. Diagram of the Liquid Solvent Extraction Process as operating at British Coal's Point of Ayr pilot plant. Reproduced from [1]. 23
Figure 2.2. Diagram of the Chevron two-stage Isocracking process [11]. 24
Figure 3.1. Diagram of the micro-bomb reactor. Reproduced from [85]. 45
Figure 3.2. Diagram of the process followed to prepare liquid and solid products for analysis. 46
Figure 3.3. Calibration of Mixed-A and Mixed-D SEC columns based on Polystyrene standards. 49
Figure 3.4. Diagram of the SEC system. 49
Figure 3.5. Calibration curve relating boiling points with temperature on the TGA pan (extracted from Zhang's PhD thesis [85]). 50
Figure 4.1. Mixed-D column SEC chromatograms of hydrocracking products obtained in three successive reactions reusing the $NiMo/Al_2O_3$ catalyst. The conditions applied were 190 bar H_2 pressure and 440°C. Tetralin was used as solvent. Area normalisation has been applied to all chromatograms. 56
Figure 4.2. Mixed-D column SEC chromatograms of Point of Ayr extract and its hydrocracking products obtained at 190 H_2 pressure and 440°C. Area normalisation has been applied to all chromatograms. 60
Figure 4.3. TGA temperature programs tested for boiling point determination. 63
Figure 4.4. "$>$450°C" content determined by three different TGA temperature programs as a function of the weight loaded on the TGA pan. 64
Figure 4.5. Mixed-A column SEC chromatograms of the Point of Ayr extract and its "$>$450°C fraction". Both chromatograms have been area normalised. 65
Figure 5.1. Mixed-A column SEC chromatograms of the Point of Ayr hydrocracking feed and the hydrocracking products for 0, 5, and 10 minutes reaction time. All chromatograms have been area normalised. 73
Figure 5.2. Mixed-A column SEC chromatograms of the Point of Ayr hydrocracking feed and the hydrocracking products for 5, 30 and 60 minutes reaction time. All chromatograms have been area normalised. 73
Figure 5.3. Synchronous UV-Fluorescence spectra of the Point of Ayr hydrocracking feed and the hydrocracking products for 0, 5 and 10 minutes reaction time. All spectra have been peak normalised. 74

Figure 5.4. Synchronous UV-Fluorescence spectra of the Point of Ayr hydrocracking feed and the hydrocracking products for 5, 30 and 60 minutes reaction time. All spectra have been peak normalised. 75
Figure 5.5. Apparent and real conversions as a function of reaction time obtained by Begon et al. [7]. 77
Figure 5.6. Apparent and real conversions as a function of reaction time obtained in the present work. 78
Figure 6.1. Diagram of a pillared clay. 81
Figure 6.2. Mixed-A column SEC chromatograms of hydrocracking products obtained with CM2b, CM6a and NiMo as catalysts. SEC chromatograms of the feed and products from the no catalyst run are also included for comparison. All chromatograms have been area normalised. 88
Figure 6.3. Mixed-A column SEC chromatograms of hydrocracking products obtained with CM3, CM16, Na montmorillonite and NiMo as catalysts. SEC chromatograms of the feed and products from the no catalyst run are also included for comparison. All chromatograms have been area normalised. 88
Figure 6.4. Mixed-A column SEC chromatograms of hydrocracking products obtained with CM3, CM6a, Na montmorillonite and NiMo as catalysts. SEC chromatograms of the feed and products from the no catalyst run are also included for comparison. All chromatograms have been area normalised. 89
Figure 6.5. Synchronous UV-F spectra of hydrocracking products obtained using CM3, CM6a and NiMo as catalysts. The feed (Point of Ayr extract) and the products from the non-catalytic run are also shown for comparison. All spectra have been peak normalised. 91
Figure 6.6. Synchronous UV-F spectra of hydrocracking products obtained using CM16 and Wyoming Bentonite (raw clay) as catalysts. The spectra of the feed (Point of Ayr extract) and the products from the runs using CM3, NiMo and no catalyst are also shown for comparison. All spectra have been peak normalised. 91
Figure 6.7. Mixed-A column SEC chromatograms of hydrocracking products obtained using SL1, SL2 and SL3 as catalysts. The SEC chromatograms of the feed (Point of Ayr extract) and the products from the runs using NiMo and no catalyst are also shown. All chromatograms have been area normalised. 93

Figure 6.8. Mixed-A column SEC chromatograms of hydrocracking products obtained using SL4, SL5, SL6 and the untreated laponite (raw clay) as catalysts. The SEC chromatograms of the feed (Point of Ayr extract) and the products from the runs using NiMo and no catalyst are also shown. All chromatograms have been area normalised. 94

Figure 6.9. Mixed-A column SEC chromatograms of hydrocracking products obtained using SL7, SL8 and SL9 as catalysts. The SEC chromatograms of the feed (Point of Ayr extract) and the products from the runs using NiMo and no catalyst are also shown. All chromatograms have been area normalised. 94

Figure 6.10. Synchronous UV-F spectra of hydrocracking products obtained with tin laponites. All spectra have been peak normalised. 95

Figure 6.11. Mixed-A column SEC chromatograms of hydrocracking products obtained using two different preparations of SL2 and SL7. All chromatograms have been area normalised. 96

Figure 6.12. Mixed-A column SEC chromatogram of hydrocracking products obtained with several pillared clays. All chromatograms have been area normalised. 97

Figure 6.13. Synchronous UV-F spectra of hydrocracking products obtained using Cr laponite, NiMo and no catalyst. All spectra have been peak normalised. 98

Figure 7.1. Mixed-A column SEC chromatogram of the hydrocracking products obtained using CM3, no catalyst and NiMo. All chromatograms have been area normalised. 103

Figure 7.2. Mixed-A column SEC chromatogram of the hydrocracking products obtained using Na montmorillonite and NiMo. All chromatograms have been area normalised. 103

Figure 7.3. Mixed-A column SEC chromatogram of the hydrocracking products obtained using CM6a, Wyoming Bentonite and NiMo. All chromatograms have been area normalised. 104

Figure 7.4. Synchronous UV-F spectra of hydrocracking products obtained with fresh and reused CM3 as catalysts. All spectra have been peak normalised. 104

Figure 7.5. Synchronous UV-F spectra of hydrocracking products obtained with fresh and reused CM6a as catalysts. All spectra have been peak normalised. 105

Figure 7.6. Mixed-A column SEC chromatogram of hydrocracking products obtained with SL2 (fresh and reused) as catalyst. All chromatograms have been area normalised. 107
Figure 7.7. Mixed-A column SEC chromatogram of hydrocracking products obtained with SL7 (fresh and reused) as catalyst. All chromatograms have been area normalised. 108
Figure 7.8. Synchronous UV-F spectra of hydrocracking products obtained using fresh and reused SL2. All spectra have been peak normalised. 108
Figure 7.9. Synchronous UV-F spectra of hydrocracking products obtained using fresh and reused SL7. All spectra have been peak normalised. 109
Figure 7.10. Mixed-A column SEC chromatogram of hydrocracking products obtained using fresh and reused CL1a. All chromatograms have been area normalised 110
Figure 7.11. Mixed-A column SEC chromatogram of hydrocracking products obtained using fresh and reused Eu montmorillonite. All chromatograms have been area normalised 110
Figure 7.12. Mixed-A column SEC chromatogram of hydrocracking products obtained using fresh and reused Ce montmorillonite. All chromatograms have been area normalised. 111
Figure 7.13. Mixed-A column SEC chromatograms of hydrocracking products obtained using fresh and reused Ce-Cr montmorillonte. All chromatograms have beeen area normalised. 112
Figure 8.1. Pore size distributions of fresh and coated NiMo 116
Figure 8.2. Pore size distributions of the starting catalyst (coated NiMo) and the catalysts recovered after 0, 10 and 30 minutes hydrocracking experiments 117
Figure 8.3. Pore size distributions of fresh Sn laponite 7 and Cr montmorillonite 3. 118
Figure 8.4. SEM of a CM3 catalyst particle (a). Its elemental composition profiles obtained by X-ray microanalysis are also shown: (b) Silicon, (c) Aluminium, (d) Oxygen, (e) Carbon. 119
Figure 8.5. (a)Fresh CM3 catalyst. (b) Fourteen points taken for elemental analysis. 121
Figure 8.6. SEM micrographs of CM3 used once. (a) shows the carbonaceous deposition in red; (b) shows the carbon distribution (red), silicon (green) and

aluminium (blue); (c) five points taken for the determination of elemental composition shown in Table 8.3. 122

Figure 8.7. (a) SEM of the CM3 used twice; the Cr distribution is shown in red; (b) Carbon X-ray microanalysis profile; (c) Si X-ray microanalysis profile; (d) Aluminium X-ray microanalysis profile; (e) Oxygen X-ray microanalysis profile; (f) The area richer in Cr is magnified; X-ray microanalysis profiles of carbon (blue), silicon (green) and chromium (red) are shown;(g) four points taken for the determination of elemental composition shown in Table 8.4..... 125

Figure 9.1. Mixed-A column size exclusion chromatograms of the $CHCl_3/CH_3OH$ soluble and insoluble fractions of pitch pyridine insoluble and its hydrocracking products. Area normalisation has been applied to all chromatograms..... 128

Figure 9.2. Mixed-D column SEC chromatograms of the pyridine insoluble pitch fraction and its $CHCl_3/CH_3OH$ soluble and insoluble sub-fractions. Area normalisation has been applied to all chromatograms. 130

Figure 9.3. Mixed D column SEC chromatograms of the pyridine insoluble, $CHCl_3/CH_3OH$ insoluble pitch fraction and its hydrocracking products. Area normalisation has been applied to all chromatograms. 131

Figure 9.4. Comparison between the mixed-D column SEC chromatograms of the whole hydrocracking products and its $CHCl_3/CH_3OH$ soluble and insoluble fractions. Area normalisation has been applied to all chromatograms. 131

Figure 9.5. Mixed-A column SEC chromatograms of the vacuum residue C and its 2-hour hydrocracking products using fresh and reused Al montmorillonite. All chromatograms have been area normalised. 135

Figure 10.1. Diagram of the MALDI spectrometer. 138

Figure 10.2. Diagram showing pulsed ion extraction (PIE) in the MALDI-TOF spectrometer used in these experiments..... 139

Figure 10.3. MALDI-MS spectra of polystyrene standard 1700 Da recorded by a) reflector b) linear mode..... 142

Figure 10.4. MALDI-MS spectra of polystyrene standard 5050 Da recorded by a) reflector b) linear mode..... 143

Figure 10.5. MALDI-MS spectra of polystyrene standard 11,600 Da recorded by a) reflector b) linear mode..... 144

Figure 10.6. MALDI-MS spectrum of polystyrene standard 22,000 Da recorded by linear mode..... 145

Figure 10.7. MALDI-MS spectrum of polystyrene standard 50,000 Da recorded by linear mode..... 145
Figure 10.8. MALDI-MS spectrum of polystyrene standard 126,700 Da recorded by linear mode..... 146
Figure 10.9. Mixed-D column SEC chromatogram of the coal tar pitch. Detection by UVA at 300 nm was employed. 148
Figure 10.10. Peak-mass of SEC fractions obtained by LD-MS compared with the PS calibration of the Mixed-D column..... 148
Figure 10.11. LD-MS spectrum of the SEC fraction collected at elution time between 17 and 17.5 min. Spectrum obtained by linear mode..... 149
Figure 10.12. Acetone soluble pitch fraction by laser desorption-MS. Reflector mode. 150
Figure 10.13. Compounds identified in the acetone soluble fraction of the coal tar pitch identified by LD-MS..... 151
Figure 10.14. MALDI-MS spectrum of the pyridine acetone soluble fraction. Dithranol was used as matrix and the laser power applied was 70%. Matrix deflection was applied..... 151
Figure 10.15. Pyridine soluble pitch fraction by laser desorption-MS. Reflector mode. 153
Figure 10.16. Compounds identified in the pyridine soluble fraction of the coal tar pitch by LD-MS. 153
Figure 10.17. Pyridine insoluble pitch fraction recorded by Laser Desorption MS using linear mode. 154
Figure 10.18. MALDI-MS of the pitch pyridine insolubles. Distribution showing a second peak around 30,000 Da. MBTA was used as matrix. 155
Figure 10.19. Mixed-D column SEC chromatogram of the pyridine insoluble pitch fraction. Mass ranges according to the PS calibration are shown..... 157

TABLE OF TABLES

Table 4.1. Hydrocracking conversion of the">450°C"fraction in experiments carried out with tetralin as solvent at 190 bar H_2 pressure and 440°C. 56

Table 4.2. Hydrocracking conversions in experiments carried out without tetralin at 190 bar H_2 pressure and 440°C. 57

Table 4.3. Hydrocracking conversions and carbonaceous deposition on the catalyst in 120 minute experiments carried out without tetralin at 190 bar H_2 or He pressure and 440°C. Duplicated runs are shown in brackets. 59

Table 5.1. Apparent and real conversions and deposition on the catalyst as a function of reaction time. Experiments were carried at 440°C, 190 bar hydrogen pressure. A catalyst previously coated was employed in these experiments. 71

Table 5.2. BET surface area, total pore volume and average pore diameter of fresh and coated $NiMo/Al_2O_3$, and the catalysts recovered from hydrocracking runs. 76

Table 6.1. Apparent and real hydrocracking conversions obtained by Begon et al. [70] in experiments at 190 bar H_2 pressure and 440°C in the presence of tetralin. .. 83

Table 6.2. Apparent and real conversions and deposition on the catalyst for Cr montmorillonites. Fresh catalysts were used in these runs. 87

Table 6.3. Apparent and real conversions and deposition on the catalysts for tin laponites. The Sn contents of the fresh catalysts shown in this table were supplied by the project partners at Aston University. 92

Table 6.4. Conversions and carbonaceous deposition on the catalyst for two preparations of Sn laponites 2 and 7. The Sn content in the fresh catalyst measured by XPS has been provided by our partner group at Aston University. 96

Table 6.5. Apparent and real conversions and deposition on the catalysts for several pillared clays. 97

Table 7.1. Apparent and real conversions and recovered solids for various reused catalysts. 102

Table 7.2. Characteristics of fresh catalysts. Values supplied by the project partners at Aston University. 106

Table 7.3. Apparent and real conversions and recovered solids for various reused catalysts. 107

Table 7.4. Apparent and real conversions and recovered solids for various reused catalysts. 111

Table 8.1. BET surface area, total pore volume and average pore diameter of fresh and coated NiMo/Al_2O_3, and the catalysts recovered from hydrocracking runs. All values shown were obtained in this laboratory. 115

Table 8.2. Particle size distribution of the fresh CM3 catalyst obtained by sieving. 120

Table 8.3. Al:Si and C:Si ratio measured by X-ray microscopy in five points shown in Figure8.6c. 120

Table 8.4. Al:Si and C:Si ratio measured by X-ray microscopy in four points shown in Figure8.7g. Points are numbered from left to right..... 123

Table 9.1. Table of conversions for experiments using Vacuum Residue C as feed. Experiments were performed at 440°C and 190 bar hydrogen pressure. The reaction time was 2 hours..... 134

Table 10.1. Experimental conditions under which the signal at 30,000 Da was obtained by LD-MS. Linear mode was employed and laser power was 80% of the maximum available in all cases..... 156

1 INTRODUCTION

1.1 COAL LIQUEFACTION

Attempts to produce coal derived liquid products started as early as the mid-nineteenth century, when processes to obtain solvents, fuels and other products were developed in France, Germany and the UK.

In 1869 Berthelot suggested that an oil-like product could be synthesised by chemical reduction of coal, but processes applying his idea were not available until Friedrich Bergius patented the direct liquefaction of coal in 1913. This method implied the hydrogenation of coal under high temperatures and pressures to produce hydrocarbons with similar properties to those of a crude oil. A few years later, during the World War I, Bergius' process found commercial application. A different approach employing gasification of coal and reaction of the molecular hydrogen and carbon monoxide over a cobalt catalyst was patented in 1925 by Fischer and Tropsch. In its origins, this indirect liquefaction process was mainly applied to the synthesis of chemical feedstocks rather than fuels. During the World War II, Germany depended on coal liquefaction processes, which produced 90% (about 4 millions tons) of its consumption of gasoline. A direct liquefaction plant was also operating in the UK between 1935 and 1939 to produce 100,000 tons per year of gasoline. In the 1950's the interest on coal liquefaction processes dropped as a consequence of the discovery of new petroleum reserves and the reduction in oil prices which followed it. The only exception was South Africa, which developed some liquefaction processes, mainly based on indirect liquefaction. Its availability of large coal reserves and the impossibility to obtain oil due to imposed embargo acted as an incentive to the commercial application of coal liquefaction.

This overall situation remained unchanged until 1973 when increases in oil prices again generated interest in the production of liquids fuels from coal. As a result, much research was devoted to direct liquefaction processes until low oil prices returned in the mid-eighties. Several direct liquefaction processes have been developed in the 1970's and early 1980's, mainly in the US, the UK, Germany and Japan. Although some of them went beyond laboratory scale, and pilot plants were commissioned and run, none of them has found commercial application. Two stage direct liquefaction processes, with a first step involving the dissolution of coal,

followed by hydrocracking at high temperature and pressure in the presence of a catalyst, were developed in that period.

Interest in coal liquefaction decreased with the return of low oil prices after the second oil shock in 1980, and it has continued at a low level since then. Although sporadic rises in oil prices which took place over those years have not changed this situation, a more permanent turn to high oil prices could alter the perception and reinstall coal liquefaction as a strategic alternative. If the current situation of oil prices in the region of 50-60 US$ per bbl continues, the economics of coal liquefaction may begin to look seriously attractive.

Viability of coal liquefaction may also be favoured by regional conditions, mainly in countries which contain vast coal reserves. This is the case of China, which is strongly dependent on imported oil, and South Africa, which developed the SASOL indirect liquefaction process during the years under trade embargoes and has continued relying on it since then.

As coal reserves are much larger than those of oil and gas, coal liquefaction may still be an option when oil and gas became less abundant or its production difficult or expensive. This may strongly depend on how far advanced technologies using renewable sources develop and whether they can close the gap between energy supply and demand.

1.2 UPGRADING HEAVY OIL FRACTIONS

By contrast with coal liquefaction, the use of hydrocracking to upgrade heavy oil fractions is becoming more attractive. Several causes can be pointed out for this. There is a decline in light oil reserves and production together with an increase in the reserves of heavy oil discovered. The market for heavy oils such as fuel oil is decreasing due to substitution by natural gas. In addition, tightening of environmental regulations involving requirements of disposal of refinery residues makes the upgrade of heavy fractions an increasingly economically viable option. However, hydrocracking is an expensive process, mainly due to the large consumption of hydrogen. The number of recent studies dealing with the main aspects of catalytic hydrocracking and the characterisation of heavy hydrocarbons, such as asphaltenes, has increased. Their aim is to improve the catalyst effectiveness and to understand the

mechanisms of catalytic activity and catalyst deactivation. Improvements in the catalysts used would allow a decrease in the amount of expensive hydrogen consumed, as well as in the temperatures and pressures at which the process takes place. In addition, a more detailed knowledge of the molecular structures involved in heavy oil fractions will contribute to the development of cheaper technological alternatives.

1.3 OBJECTIVES OF THE PRESENT STUDY

The main aim of this work is to test the suitability of several catalysts for the hydrocracking of heavy hydrocarbons. Ideally, a catalyst should lead to high conversions of the starting material into a liquid with lower molecular mass and boiling point distributions. It should also provide reaction pathways that would reduce hydrogen consumption. In previous work in a joint project between this group at Imperial College London and the Chemical Engineering and Applied Chemistry Department of Aston University, clays pillared with different ions have been identified as potentially active catalysts for the hydrocracking of heavy oil and coal feedstocks.

The present project, which is run in collaboration with the Chemical Engineering and Applied Chemistry Department of Aston University and the Department of Chemistry of the University of Birmingham, has been a continuation of that work. New routes to synthesise the more promising catalysts, Sn laponite and Cr montmorillonite, have been explored at Aston University. Microwave irradiation has been employed in the synthesis of Sn laponites in addition to conventional methods. New compounds such as Cr laponite, Eu montmorillonite, Ce montmorillonite and Ce-Cr montmorillonite have also been prepared. The hydrocracking activities of all these catalysts have been tested at Imperial College.

In the case of Sn laponites and Cr montmorillonite, comparison has been made among the performances of catalysts synthesised under different experimental conditions. The ability of the raw clays used in the synthesis of pillared clays to hydrocrack the same feedstocks has also been evaluated in order to assess the effects of pillaring on catalytic activity.

The experimental procedures applied to catalyst testing have been modified. First, the use of tetralin as solvent in hydrocracking experiments has been avoided since it generates its own reaction products interfering with product characterisation. The use of no solvent has been proven feasible and allowed the generation of more reliable data. Second, previously coated catalysts have been used in several experiments in order to study the catalyst behaviour under conditions independent from the initial deposition.

Characterisation of heavy hydrocarbon materials is relevant to a variety of processes involving coal and oil utilisation, amongst them hydrocracking. One of the objectives of this project has been to further develop the techniques used to evaluate the materials in the samples before and after hydrocracking. Among the analytical techniques which have usually been applied in this laboratory in the characterisation of coal and petroleum-derived samples are size exclusion chromatography (SEC), ultraviolet fluorescence spectroscopy (UV-F), thermogravimetric analysis (TGA), nuclear magnetic resonance spectroscopy (NMR), gas chromatography (GC) and some mass spectroscopy techniques such as laser desorption (LD-MS), matrix-assisted laser desorption/ionisation (MALDI-MS), and probe-MS.

In the present project, coal derived samples which had been widely studied by several techniques in this laboratory were analysed with newly available methods, principally MALDI-MS. This work focused on the development of MALDI-MS as a useful technique to analyse heavy hydrocarbons. The agreement between results from size exclusion chromatography and MALDI-MS has been studied.

1.4 THE STRUCTURE OF THIS THESIS

The general background to the catalytic hydrocracking of coal and petroleum-derived materials and to the analytical techniques applied to the characterisation of heavy hydrocarbon liquids is discussed in the next chapter. More detailed background, specific to the content of each chapter is given in their respective introductions.

The experimental chapter describes the equipment as well as the procedures used in both hydrocracking experiments and sample characterisation. The changes made to experimental procedures, particularly experiments carried out in the absence

of solvent, are discussed in Chapter 4. Chapter 5 analyses the effect of reaction time on hydrocracking conversions and product distributions. Chapters 6 and 7 describe the results from the first use of pillared clays and their reuse, respectively.

An insight into the behaviour of the catalysts used for catalytic hydrocracking is given in Chapter 8. Work on hydrocracking of two feeds other than the Point of Ayr extract, namely a vacuum residue and the pyridine insoluble fraction of a coal tar pitch, is presented in the Chapter 9. Chapter 10 describes the work carried out on characterisation of heavy hydrocarbon liquids. Finally, the conclusions of this work are presented in Chapter 11, as well as recommendations for further work.

2 BACKGROUND

2.1 PROCESSES IN HYDROCRACKING OF COAL AND OIL-DERIVED LIQUIDS

2.1.1 Coal liquefaction

Direct coal liquefaction can be carried out in single or two-stage processes depending on whether the hydrocracking step is performed on the raw coal (single stage) or a coal extract is first obtained and subsequently hydrocracked (two-stages).

As mentioned in the introduction, there are no direct liquefaction processes currently operating in commercial scale. However, several processes have been developed at pilot scale and some of them, such as Kohleoel in Germany, Nedol in Japan and Liquid Solvent Extraction (LSE) in the UK [1, 2] would be ready for commercialisation if the economics were to become viable.

The LSE process, a two-stage process developed by British Coal at the liquefaction facility at Point of Ayr [1], is especially relevant for the present work. The development of this process included the commissioning and operation of a 2.5 tonnes per day pilot plant. These facilities were located in Point of Ayr, Wales, and have been decommissioned in 1992. The LSE pilot plant operated by British Coal Corporation has been a direct antecedent of this project. The Point of Ayr hydrocracker feed has been thoroughly characterised and used as feed in hydrocracking experiments in this laboratory [3-10].

A schematic diagram of the LSE process is shown in Figure 2.1. At the Point of Ayr plant coal was mixed with a solvent recycled from the same process. The ratio between recycled solvent and coal was 2.2. Then the mixture was preheated and extracted in a continuous digestor, a stirred tank reactor (CSTR), operating at approximately 15 bar and temperatures between 410-430°C. The digest was filtered to remove mineral matter and undissolved coal particles. The light fractions of the digest were removed by distillation and the main stream fed to the hydrocracker. It operated at a hydrogen pressure of 200 bar and a temperature normally in the range 420-430°C. The space velocity was 0.76 kg-feed/kg-cat/h. The hydrocracked products were cooled and sent to an atmospheric pressure distillation column. The atmospheric pressure distillate was the output of the process, and it was successfully upgraded to a transport fuel by the procedures normally applied in the petroleum industry. The

bottoms of the atmospheric pressure column were vacuum distilled. The distillate from the vacuum column, mixed with a fraction of the bottoms of the atmospheric distillation, formed the recycled solvent.

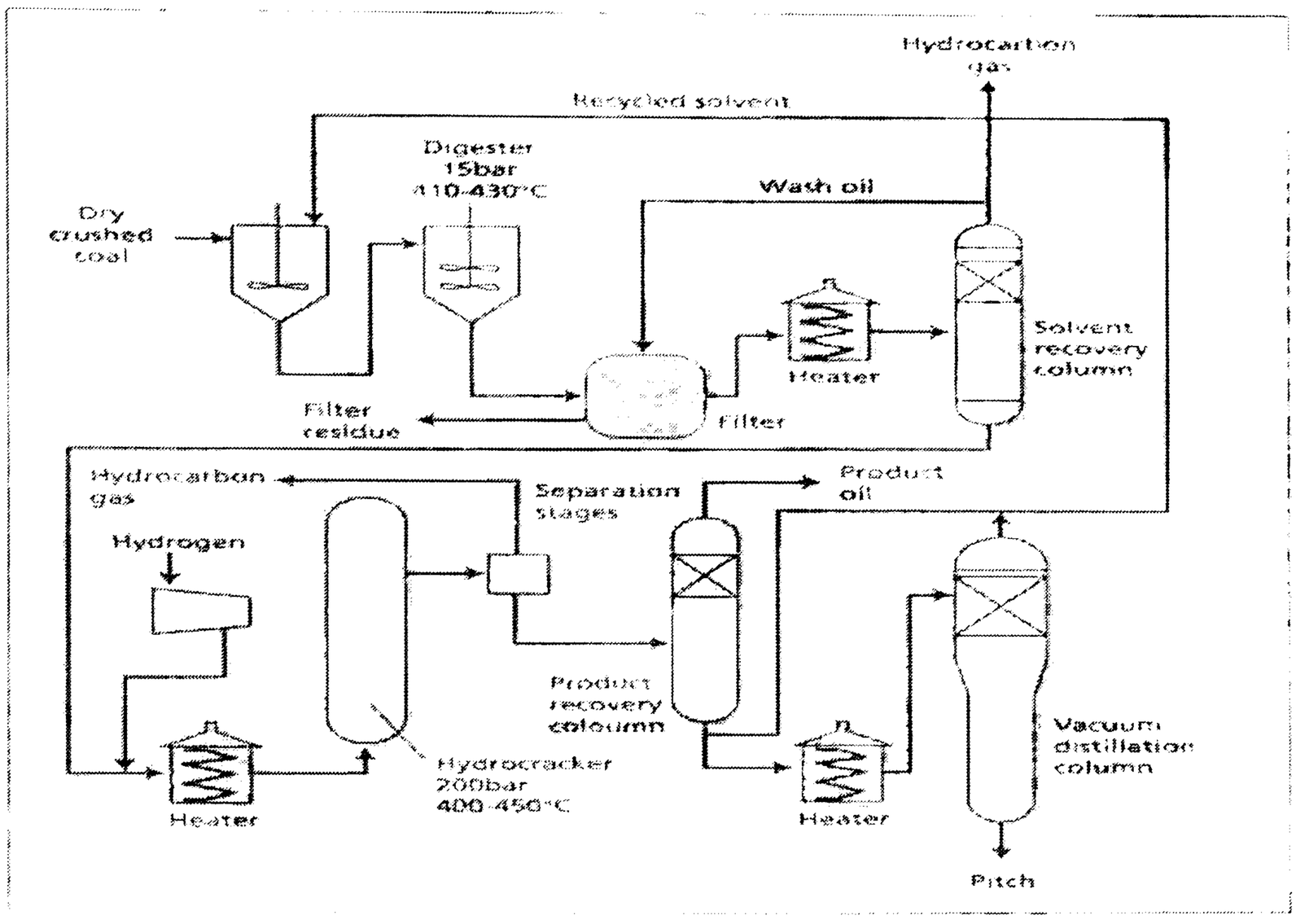


Figure 2.1. Diagram of the Liquid Solvent Extraction Process as operating at British Coal's Point of Ayr pilot plant. Reproduced from [1].

About 15% of the dry ash-free coal was recovered as hydrocarbon gases (C_1 to C_4), nearly 50% as distillate product with boiling point lower than 300°C, 10% with boiling points between 300°C and 450°C, about 1 % as pitch and 24% as organic matter in the filter cake [2]. Special attention was devoted in that work to parameters affecting the selection of the catalyst. The most relevant properties identified in a catalyst were hydrocracking activity, hydrogenation activity, attrition resistance, thermal-shock resistance and particle size distribution.

2.1.2 Hydrocracking in the petroleum industry

Numerous hydrocracking processes are currently used in the petroleum industry to produce lighter materials from heavier fractions. Hydrocracking has been applied to relatively light feeds to produce higher yields of lighter distillates and to upgrade heavier feeds such as atmospheric and vacuum residues, heavy crudes, bitumen, tar sands and shale oils. The industrial applications of hydrocracking include

obtaining LPG from naphthas and vacuum gas oils, naphthas from atmospheric and vacuum gas oils and diesel from vacuum gas oils and residues [11].

Hydrocracking is one of the processes involved in the hydroprocessing of oil derived liquids. Hydroprocessing also comprises hydrodesulphurisation (HDS), hydrodenitrogenation (HDN), hydrodeoxygenation (HDO) and hydrodemetalisation (HDM). The conditions under which all these reactions take place are similar and involve high temperatures and hydrogen pressures. Depending on the characteristics of the feed and the desired products, some of these functions will be more relevant to a specific process.

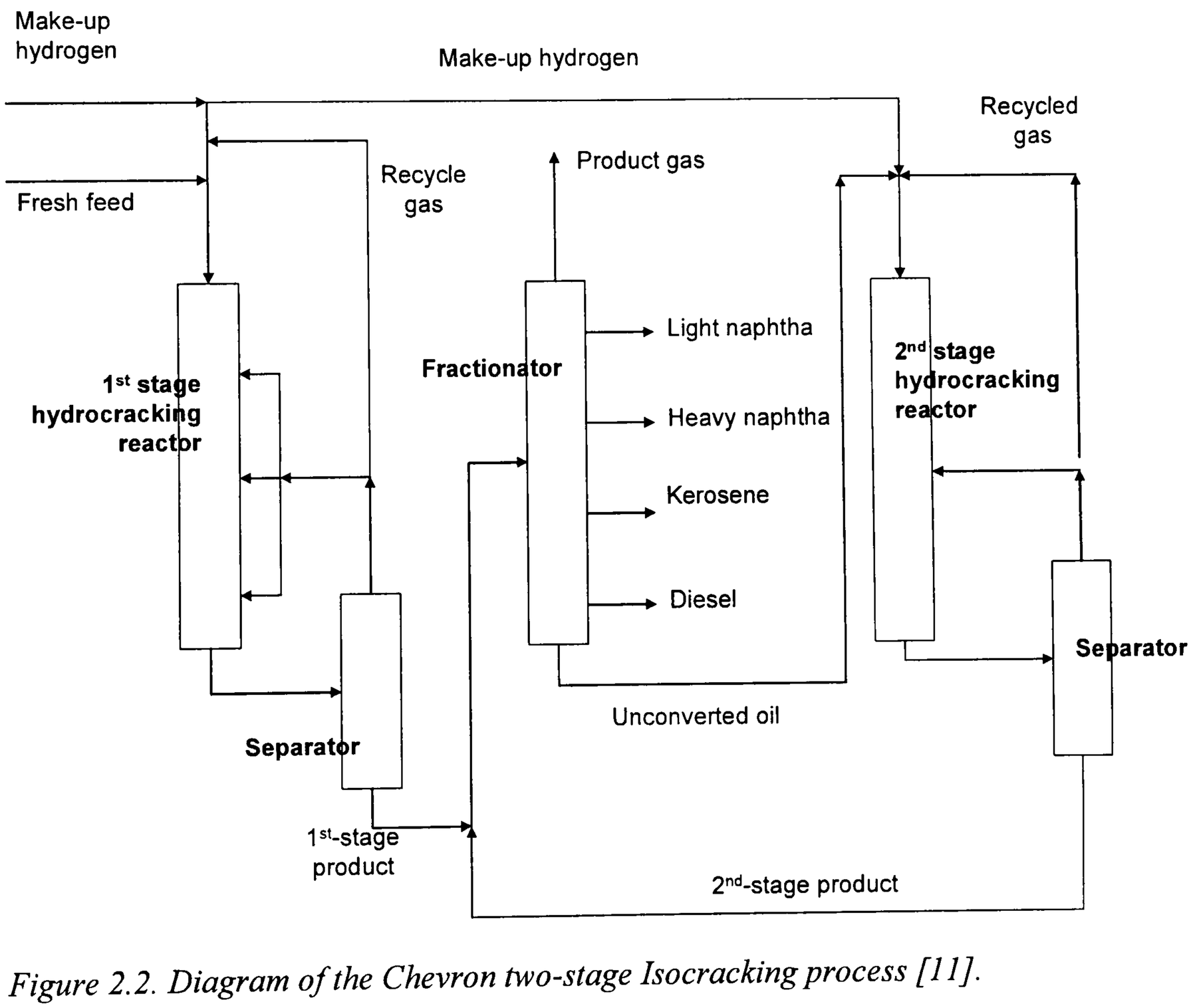


Figure 2.2. Diagram of the Chevron two-stage Isocracking process [11].

Numerous hydrocracking processes are currently commercially employed. A summary can be found in [12]. All processes have some common features. The heavy hydrocarbon mixture is preheated to reaction temperature and transferred to a reactor.

The retention times applied are usually in the range between 1 and 10 hours. Hydrogen can be added either during the preheating or in the reactor. There are single and two-stage processes, with and without recycle. An example of a two-stage process is Chevron's two-stage "Isocracking" shown in Figure 2.2. The three main groups of reactors used for hydrocracking are fixed-bed, expanded-bed and moving-bed. Fixed bed hydroprocessing is the simplest and most commonly used system currently operating and is usually operated in the downflow mode.

The H-oil and the LC-Fining processes employ ebullated-bed reactors. In this type of reactor, recirculation of the feed helps to achieve the speeds required to fluidise the catalyst bed. These processes were initially designed for petroleum–derived feeds and have been adapted to coal liquefaction processes and the coprocessing of heavy feeds, coal and plastics. New systems applying moving bed reactors, where the catalyst can be replaced without stopping the reactor operation, have been reported in the literature [13].

2.2 CATALYSTS AND CATALYST DEACTIVATION

2.2.1 Hydroprocessing Catalysts

A mechanism of catalytic activity in which molecular hydrogen dissociates on the catalyst and then migrates and reacts with the products of thermal bond cleavage has been proposed [14]. Hydrogen itself is very mobile through the coal structure. The transport of hydrogen atoms in solution could be favoured by the use of a hydrogen donor solvent. According to this model the bond cleavage reactions are not catalytically but thermally induced [14]. An alternative mechanism was suggested by McMillen et al. [15]. In their view, the addition of hydrogen atoms to aromatic rings in the coal structure precedes bond cleavage. Cyclohexadienyl-type radicals are thought to play an important role in this model transferring atomic hydrogen to the ipso positions of linkages to aromatic systems in the coal structure.

There are two separate functions involved in the hydrocracking mechanism, cracking and hydrogenation. This was deduced from the synergism between CoS and SiO_2/Al_2O_3 in work done by Quader and co-workers, cited in [16 page 195]. It was found in that work that a mixture of CoS and SiO_2/Al_2O_3 had a higher hydrocracking activity than any of the components separately. CoS is active towards hydrogenation

while SiO_2/Al_2O_3 provides cracking activity. The hydrocracking catalysts are expected to have both functions.

Acid catalysts, such as the $ZnCl_2$ melt catalyst used in the Consol liquefaction process [16, 17], promote the rupture of C-C bonds but they do not perform the hydrogenation function. In the absence of hydrogenation, condensation of the products of cracking may lead to the build-up of higher molecular mass materials.

Supported catalysts have also been used in the hydrocracking step of two-stage coal liquefaction, whilst dispersed catalysts were preferred for the first stage involving coal dissolution [14]. The catalysts normally used in hydroprocessing contain molybdenum, or less frequently, tungsten, promoted by either nickel or cobalt and supported on alumina, silica, silica-alumina or zeolites [13, 14]. Catalysts supported on carbon have also found some applications. Recently developed catalysts have incorporated the use of phosphorus and boron as supports and Mo carbides and nitrides as active phases [13].

CoMo catalysts supported on Al_2O_3 are generally considered as better for hydrodesulphurisation, whereas NiMo supported on Al_2O_3 is preferentially used as catalyst for hydrodenitrogenation, hydrodemetalisation and hydrocracking [13, 18]. A molybdenum sulphide is the active catalytic form of these catalysts. Sulphidation can take place in-situ by reaction with sulphur present in the feed or else a presulphided catalyst may be used. Due to its hydrocracking properties, NiMo is the catalyst preferred for coal derived materials, which have a large content of aromatic materials [13]. The molybdenum sites are active towards hydrogenation whereas cracking takes place mainly on the acidic support.

Typical support surface areas are of the order of 200 m^2/g and average pore sizes in the range 75-300 Å [19]. Petroleum hydrotreating was achieved in the 1970s through the use of catalysts with high metal loadings and small pores, in the range of 30 to 80Å pore diameter. The need to process heavier feeds led to the introduction of catalysts with larger mesopores in the 1980s and bimodal catalysts in the early 1990s. Bimodal catalysts have a cracking component which consists of a mildly acidic phase and a hydrogenating component with lower acidity. In bimodal catalysts the macropores allow the transport of large molecules to the meso and micropores where most catalytically active sites are [20].

2.2.2 Catalyst deactivation by coke deposition

The processes leading to catalyst deactivation have been reviewed by Absi-Halabi [18] and Furimsky et al. [19]. Three main mechanisms have been identified: deactivation by coke deposition or "fouling", by metals and by pore mouth constriction and blockage. Coke deposition occurs in the early stages of hydroprocessing and it reaches a pseudo steady state, whereas deactivation by metal deposits continues over a longer time scale [18, 19, 21, 22]. At commercial scale the reaction rate is often maintained by means of increasing the reactor temperature, although this also increases the deactivation rate. Pore blockage becomes relevant at later stages and it is irreversible, forcing the end of the run and the regeneration or replacement of the catalyst.

The effect of coke deposition on the deactivation process is more marked than that of metal deposits. Cable et al. [23] qualitatively described the deactivation effects of metals as very weak on hydrogenation and weak on the cracking function. By contrast, the effects of coke deposition on the catalytic activity were regarded as strong on hydrogenation and very strong on cracking. Hence the study of catalyst deactivation in the present work focuses on the latter.

The effect of deposition on catalytic activity has been assessed in several works. This literature review is not exhaustive. The references quoted are either the most relevant to the present project or examples of the trends commonly agreed by several research works. Yamamoto et al. [24] showed that complete deactivation of a CoMo catalyst used to hydroprocess a coal-derived middle distillate would occur when its carbon content was around 20%. Diez et al. [25] observed a 20% and 75% decrease in the hydrogenation function of a hydroprocessing catalyst with coke amounts of 3% and 10.6% weight respectively.

The main factors affecting catalyst deactivation by coke deposition are feed composition, catalyst composition and structure, and the hydroprocessing conditions. These factors will be discussed in the next few sections.

2.2.3 Effect of catalyst properties in coke deposition

The deactivation process is very dependent on catalyst structure and pore size distribution. A higher acidity of the support promotes coking, as well as cracking [18, 19]. A larger deposition of anthracene under nitrogen has been observed on a bare

Al_2O_3 support than on a $CoMo/Al_2O_3$ catalyst. The addition of Mo to the alumina support produced a drop in the amount of deposits when a vacuum gas oil was hydroprocessed [26]. Remarkable differences in deposition after five months on stream were observed between two different aluminas. A γ-alumina with a lower acidity ("chestnut burr" γ-alumina type) generated 12% of coke on the catalyst instead of the 20% shown by the normal γ-alumina [27].

Although catalyst porosity seems not to be very relevant in the hydroprocessing of light feeds, it becomes an essential parameter in the case of heavy feed hydroprocessing. Catalysts of small porosity are more likely to deactivate by pore plugging, whereas those with larger pores may suffer core deactivation. This may lead to two different profiles of coke deposits within the catalyst. A uniform surface deposition is observed in large-pore catalysts whereas small-pore catalysts show a gradient in coke concentration across the catalyst [13, 28]. This reflects pore diffusion limitations of the material with potential for coking. In the hydroprocessing of an atmospheric residue from coal liquefaction, Yoshimura et al. [29] found that the catalyst with the smallest pore diameter had the lowest activity, although small differences in the loss of surface area were observed after the catalysts were extracted with toluene. Small catalyst particle size has been found more advantageous in the hydroprocessing of heavy feeds, since the diffusion limitations are overcome, at least partially. In hydroprocessing using extrudates, a gradient of coke was observed through the catalyst particle. The carbon was initially seen to deposit on the surface to then migrate inside the catalyst. The concentration gradient depends on catalyst pore size, decreasing for the catalysts with larger pores [29].

The deposition markedly affects the surface area and pore volume of the catalyst. During the hydrocracking of maya heavy crude oil in isothermal operation at 400°C, Ancheyta et al. observed [21] that the surface area decreased after 500 hours from 175 to 88 m^2/g and the pore volume from 0.56 to 0.33 cm^3/g. The mean pore diameter actually increased from 127 to 152Å due to blockage of the smaller pores.

In a separate work, Ancheyta et al. [22] observed a reduction of surface area and pore volume of the order of 70%. The percentage of pores with diameters larger than 250Å decreased, whereas there was a larger fraction of small pores (<100Å) in the catalyst coated with carbonaceous material. Gray et al. [28] found that the relative pore volume, the surface area and the relative median pore diameter were very

sensitive to the carbonaceous deposits in the range 0 to 5% carbon on the catalyst. This is in agreement with the large drop in all these parameters observed during the early stages of hydrocracking, when greater and faster deposition takes place, and the relative stabilisation afterwards.

Reddy et al. [30] showed that a pore diameter of around 28Å in a CoMo catalyst supported on a mesoporous molecular sieve, MCM-41, was not large enough to achieve high conversions in the hydroprocessing of asphaltenes of petroleum residues. In that work Reddy et al. found an increase in the conversion of the fraction with boiling point above 540°C with increasing temperature. It has been suggested that the catalyst did not promote C-C cleavage but that the cracking was thermal in nature. However, the product distribution varied and larger amounts of gas and coke were obtained in the non-catalysed run.

A study on the effect of catalyst pore size on hydrocracking conversions was carried out by Song et al. [20, 31]. In that work, NiMo catalysts with median pore sizes 120, 150, 290 and 730Å were used to hydrocrack two samples of solvent refined coal. The asphaltene and preasphaltene fractions of the solvent refined coals were hydrocracked separately. Conversions of the preasphaltenes steadily increased with mean pore diameter up to 730Å. By contrast, the conversion of the asphaltenes increased with pore diameter up to 290Å to become constant for larger pore sizes. The authors attributed these pore size effects are attributed to steric hindrance of large molecules [31]. The diffusion of preasphaltenes into the catalyst porosity is enhanced by large porosity catalysts and therefore the preasphaltene conversions improved with increasing pore sizes.

Hydrocracking experiments were also performed on the whole solvent refined coals [20]. The conversions of asphaltenes and preasphaltenes present in the solvent refined coal were observed to increase with increasing pore size up to 150Å. A further increase in the catalyst pore diameter up to 730Å enhanced the preasphaltene conversion but that of the asphaltenes dropped [20].

The difference in the behaviour of the asphaltene fraction when isolated from that observed in the solvent refined coal was interpreted in terms of the preasphaltene fraction suppressing the conversion of the asphaltenes. The preferential adsorption of the preasphaltenes on the active sites and the production of asphaltenes from

preasphaltenes were the causes of the lower asphaltene conversions achieved when hydrocracking the whole solvent refined coal. By contrast, the asphaltenes had little effect on the preasphaltenic conversions [20].

The pore size distribution is therefore an important parameter to take into account in catalyst evaluation. A study of the pore size distribution of the pillared clay catalysts is presented in Chapter 8.

2.2.4 Effect of feed composition on coke deposition

The rate of catalyst deactivation is strongly dependent on feed composition. Deactivation during the hydroprocessing of light petroleum fractions has been found to be very slow, allowing the catalyst to be active for longer periods than during the hydroprocessing of heavier feeds. Hydroprocessing of heavy fractions such as asphaltenes and preasphaltenes as well as coal liquefaction extracts leads to high levels of catalyst fouling and short catalyst life.

Increases in molecular weights, boiling point ranges and in the content of heteroatoms and aromatic rings in the feed lead to larger coke deposition. Heterocycles, alkenes and aromatics are more likely to be the coke precursors since they can interact more strongly with the catalyst surface. Stohl et al. [19] found larger deactivation rates when the composition of the feed was changed in the order: aliphatic hydrocarbons, neutral polycyclic, nitrogen polycyclic and hydroxyl polycyclic aromatics. Banerjee et al. [32] reported that the amount of coke during the thermal pyrolysis in gas phase of various fractions decreased in the order: asphaltene, resins, aromatic and saturates. The asphaltenes are defined as the hexane insoluble – toluene soluble fraction. Resins are soluble in light alkanes but insoluble in liquid propane. Curtis et al. used spent catalyst from the hydroprocessing of mixtures of solvent refined coal and hydrogenated creosote oil to hydrocrack naphthalene [33]. No deactivation was observed in catalysts used in the hydrocracking of hydrogenated creosote oil only. However, deactivation was observed when solvent refined coal was used in the blend and it increased with increasing proportions of solvent refined coal employed.

The deposits can also include insoluble materials which have precipitated out of solution. Precipitation has been reported to occur in the hydroprocessing of oil derived feeds containing asphaltenes. Asphaltenes are stabilised in solution by resins

and they precipitate if the balance between resins and asphaltenes in the liquid is altered as a consequence of hydrocracking reactions.

Hydrocracking experiments on coal extracts fractionated by solubility in pentane and toluene [34] have shown that greater carbonaceous deposits on the catalyst are produced by the heaviest sample, the toluene insoluble fraction, or preasphaltenes, of a coal tar pitch.

2.2.5 Effect of hydroprocessing conditions on coke deposition

The conditions applied during hydroprocessing are also relevant to the deposition phenomenon. The amount of coke was observed to increase with the temperature of operation up to 375°C, due to slow conversion of coke precursors to lighter species. This stage is followed by a constant level of deposits between 375 and 440°C. In this range of temperatures, hydrogenation seems to be quicker than condensation. Above 440°C, the coke resumed its increase with temperature [18] since the rate of condensation reactions increases at higher temperatures. However, the exact temperature ranges may depend on the composition of the feed, the catalyst and other operation parameters such as hydrogen pressure. In particular, the use of higher hydrogen pressure may extend the range of temperatures at which hydrogenation is favoured.

By contrast, Gualda et al. found that the amount of coke deposited on $NiMo/Al_2O_3$ catalysts during residue hydrodemetallisation actually decreased with increasing temperature, although the H/C ratio varied, going through a maximum [35]. A decrease in the coke deposition with hydrogen operation pressure was reported by several researchers [18, 35, 36].

Performing studies in a batch reactor, Gualda et al. [35] observed a decrease in the amount of coke with reaction time. On the other hand, a larger amount of deposits were found in a continuous system due to the uninterrupted supply of coke precursors. An extension of time on stream before deactivation takes place was achieved by using graded catalytic systems with three or more types of catalysts [37].

2.2.6 Effect of reaction time on the carbonaceous deposits.

The initial coke deposition is especially relevant to the present work since the catalysts are tested in relatively short runs. The initial deposition leads to great losses in surface area and pore volume. Processing Maya heavy crude oil in a flow reactor,

Ancheyta et al. [21, 22] found that strong deactivation takes place during the first 100 hours of operation. Deactivation led to a sharp increase in the asphaltenic content of the products within that period. The increase in deactivation and therefore in the concentration of asphaltenes in the outflow slowed down afterwards. Despite increases in temperature, which was changed from 400°C to 420°C after 280 hours and then to 430°C after 700 hours of operation, the subsequent catalyst deposition increased only slightly (from 18.3% weight at 490 hours to 18.5% at 1120 hours). This is in line with work by Benito et al. [38] who observed that the coke content did not show significant variations with time after the initial deposition during the hydrocracking of a residue from deasphalting a syncrude obtained by direct coal liquefaction. Similar findings have been published by Richardson et al. [36].

During the hydrocracking of a Kuwaiti atmospheric residue, Matsushita et al. [39] found that the quick deposition of carbonaceous material on an industrial MoO_3/Al_2O_3 took place over the first 12 hours reaching 15% of the fresh weight of the catalyst. They also observed the deposition to slow down afterwards to reach 20% after 240 hours on stream.

The composition of the deposits changes with time, becoming more graphitic during the first days on stream. According to Matsushita et al. [39], the aromatic fraction of the coke deposited on CoMo and NiMo catalysts increase markedly during the first 4 days and more slowly afterwards. The graphitic structures showed a decrease after the 4^{th} day, which was attributed to the lack of space for rearrangements available on the catalyst surface. An independent work showed that the H/C ratio of the coke was observed to decrease compared to that of the coke precursor [28].

The same authors [39] differentiate between two types of coke formed on the catalyst, soft and refractory. Soft coke consisted of extractable material reversibly adsorbed on the catalyst. It was burnt at lower temperatures during temperature programmed oxidation (TPO) carried out in a thermogravimetric analyzer (TGA) than the refractory coke. Refractory coke was not extractable and required higher temperatures to be removed from the catalyst surface by TPO. The authors found that the initial deposits were mainly composed of soft coke. Soft to refractory ratio decreased with time on stream. Moreover, the deposits showed an increase in the intensity of the band corresponding to condensed aromatic coke observed by Fourier

transform infra-red spectroscopy (FT-IR) [39]. Chu et al. [40] showed that a portion of the deposits that can be extracted with heptane and chloroform was causing a decrease in the porosity and hydrogenation activity.

Gray et al. distinguished between thermal and catalytic coke. The former is formed through a mechanism involving aromatic radicals in the bulk of the liquid, whereas the latter implies dehydrogenation on the catalyst [41]. Asphaltenes have been identified as the main cause of thermal coking. The fraction of asphaltenes ending up as coke on the catalyst dropped as the concentration of asphaltenes increased, showing a certain saturation phenomenon. However, the composition of the coke changed with the composition of the feed. Higher asphaltenic concentrations in the feed led to higher carbon contents and aromaticities on the catalyst.

The reversible character of the initial deposition is in line with observations by Richardson et al. [36]. They found that the initial deposits during the hydroprocessing of Athabasca bitumen on a $NiMo/Al_2O_3$ catalyst were removable with tetralin at the conditions of operation. Gray et al. [28] also showed that a fraction of the deposits resulting from the hydroprocessing of an Athabasca bitumen vacuum residue over a $NiMo/Al_2O_3$ catalyst was able to equilibrate with the liquid phase. This material becomes immobile at lower temperatures but is capable of reaching an equilibrium with the liquid phase at higher temperatures.

Preferential deposition of carbonaceous material on the catalyst support rather than on the active sites has been reported. Asphaltenes and coke precursors were found to preferentially adsorb on the acidic sites of the support whereas nitrogenated species tended to adsorb preferentially on the hydrogenation active sites [39]. Deposition of coke leads therefore to plugging of small pores and loss of surface area. On the other hand, nitrogenated compounds act as poisons, decreasing the catalytic activity of the active sites.

Fleisch et al. [42] reported an increase in the superficial Mo/Al ratio measured by XPS with increasing coke deposition, which provides evidence of a preferential deposition of coke on the alumina support rather than on the Mo active phase. A model proposed by Diez et al. [25] suggested that the deposits were thinner near the NiMo crystallites than on the catalyst support due to the hydrogenation activity of these active sites. Richardson et al. followed this model and assumed a monolayer of

coke deposited on the catalyst support with no coke deposits in an annular region surrounding the active sites [36]. They found good agreement with the experimental dependence of coke deposition on hydrogen pressure, reaction time, feed to catalyst ratio and feed composition [36]. van Doorn et al. [43, 44] suggested that at larger distances from the active sites, the coke could consist of a three dimensional network, rather than a monolayer deposit.

Chu et al. observed [45] that in a large pore size NiMo (around 180Å) catalyst the initial deactivation was linear up to a carbon content of about 4% and then slowed down. They proposed that at this point the growth of the carbonaceous layer is more upon itself than on new sites. The hydrogenation function was seen to be less affected than other functions, suggesting that the active sites are relatively clear of deposits.

2.3 MOLECULAR MASS DISTRIBUTIONS IN COAL AND OIL DERIVED SAMPLES.

The evaluation of hydrocracking catalysts requires an extensive characterisation of both feeds and products in terms of their molecular mass distributions. Several analytical techniques have been developed and applied to the analysis of molecular mass distributions and chemical structures of coal and petroleum derived liquids. The analysis of the larger molecular mass fractions is particularly important since they are the main objective of the hydrocracking process. Fractionation has been usually performed before analysis since the presence of larger quantities of lighter molecular masses avoids the detection of a relatively small amount of heavy material.

As discussed below, many of the analytical techniques showed the presence of materials of apparently high masses. The upper molecular mass limit in coal and petroleum derived samples has been debated in some detail and the discussion about whether those techniques are showing large molecules or aggregates of smaller ones is ongoing. A short review of the findings and limitations of the most relevant analytical techniques follows.

2.3.1 Size Exclusion Chromatography

Size exclusion chromatography (SEC) has been applied in this laboratory to the characterisation of heavy petroleum fractions [46, 47] and coal derived materials

including a coal tar pitch, a low temperature tar, the Point of Ayr extract, and several fractions obtained from them by different methods [3, 48-56]. Early work was performed using tetrahydrofuran (THF) as eluent. However, it was found that THF does not dissolve the whole sample and some material precipitated in the column, causing partial blockage and forcing an increase in pressure to keep a constant flow of solvent. In addition, its low solvent power allowed adsorption of sample on the column packing to take place. Adsorption effects were detected as signal appearing at longer elution times than the permeation limit of the column. Following work by Lafleur and Nakagawa [57], THF has been substituted by N-methyl pyrrolidinone (NMP) as solvent for SEC, as it seems to entirely dissolve most coal-derived liquids and no adsorptive effects have been observed.

Typical SEC chromatograms of coal and oil derived materials show two peaks. The material excluded from the column porosity appears at shorter retention times than the material retained in the column (excluded and retained peaks, respectively). Both peaks are separated by a valley of zero intensity.

Columns with different porosities have been employed. Their details are given in the experimental section. SEC is not an absolute method to evaluate molecular masses and therefore its validity relies on finding a suitable calibration of the columns. In this laboratory, SEC columns were calibrated employing polystyrene (PS) and poly (methyl methacrylate) (PMMA) standards with molecular masses ranging up to 15.4 million Da. Calibration curves relating molecular mass and elution time obtained with both sets of polymers match each other very closely. Extensive work has been carried out to evaluate the validity of these calibrations by independent experiments and techniques. This has led to the application of MALDI-MS and LD-MS to SEC fractions of samples as described below.

Numerous model compounds with different structures and polarities have been found to elute in reasonable agreement with the polystyrene calibration [48, 58, 59]. These include small aromatic and polycyclic aromatic compounds, heterocyclic nitrogen and heterocyclic oxygen compounds known to be present in coal. A separate calibration line was found for a set of polysaccharides (PSAC), which eluted earlier than PS and PMMA of similar masses. The mass deviation of PSAC from the PS/PMMA calibration is within a factor of 2.5 as maximum up to 15,000 Da and it was the largest observed for any sample. The important structural differences between

polysaccharides and heavy hydrocarbons make this deviation an upper limit to the errors in the estimation of molecular masses of coal and oil-derived samples by SEC using these columns. Other polymers including nitrogenated and oxygenated species with masses between 3,500 and 170,000 Da eluted in closer agreement with the PS/PMMA calibration line than the polysaccharides [59]. Their elution times were within one minute of the values predicted by the calibration.

The coal tar pitch was fractionated by TLC, using acetonitrile and pyridine as solvents. Three fractions were obtained in that way: acetonitrile mobile, pyridine mobile and pyridine immobile. SEC and UV-F have been carried out on those fractions. The excluded signal by SEC decreases and there is a shift towards shorter fluorescence wavelengths when increasing the fraction mobility [60]. Similar results have been obtained with fractions prepared by column chromatography and solvent solubility [3].

Materials eluting under the excluded peak would be large according to the polystyrene calibration. However, some studies have shown that molecular shape may have a strong influence on the elution time of the samples. A mixture of fullerenes with masses between 720 and 840 Da elutes in the mixed-D column at a time corresponding to a mass about 1 million Da according to the polystyrene calibration. Clearly, the particular shape of fullerene represents a departure from the relationship between shape and size [58] exhibited by most compounds.

An alternative explanation has therefore suggested [61] that signal under the excluded peak could also be generated by non-planar, three-dimensional rigid molecules. Although having relatively low molecular masses, these materials would be unable to pass through the small pores of the SEC column because of their voluminous and rigid structure, as observed for fullerenes. A good correlation showing a linear relation between $\log_{10}$ particle diameter and elution time has been observed in recent work on spherical soot and silica particles [59].

Several experiments have ruled out the possibility of the excluded peak being composed of aggregates of smaller molecules. Although proof of aggregation of coal derived materials was found in weaker solvents such as d_{10}-1-methyl naphthalene, chloroform, toluene and others (see below), no work has reported the presence of aggregates in a stronger solvent as NMP. It must emphasised that the whole pyridine

insoluble fraction of the coal tar pitch, which represents about 15% of the sample, is soluble in NMP.

Aggregation has not been observed in NMP solutions of standard polycyclic aromatic compounds which are known to be present in coal, even for the most polar compounds, which would be more likely to form aggregates. As mentioned above, the SEC retention times of these molecules were in good agreement with the PMMA and PS calibration [46, 58]. The concentration of the standard compound solutions was increased to favour agglomeration, but UV-F has shown no shift in the maximum fluorescence wavelength [46].

Independent techniques such as MALDI, UV-F and others have shown structural differences between the apparently high and the low mass material. This would indicate that the first is not merely composed of aggregates of the second, although in itself it does not rule out the possibility of the excluded peak being formed by aggregates of smaller molecules other than those appearing under the retained peak.

In an attempt to find evidence of aggregation in NMP, a coal tar pitch was fractionated by SEC and the fractions were re-injected in the SEC column as diluted solutions. No significant shift towards longer retention times was evident, as it would have been expected from the favourable conditions for disaggregation [58].

A shift towards longer elution times of the signal eluting under the excluded peak was observed when LiBr was added to the SEC solvent [62]. Claims that this shift was due to disaggregation have been challenged. Further work has demonstrated that the addition of LiBr to an SEC column decreases the NMP solvent power and precipitates some of the coal derived material. In the presence of this salt the elution mechanism was not purely by size, but adsorption of the sample on the column also played a role. Adsorption phenomena were observed even in the analysis of a non-polar material like a naphthalene mesophase [52].

2.3.2 Mass Spectroscopy

Independent confirmation of the SEC calibration has been attempted by applying several mass spectroscopy techniques. Most of them, however, are only suitable for the molecular mass range up to 500-1000 Da. The analysis of higher masses is only achievable by MALDI and laser desorption-MS.

A comparison between different mass spectrometry methods applied to coal tar analysis was made by Herod et al. [63]. That work included high performance liquid chromatography (HPLC-MS), desorption chemical ionisation (D.C.I.-MS), field ionisation (F.I.-MS), field desorption (F.D.-MS) and fast atom bombardment (F.A.B.-MS). The use of the latter technique made it possible to detect components with molecular masses up to about 2000 Da in the asphaltene fraction of a coal tar. However, no individual compounds could be recognised due to the complexity of the spectrum. Other techniques have also shown limitations in their applications to coal derived samples: GC-MS is restricted to molecules which can pass through the chromatographic column, which imposes an upper limit of about 300u for aromatics. The observed limit in Probe-MS has been established around 500u [64, 65]. Pyrolysis GC-MS, which has the same limitations as GC and GC-MS regarding operational mass range of products, has also been applied to structural elucidation of some samples [49, 50, 66, 67].

Coal and petroleum-derived samples have wide polydispersities. When using MALDI and LD-MS, the signal from the high molecular weights (MW), whose abundance is relatively low, is hidden by smaller MW materials, present in larger proportions. Fractionation of the samples has been performed to isolate the heaviest material and characterise it more effectively by mass spectroscopic techniques.

Preparative scale SEC, planar chromatography column chromatography and separation by solubility in acetone and pyridine have been used in sample fractionation. These methods have been compared [46, 53]. Every technique used to fractionate a coal tar pitch led to fractions which showed structural differences among themselves. SEC fractions of a coal tar pitch were studied by Probe-MS and no signal was obtained from the excluded material whereas decreasing MWs were observed with increasing elution time in fractions appearing under the retained peak [58].

Early work on Laser Ionisation Mass Analysis expanded the limit of mass spectroscopy techniques applied to coal tars and extracts up to 12,000 Da [68]. These limitations of mass spectroscopic techniques to the analysis of small molecular masses have been recently overcome by the use of MALDI-MS. The application of MALDI-TOF to the analysis of coal and petroleum derived materials is discussed in Chapter 10.

2.3.3 UV-Fluorescence Spectroscopy

Li et al. [69] reviewed the application of UV-fluorescence (UV-F) spectroscopy to coal tars. UV-F shows a shift towards longer wavelengths and a reduction in signal intensity with increasing size of the polynuclear aromatic ring systems. However, shifts towards shorter wavelengths can be produced by loss of alkyl or alkoxy groups, loss of heteroatom content, reduction in linear polynuclear aromatic ring system size and loss of fused 5-membered rings [61]. These multiple causes for changes in fluorescence wavelengths together to the wide range of chemical structures present in coal and oil-derived samples, set limits to the interpretation of the results. UV-F has widely been applied to confirm the differences among sample fractions shown by SEC [48-51, 67, 69] as well as to measure changes in samples after liquefaction and hydrocracking. Shifts towards shorter wavelengths have been detected which parallel the changes seen in SEC chromatograms after hydrocracking [5-10, 34, 70-74].

UV-F has also been applied to the analysis of SEC fractions of a coal tar pitch [58], showing stronger fluorescence under the retained peak. More recently [75] the use of UV-F as on line SEC detector in the analysis of coal and petroleum derived materials showed no signal at short elution times while an excluded peak was observed using UV-A detection. These results suggest that the light material is structurally different to that appearing as heavier fractions under the excluded peak by SEC. It could be argued that the excluded peak is still composed of aggregated material but structurally different from the retained peak. However, several attempts to disaggregate it have resulted unsuccessful, as discussed above.

A sample of heavy petroleum residue was fractionated by solubility in acetonitrile, pyridine and NMP. Three fractions: acetronitrile solubles, pyridine solubles and NMP solubles were generated in this way. A second fractionation involved the use of heptane, producing two fractions: heptane solubles and heptane insolubles. UV-F was applied to all these fractions. The maximum intensity of the spectra shifted towards longer wavelengths with decreasing solubility of the fraction [47], indicating increasing size of aromatic rings in this series.

2.3.4 Other techniques

A number of techniques have been applied to investigate the structures and molecular weights and sizes in coal and petroleum derived samples. Size distribution of asphaltenes from a vacuum petroleum residue have been analysed by small angle neutron scattering (SANS). A reduction in size, attributed to a disaggregation process, was observed with increasing temperature in an experiment carried out using d_{10}-1-methyl naphthalene as solvent [76]. Studies on dilute asphaltene solutions in DCM showed continuous shifts in retention times by size exclusion chromatography in the fourteen days after the first injection. These shifts towards longer elution times (lower sizes) were interpreted as indication of an ongoing disaggregation process [77].

Fluorescence depolarisation was used [78] to measure the size of several petroleum asphaltenes in very dilute solutions in toluene. These measurements led to calculated molecular weight in the range of 500 to 1000 Da. This work was extended into a coal-derived sample. The toluene soluble – pyridine soluble fraction of a coal liquefaction residue was obtained. The hexane insolubles from this fraction were analysed by fluorescence depolarisation measurements. This sample showed a UV-F spectrum shifted towards shorter wavelengths than those of the petroleum derived samples. This suggested that the MWs in this sample were even smaller than those of the petroleum asphaltenes [78]. However, it has been claimed that large material could not be observed in experiments involving UV-Fluorescence [75]. It has recently been demonstrated that UV-F failed to detect material eluting under the excluded peak by SEC [75], due to lack of fluorescence of these materials. Therefore, the upper value of 1000 Da for MW measured by fluorescence depolarisation experiments may show a limit in the technique rather than the actual upper mass limit of the sample.

The dependence of aggregation on solution concentration was studied by Sheu et al. [79] by surface tension measurements. The behaviour of solutions of asphaltenes in nitrobenzene and pyridine was claimed to be similar to that of surfactants. A discontinuity appearing in the graph of surface tension against concentration suggested that there is a threshold concentration where asphaltene micelles aggregate [79]. It has been calculated [59] that the threshold concentration is at least ten times higher than the actual concentration used in SEC experiments in this laboratory. This supports the lack of aggregation under the conditions applied in the present application of SEC.

Several toluene-pyridine mixtures were used as solvent in a study on the dependence of particle radius with solvent permittivity. The particle radius was measured by small angle neutron scattering and it decreased when solvent permittivity increased, as a result of a disaggregation process. This result illustrates that the occurrence of aggregation depends strongly on the chosen solvent, even when only two solvents mixed in different ratios are used [80]. In an independent study, the average molecular weight of a sample of asphaltenes from a vacuum residue in several solvents was determined by the same technique. The solutions were prepared in ortho-xylene, benzene, THF, pyridine, toluene and their mixtures. Changes in average MW have been investigated in relation with both temperature and solvent. Decreasing MW were evident when increasing either temperature or dipole moment of the solvent [81].

On the other hand, results obtained by small angle X-ray scattering (SAXS) and small angle neutron scattering (SANS) on asphaltenes from a petroleum vacuum residue have suggested that the particle size in the vacuum residue is the same as in solutions in toluene and toluene-pyridine mixtures [82]. The residue was dispersed in the de-asphalted oil and measured by SAXS. SANS was applied to solutions of the same sample in different toluene-pyridine mixtures. Those results together with rheological measurements in the vacuum residue as well as mass spectroscopy and surface tension determinations in asphaltenes have given average particle mass values around 100,000 Da and an estimation of approximately 100 molecules in each micelle. Therefore they have proposed an average MW about 1000u. According to an early model suggested by Pfeiffer and Saal [83] non-asphaltenic molecules would solvate these asphaltenic micelles in the vacuum residue.

A slightly different view came from a work by Gutierrez [84] et al. where asphaltenes from Venezuelan crude oils have been separated in two fractions by complex formation with p-Nitrophenol. One of these fractions is insoluble in toluene but it becomes soluble when mixed with the other. It is thought that the toluene soluble fraction plays a role as a dispersing agent. It has thus been suggested that the asphaltenic fraction is composed of materials which differ widely in solubility and the soluble part would help to disperse the insoluble one [84].

The present work focused on the elucidation of the higher molecular mass limit of heavy hydrocarbons. The validity of the application of the SEC polystyrene

calibrations to the analysis of these samples was studied. The approach used in this work consisted in the comparison of SEC results with an independent technique such as LD-MS or MALDI-MS. As mention above, aggregation of these materials has not been observed in a strong solvent such as the NMP used as SEC eluent. The use of LD-MS and MALDI-MS provide a valuable tool to examine the actual MWs present in these samples, since aggregation is unlikely to take place under the conditions used to generate the mass spectra.

3 EXPERIMENTAL

Batch hydrocracking experiments are carried out in the present study. In previous work in this laboratory [8], batch hydrocracking was performed on coal extracts obtained from a continuous flowing solvent reactor (FSR). This reactor allowed the coal extracts to have larger molecular mass distributions than extracts produced in batch systems due to the short residence times applied. The FSR made it also possible to obtain products with narrow residence time distributions. However, due to its larger availability, a coal extract from the Point of Ayr pilot plant was used in experiments in this work.

This batch hydrocracking scheme is applied in the present work to study the effectiveness of pillared clays as hydrocracking catalysts and the dependence of hydrocracking extent on reaction time and nature of the feed. As mentioned in Chapter 1, pillared clays identified in a previous project as active hydrocracking catalysts have been further tested in this work together with new pillared clay preparations.

Procedures and analytical techniques common to several chapters are described in this chapter. Experimental sections describing the methods in greater detail can be found in the corresponding chapters.

3.1 HYDROCRACKING EXPERIMENTS

3.1.1 Micro-bomb Reactor

Detailed information about the micro-bomb reactor, originally designed and commissioned by Zhang is available elsewhere [85] and a diagram is given in Figure 3.1. Briefly, it consists of a ½" Swagelock union tee sealed by caps at two ends and connected to a ¼" diameter line through the third one. The reactor is pressurised through this line.

The control head with connections for temperature and pressure sensors is placed at the top of the rig. The temperature is measured by means of two K type thermocouples. One of them shows the temperature in the reactor (reaction temperature) while the other indicates the temperature in the control-head. The pressure transducer is placed there and it must not be exposed to temperatures higher

than 80°C; hence the temperature in the control-head must be monitored and controlled. Cooling water flows through a heat exchanger to keep temperature in the upper section low. The reactor can be operated at temperatures up to 500°C and pressures up to 200 bars.

The reactor operates immersed in a fluidised sand bath, which is electrically heated and fluidised by a flow of air through the sand. The temperature of the sand bath is controlled by a Skil-S9C external temperature controller. Calibration curves have been established relating the temperature of the sand bath and the reaction temperature [85].

Digital indicators display the reaction, sand bath and transducer temperature as well as the reaction pressure. A PC-30B data acquisition board is used to record reactor pressure and both reactor and control-head temperatures. The reactor is shaken at a rate of 80 cpm to homogenise the sample and provide better thermal transfer.

3.1.2 Procedure

The reactor is charged with sample, catalyst and solvent (if used). Tetralin is used as solvent in experiments where a solvent is employed. The usual amounts of solvent, sample and catalyst are 1g:200mg:100mg respectively. When no solvent is used, 1g of sample and 250 mg of catalyst are place in the reactor. Comparison between the two methods is made in Chapter 4.

Next, the reactor is attached to the ¼" line and pressurised with helium. The absence of leaks is then tested. Afterwards, it is depressurised and pressurised with hydrogen. A calibration curve which relates the pressure at ambient temperature to the pressure at reaction temperature is available [85]. The absence of leaks is checked again, this time with the system pressurised with hydrogen. A period of about 20 minutes after pressurisation is usually necessary to stabilise the temperature and therefore the pressure inside the reactor. After stabilisation, a drop in pressure lower than 0.2 bars in 15 minutes is considered reasonable in order to start the experiment. After the leak test, cooling water lines are connected to the heat exchanger and then the reactor is placed in the fluidised sand bath. Subsequently the shaker is turned on. The reaction time is measured from the point when the reactor reaches the reaction

temperature. The heating up period usually lasts for two minutes since the reactor is immersed in the sand bath.

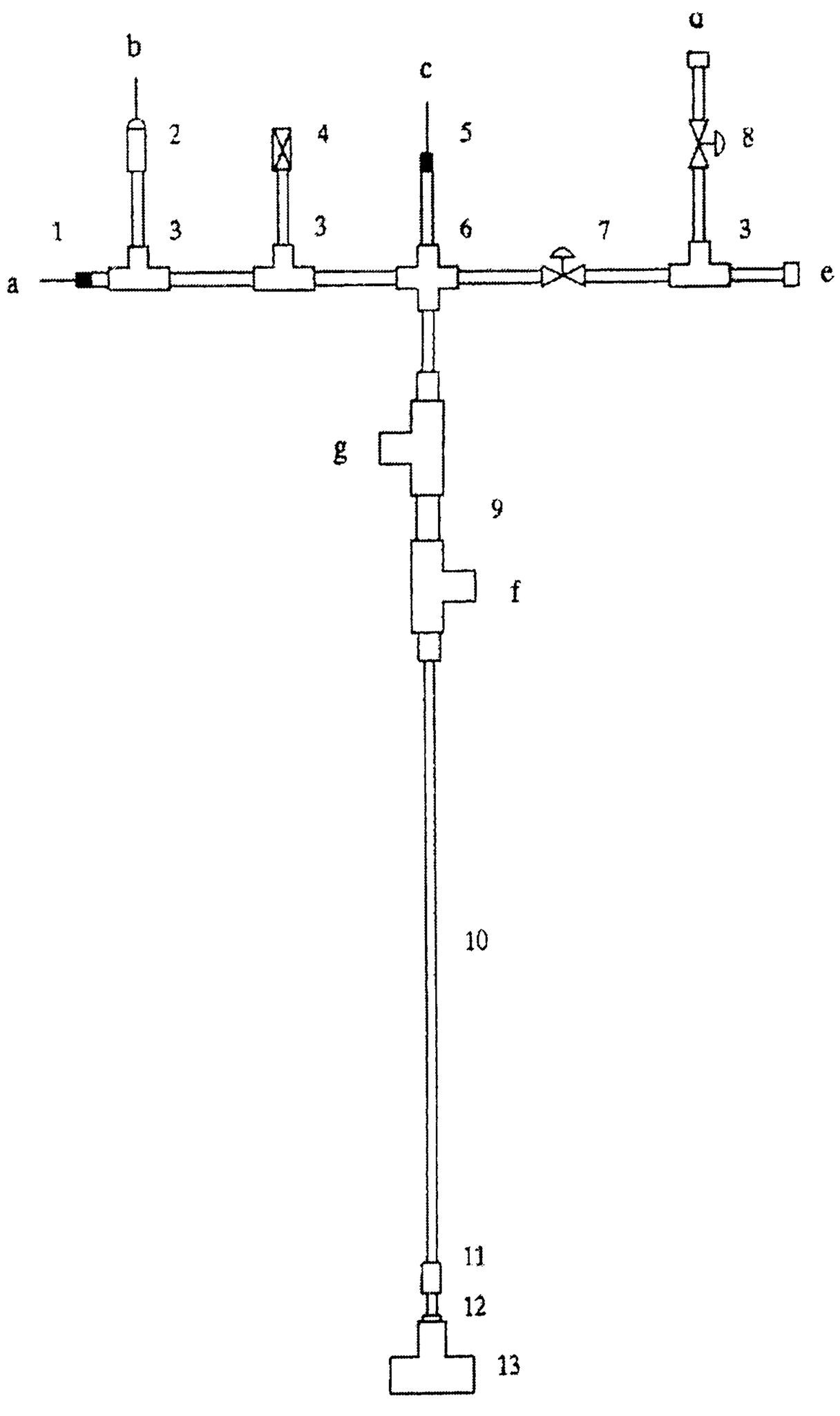


Figure 3.1. Diagram of the micro-bomb reactor. Reproduced from [85].

1.thermocouple 2.pressure transducer 3.union tee 4.auto pressure relief valve 5.thermocouple 6.union cross 7.ball valve 8. needle valve 9. heat exchanger 10.vertical pressure extender 11.union connector 12. adapter 13. reactor. Connectors: a. temperature indicator 1 b.pressure indicator c.temperature indicator 2 d.flexible vent tube e.hydrogen cylinder f. cooling water in g. cooling water out.

Once the reaction time is reached, the reactor is cooled down to ambient temperature and then depressurised. After it has reached atmospheric pressure, the reactor is detached from the ¼" line and washed with a mixture of chloroform and methanol 4:1 v/v until the washing liquid is colourless. The line and the reactor thermocouple are also washed and the liquid recovered is mixed with that from the reactor.

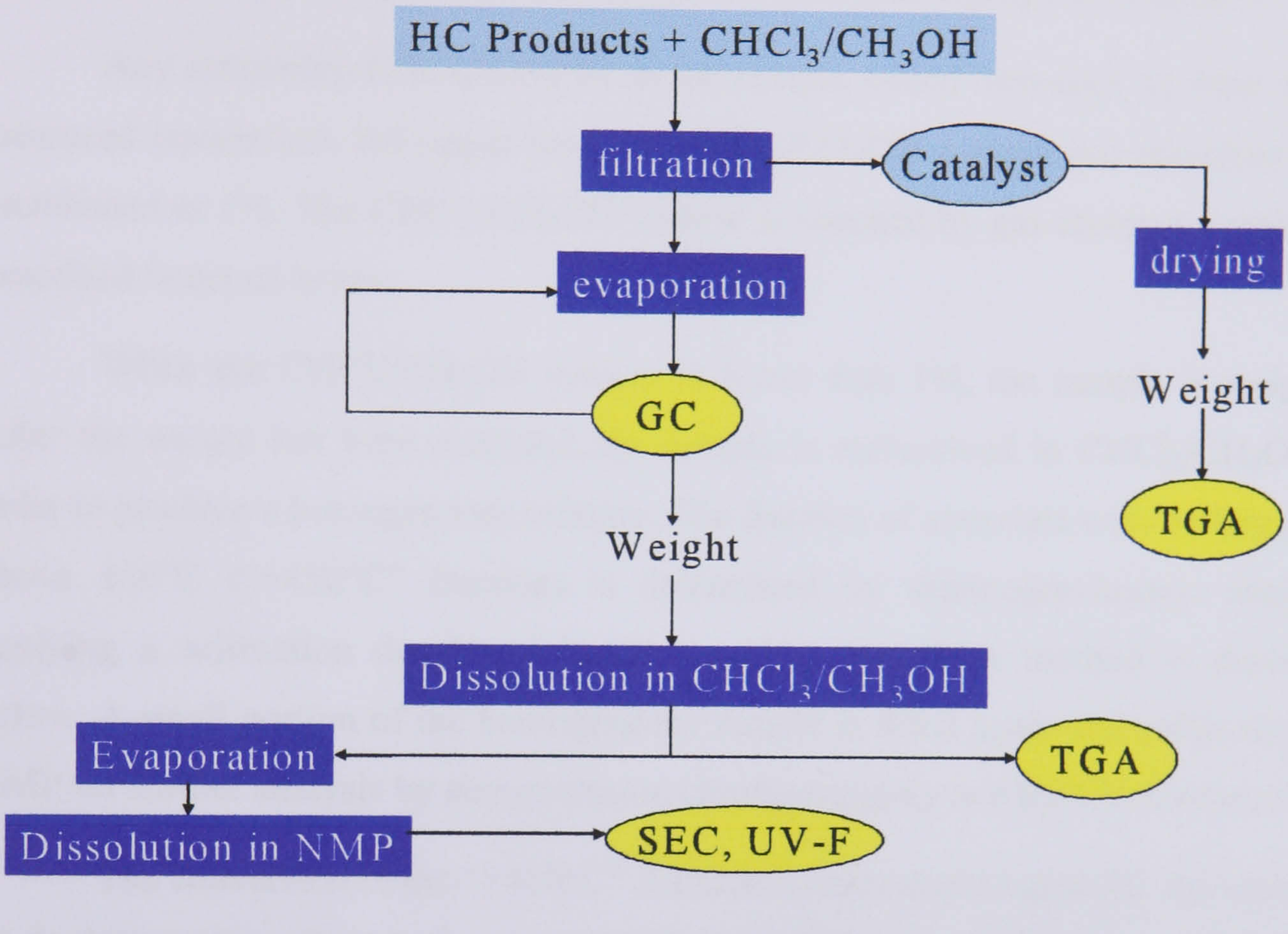


Figure 3.2. Diagram of the process followed to prepare liquid and solid products for analysis.

The reaction products in $CHCl_3/CH_3OH$ are filtered to separate the soluble products from the solids as shown in the diagram (Figure 3.2). The latter are composed of catalyst particles with carbonaceous material adsorbed on them and reaction products insoluble in $CHCl_3/CH_3OH$. A Millipore glass filter holder with Whatman No 1 qualitative filter paper is used. The filter cake is carefully washed to remove all the soluble material. Afterwards it is dried in a vacuum oven at 60°C for 3 hours to eliminate $CHCl_3/CH_3OH$ and weighed. The carbonaceous content of the solids is measured by thermogravimetric analysis (TGA) as described below.

The $CHCl_3/CH_3OH$ is evaporated and then the remaining products are weighed. Two methods have been used for solvent removal; the first consisted of

drying by a nitrogen stream bubbling in the liquid under gentle heating. It has been observed that this method produces losses of lighter material from the sample and its repeatability is low. In the present work a second method employing a rotary evaporator has given higher recoveries of material. In this procedure the water bath is kept at 85°C and the mixture is dried until no more solvent is seen to condense. No vacuum is applied. Comparison between the two methods is given in Chapter 4.

Any remaining $CHCl_3/CH_3OH$ in the sample would introduce an error in the measured conversion. An upper limit for $CHCl_3/CH_3OH$ content has therefore been established as 1%. The $CHCl_3/CH_3OH$ content is checked by gas chromatography, as described in detail below.

When the $CHCl_3/CH_3OH$ content is lower than 1%, the sample is weighed. After the weight has been recorded, the sample is redissolved in $CHCl_3/CH_3OH$ in order to produce a homogeneous mixture. The fraction of materials with boiling point above 450°C (">450°C" fraction) is determined by thermogravimetric analysis, applying a calibration developed by Zhang [85]. The TGA method is described below. A small portion of the homogeneous sample is dried again and redissolved in NMP for further analysis by size exclusion chromatography and by UV fluorescence.

The conversion of the ">450°C" fraction is calculated to quantify the extent of the hydrocracking. The "apparent conversion" is obtained by taking into account only the $CHCl_3/CH_3OH$ soluble fraction of the products:

$$Apparent \quad Conversion = \frac{m_{feed} \cdot (f_{>450C})_{feed} - m_{liq} \cdot (f_{>450C})_{liq}}{m_{feed} \cdot (f_{>450C})_{feed}} \qquad \text{(Equation 3.1)}$$

where $m_{feed,}$ and m_{liq} are the weight of the feed and the liquid recovered after hydrocracking respectively. $(f_{>450C})_{feed}$ and $(f_{>450C})_{liq}$ are the fraction of material with boiling point above 450°C in the feed and liquid products respectively.

As high apparent conversions could be achieved just by removal of ">450°C" material as deposits on the catalyst, the evaluation of the catalyst effectiveness cannot only be based on this parameter. The solids deposited on the catalyst are considered as part of the ">450°C" fraction of the products to calculate the real conversion. It is defined as:

$$Real\quad Conversion = \frac{m_{feed}\cdot(f_{>450C})_{feed} - m_{liq}\cdot(f_{>450C})_{liq} - m_{sol}\cdot\Delta f_{carb}}{m_{feed}\cdot(f_{>450C})_{feed}} \quad \text{(Equation 3.2)}$$

where m_{sol} is the weight of solids recovered and Δf_{carb} is the carbonaceous fraction of the solids deposited during the run.

3.2 ANALYTICAL TECHNIQUES

3.2.1 Gas Chromatography

Gas chromatography (GC) is applied to determine the residual content of $CHCl_3/CH_3OH$ in the liquid products. As stated above, it must be less than 1% in order to proceed to weigh the sample.

Two columns, an approximately 15 m x 0.54mm megabore column coated with a liquid phase of phenylmethylpolysiloxane and a 2 meter long, ¼" OD metal tube column packed with Porapak-Q are installed in a GCD Gas Chromatograph. It is equipped with Flame Ionisation Detection (FID). Both columns are suitable to determine $CHCl_3/CH_3OH$ content. Helium is used as gas carrier. The injector and detector temperature are set at 250°C and 300°C respectively.

Comparison of the area under both the $CHCl_3$ and CH_3OH peaks in the sample is made against a chromatogram of the $CHCl_3/CH_3OH$ solvent. The standard $CHCl_3/CH_3OH$ solution is always checked under the same conditions as the sample.

3.2.2 Size Exclusion Chromatography

NMP solutions of coal and oil derived material have been analysed by size exclusion chromatography. Two SEC columns from Polymer Laboratories packed with polystyrene/polydivinylbenzene were used in this work: Mixed-A and Mixed-D. The Mixed-D column has a smaller porosity than the Mixed-A and its temperature must be increased to 85°C in order to reduce the NMP viscosity and make it flow more easily. The porosity ranges of these columns are not available due to manufacturer confidentiality. Work using the Mixed-A column has been performed at room temperature. The linear ranges of $\log_{10}$ MM vs. retention time for polystyrene are up to 15 million for Mixed-A, and 200,000 for Mixed-D. The polystyrene calibration curves are shown in Figure 3.3.

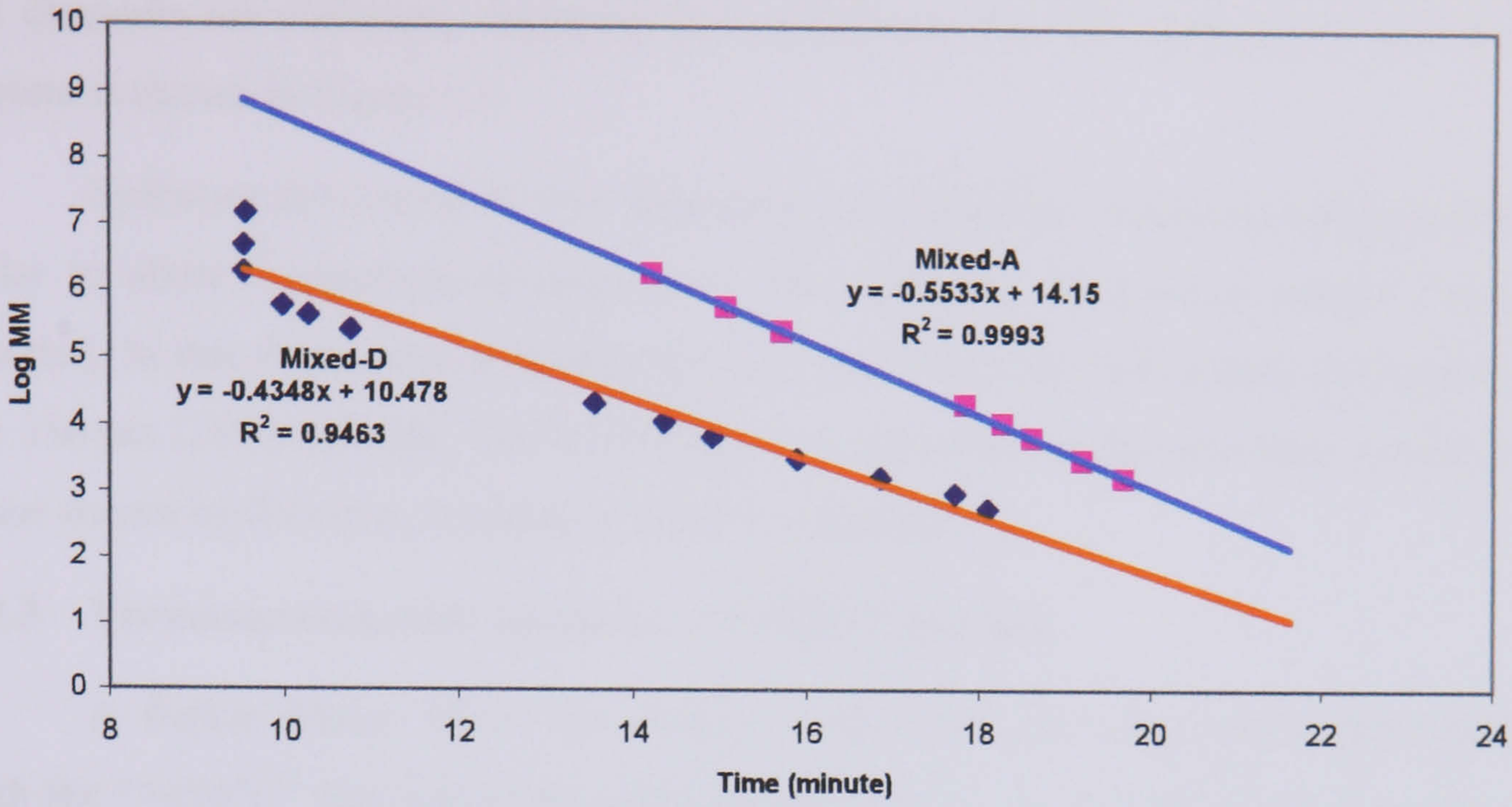


Figure 3.3. Calibration of Mixed-A and Mixed-D SEC columns based on Polystyrene standards.

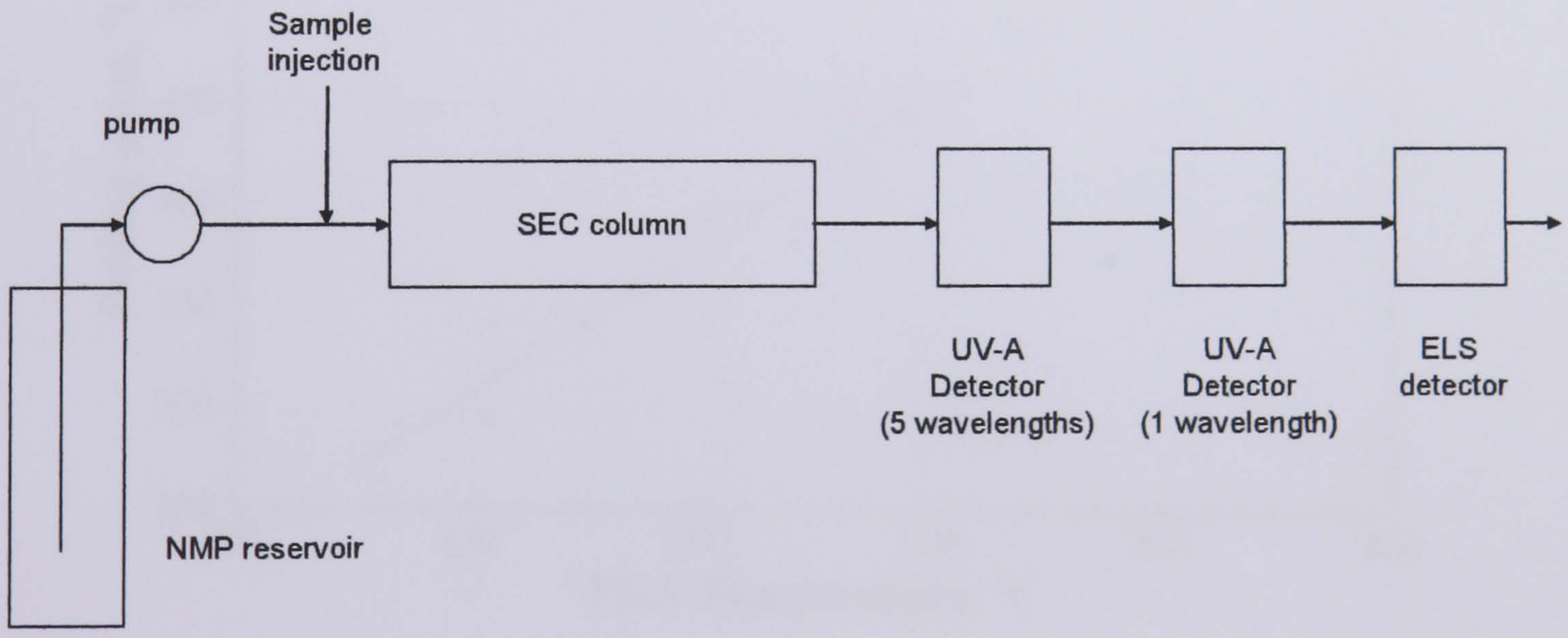


Figure 3.4. Diagram of the SEC system.

A 0.5 mL/min flow of NMP is pumped through the system. The signal is detected by ultraviolet absorption at five wavelengths 280, 300, 350, 370 and 450 nm. The latter is recorded by a variable wavelength Perkin-Elmer LC250 UV detector set at 450nm whereas the rest are measured by a Diode Array detector. An Evaporative

BIBL. LONDIN. UNIV.

Light Scattering detector is also connected in series with the UV ones. Data from all six channels are collected, displayed and saved in a PC. The diagram of the SEC system is shown in Figure 3.4.

Software developed in this laboratory is applied to normalise intensities in order to allow comparison among runs where different amounts of material were injected. In this work, area normalisation was applied to chromatograms recorded by the 350 nm UV-A detector. The trends shown at this wavelength have been similar to those shown by detectors working at other wavelengths.

3.2.3 Thermogravimetric Analysis – ">450°C" fraction

A Perkin Elmer TGA7 thermogravimetric analyser was used to determine both the ">450°C" fraction of the liquid products, $(f_{>450C})_{liq}$, and the feeds $(f_{>450C})_{feed}$, and the carbonaceous deposition on the catalyst, f_{carb}.

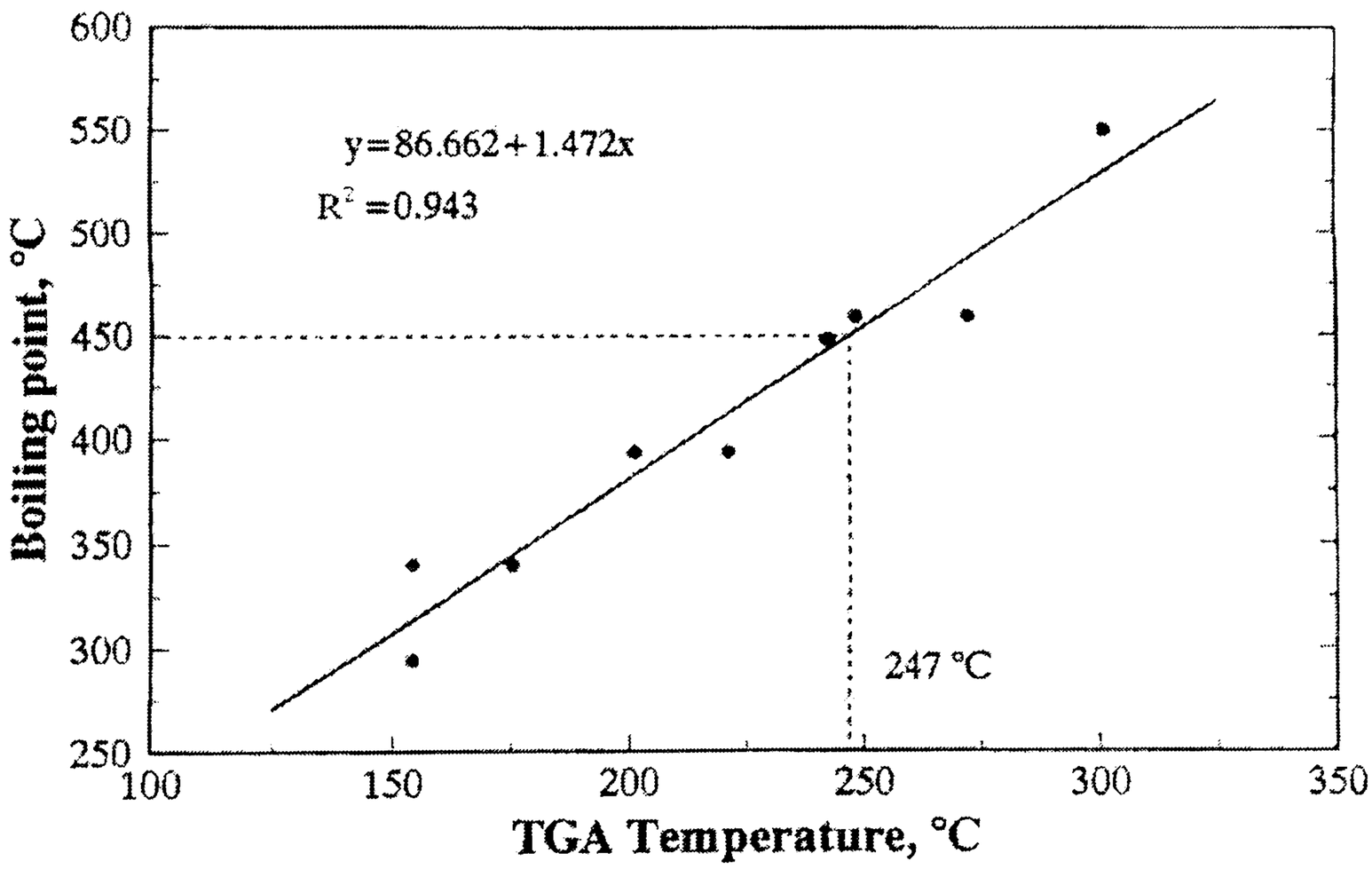


Figure 3.5. Calibration curve relating boiling points with temperature on the TGA pan (extracted from Zhang's PhD thesis [85]).

In the first case, a calibration performed by Zhang using polycyclic aromatic compounds [85] is applied to relate evaporation temperature on the TGA pan with the normal boiling point. As the experiments are run under a flow of helium, which reduces the vapour pressure of the compounds, the required temperatures are lower

than the actual boiling point of the substance. The calibration curve obtained by Zhang is shown in Figure 3.5. According to the calibration, a boiling point of 450°C corresponds to a TGA temperature of 247°C.

Between 1 and 5mg of hydrocracking products in $CHCl_3/CH_3OH$ solution are loaded on the TGA pan. The sample is heated in a helium flow of 60 mL/min according to the following temperature programme: 15 minutes at 30°C in order to remove $CHCl_3/CH_3OH$, then the temperature is increased at 4°C/min to 50°C and it is maintained at that temperature for 120 minutes to remove tetralin. Afterwards a ramp of 4°C/min is applied up to 247°C; this temperature is kept for 10 minutes. A modification has been introduced to this programme to adapt it to experiments where solvent is not used. The long step at 50°C to remove tetralin has been eliminated to adapt the method to runs without tetralin. Instead, the sample is heated directly from 30°C to 247°C. A comparison among different temperatures programmes is given in the next chapter.

3.2.4 Thermogravimetric analysis - Carbonaceous deposition on the catalyst

The programme for carbonaceous content measurement consist in heating the sample under a flow of air during 15 minutes at 50°C, followed by a ramp of 10°C/min up to 600°C. The sample is kept at 600°C for 30 minutes. The carbonaceous deposits are burnt and their fraction is calculated by difference with the remaining weight on the TGA pan. The air flow rate during the determination is 40 mL/min.

When an already coated catalyst is reused the amount of material added to the carbonaceous layer must be calculated. From TGA measurements the carbonaceous contents as fraction of the total solids before (f_{carb}^{O}) and after (f_{carb}^{F}) the run are known. Since the initial and final carbonaceous deposits are measured on different bases, a correction must be performed to calculate the fraction of newly deposited material. As the amount of fresh catalyst remains constant, it is convenient to express the weight of "old" and "total" deposits per weight unit of fresh catalyst as: $f_{carb}^{O} / (1 - f_{carb}^{O})$ and $f_{carb}^{F} / (1 - f_{carb}^{F})$ respectively. The fraction of carbonaceous layer due to new deposition on the catalyst "ΔC" can be calculated by subtracting the "old" deposits per catalyst weight unit from the total ones and multiplying by the fraction of catalyst after the second run, $(1-f_{carb}^{F})$:

$$\Delta f_{carb} = [f_{carb}^{F} / (1 - f_{carb}^{F}) - f_{carb}^{o} / (1 - f_{carb}^{o})] * (1 - f_{carb}^{F}) \quad \text{(Equation 3.3)}$$

which may be simplified to:

$$\Delta f_{carb} = f_{carb}^{F} - f_{carb}^{o} * (1 - f_{carb}^{F}) / (1 - f_{carb}^{o}) \quad \text{(Equation 3.4)}$$

This value of Δf_{carb} is applied to the calculation of conversion for runs where the catalyst has been reused.

3.2.5 UV Fluorescence Spectroscopy

A Perkin-Elmer LS50 Luminescence Spectrometer has been used in the static-cell mode determinations. Solution of the samples in NMP have been measured at 240 nm/min between 250 and 800 nm. The spectra have been recorded in three modes. The emission spectrum is obtained by exciting the sample at a constant wavelength and recording the emission in the full range of wavelengths. The excitation spectrum is recorded at a fixed wavelength while the excitation frequency is changed over the range. In the synchronous spectrum both excitation and emission are simultaneously varied but the wavelength difference is 20nm at any time.

3.2.6 Surface area measurements

A Micromeritics 2000 ASAP surface area analyser was used for the surface area measurements. Approximately 200 mg of sample were used for each analysis. The standard method based on the adsorption of nitrogen on the surface was applied [86]. The samples were dried overnight at 150°C in a vacuum oven prior to the experiment to remove moisture and adsorbed gases from the catalyst pores. The method developed by Brunauer, Emmett and Teller (BET method) to calculate the surface area was applied. Pore size distributions were obtained by the BHJ method (developed by Barret, Joyner and Halenda) based on the desorption isotherm.

3.3 FRACTIONATION TECHNIQUES

Fractions prepared by solvent solubility of a coal tar pitch have been used for hydrocracking and characterisation experiments described in Chapters 9 and 10. Fractions of the coal tar pitch sample were generated by solvent separation using acetone and pyridine as solvents. The following procedure was applied in previous work [3, 87] to fractionate the sample used in the present experiments. 10 g of the coal tar pitch were successively mixed with acetone and pyridine with separation of

the solids by settling and transfer of the solution by pipette. Contact with filtration media was avoided in order to maximise sample recovery. The residual solids at each stage were washed with excess solvent, allowed to stand after shaking, and the solution removed by pipette as before. Each stage was repeated several times; acetone washings were collected and dried by gentle heating under a nitrogen stream and weighed. Pyridine washings were collected and dried before weighing to recover the pyridine soluble pitch fraction. The residual pyridine insolubles were also dried and weighed. All three solid fractions were further dried in vacuum to constant weight to remove residual solvents.

Three fractions were produced in this way: one soluble in acetone, another soluble in pyridine but insoluble in acetone and the third insoluble in both solvents.

4 MODIFICATIONS TO THE EXPERIMENTAL PROCEDURE FOR HYDROCRACKING EXPERIMENTS

Some changes in the experimental procedure in comparison with previous experiments carried out in this laboratory [85, 88] were introduced in the present work. First, no solvent was used in coal extract hydrocracking experiments. This in turn allowed modifications in the boiling point determination based on the TGA method to be introduced, shortening the analysis time. Secondly, a catalyst previously coated with carbonaceous material has been used in some experiments (see Chapter 5). This was done to evaluate conversions in a way independent of the initial deposition of carbonaceous material on the catalyst. The application of a different method to dry $CHCl_3/CH_3OH$ from the liquid products is also analysed in this chapter. All these changes are analysed in this chapter and comparisons with the previous methods are made. Finally, a study on the relation between SEC and the fraction with boiling points above 450ºC recovered from the TGA is presented in section 4.5.

4.1 THE USE OF NO SOLVENT IN HYDROCRACKING EXPERIMENTS

Within the two-stage liquefaction framework followed in previous work in this laboratory, tetralin was used as solvent in coal extraction (first stage) and coal hydrocracking (second stage) experiments. Carrying out hydrocracking experiments using tetralin enabled the use of small amounts of sample (200 mg). This was particularly important when the availability of the coal extract was low due to the small amounts obtained in a laboratory scale Flowing Solvent Reactor [5, 8, 72, 73]. As a hydrogen donor, tetralin promotes the transfer of hydrogen to the sample. However, its utilisation has a drawback in the analysis of the products. Tetralin generates dimers and other reaction products whose boiling points reach as high as 450°C [85]. These products interfered with the characterisation of materials with boiling points below 450°C. For this reason, only the conversion of the fraction of the sample with boiling points above 450°C (“>450°C” fraction) was assessed in previous work [85]. The presence of tetralin and tetralin derivatives also affected the results of SEC and UV-fluorescence experiments. Hence there was a lack of

information on the lighter fractions, which represent about 60-80% of the whole products.

The use of no solvent in hydrocracking experiments would allow more accurate distributions to be generated by TGA, SEC and mass spectrometry techniques. In addition, conditions used in larger scale processes, such as the Point of Ayr pilot plant, would be more closely replicated. On the other hand, without tetralin the feed to the reactor would become more viscous and the sample less homogeneous. This could lead to poorer contact with the catalyst, higher levels of carbonaceous deposition and larger amounts of $CHCl_3/CH_3OH$ needed to remove the product from the reactor. Moreover, the addition of hydrogen to the sample could be limited by the new conditions. Although the Point of Ayr extract contains a recycle solvent, it is heavier than tetralin and it is unlikely to have the same hydrogen donor properties. The suitability of hydrocracking the Point of Ayr hydrocracking feed in the absence of solvent has been evaluated in the present work. These possible drawbacks have been examined. The results are presented and discussed below.

4.1.1 Hydrocracking experiments with solvent

Experiments with solvent were run under the same conditions as in Begon's work [88]. The procedure followed was described in the experimental chapter (section 3.1.2). Briefly, the reactor was loaded with 1g of tetralin, 200 mg of Point of Ayr hydrocracker feed and 100 mg of fresh $NiMo/Al_2O_3$ as catalyst. The reaction temperature was 440°C and the hydrogen pressure 190 bar. Three successive runs reusing the catalyst were performed. The $NiMo/Al_2O_3$ coated with carbonaceous material recovered after reaction was used again in the second run. This procedure was repeated in the third experiment.

The conversions obtained are shown in Table 4.1. Decreasing conversions in successive experiments were observed along the 3 x 120 minute series, reflecting catalyst deactivation. The real conversion showed a large drop between the first and the second run. As found in previous work [7], the deposition on the fresh catalyst was very intense and 18% of the recovered solids were carbonaceous deposits. The carbonaceous layer showed only a marginal increase when the catalyst was reused.

Table 4.1. Hydrocracking conversion of the ">450°C" fraction in experiments carried out with tetralin as solvent at 190 bar H_2 pressure and 440 °C.

Reaction time	Catalyst	Apparent conversion (%)	Carbonaceous Deposits (as % of the recovered solids)	Real conversion (%)
1 x 120 min	Fresh $NiMo/Al_2O_3$	66	16	49
2 x 120 min	Reused NiMo from 1x120min	32	4	28
3 x 120 min	Reused NiMo from 2x120 min	24	3	22

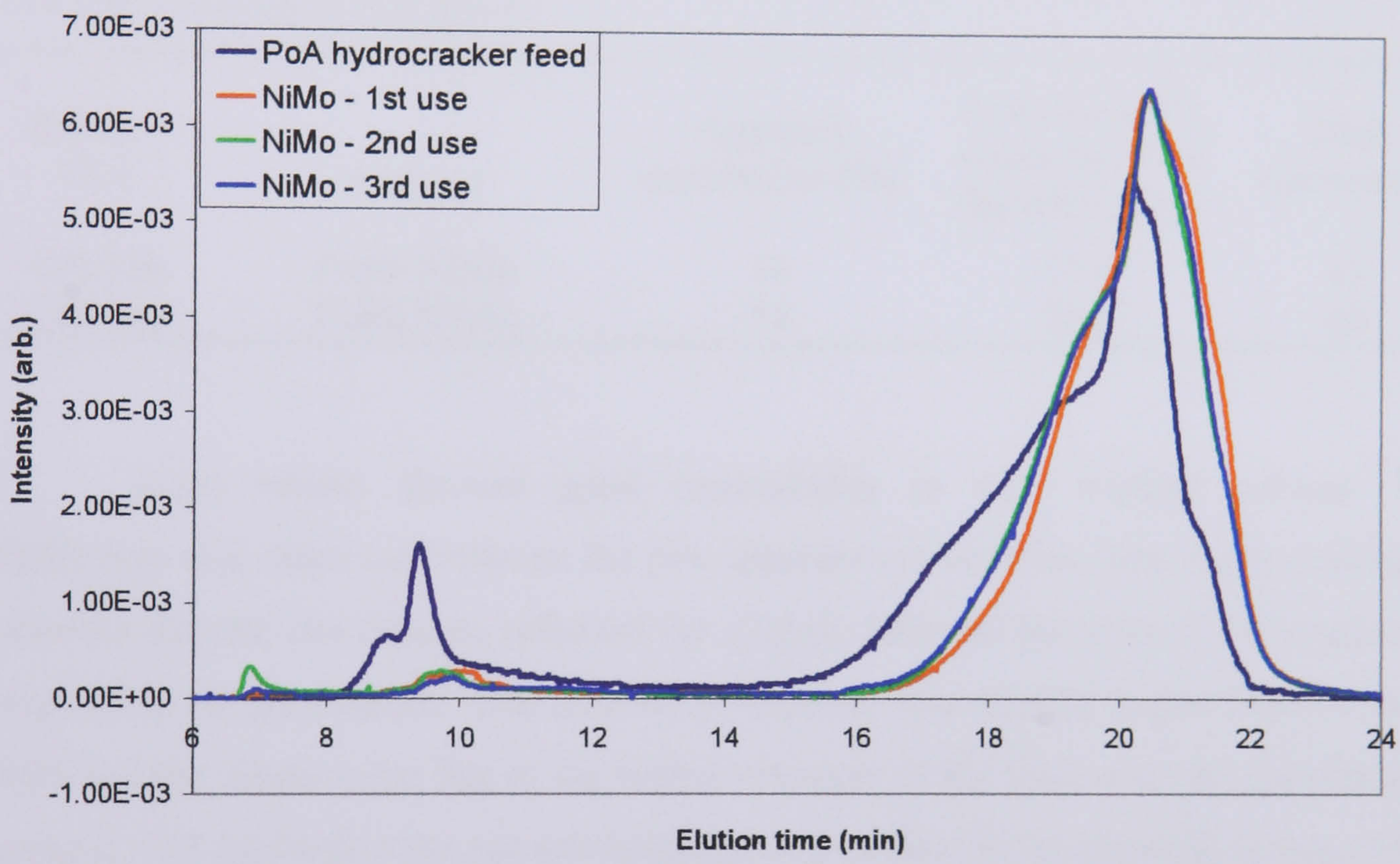


Figure 4.1. Mixed-D column SEC chromatograms of hydrocracking products obtained in three successive reactions reusing the $NiMo/Al_2O_3$ catalyst. The conditions applied were 190 bar H_2 pressure and 440 °C. Tetralin was used as solvent. Area normalisation has been applied to all chromatograms.

Figure 4.1 shows the normalised SEC chromatograms of the feed and products from the four runs. All runs showed a reduction in the excluded peak and a shift of the retained peak towards longer elution times. The differences between the three catalysed runs are not as large as it would be expected from the apparent conversions. A slight shift in the retained peak towards longer retention times (smaller molecules)

was seen in the first run compared to the two others. Chromatograms from the second and third runs are almost undistinguishable. Judging by these three runs, it is clear that the differences observed in conversions are not necessarily reproduced in SEC chromatograms. The relation between boiling point as determined by TGA and elution times in SEC will be discussed later on, in this chapter.

4.1.2 Hydrocracking experiments without solvent

Experiments have also been performed in the absence of an added solvent. Results shown in Table 4.2 show conversions and carbonaceous deposition from two duplicated runs using Point of Ayr "hydrocracker feed" as feed and fresh NiMo as catalyst.

Table 4.2. Hydrocracking conversions in experiments carried out without tetralin at 190 bar H_2 pressure and 440 ℃.

Reaction time	Catalyst	Apparent conversion (%)	Carbonaceous solids (as % of the filter cake)	Real conversion
120 min	Fresh NiMo	54	17.4	43
120 min	Fresh NiMo	54	21.6	40

These results showed good repeatability in runs without solvent. No difference was observed between the two apparent conversions from duplicated runs whereas the real conversions reflected the slightly different amounts of carbonaceous deposition on the catalyst. The amount of deposits was slightly higher than in runs with tetralin, likely to be due to the higher viscosity of the feed when no solvent was present. The products were not substantially heavier than those obtained in runs using tetralin. The reactor was easily washed using $CHCl_3/CH_3OH$ as solvent by the same procedure applied to runs with solvent.

The conversion obtained in the corresponding run with the addition of tetralin was slightly higher (49 %). The difference in conversions observed in experiments with and without tetralin can be attributed to the hydrogen-donor properties of tetralin. The difference found between runs with and without solvent was relatively small. The use of no tetralin as solvent as a viable alternative in the hydrocracking of the Point of Ayr coal extract was therefore established.

4.2 THE USE OF COATED CATALYST

The catalyst performance at short reaction times differs from that observed at longer time scales. The bulk of the carbonaceous deposition on the catalyst surface was observed to take place in the early stages of hydrocracking. The weight of material coating the catalyst was observed to decrease continuously with reaction time in batch experiments [7]. The remaining deposit after 120-minute reaction seemed to be harder than the original [7].

Catalysts should be evaluated under conditions which minimise the effect of the intense initial deposition. Coating the $NiMo/Al_2O_3$ catalyst beforehand was attempted as a way of studying the hydrocracking process independently of the initial deposition. The coating process was performed on the $NiMo/Al_2O_3$ catalyst in an independent experiment using a coal tar pitch. This coal tar pitch was selected for coating the catalyst instead of the Point of Ayr coal extract due to the limited available amount of the latter. The coated catalyst was subsequently used in hydrocracking experiments as described below.

The coating procedure was as follows. 1.5 g of coal tar pitch and 750mg of $NiMo/Al_2O_3$ were loaded into the microbomb reactor. The mixture was hydrocraked for 2 hours under 190 bars of hydrogen. A lower temperature than the usual in hydrocracking experiments, 355°C, has been applied in order to avoid excessive hard-fouling of the catalyst. The products were collected, filtered and washed with NMP to remove solubles. Two of these hydrocracking runs were performed in order to obtain larger quantities of catalyst. The catalysts obtained from these two runs were dried in a vacuum oven at 60°C for 3 hours, mixed and used again to hydrocrack coal tar pitch. In the second step 1.66g of coated catalyst and 1g of coal tar pitch were heated up to 375°C under hydrogen pressure of 190 bars. Levels of carbonaceous deposition of about 30 % weight of the total solids were observed after the first stage. This figure remained constant after the second step (31 %).

In order to obtain a more complete picture of the hydrocracking process in the absence of solvent, several runs have been carried out on the Point of Ayr hydrocracker feed. All of them were performed at 440°C and 190 bars. In some of them the reactor was pressurised with helium rather than hydrogen to isolate thermal effects from the hydrogenation process. Runs without catalyst, with fresh

$NiMo/Al_2O_3$ and with the $NiMo/Al_2O_3$ coated by the procedure described above were performed. The results are shown in Table 4.3. In the first run using no catalyst under hydrogen, the filtration step in product processing was omitted and therefore the insoluble products were not separated; hence the apparent and real conversions were identical. A change in procedure was introduced for the rest of the non-catalysed runs. The filtration step did take place, enabling a separation of the products in $CHCl_3/CH_3OH$ solubles and insolubles.

Table 4.3. Hydrocracking conversions and carbonaceous deposition on the catalyst in 120 minute experiments carried out without tetralin at 190 bar H_2 or He pressure and 440 ℃. Duplicated runs are shown in brackets.

Catalyst	Gas	Apparent conversion (%)	Carbonaceous Deposits (as % of the recovered solids)	Total Conversion (%)
No catalyst	He	43 (35)	100 (100)	3 (-4)
Coated NiMo	He	43 (38)	29 (29)	12 (6)
No catalyst	H_2	16 (28)	--- (100)	16 (20)
Coated NiMo	H_2	40 (50)	5 (13)	37 (42)
Fresh NiMo	H_2	54 (54)	17 (22)	43 (40)

As can be seen in Table 4.3, negligible conversions and a large amount of carbonaceous solids were produced when helium was used instead of hydrogen. The apparent conversions in these runs were only representative of a small fraction of the products, since most of them were recovered as a char insoluble in $CHCl_3/CH_3OH$. Among runs using helium, those in the presence of the catalyst exhibited a slightly higher conversion.

As expected, a larger reduction in the ">450°C" content was observed when hydrogen was used, even if no catalyst was present. A substantial reduction in the ">450°C" fraction was achieved in the two catalysed runs. In line with the expectations, the amount of new carbonaceous material deposited on the catalyst surface was significantly lower for the case of previously coated catalyst compared with the run with fresh $NiMo/Al_2O_3$. However, the conversions achieved with fresh NiMo were marginally higher.

In Figure 4.2, SEC chromatograms of the Point of Ayr hydrocracking feed and the hydrocracking products using fresh $NiMo/Al_2O_3$, coated $NiMo/Al_2O_3$ and no catalyst are shown. The feed showed the largest signal in the excluded region and a retained peak eluting at relatively short elution times. A considerable reduction in the excluded material was observed in all three products. In addition, all products exhibited a shift in the retained peak towards longer elution times in comparison with the coal extract. As expected, the shift towards longer elution times was larger for the products of the run using fresh $NiMo/Al_2O_3$.

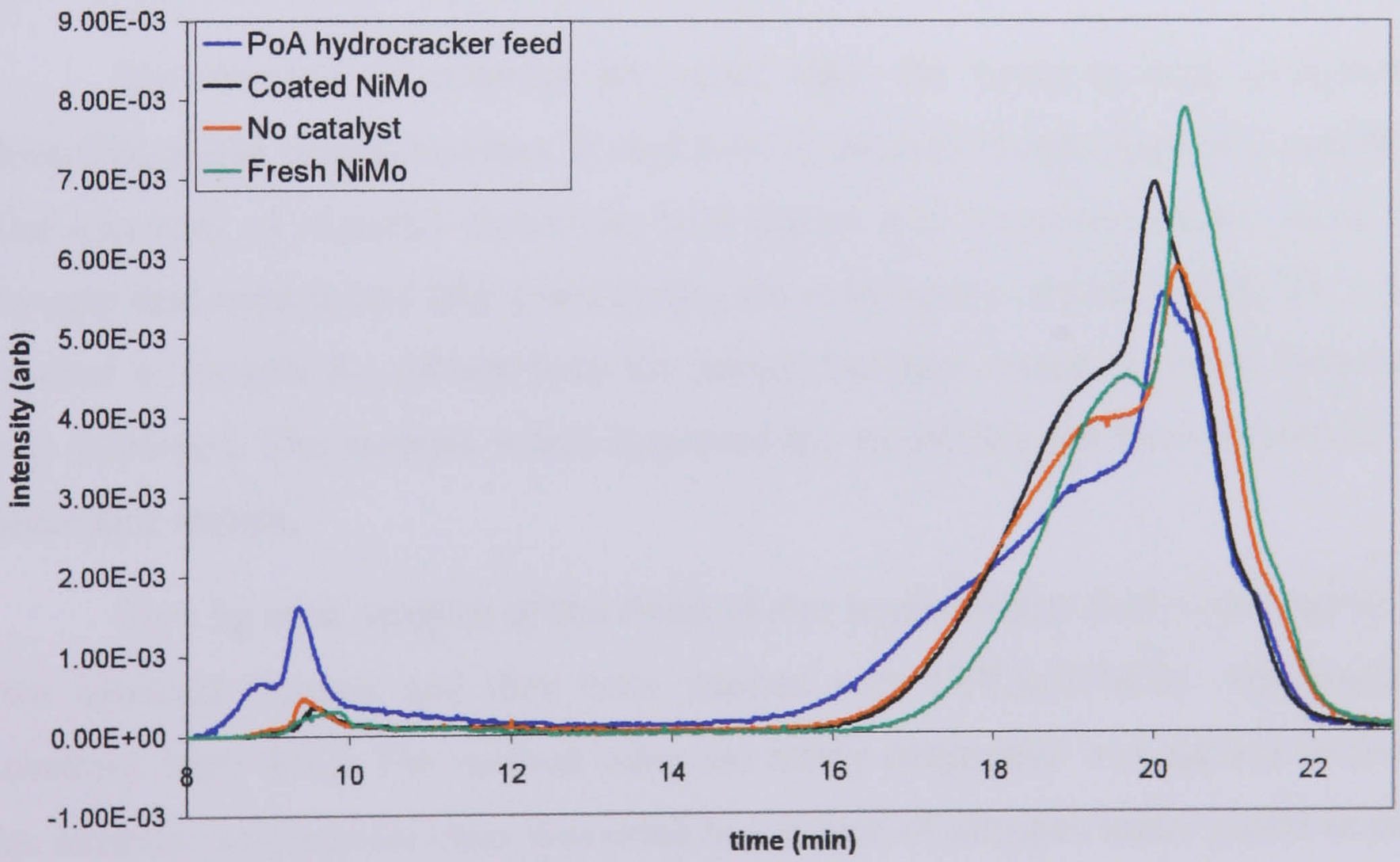


Figure 4.2. Mixed-D column SEC chromatograms of Point of Ayr extract and its hydrocracking products obtained at 190 H_2 pressure and 440 ℃. Area normalisation has been applied to all chromatograms.

The non-catalysed run produced a slightly larger excluded peak in the area normalised SEC chromatograms. However, its retained peak showed an unexpected shift towards smaller molecules than that from the products obtained using coated $NiMo/Al_2O_3$. The loss of an important fraction of the lighter material during the drying process in the two catalysed runs provides at least a partial explanation for this shift. The sample recovered in the non-catalysed run after drying the $CHCl_3/CH_3OH$ was 96% of the initial weight of the feed. On the other hand, much lower quantities were recovered for the two catalysed runs: 73.5 % and 72.1 % for fresh and coated $NiMo/Al_2O_3$ respectively. This includes between 1 and 4% of the original sample weight recovered as deposits on the catalyst. The removal of the light ends during the drying process would explain the apparently lower hydrocracking extent measured by SEC for the coated catalyst in comparison with the no-catalyst run. The lack of repeatability in the amounts recovered using this drying method led to the changes described in the next section.

4.3 CHANGES TO THE DRYING METHOD

The fraction of material recovered after the hydrocracking experiments described above ranged between 71 and 96% of the feed weight, typically near 80%. The recovery of material should be both higher and more repeatable. As it was thought that most losses take place during the evaporation of $CHCl_3/CH_3OH$, a new method to remove the solvent from the sample has been tested. A rotary evaporator was employed. The method, which improved the recoveries, has been detailed in the procedure section.

Two 1g each samples of the Point of Ayr hydrocracker feed were loaded into two identical reactors and they were washed with $CHCl_3/CH_3OH$. The resulting solutions were dried. The method using the rotary evaporator was applied to one of the samples, whereas the other was dried in a stream of nitrogen under gentle heating. Both samples were weighed after drying. The recovery was 96.3% from the rotary evaporator and 89.8% by the usual method. As the Point of Ayr hydrocracker feed used in these tests is heavier than the hydrocracking products, the method will be usually applied to more volatile samples than those employed here. It is expected that the difference between the two methods becomes larger when lighter fractions are

dried. The application of the new drying method to hydrocracking products from the experiments described in this thesis led to recoveries typically above 90%. The formation of gas products and losses of material during sample processing, mainly in the filtration and evaporation stages, account for the remaining 10%. The amount of gas products generated during the hydrocracking of the Point of Ayr coal extract can therefore be roughly estimated as around 5%.

4.4 CHANGES TO THE BOILING POINT DETERMINATION METHOD

The TGA method applied to determine the ">450°C" fraction of the sample was developed by Zhang [85] and has been described in the experimental section. A modification to the temperature program has been made in this work to adapt it to runs without solvent. The temperature programs are shown in Figure 4.3. The curve labelled as "old method" corresponds to the temperature program used by Zhang [85]. It includes a 2-hour long step at 50°C applied in order to dry off the large amounts of tetralin present in those experiments. This step was suppressed in the temperature program shown as "new method 1". This program applies a 4°C/min ramp from 30°C to 247°C (equivalent to a 450°C boiling point according to the calibration shown in the experimental section) followed by a 10 minute period at that temperature. A third temperature program, "new method 2", which applies a 4°C/min ramp in temperature from 30°C to 400°C (equivalent to a 675°C boiling point) has also been tested. In this case the ">450°C" fraction is calculated from the point in the ramp, where the temperature is 247°C.

The calculation of conversions is based on the determination of the ">450°C" fraction by TGA in feeds and products. Therefore the method for boiling point distribution measurement plays a key role in catalyst evaluation. However, disagreement in the Point of Ayr hydrocracker feed ">450°C" content between different TGA determinations has been found. This was due to differences in the amount of sample loaded on the TGA pan. A strong dependence of the ">450°C" fraction of the sample determined by TGA on the sample weight was observed. A more detailed study on that dependence has been carried out in the present work and will be outlined below. As a result of this study, 38.3% has been established as ">450°C" fraction in the Point of Ayr hydrocracker feed in place of 47.3 %, which

was the value used in previous work. Calibration curves linking the ">450°C" fraction in the Point of Ayr hydrocracker feed with the weight loaded on the TGA pan have been produced and are shown in Figure 4.4.

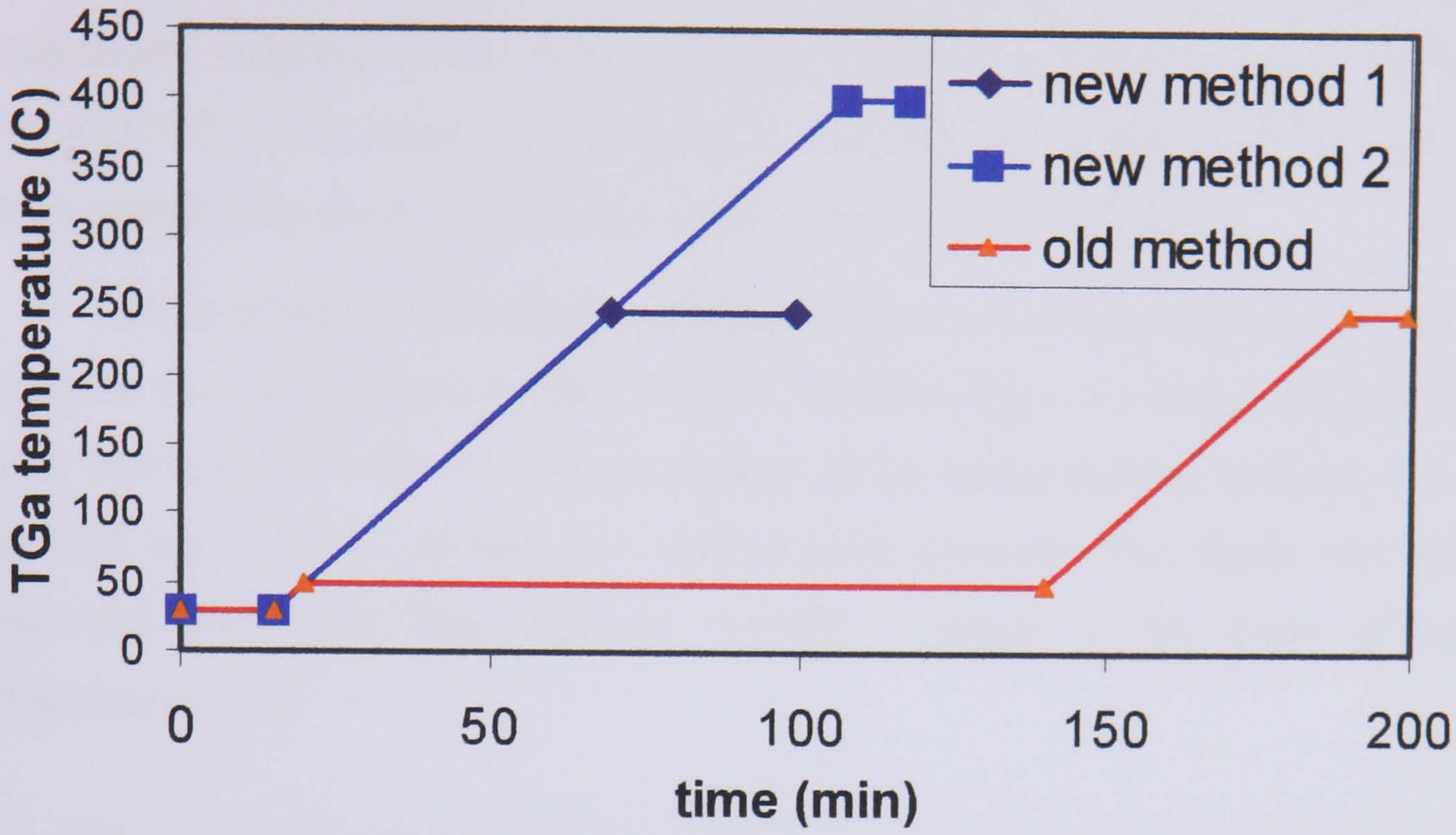


Figure 4.3. TGA temperature programs tested for boiling point determination.

All temperature programs showed an increase in the ">450°C" fraction of the Point of Ayr hydrocracker feed as determined by TGA with increasing weights loaded on the TGA pan. In the light of these results, the figure of 47.3 % found in early work seems to overestimate the actual value of ">450°C" material, since it corresponds to the use of relatively large amounts of sample. The new method showed a linear relationship between the value obtained for the ">450°C" fraction and the sample weight for weights above 7 mg. Below 7 mg, the ">450°C" fraction measured was 38.3 % of the sample and it did not show a dependence on the amount of sample used. 38.3 % was the value adopted as the ">450°C" fraction of Point of Ayr hydrocracker feed in conversion calculations, since the weight normally loaded on the TGA pan is below 5 mg of sample. This weight does not take into account the solvent, $CHCl_3/CH_3OH$, which is promptly evaporated within the first 15 minutes of the run.

The "old method" showed a higher dispersion of the data than the new method, probably due to the longer experimental time. When the tetralin-drying step

is removed ("new method 1") the results perfectly match the "old method". The difference in ">450°C" fraction found by both methods has been negligible over the whole range of weights used in the present study.

Higher values for the ">450°C" fraction have been found for the third temperature program, where there is neither a tetralin-drying step nor a holding period at 247°C. The absence of the period at a constant temperature of 247°C did not allow enough time for the evaporation of the whole ">450°C" fraction.

These results showed that the removal of the two-hour long step at 50°C does not alter the determination of the ">450°C" fraction while it reduces the analysis time. 38.3% is the ">450°C" content determined for loaded weights between by 2.7 and 6.8 mg by both old and new boiling point methods. This figure has been employed throughout this work as ">450°C" fraction in the Point of Ayr hydrocracker feed.

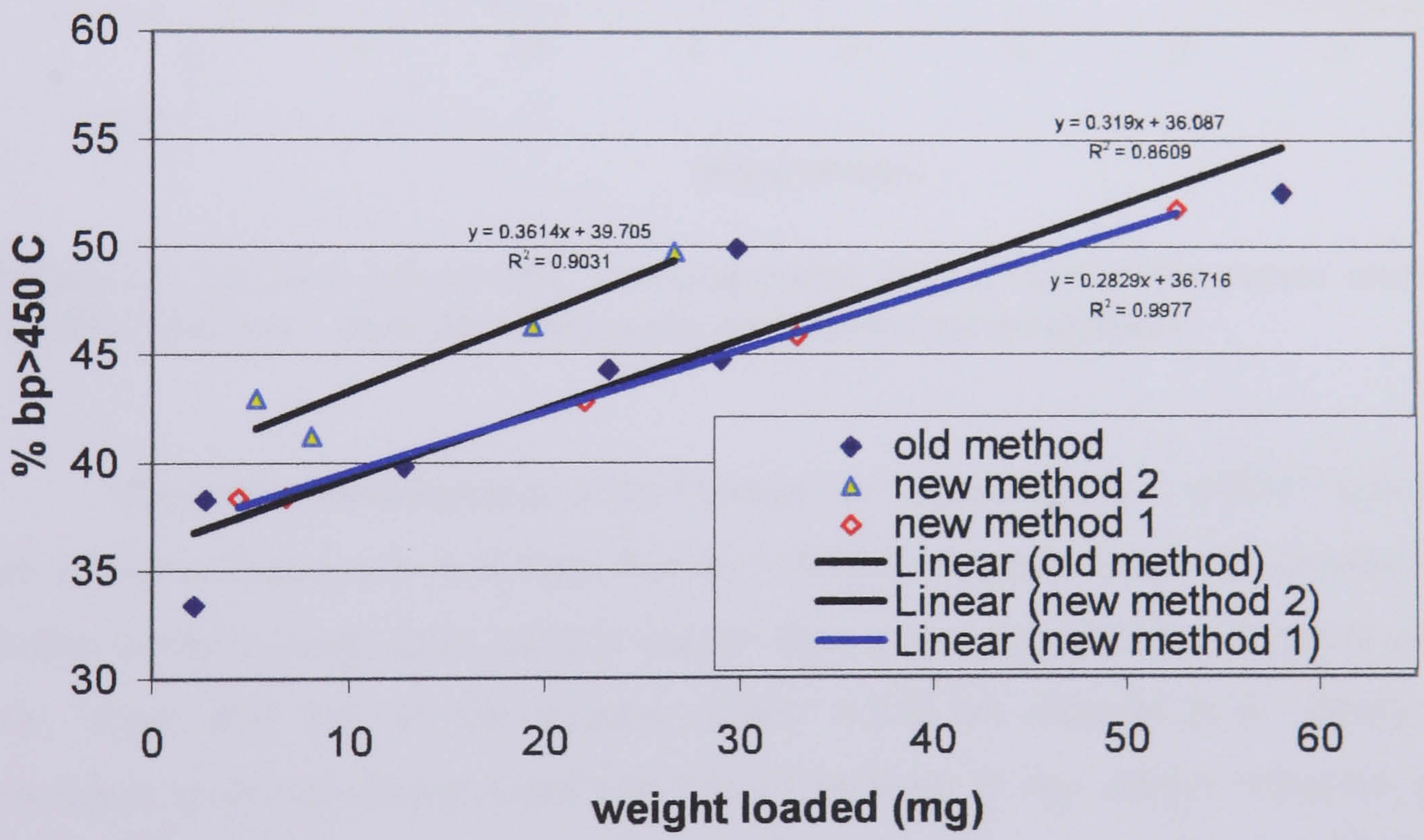


Figure 4.4. ">450℃" content determined by three different TGA temperature programs as a function of the weight loaded on the TGA pan.

4.5 SEC ON THE ">450°C" FRACTION OF THE POINT OF AYR EXTRACT

Size exclusion chromatography has been widely employed in the characterisation of hydrocracking products throughout this work. It is important to

know the correlation that may be expected between the conversions based on TGA experiments and SEC results. In particular it would be desirable to know the elution times of the ">450°C" material. In order to find out if such a relation can be established, the residue left on the TGA pan representing the ">450°C" fraction of several samples has been dissolved in NMP and analysed by SEC.

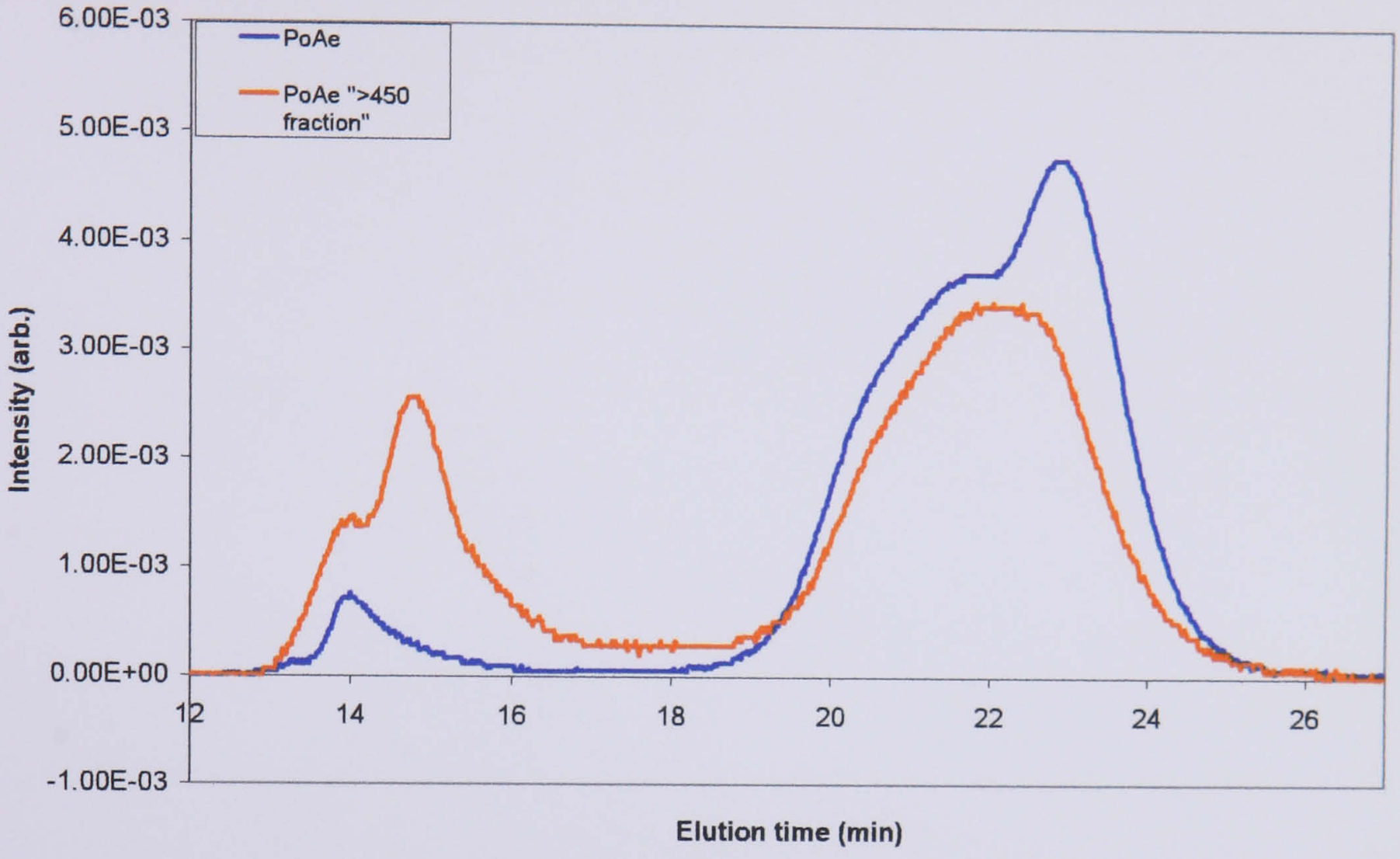


Figure 4.5. Mixed-A column SEC chromatograms of the Point of Ayr extract and its ">450°C fraction". Both chromatograms have been area normalised.

The SEC chromatograms of the Point of Ayr extract and its ">450°C" fraction are shown in Figure 4.5. It is clear that the ">450°C" fraction has a size distribution shifted towards larges sizes (shorter elution times), as expected. The excluded peak was larger than that of the original sample while the retained peak showed a maximum at shorter elution times than that of the Point of Ayr extract. However, the range of elution times covered by the ">450°C" is the same as that covered by the original sample. The difference between the whole sample and its ">450°C" fraction is quantitative rather than qualitative. Similar experiments comparing the liquid products from eight different hydrocracking runs with their respective ">450°C" fractions led to the same conclusions.

Summarising, there is not a straightforward relation for these samples between elution time of certain material by SEC and its boiling point. This explains why in

some hydrocracking experiments described in this thesis, the trends shown by SEC chromatograms and UV-F spectra are in apparent disagreement with those from apparent conversion. While conversions refer exclusively to the ">450°C" fraction (including the solids, in the case of real conversions), SEC gives information on the size distribution of the liquid products and UV-F mainly on the size of aromatic rings.

5 EFFECT OF REACTION TIME ON EXTENT OF HYDROCRACKING USING A COATED NiMo CATALYST

5.1 INTRODUCTION

Catalyst deactivation by coke deposition has a direct impact on the economic viability of heavy hydrocarbon upgrading processes, such as coal liquefaction and oil residue hydroprocessing. Several strategies, representing high operational costs, have been applied to deal with the loss in catalytic activity. Some examples include progressively increasing the reactor temperature as the catalyst becomes less active, regenerating the catalyst frequently or continuously adding fresh catalyst while purging the catalyst bed. As the necessity for heavy hydrocarbon hydroprocessing grows, the understanding of processes involved in catalyst deactivation becomes increasingly more compelling.

Coke deposition is responsible for a quick loss of catalytic activity while metal deposition, the other main deactivation mechanism present in heavy hydrocarbon hydroprocessing, takes place over a longer time scale. Moreover, metal deposition does not affect the hydrogenation and cracking performances of the catalyst as much as coke deposition does [19].

As discussed in Chapter 2, the deactivation rate by coke deposition strongly depends on the characteristics of the feed processed. While very slow deposition takes place in the hydroprocessing of light feeds, the deposition of heavy hydrocarbons on the catalyst surface is a rapid process [19]. Molybdenum promoted either by cobalt or nickel and supported on alumina are usually employed in the oil industry as hydroprocessing catalysts.

A commercial $NiMo/Al_2O_3$ widely used in the oil industry as hydrotreating catalyst has been extensively employed in this laboratory to hydrocrack several heavy petroleum-derived liquids and coal liquefaction extracts. This class of catalysts shows a rather quick deactivation and settles down to operate at a relatively low level of hydrocracking activity. This has led to the search for more suitable hydrocracking catalysts [6, 10, 70, 71]. The availability and widespread use of $NiMo/Al_2O_3$ also makes it a suitable reference for the study of catalytic hydrocracking.

Hydrocracking of the fraction with a boiling range above 450°C (">450°C" fraction) as a function of reaction time was investigated by Zhang et al. [5, 8]. Those experiments used Point of Ayr coal liquefaction extract as feed and tetralin as solvent. The reactions were catalysed by $NiMo/Al_2O_3$.

Within this framework, a remarkable conversion took place within the first 30 minutes of hydrocracking. It was followed by a continuous slow down in the reaction rate up to 120 minutes [5, 8]. No significant changes in conversion were detected at reaction times longer than 120 minutes. Clearly, the decrease in conversion rate could have been due to a combination of loss of sample reactivity and catalyst deactivation.

In an attempt to distinguish between these two processes Begon et al. [7, 88] performed successive 120 minute hydrocracking experiments, reusing the carbon coated catalyst from the previous run together with fresh feed. Although some degree of deactivation was found, the catalyst was still considerably active after 6 hours of hydrocracking. Loss of sample reactivity was therefore identified as the main cause of the slow down in conversion rates.

Changes in extent of hydrocracking during early stages (times shorter than 30 minutes) have also been studied in that work [7]. A somewhat unexpected pattern of hydrocracking conversions was observed within the first 10 minutes of the reaction catalysed by $NiMo/Al_2O_3$. A drop in ">450°C" material took place during the heat up of the sample to 440°C. Conversion increased in the next 5 minutes to show a maximum, which was followed by a diminution leading to a minimum at 10 minutes. Afterwards the conversion increased again according to the behaviour described by Zhang et al. [5, 8]. Only apparent conversions were published in that work. However, the real conversion have been calculated from those data as a part of the present work and the trend is maintained when deposits on the catalyst are included as part of the ">450°C" fraction.

In that work, lack of full catalytic activity of the fresh $NiMo/Al_2O_3$ catalyst in the early stages of hydrocracking was suggested to explain the drop in conversion taking place within the first 10 minutes. Retrogressive reactions between primary hydrocracking products have been indicated as causing the decrease in conversion observed between 5 and 10 minutes. The active form of the $NiMo/Al_2O_3$ catalyst is molybdenum sulphide, which was generated in-situ through reaction of Mo with a

proprietary sulphur dopant present in the commercial catalyst. Thermal cracking released reactive molecules or radicals which, in the absence of an active catalyst to hydrogenate them, polymerised to form heavier materials. It is thought that the activation of the catalyst by sulphidation may take some minutes and retrogressive reactions may have occurred before its completion. Once the catalyst was fully active, the increase in conversion as a function of reaction time was steady.

Deposition on the catalyst was found to be strong when the fresh catalyst was placed in contact with fresh feed. The carbonaceous layer coating the catalyst after the "heat up only" run represented almost 20% of the total filter cake weight. The amount of deposits steadily decreased with reaction time and after the 120 minute run only 11% of the filter cake consisted of carbonaceous material. A process of reaction and re-dissolution of the deposits in the liquid phase was evident.

When an already coated catalyst was reused in contact with fresh feed in successive 120 minutes experiments some new deposition took place, leading to an increase in the total amount of carbonaceous on the catalyst. However, the amount of deposit added to the carbonaceous layer became progressively smaller and therefore the carbonaceous layer tended to stabilise. This finding is in agreement with observations suggesting the relative insensitivity of the amount of deposits to time on stream in continuous reactors [36, 38, 39], as discussed in Chapter 2.

Early stages of the hydrocracking process are addressed again in the present work with two main modifications in experimental procedure. Firstly, the Point of Ayr coal extract is hydrocracked in the absence of solvent, allowing the collection of meaningful data over the whole range of boiling points. Moreover, experiments without solvent resemble more closely the conditions likely to occur during the actual hydrocracking process. Secondly, an already coated $NiMo/Al_2O_3$ catalyst has been employed to study the processes taking place in the first few minutes of contact between a coated catalyst and fresh feed. This simulates the continuous process and is expected to minimise effects due to the initial carbon deposition.

5.2 EXPERIMENTAL

5.2.1 Hydrocracking experiments

The micro-bomb reactor and the experimental procedure have been described in the experimental chapter (section 3.1). 1 g of hydrocracker feed from the Liquid Solvent Extraction process development pilot plant at Point of Ayr [1] and 250 mg of a previously coated $NiMo/Al_2O_3$ catalyst (see below) were charged into a 5 mL reactor. No solvent was added to the reaction mixture. Reaction time, defined as the time at 440°C, was varied from 0 (heat up immediately followed by cooling down) to 120 minutes.

The liquid products were analysed by SEC and UV-F. Conversions of the ">450°C" fraction were calculated from TGA data, as described in Chapter 3. Surface area measurements were applied to the fresh $NiMo/Al_2O_3$, the coated $NiMo/Al_2O_3$ used as catalyst in these runs and the catalysts recovered from the 0, 10 and 30 minute runs.

5.2.2 Precoating of catalyst with carbon deposit

1.5 g of coated $NiMo/Al_2O_3$ were prepared in two steps. First, 900 mg of fresh $NiMo/Al_2O_3$ were used to hydrocrack 1.5 g of a coal tar pitch during 2 hours at 350°C and 170 bar. That process was repeated to duplicate the amount of catalyst prepared. The solids recovered from the two runs were washed with NMP and mixed. 1 g of the coal tar pitch was hydrocracked in presence of 1.5 g of that mixture at 370°C and hydrogen pressure 170 bar. NMP was again used to wash the reaction mixture. The whole process was repeated to generate more coated catalyst. The recovered catalyst was heavily coated; its carbonaceous content was between 30 and 35% of the total solids.

5.3 RESULTS

5.3.1 Conversions

Table 5.1 shows apparent and real conversions as a function of reaction time. As described in Chapter 3, the difference between these two conversions consists in the inclusion of the carbonaceous deposits on the catalyst as part of the ">450°C" fraction in order to calculate the real conversion. All these experiments employed the

coated $NiMo/Al_2O_3$ as catalyst. Hydrocracking of the ">450°C" fraction exhibited some progress during the reactor heat-up to 440°C. 13% of the ">450°C" fraction was converted to lower boiling point materials within that period. The real conversion steadily increased with time up to 120 minutes, the longest time tested. Certain slow-down in the reaction rate observed after 60 minutes was probably due to loss of sample reactivity as observed in previous work [5, 7, 8]. By contrast, the apparent conversion showed a marked reduction between 0 and 10 minutes to continuously increase afterwards.

Table 5.1. Apparent and real conversions and deposition on the catalyst as a function of reaction time. Experiments were carried at 440°C, 190 bar hydrogen pressure. A catalyst previously coated was employed in these experiments.

Time (min)	Apparent conversion (%)	New carbonaceous deposits (as % of the filter cake)	Real conversion (%)
0	26	18	13
5	25	14	14
10	16	0	16
30	26	6	22
60	29	- 2	30
120	45	12	37

The amount of carbonaceous material added to the deposits on the catalyst during the hydrocracking is also shown in Table 5.1. Despite the previous coating, a new deposition of carbonaceous material took place on the catalyst during the 0 minute run. The amount of deposits sharply decreased within the first 10 minutes of reaction, presenting variations at lower levels between 10 and 60 minutes. The negative additional carbonaceous deposition shown in Table 5.1 for the 30 minute run means that a net dissolution of material coating the catalyst has taken place in that experiment. Although the carbonaceous deposits showed an increase in the 120 minute run, they were kept at lower levels than the initial deposition.

The trend followed by the apparent conversion was the result of two different processes simultaneously occurring in the reactor. First, longer reaction times allowed

hydrocracking to proceed to greater extents, producing further reductions in the ">450°C" fraction. On the other hand, the material deposited on the catalyst during the heat-up ramp partially dissolves in the liquid mixture, producing a diminution in the total amount of carbonaceous deposits (see Table 5.1). As discussed in Chapter 2, the deposits on the catalyst tend to preferentially form from heavy fractions. Therefore their dissolution was likely to generate an increase in the amount of ">450°C" material in solution.

Within the first 10 minutes the dissolution rate of the deposits was higher than the hydrocracking rate and consequently the apparent conversion dropped. After 10 minutes, both apparent and real conversion increased. Although differences between conversions at 0 and 5 minutes were within experimental error, they were consistent with the process described above showing a drop in apparent conversion while the real conversion rose. Real conversions are not affected by the re-dissolution of ">450°C" material since the deposits were already taken as part of the ">450°C" fraction. These parallel events explain the difference in behaviour followed by apparent and real conversion.

5.3.2 Size Exclusion Chromatography

SEC chromatograms of the Point of Ayr hydrocracker feed and its hydrocracking products are shown in Figure 5.1 and Figure 5.2. These data refer only to liquid products; clearly, the material deposited on the catalyst is not seen in the SEC chromatograms. All chromatograms exhibited two peaks: one showing material resolved by the column porosity and the other showing signal for material excluded from column porosity. This is similar to the pattern generally shown by coal and petroleum-derived samples [9, 46, 47, 51, 52, 58, 72], as discussed in Chapter 2.

All products exhibited a smaller excluded peak than that from the feed. The size of this peak decreased with reaction time. A shift of the retained peak towards longer elution times was also observed with a progression in time in the series feed, 0 min, 10 min, 30 min, 60 min and 120 min. These changes in the SEC chromatograms showed a reduction in molecular sizes with reaction time.

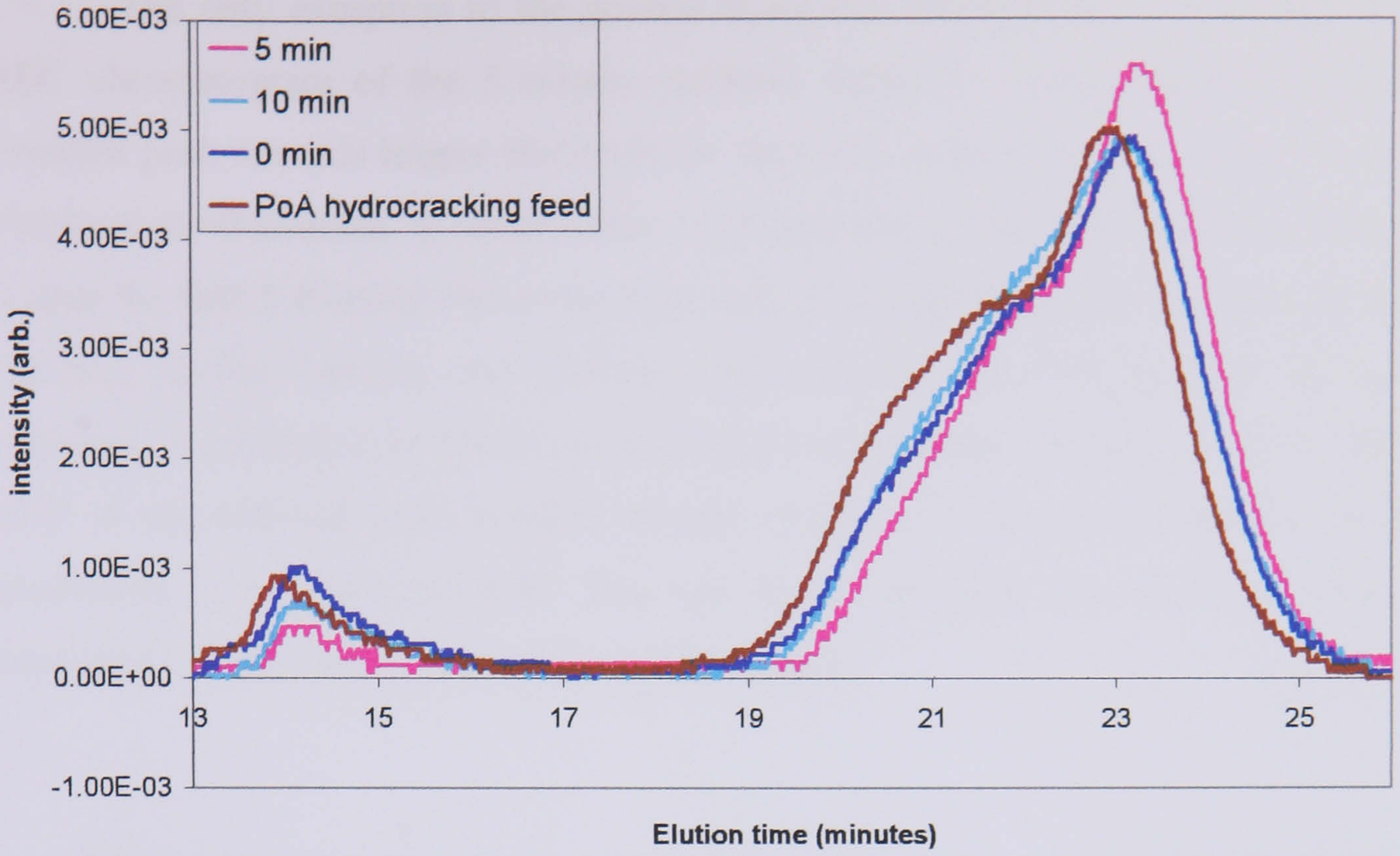


Figure 5.1. Mixed-A column SEC chromatograms of the Point of Ayr hydrocracking feed and the hydrocracking products for 0, 5, and 10 minutes reaction time. All chromatograms have been area normalised.

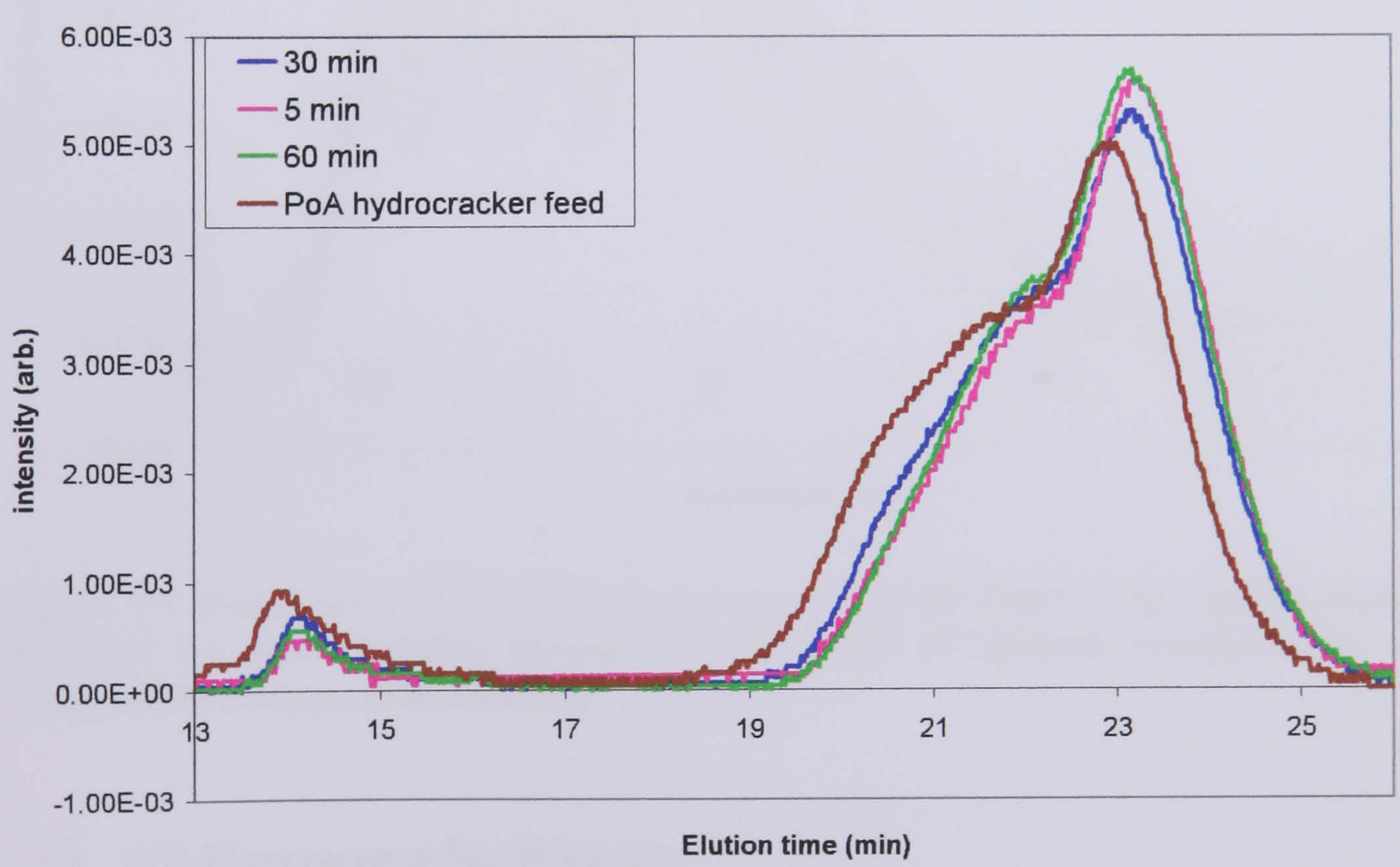


Figure 5.2. Mixed-A column SEC chromatograms of the Point of Ayr hydrocracking feed and the hydrocracking products for 5, 30 and 60 minutes reaction time. All chromatograms have been area normalised.

The only exception to the general trend was found in the 5 minute run. The SEC chromatogram of the 5 minute products showed a considerable shift of the retained peak towards longer elution times than that of the 0 min run, similar to that observed at 60 minutes. A combination of progression of the hydrocracking reactions within the first 5 minutes and a still large amount of carbonaceous materials forming deposits on the catalyst, and therefore not observed by SEC, explain the trend obtained. A retrogressive behaviour was observed between 5 and 10 minutes, with a shift of the retained peak towards shorter retention times and an increase in the proportion of excluded material. This was due to the large dissolution of material deposited on the catalyst between 5 and 10 minutes.

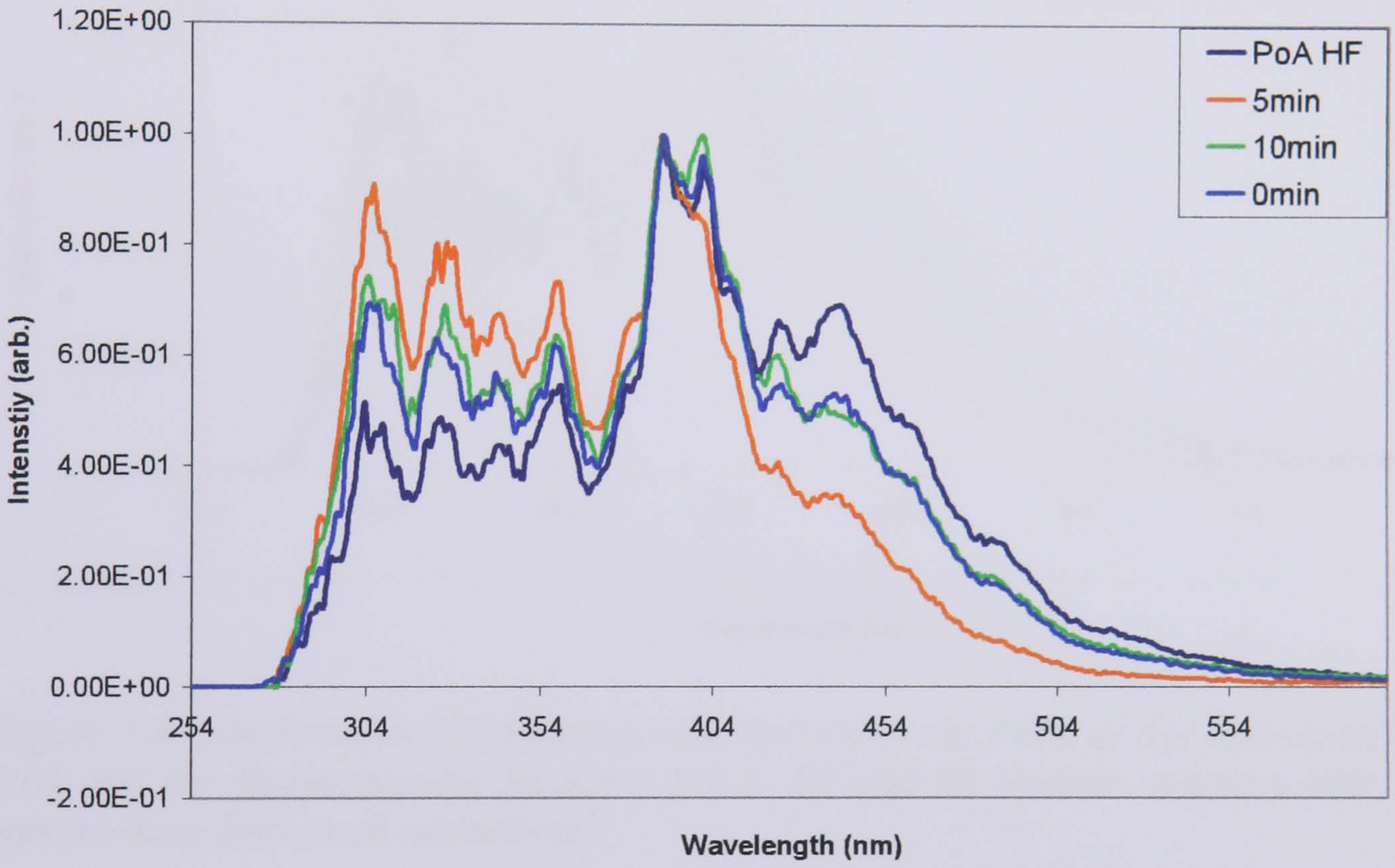


Figure 5.3. Synchronous UV-Fluorescence spectra of the Point of Ayr hydrocracking feed and the hydrocracking products for 0, 5 and 10 minutes reaction time. All spectra have been peak normalised.

5.3.3 UV-Fluorescence Spectrometry

The UV-F spectra of the Point of Ayr hydrocracker feed and its hydrocracking products are shown in Figure 5.3 and Figure 5.4. The Point of Ayr hydrocracker feed showed signal at longer wavelengths than the hydrocracking products, indicating that higher concentrations of larger polynuclear aromatic rings are present in the feed. The

spectra of the 0 min, 10 min, 30 min and 60 min runs were almost undistinguishable. The 5 minute run spectrum was clearly shifted towards shorter wavelengths. This suggests the presence of smaller aromatic rings in solution than those observed in the rest of the samples. Between 5 and 10 minutes the spectrum shifted towards longer wavelengths as a consequence of the dissolution of material which was deposited on the catalyst. This is a similar behaviour to that exhibited by the SEC chromatograms of the liquid products discussed above.

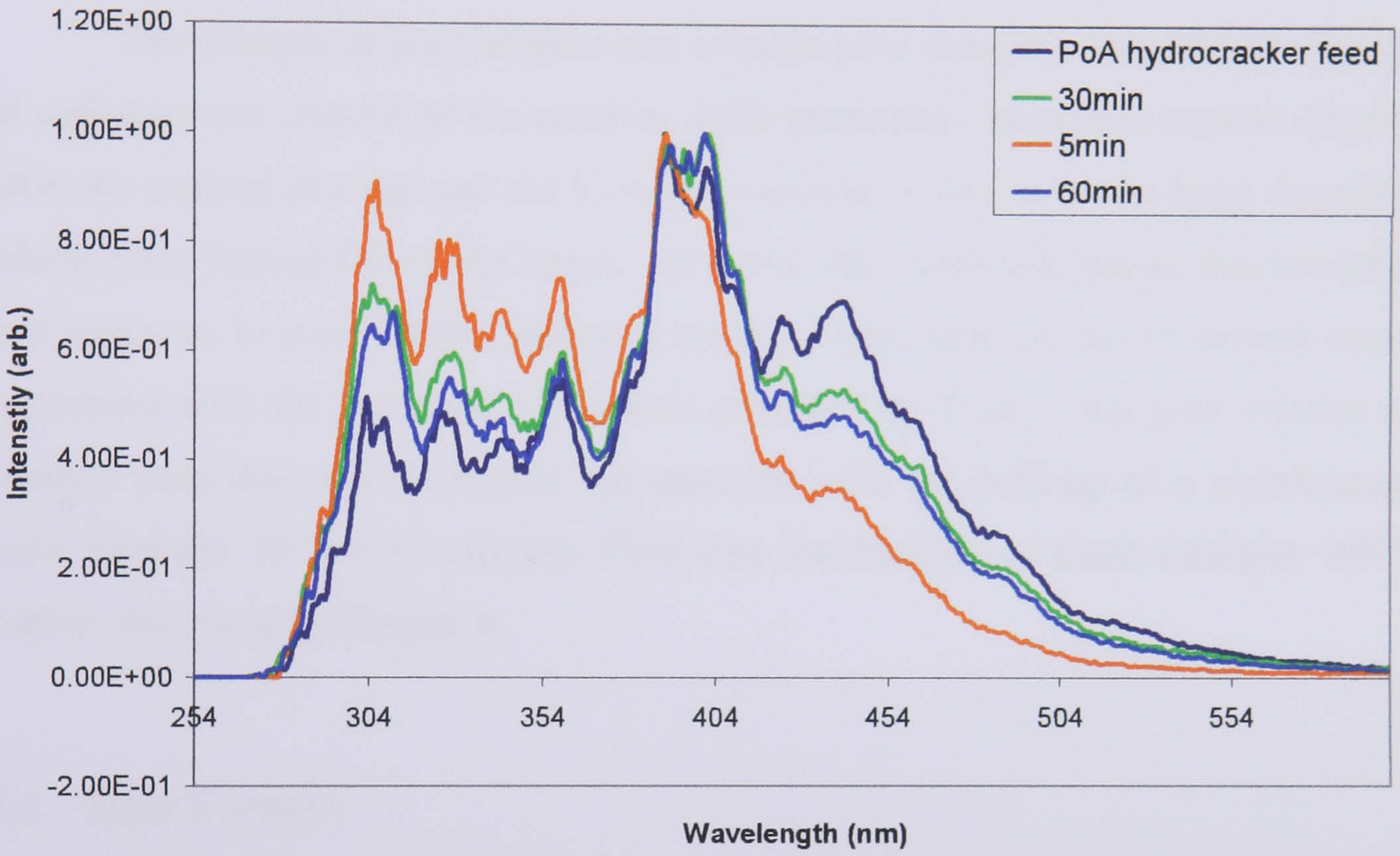


Figure 5.4. Synchronous UV-Fluorescence spectra of the Point of Ayr hydrocracking feed and the hydrocracking products for 5, 30 and 60 minutes reaction time. All spectra have been peak normalised.

5.3.4 Surface Area Measurements

Surface area measurements were carried out on fresh $NiMo/Al_2O_3$, the coated $NiMo/Al_2O_3$ used as feed in these experiments and the catalysts obtained from the 0, 10 and 30 minute runs. A summary of the results can be seen in Table 5.2. A significant decrease in surface area takes place during the catalyst coating. A slight increase in surface area was observed after the 0 min reaction. The variations in surface area observed afterwards are negligible.

Table 5.2. BET surface area, total pore volume and average pore diameter of fresh and coated $NiMo/Al_2O_3$, and the catalysts recovered from hydrocracking runs.

Sample	BET Surface Area (m^2/g)	Total Pore Volume (cm^3/g)	Average Pore Diameter (nm)
Fresh $NiMo/Al_2O_3$	78	0.28	14.7
Coated $NiMo/Al_2O_3$	45	0.12	11.0
0 minute run	51	0.09	7.3
10 minute run	52	0.13	10.2
30 minute run	51	0.12	9.4

The changes in pore volume and average pore diameter followed the changes in carbonaceous content of the catalyst. Both parameters showed a marked decrease after the coating process and the 0 minute reaction in line with the large deposition taking place during the initial stages. However, the initial deposition was reversible and increases in pore volume and pore diameter were seen for the 10 minute run, in agreement with the reduction of deposits observed by TGA. Total pore volume and average pore diameter decreased subsequently with the built-up of a carbonaceous layer between 10 and 30 minutes. Pore size distributions of these catalysts will be further discussed in Chapter 8.

5.4 DISCUSSION

Hydrocracking, defined as increasing real conversion, showed a continuous progression between 0 and 120 minutes as a function of reaction time. This marks a difference with previous work which showed a drop in real conversion during the first 10 minutes of reaction [7]. Data presented in that work only referred to apparent conversion. However, the corresponding real conversions have been calculated here using data from Begon's thesis [88]. Conversions obtained with these data are plotted in Figure 5.5 as a function of reaction time. The drop in apparent conversion at short reaction times has been explained in that work in terms of a period needed to achieve the activation of the catalyst by sulphidation [7]. The fragments produced by thermal cracking of the sample were not hydrogenated due to the absence of an active catalyst and recombined to form larger molecules. As shown in Figure 5.5, the trend followed by real conversion is identical to that of the apparent conversion and the conclusions of that work remain valid. The use in this work of an already coated catalyst, which

has been sulphided during the coating process, eliminated this activation period and therefore the real conversion was observed to continuously increase.

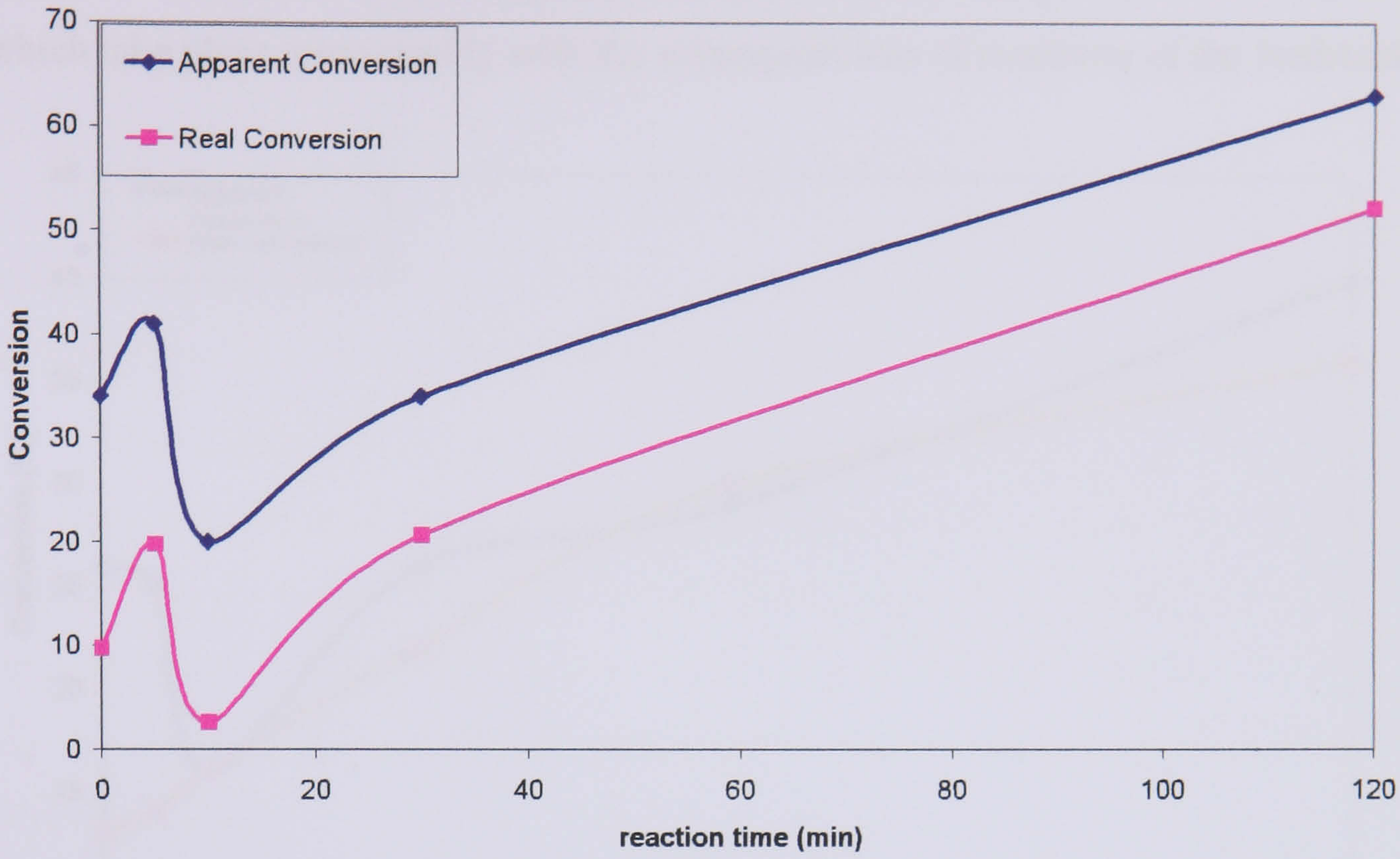


Figure 5.5. Apparent and real conversions as a function of reaction time obtained by Begon et al. [7].

A large deposition on the fresh catalyst in the early stages of hydrocracking has been extensively reported in the literature [7, 21, 22, 38, 39]. The present work shows that a relatively large deposition also takes place even though a previously coated catalyst with a high carbonaceous content (30%) is used. This suggests that a fraction of the feed has a strong tendency to adsorb on the solid surface provided by the catalyst. Although a previously coated NiMo was used, the amount of deposits was significant in the first five minutes of hydrocracking.

The deposits seem to quickly re-dissolve in the liquid mixture. The re-dissolution process is slower during the first 5 minutes, but it speeds up between 5 and 10 minutes. As a result, a weight equivalent to all the material initially deposited on the catalyst has been transferred to the solution within the first 10 minutes. This shows that the carbonaceous deposits are dynamic and material is exchanged between them and the solution. The re-dissolution of heavy material coating the catalyst produced a decrease in apparent conversion between 5 and 10 minutes and shifted the SEC and UV-F profiles towards smaller sizes. After the first 10 minutes the apparent

and real conversions increase with time. The curves of apparent and real conversion as a function of time are shown in Figure 5.6. The increase in real conversion slowed down in the second hour of hydrocracking due to the completion of the reactions which take place more readily with the subsequent loss of reactivity of the feedstock.

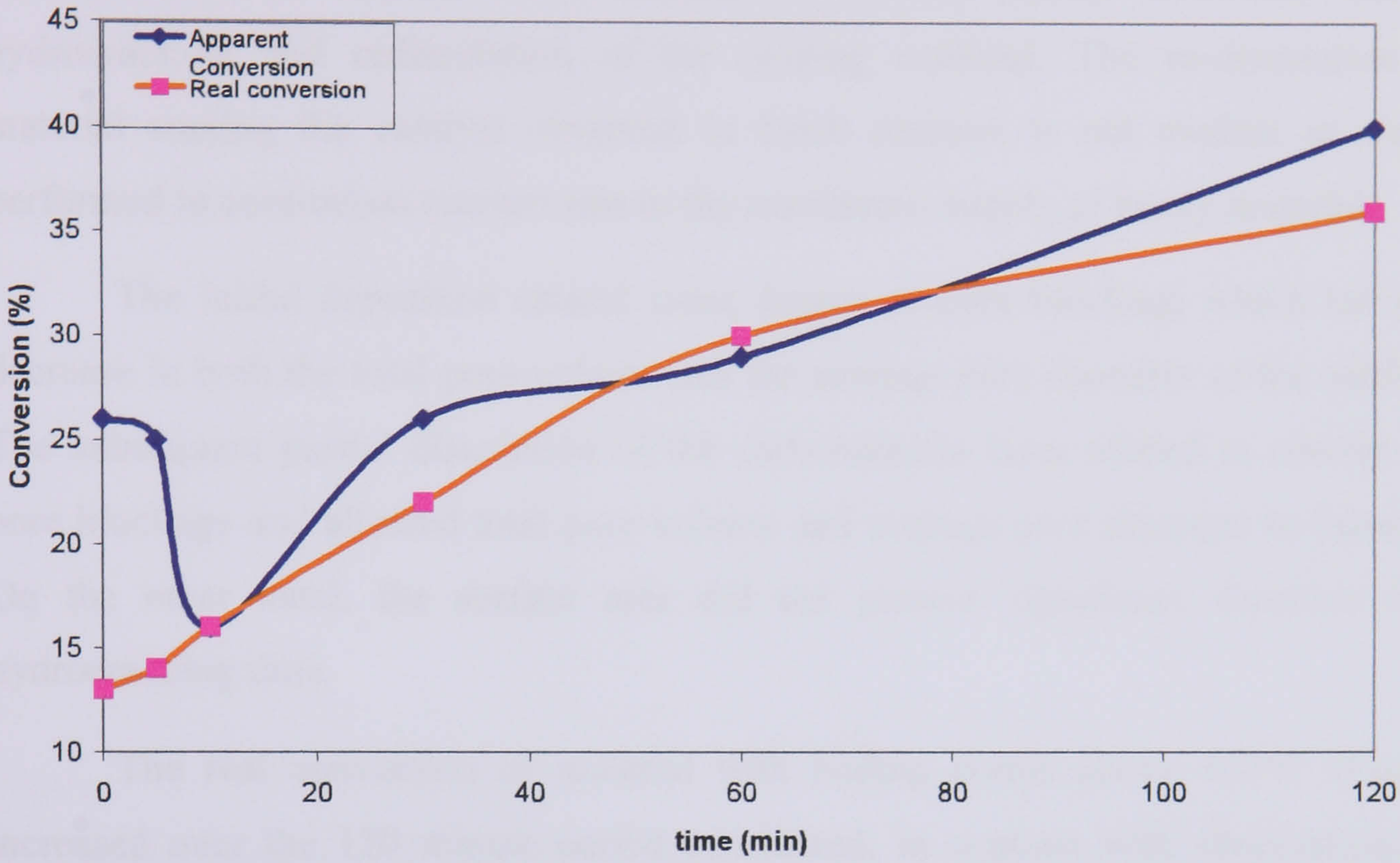


Figure 5.6. Apparent and real conversions as a function of reaction time obtained in the present work.

Despite the use of a pre-coated catalyst, similar amounts of material deposited on the catalyst as those reported by Begon et al. [7] on the fresh catalyst were observed. The absence of tetralin in the reactor made the feed heavier, which may have had an effect on this observation.

5.5 CONCLUSIONS

The behaviour of a $NiMo/Al_2O_3$ catalyst in the early stages of hydrocracking has been studied in this work. The use of an already coated catalyst and no solvent are the main differences in experimental procedure with previous work. By not adding solvent to the reaction mixture, the interference of the solvent in product characterisation has been avoided. Despite the use of a pre-coated catalyst, the initial deposition was large. This shows that a heavy fraction of this particular feed has a strong tendency to form deposits. This behaviour is in line with the larger deposition

observed in continuous reactors than in batch systems due to the permanent supply of heavy materials.

The carbonaceous layer coating the catalyst is largely dynamic and exchanges material with the solution. The amount of deposits rapidly decreased due to hydrocracking and redissolution of the coating material. The re-dissolution of material coating the catalyst observed in batch reactors is not evident in works performed in continuous reactors due to the continuous supply of heavy materials.

The initial deposition caused some degree of pore blockage which led to a decrease in both the total pore volume and the average pore diameter of the catalyst. The subsequent partial dissolution of the carbonaceous layer tended to reverse the pore blockage and allowed total pore volume and average pore diameter to increase. On the other hand, the surface area did not present significant variation with hydrocracking time.

The real conversion of material with boiling points above 450°C steadily increased over the 120 minute period considered, in contrast with observations in earlier work [7]. This supports the interpretation of the drop in conversions observed in previous work as caused by the lack of catalytic activity of the $NiMo/Al_2O_3$ during the sulphidation period.

6 PILLARED CLAYS AS HYDROCRACKING CATALYSTS: TESTS WITH FRESH CATALYSTS

6.1 INTRODUCTION

As described in Chapter 2, NiMo and CoMo catalysts supported on alumina have been developed and used mainly as petroleum hydrodesulfurisation catalysts. Subsequently, their use has been extended to hydrocracking processes including those from coal liquefaction, such as in the liquid solvent extraction (LSE) process developed by British Coal. The main advantages of molybdenum based catalysts supported on alumina are their availability and robustness. However, these catalysts suffer from quick deactivation and their activities at steady state are low. Improvements in hydrocracking catalysts should reduce the hydrogen consumption. It currently represents a high proportion, nearly 25%, of the operating cost of hydrocracking plants. The hydrogen consumption in the hydrocracking of a petroleum residuum is estimated in 1200 to 1600 standard cubic feet per barrel (scfb) [11]. Higher conversions of the heaviest fraction of coal and oil samples into lighter materials and longer catalyst lifetimes are also desirable.

The $NiMo/Al_2O_3$ and $CoMo/Al_2O_3$ formulations have also provided bases for comparison in studies on the suitability of a number of novel hydrocracking catalysts carried out in several laboratories. In this laboratory, the search for catalysts able to hydrocrack the larger molecules present in coal and heavy oils led to the testing of dispersed catalysts [10]. A number of metal carbonyls, organometallic catalyst precursors, as well as a mixture of C_{60} and C_{70} fullerenes in a 10:1 ratio were tested on a coal extract by Zhang et al. [6, 10]. None of the metal carbonyls gave significantly greater catalytic activities than the $NiMo/Al_2O_3$ in terms of their hydrocracking conversions, whereas the fullerenes were not stable at the reaction conditions.

As discussed in Chapter 2, the pore size of $NiMo/Al_2O_3$ catalysts was reported to be an important factor in hydrocracking and heteroatom removal of asphaltenes and preasphaltenes [20]. Larger pores allow for better contact between the catalysts and large molecules in the feed. Following that approach, in an attempt to design materials which can accommodate larger molecules, pillared clays have been tested in this laboratory [70, 71]. In these compounds, the separation between clay layers is

modified by inserting an ion, which must provide both structural stability and an adequate gap between layers to allow the reactants to get into the catalyst. A diagram of these materials is shown in Figure 6.1. A lower pillar density leads to bigger galleries in the catalyst, which it is thought, would favour the access of bigger molecules into the catalyst pores. However, a high pillar density provides higher mechanical stability. Hence the catalyst design must be a compromise between these two factors.

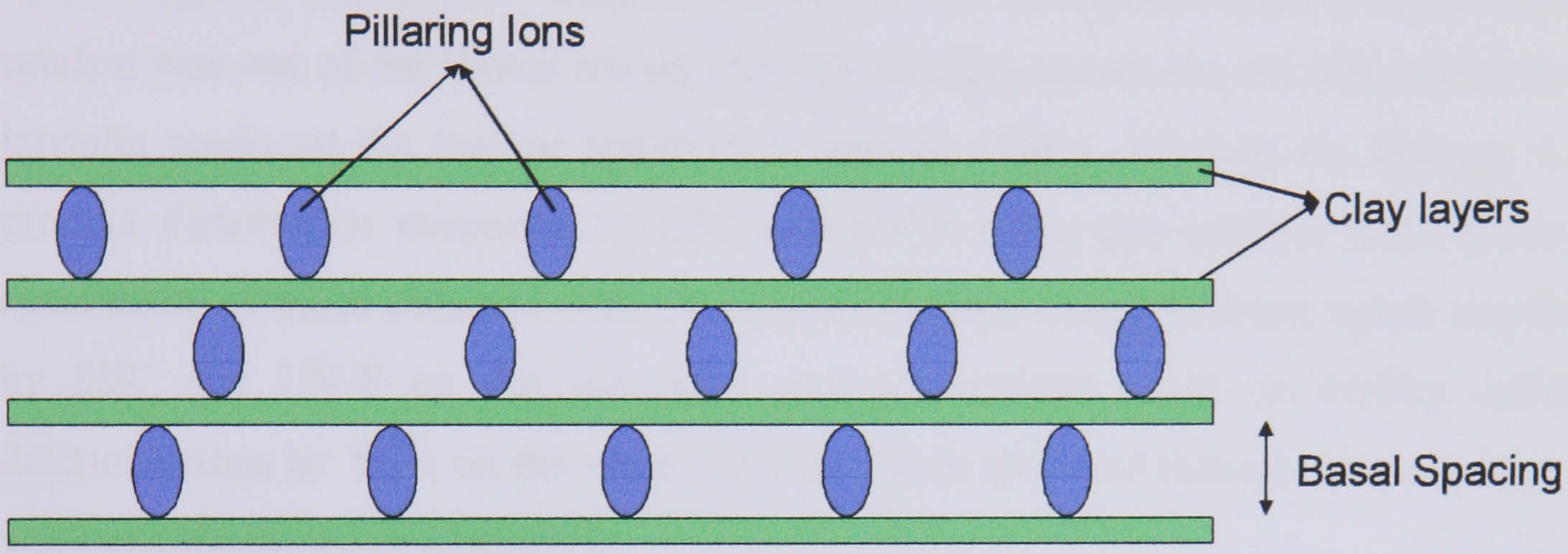


Figure 6.1. Diagram of a pillared clay.

Pillared clays have been tested as catalysts for fuel upgrading [89-91]. Other applications include several different processes such as polyethylene recycling [92], denox processes [93], clean up of aqueous environments [94, 95] and sorption of humic substances [96].

Promising levels of activity were observed when using some pillared clays as catalysts for coal and oil hydrocracking [70, 71]. A number of pillared clays prepared by Bodman [97] were tested in previous work in this laboratory [70, 71]. A screening study was performed at short reaction times (10 min) to assess the effectiveness of some pillared clays and layered double hydroxides (LDH) in hydrocracking coal extract from the Point of Ayr pilot plant. Four different Al montmorillonites calcined at different temperatures between 400°C and 525°C, two Cr montmorillonites, a Sn laponite and an Al/Fe montmorillonite were tested as well as a LDH. Conversion of the ">450°C" fraction was used as a criterion of the catalytic performance of these materials following the method described in Chapter 3.

In these 10 minute runs, most pillared clay catalysts achieved higher apparent conversions than the $NiMo/Al_2O_3$ and all of them showed higher real conversions [70]. The tin laponite and the chromium montmorillonite calcined at 500°C were identified as the most effective catalysts in reducing the size of the molecules in the feedstock [70]. In the case of Cr-montmorillonite, the authors based this assertion on the larger shift towards smaller molecules observed by SEC and UV-F than those seen using the rest of the catalysts. However, the conversion achieved with this catalyst was one of the lowest among the pillared clays tested. On the other hand, tin laponite produced the highest apparent conversion (70%), although the changes in product distribution measured by SEC and UV-F using this catalyst were not as remarkable as those obtained with Cr-montmorillonite. These different trends shown by SEC and UV-F on the one hand, and conversions based on boiling point determinations by TGA on the other, have also been observed throughout the present work and discussed in Chapter 4.

Further tests were run on the Cr montmorillonte and the Sn laponite selected from the 10-minute studies [70]. As mentioned above, this selection was esentially based upon the properties of the liquid products. The amount of carbonaceous material deposited on the catalyst had not been considered. As seen in Chapter 5, deposits in the early stages of hydrocracking are extremely large and therefore they affect the real conversions achieved. Moreover, a large deposition has also an indirect effect on the SEC chromatograms and UV-F spectra by removing a heavier fraction of the sample from solution. When the conversion was corrected to take into account carbonaceous deposition on the catalyst surface, the figure achieved with the Sn laponite dropped from 70% (apparent conversion) to 28% (real conversion). The difference was remarkable although the real conversion of this catalyst was still one of the highest among the pillared clays.

Studies at a longer time scale were required in order to assess the catalyst performance [7] as distinct from the effects of the strong deposition observed at short times. Therefore, a series of 2 hour runs were conducted by Begon et al. [71] using both Sn laponite and Cr montmorillonite to hydrocrack the Point of Ayr hydrocracker feed as well as other samples [71]. As in the short time series, comparison was made against NiMo based on alumina and $Mo(CO)_6$ [71]. The catalysts were recovered and reused in series of three successive two-hour experiments.

The conversions and carbonaceous deposition found in that work are shown in Table 6.1. The figure for the ">450ºC" fraction of the feed used in that work was 47.3% as opposed to 38.3% found as a more suitable value in the present work. As described in Chapter 4, this figure has been arrived at following a careful study of the dependence of the ">450°C" fraction measured by TGA on the weight loaded on the TGA pan. Both pillared clays showed a distinctive pattern of real conversion against time with a maximum achieved in the second run. By contrast, a steady decrease in apparent conversion was observed from the first to the third run. The maximum in real conversion observed in the second run could be the result of two opposite effects. Firstly, a diminution in the carbonaceous deposition on the catalyst would lead to an increase in conversion, since that material is considered as part of the ">450°C" fraction. Secondly, a decrease in the catalyst activity would lead to higher amounts of ">450°C" in the liquid and then smaller apparent conversions. The combination of these two factors could generate a pattern of conversion vs. time as the observed with a maximum in the second run. However, it is not possible to conclude that the activity of the catalyst is decreasing based on the drop in apparent conversions only, since this could also be reflecting the higher deposition of ">450°C" materials on the catalyst in the earlier runs. The $NiMo/Al_2O_3$ did not present the same behaviour, but it showed a marked drop in total and apparent conversions following its reuse. This suggested that this catalyst presents a more marked deactivation process than the pillared clays.

Table 6.1. Apparent and real hydrocracking conversions obtained by Begon et al. [70] in experiments at 190 bar H_2 pressure and 440 ℃ in the presence of tetralin.

Catalyst	Run	Apparent conversion (%)	Carbonaceous Deposits (% of the recovered solids)	Real conversion (%)
Cr montmorillonite	1 x 120	66.2	18.1	40.8
Cr montmorillonite	2 x 120	59.1	4.4	54.4
Cr montmorillonite	3 x 120	50.6	1.1	49.6
Sn laponite	1 x 120	67.2	25.5	35.4
Sn laponite	2 x 120	68.1	4.3	63.8
Sn laponite	3 x 120	60.1	1.2	59.0
$NiMo/Al_2O_3$	1 x 120	72.6	15.6	59.1
$NiMo/Al_2O_3$	2 x 120	45.0	4.0	41.9
$NiMo/Al_2O_3$	3 x 120	38.8	2.8	36.9

A reduction in the molecular sizes of the feedstock has been observed by both SEC and UV-F in all experiments using Cr-montmorillonite or Sn laponite as catalysts to hydrocrack the Point of Ayr hydrocracker feed. However, these two techniques showed that the differences between feed and products decreased as the catalysts were reused. This paralleled the trend observed in the apparent conversions, which decrease when the catalysts were reused. This may be due to a combination of loss of hydrocracking activity and lower capacity to adsorb carbonaceous material on the catalyst surface, which would lead to a larger amount of heavy materials in the liquid products.

To summarise, Begon et al. [71] concluded that the pillared clays were more efficient as hydrocracking catalysts than the two catalysts used as benchmark, $NiMo/Al_2O_3$ and $Mo(CO)_6$, exhibiting good resistance to rapid deactivation. The catalytic activities of Cr montmorillonite and Sn laponite prepared by different methods have been assessed in the present work. In addition, new pillared clay catalysts such as Eu, Ce and Ce-Cr montmorillonites as well as a Cr laponite have been tested. In order to appreciate the effect of pillaring upon the catalytic activity, the raw clays used in the synthesis of the catalysts have also been evaluated as hydrocracking catalysts.

A screening test was conducted to select among the different preparations those Cr montmorillonites and Sn laponites which lead to higher conversions and better product distributions. By contrast with earlier work [70], these first tests were performed in 2 hour long runs, in order to minimise short time effects due to intense early deposition on the catalyst (see Chapter 5 and ref. 7). However, due to the large number of catalysts to be tested, it was not possible to pre-coat them beforehand. Other relevant changes to the testing procedure have been discussed in Chapter 4 and include not adding solvent to the reaction and using a different method to dry the $CHCl_3/CH_3OH$ used to recover the sample from the reactor. The aim of these modifications is to enable a more complete characterisation of the products.

The use of tetralin in hydrocracking runs affected the distribution of liquid products and did not allow significant boiling point data to be collected in the range below 450°C. Moreover, the addition of a solvent, unless derived from the same process, such as the recycled solvent in Point of Ayr pilot plant, cannot be part of a

large scale commercial process. Therefore, working without solvent is thought to resemble more closely the real application conditions. The feed used in this study was the coal digest produced at the Point of Ayr plant, which already contains a solvent recycled from the same process. In addition, changes to the method followed to evaporate $CHCl_3/CH_3OH$ from the liquid products allow a more reproducible sample recovery from run to run. Broad variations in the amount of sample recovered, which differed by up to a factor of 10 in previous work [70], will affect any measurement of the product distribution by SEC, UV-F or boiling points. These modifications to the experimental procedure have been discussed in Chapter 4.

A preliminary assessment of the catalytic activity towards hydrocracking of heavy feeds faces a major difficulty derived from the large deposition of carbonaceous materials on the fresh catalyst surface. There is evidence suggesting that the material deposited on the catalyst is mainly composed of the heaviest fraction of the feed [34], which is the main object of the hydrocracking process. Hence evaluation of the catalytic activity of fresh catalysts must take into account that an important fraction of the material will be lost on the catalyst on that first use, whereas this is not expected to happen when the catalyst has been operating for some time.

Interpretation of the results is not straightforward since the amount of deposits varies with different catalysts. Moreover, a larger deposition does not necessarily mean that the catalyst is not suitable; larger amount of deposits may be related to parameters inherent to the catalytic activity such as a higher surface area or a stronger interaction between catalyst and the sample. The complementary use of several analytical techniques is therefore required to interpret the results of catalyst testing.

6.2 EXPERIMENTAL

The preparation of the Cr montmorillonites used in this study has been described elsewhere [98]. Briefly, a conventional and a microwave method have been followed to pillar two different starting materials: a Na montmorillonite and a Wyoming Bentonite. In the conventional method, a pillaring solution composed of sodium carbonate and chromium nitrate was added to a suspension of the raw clay. The resulting material was filtered under vacuum, air dried, and calcined under argon for 1 hour at 500°C. The microwave method implied the irradiation of the suspension

with microwaves at different powers. Ce, Eu and Ce-Cr montmorillonites were prepared from Na montmorillonite.

Several pillared laponites were also prepared using conventional and microwave methods. Both methods involved the reaction between a sodium exchanged laponite and triphenyltin chloride in a suspension in dry ethanol. Sn and Cr were used as pillaring ions.

All these catalysts were tested in 2 hour experiments to hydrocrack the Point of Ayr coal extract in the microbomb reactor at 440°C and 190 bar of hydrogen. A Cr montmorillonite, CM B61, and a Cr laponite, CL B14, synthesised in a previous project by Bodman [97] have also been included in this study for comparison. The catalysts were evaluated taking into account the conversion of the ">450°C" fraction measured by TGA based boiling point distribution, size exclusion chromatography and UV-Fluorescence spectrometry. Fresh catalysts have been employed in all runs described in this chapter.

6.3 RESULTS AND DISCUSSION

6.3.1 Evaluation of Cr montmorillonites

Six Cr montmorillonites prepared at Aston University have been tested, four of them prepared from Wyoming Bentonite as raw clay, namely CM2a, CM2b, CM2c and CM6a, whereas a montmorillonite already pillared with Na was used to synthesise the two others, CM3 and CM16. CM2a, CM2b and CM2c were prepared by the same method, which was different from that applied to the preparation of CM6a. CM3 and CM16 were synthesised following different preparations. Runs using the two raw clays were performed to evaluate the effect of pillaring upon the catalytic activity. The reference catalyst, $NiMo/Al_2O_3$, has also been included in this study for comparison.

Most Cr-montmorillonites exhibited catalytic activity. The exceptions were CM2a and CM2c, which led to a conversion comparable to that obtained in the non-catalysed run (see Table 6.2). The CM3 catalyst showed the highest apparent and real conversions among the Cr montmorillonites. It performed better in terms of conversion of the ">450°C" material than the catalysts prepared from Wyoming

Bentonite following the same method, CM2a, CM2b and CM2c. In these series of runs, all catalysts showed lower conversions than the reference catalyst, the NiMo supported on alumina.

CM3 also exhibited a higher conversion than that obtained with the Na-montmorillonite used as starting material in its synthesis. By contrast, the conversion achieved by using CM16 was roughly the same as that obtained with the raw clay. Regarding the Cr montmorillonites prepared from Wyoming Bentonite, two of them, CM6a and CM2b, showed higher and the two others, CM2a and CM2c, lower conversions than the raw clay, although in the latter case those differences are not experimentally significant.

Table 6.2. Apparent and real conversions and deposition on the catalyst for Cr montmorillonites. Fresh catalysts were used in these runs.

Catalyst	Apparent conversion (%)	Carbonaceous Deposits (as % of the filter cake)	Real conversion (%)
NiMo	55	26	36
CM3	64	35	29
CM6a	50	27	27
CM B61	62	38	26
CM2b	55	30	26
Na montmorillonite	47	28	24
CM16	50	29	23
Wyoming Bentonite	44	26	23
CM2c	43	26	21
No catalyst	41	64	21
CM2a	41	28	20

SEC of the products from 2 hour long reactions obtained with the fresh Cr-montmorillonites, the raw clays, the reference catalyst and without catalyst are shown in Figure 6.2, Figure 6.3 and Figure 6.4. In all reactions, including the non-catalysed case, the excluded peak decreased in size and shifted towards longer elution times from feed to products. The retained peak also showed a shift indicating the presence of lighter materials for all hydrocracked products.

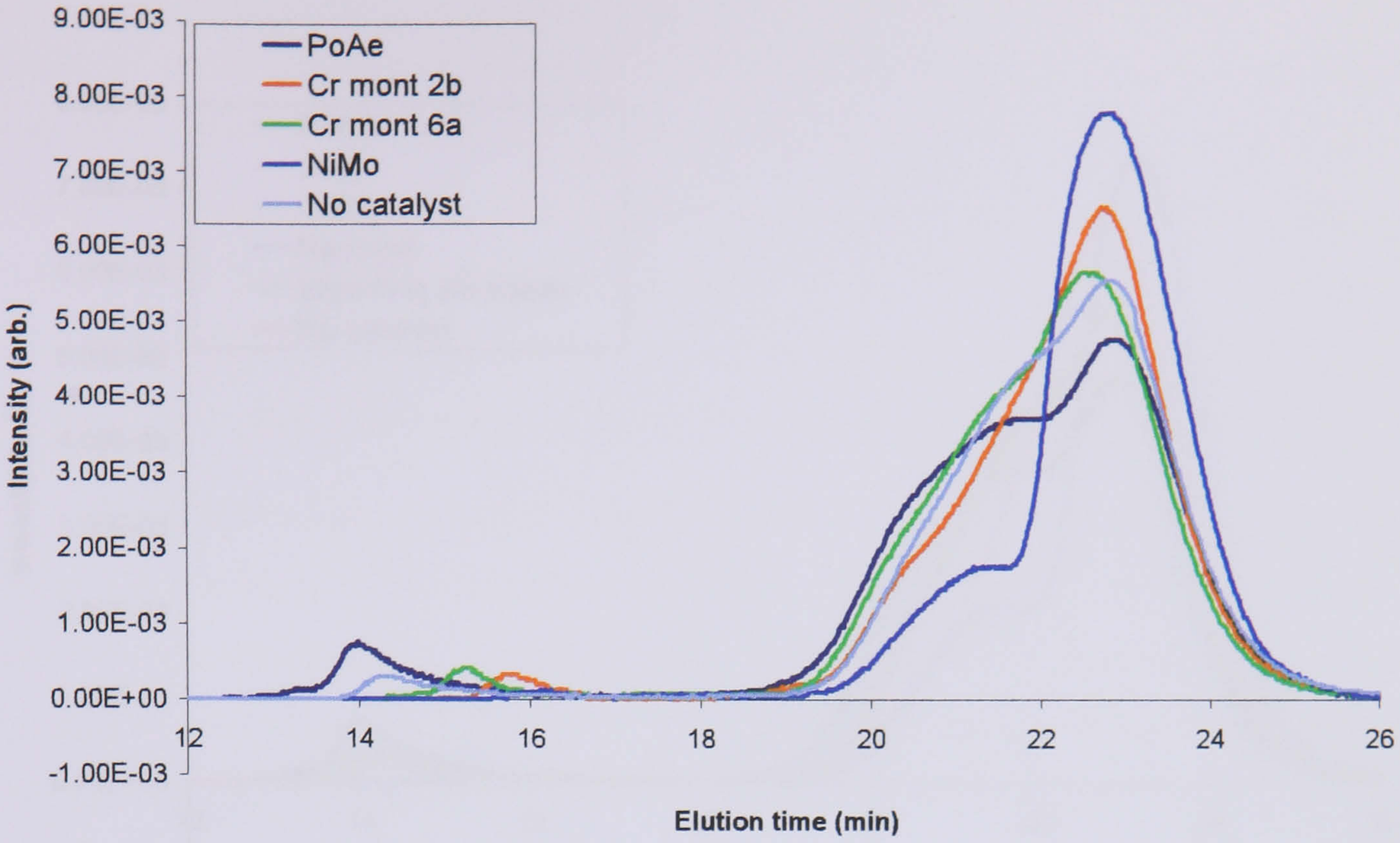


Figure 6.2. Mixed-A column SEC chromatograms of hydrocracking products obtained with CM2b, CM6a and NiMo as catalysts. SEC chromatograms of the feed and products from the no catalyst run are also included for comparison. All chromatograms have been area normalised.

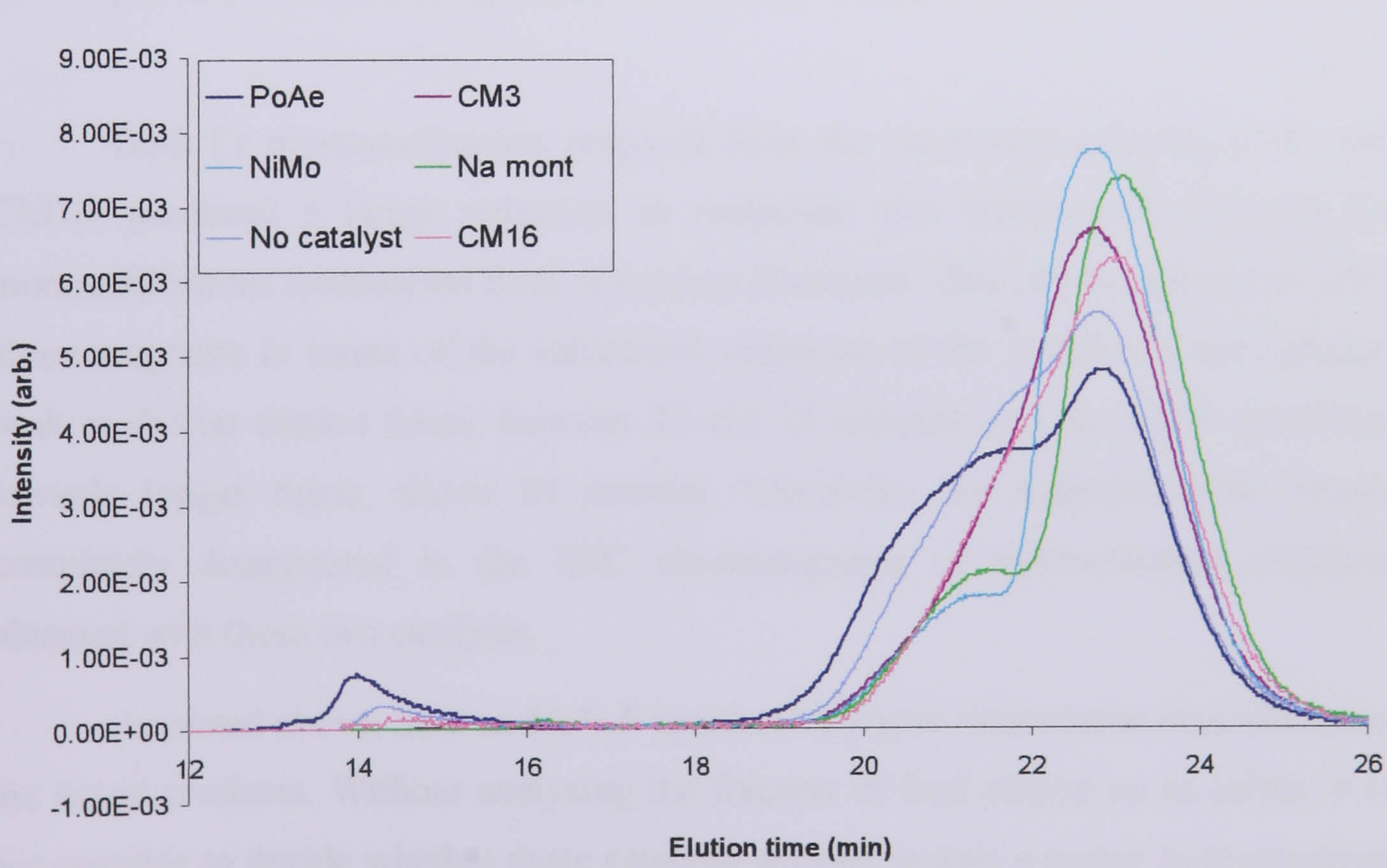


Figure 6.3. Mixed-A column SEC chromatograms of hydrocracking products obtained with CM3, CM16, Na montmorillonite and NiMo as catalysts. SEC chromatograms of the feed and products from the no catalyst run are also included for comparison. All chromatograms have been area normalised.

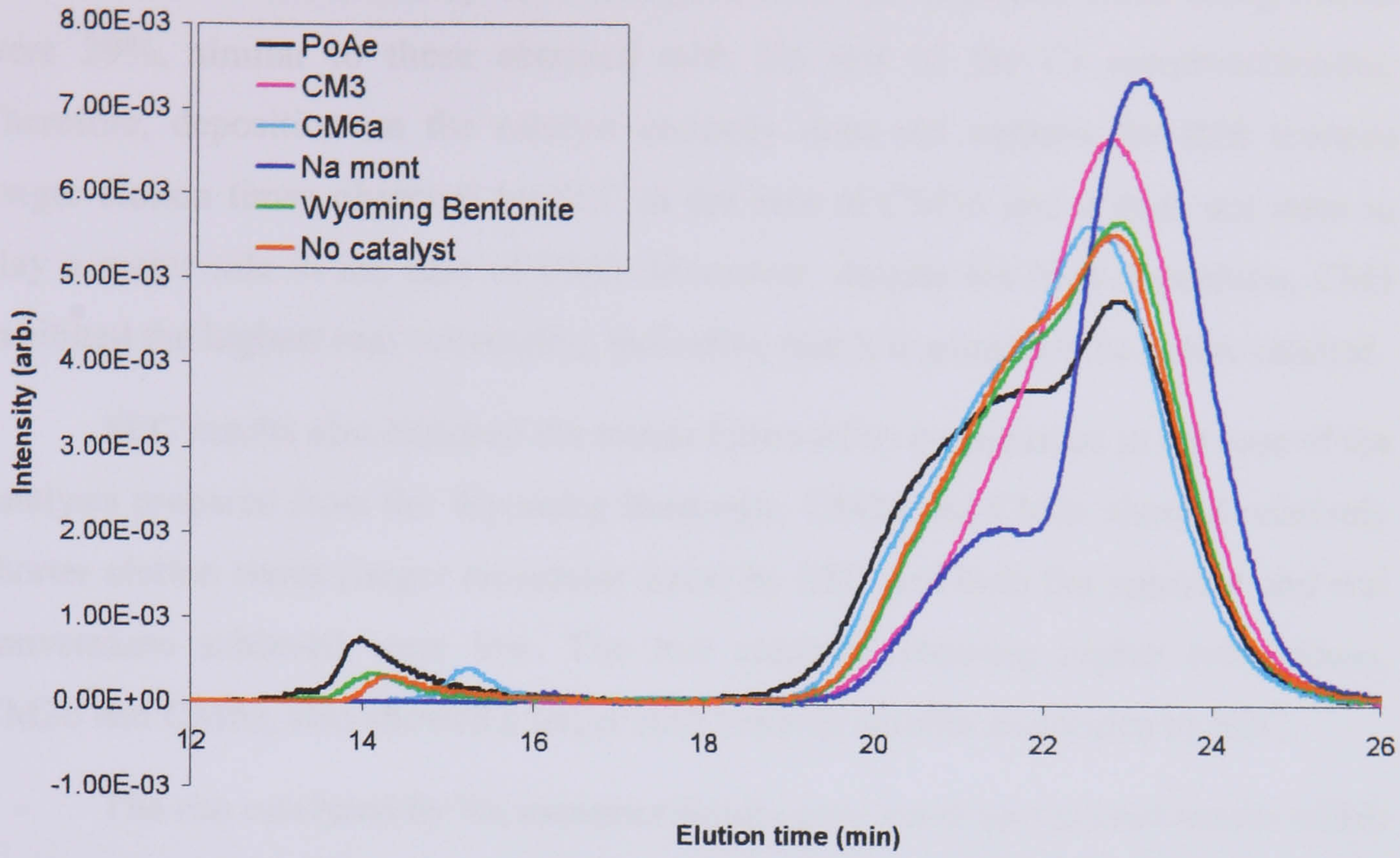


Figure 6.4. Mixed-A column SEC chromatograms of hydrocracking products obtained with CM3, CM6a, Na montmorillonite and NiMo as catalysts. SEC chromatograms of the feed and products from the no catalyst run are also included for comparison. All chromatograms have been area normalised.

Both Cr montmorillonites prepared from the Na-montmorillonite, CM3 and CM16, produced a larger reduction in molecular size distributions than the Cr montmorillonites synthesised from Wyoming Bentonite. This can be seen in the SEC chromatograms in terms of the substantial reduction of the fraction of the retained peak at shorter elution times, between 20 and 22 minutes, and the signal extending towards longer times, above 24 minutes. Moreover, the excluded peak almost completely disappeared in the SEC chromatograms of hydrocracking products obtained with these two catalysts.

As stated above, SEC and UV-F spectrometry give information exclusively on the liquid products. Without analysing the fraction of feed ending up as solids, it is not possible to decide whether these catalysts actually posses a higher hydrocracking activity or were simply removing a larger amount of heavy material as deposits on the catalyst or as condensed, precipitated carbonaceous solids. The relative weight of carbonaceous solids is shown in Table 6.2 as well as apparent and real conversions. CM3 led to 35% of carbonaceous material on the filter cake, slightly higher than the

amount of solids exhibited by other catalysts, while the deposits, when using CM16, were 29%, similar to those obtained with the rest of the Cr montmorillonites. Therefore, deposition on the catalyst certainly does not explain the shift towards longer elution times observed by SEC in the case of CM16 and it does not seem to play a major role in the case of CM3. Moreover, despite the high deposition, CM3 exhibited the highest real conversion, indicating that it is genuinely an active catalyst.

SEC results also matched the trends followed by conversions in the case of the catalysts prepared from the Wyoming Bentonite. CM2a and CM2c showed relatively shorter elution times (larger molecular sizes) by SEC and both the apparent and real conversions achieved were low. The two catalysts showing higher conversions, CM2b and CM6a, also showed a larger shift towards smaller molecules by SEC.

The run catalysed by Na montmorillonite gave some unexpected results which need to be discussed. Interestingly, it produced the largest shift of the retained peak towards longer retention times and an almost complete disappearance of the excluded peak. However, the conversion achieved with this catalyst is significantly lower than that achieved with the best Cr montmorillonites. This cannot be explained in terms of a large fraction of the sample forming deposits on the catalyst, since the amount of deposits is rather low, comparable to CM2a and CM6a and lower than CM2b and CM3. The main contribution to the low real conversion comes from the apparent conversion term. This indicates that although the shift towards longer retention times is significant, the proportion of ">450°C" material did not show significant changes. The lack of a straightforward relation between boiling points and retention times by SEC has been discussed in Chapter 4.

From these experiments the two Cr montmorillonites showing higher conversions, CM3 and CM6a, were selected for further tests at longer time scales involving the reuse of the catalysts recovered from these first runs. CM3 was selected due to the higher real conversion exhibited and the considerable lighter liquid products obtained with this catalyst as the SEC and UV-F measurements and the apparent conversion calculation suggested. The selection of CM6a was based on its higher performance in comparison with the other catalysts derived from the Wyoming Bentonite. Results from this second series of runs will be presented in Chapter 7.

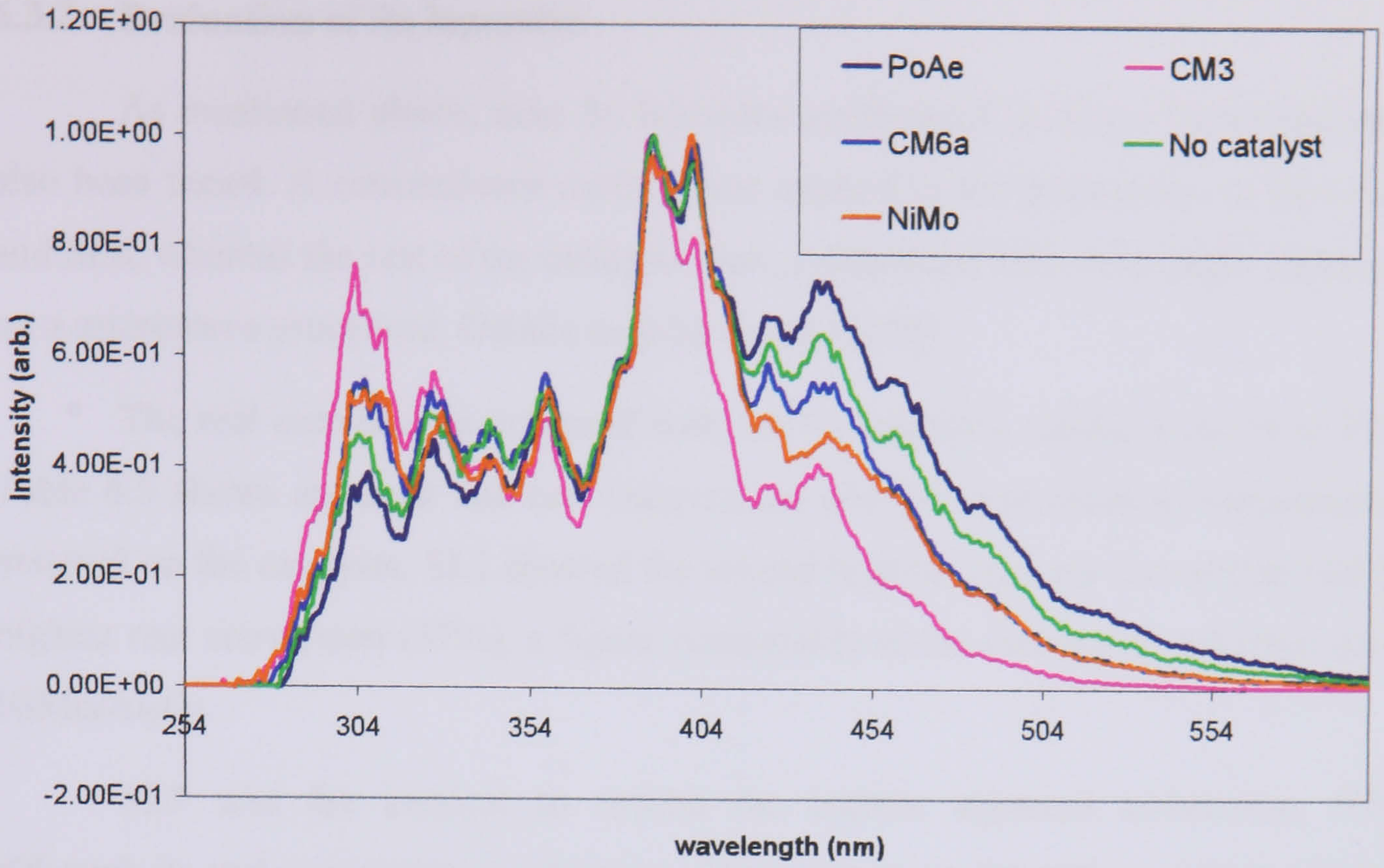


Figure 6.5. Synchronous UV-F spectra of hydrocracking products obtained using CM3, CM6a and NiMo as catalysts. The feed (Point of Ayr extract) and the products from the non-catalytic run are also shown for comparison. All spectra have been peak normalised.

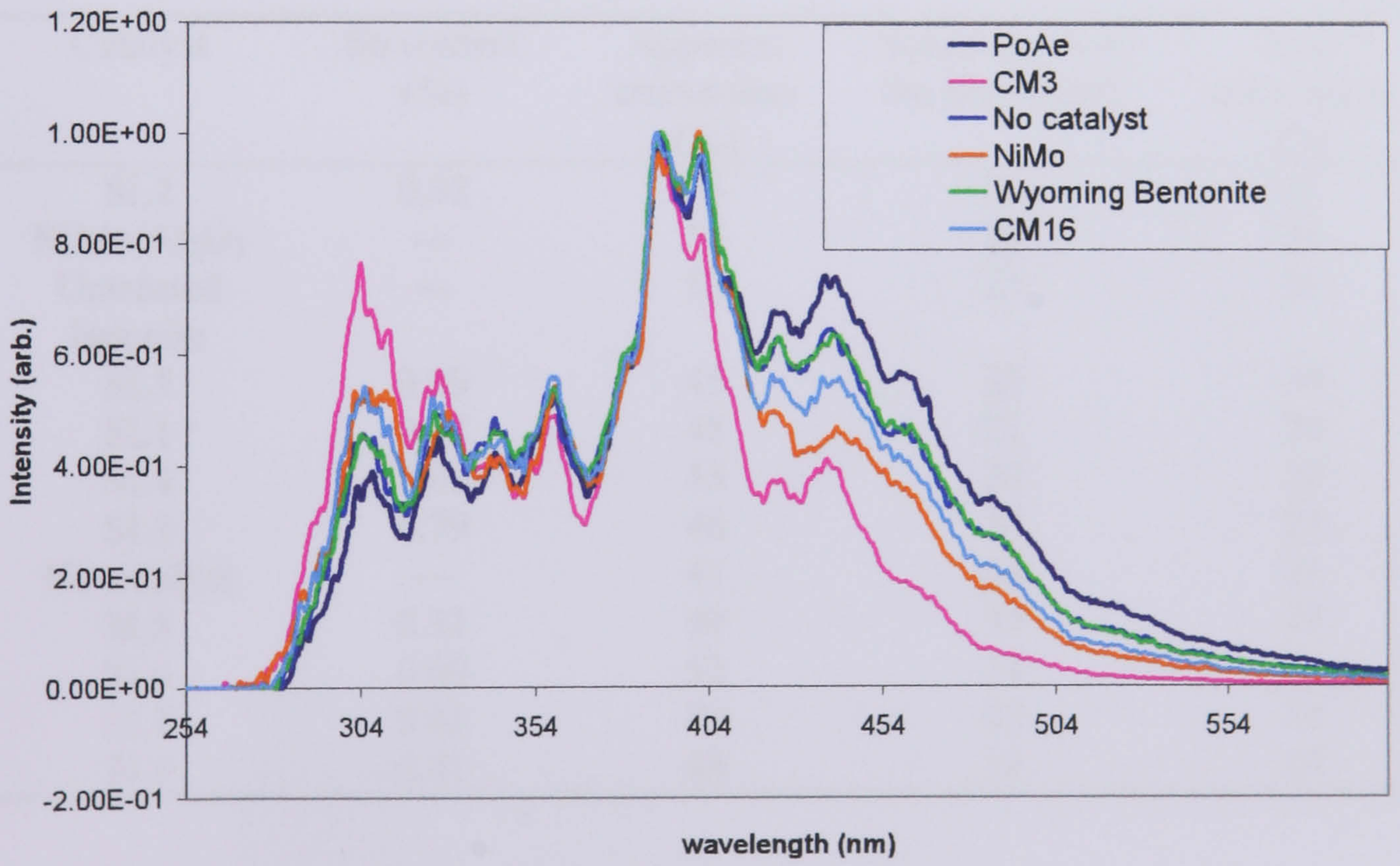


Figure 6.6. Synchronous UV-F spectra of hydrocracking products obtained using CM16 and Wyoming Bentonite (raw clay) as catalysts. The spectra of the feed (Point of Ayr extract) and the products from the runs using CM3, NiMo and no catalyst are also shown for comparison. All spectra have been peak normalised.

6.3.2 Evaluation of Sn laponites

As mentioned above, nine Sn laponites synthesised at Aston University have also been tested. A conventional method was applied in the preparation of SL4, SL5 and SL6, whereas the rest of the catalysts were synthesised following slight variations on a microwave procedure. Details may be found in [98].

The real conversions achieved with the Sn laponites ranged from 15 to 37%. Table 6.3 shows apparent and real conversions and the deposition of carbonaceous material on the catalysts. SL2 showed the second highest apparent conversion and the highest real conversion (37%), a figure comparable to the conversion achieved using $NiMo/Al_2O_3$.

SL7 was the catalyst to exhibit the highest apparent conversion, 59%, although its real conversion is quite low, due to the large deposition of carbonaceous material on the catalyst surface. It accounts for 43% of the filter cake recovered after the experiment or 41% of the initial ">450°C" fraction of the Point of Ayr extract.

Table 6.3. Apparent and real conversions and deposition on the catalysts for tin laponites. The Sn contents of the fresh catalysts shown in this table were supplied by the project partners at Aston University.

Catalyst	Sn content (%)	Apparent conversion (%)	Solids (as % of the filter cake)	Real conversion (%)
SL2	0.32	55	21	37
$NiMo/Al_2O_3$	---	55	26	36
Untreated laponite	---	52	22	32
SL5	0.09	45	25	30
SL1	0.37	48	21	29
SL4	0.09	45	20	28
SL3	0.79	46	24	25
No catalyst	---	41	64	21
SL8	0.31	50	34	21
SL6	0.09	52	34	21
SL7	0.42	59	43	18
SL9	0.41	48	35	15

Even minor differences in the pillaring method led to very different results in terms of conversion of the >450°C material. Moreover, there was lack of repeatability in the synthesis of the Sn laponites as shown below. The hydrocracking conversions

could not be related the Sn contents measured by XPS shown in Table 6.3. XRD has not been suitable to determine the basal spacing in laponites due to the lack of a first order reflection. The small size of individual particles and the random orientation of the clay platelets were pointed out as causing the absence of first order reflection.

As shown in Figure 6.7, Figure 6.8 and Figure 6.9, all catalysts produced a shift in the SEC chromatograms towards longer retention times compared to the original sample. Most Sn laponites showed similar chromatograms with an excluded peak in the vicinity of 16 minutes and a retained peak between 19.5 and 26 minutes with a maximum at 23 minutes. Only two catalysts markedly differed from that trend. They were SL5, which showed a retained peak with lower intensity in the region 20 to 22 minutes, and SL7, whose retained peak appeared shifted towards shorter elution times, closer to the chromatogram of the feed.

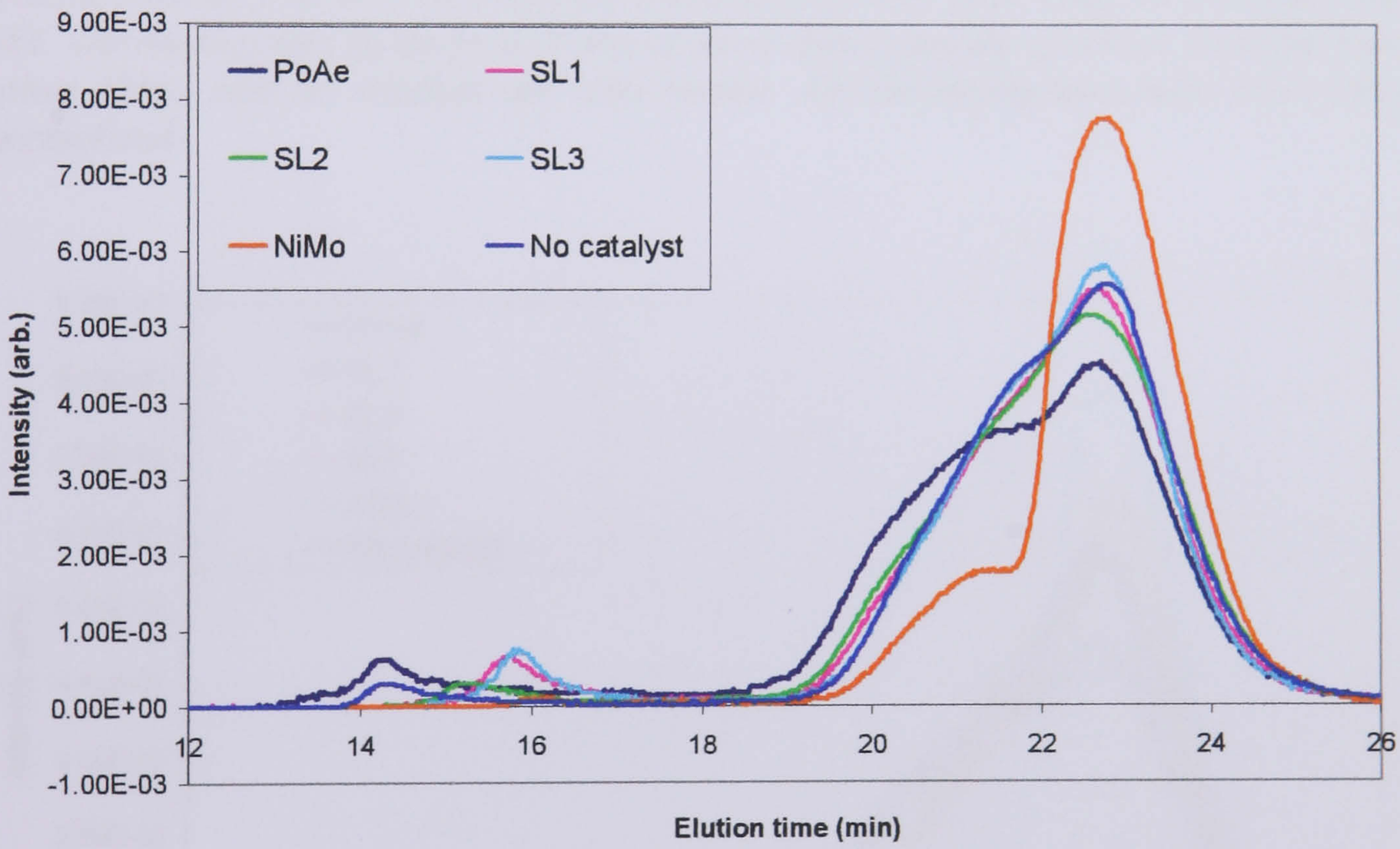


Figure 6.7. Mixed-A column SEC chromatograms of hydrocracking products obtained using SL1, SL2 and SL3 as catalysts. The SEC chromatograms of the feed (Point of Ayr extract) and the products from the runs using NiMo and no catalyst are also shown. All chromatograms have been area normalised.

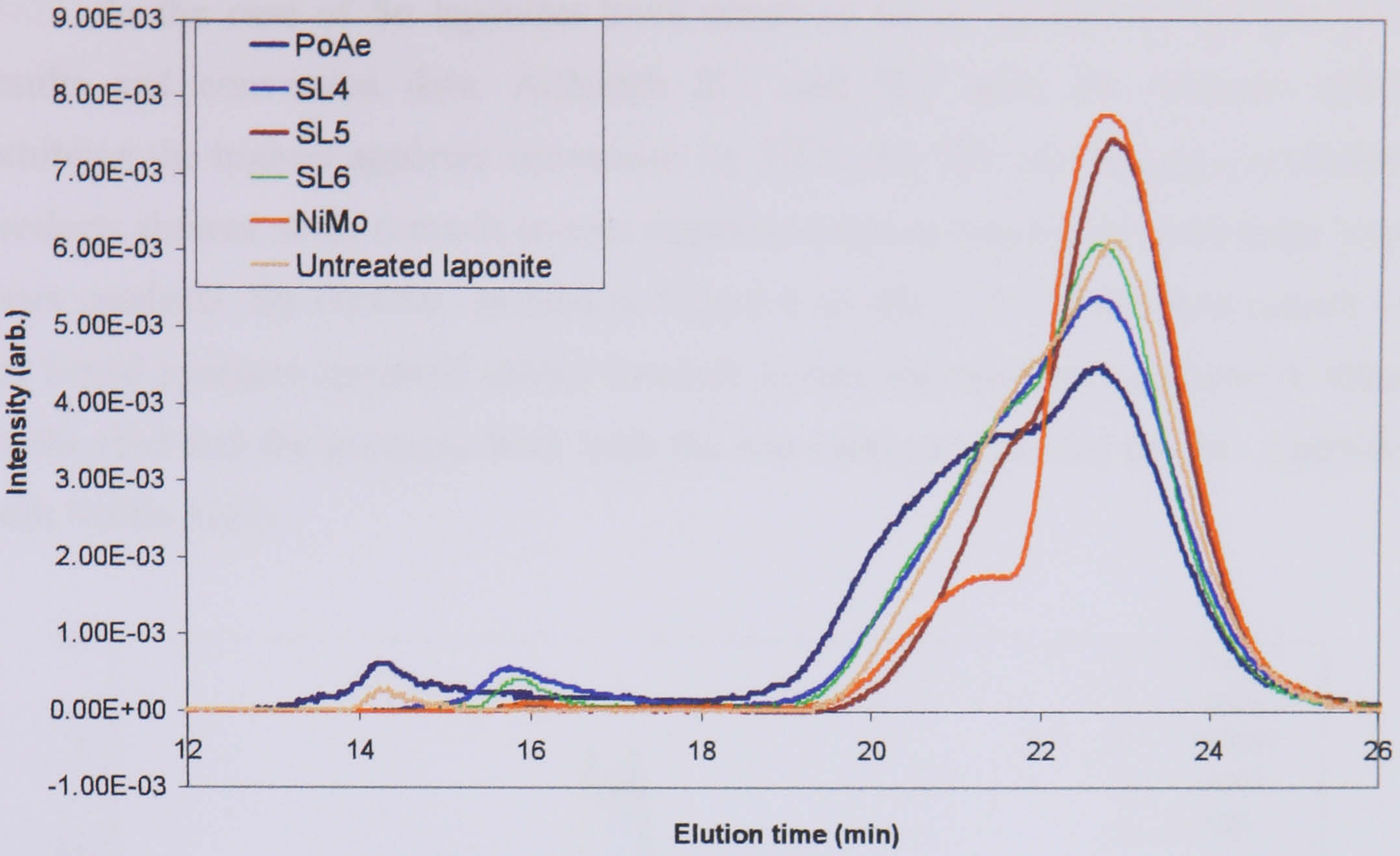


Figure 6.8. Mixed-A column SEC chromatograms of hydrocracking products obtained using SL4, SL5, SL6 and the untreated laponite (raw clay) as catalysts. The SEC chromatograms of the feed (Point of Ayr extract) and the products from the runs using NiMo and no catalyst are also shown. All chromatograms have been area normalised.

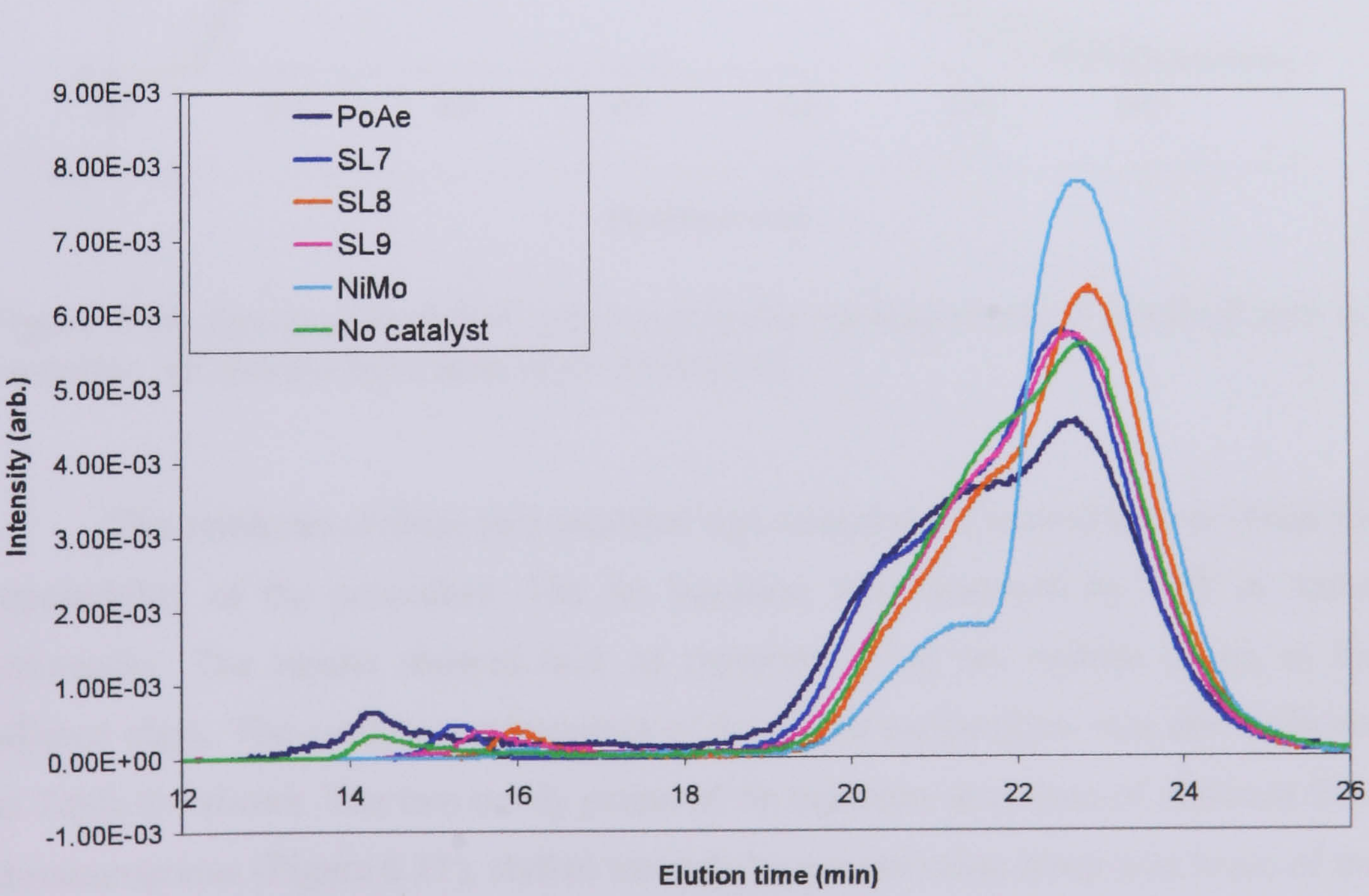


Figure 6.9. Mixed-A column SEC chromatograms of hydrocracking products obtained using SL7, SL8 and SL9 as catalysts. The SEC chromatograms of the feed (Point of Ayr extract) and the products from the runs using NiMo and no catalyst are also shown. All chromatograms have been area normalised.

In the case of Sn laponites there seems to be no agreement between SEC results and conversion data. Although SL2 and SL7 were the catalysts which exhibited the highest apparent conversion by TGA, the SEC chromatograms of their products showed shifts towards shorter retention times in comparison with those from other catalysts. By contrast, as seen in Figure 6.10, the UV-Fluorescence spectra of the liquid products appeared shifted towards shorter wavelengths compared to those of the feed and the products from both the non-catalysed run and the run catalysed with $NiMo/Al_2O_3$.

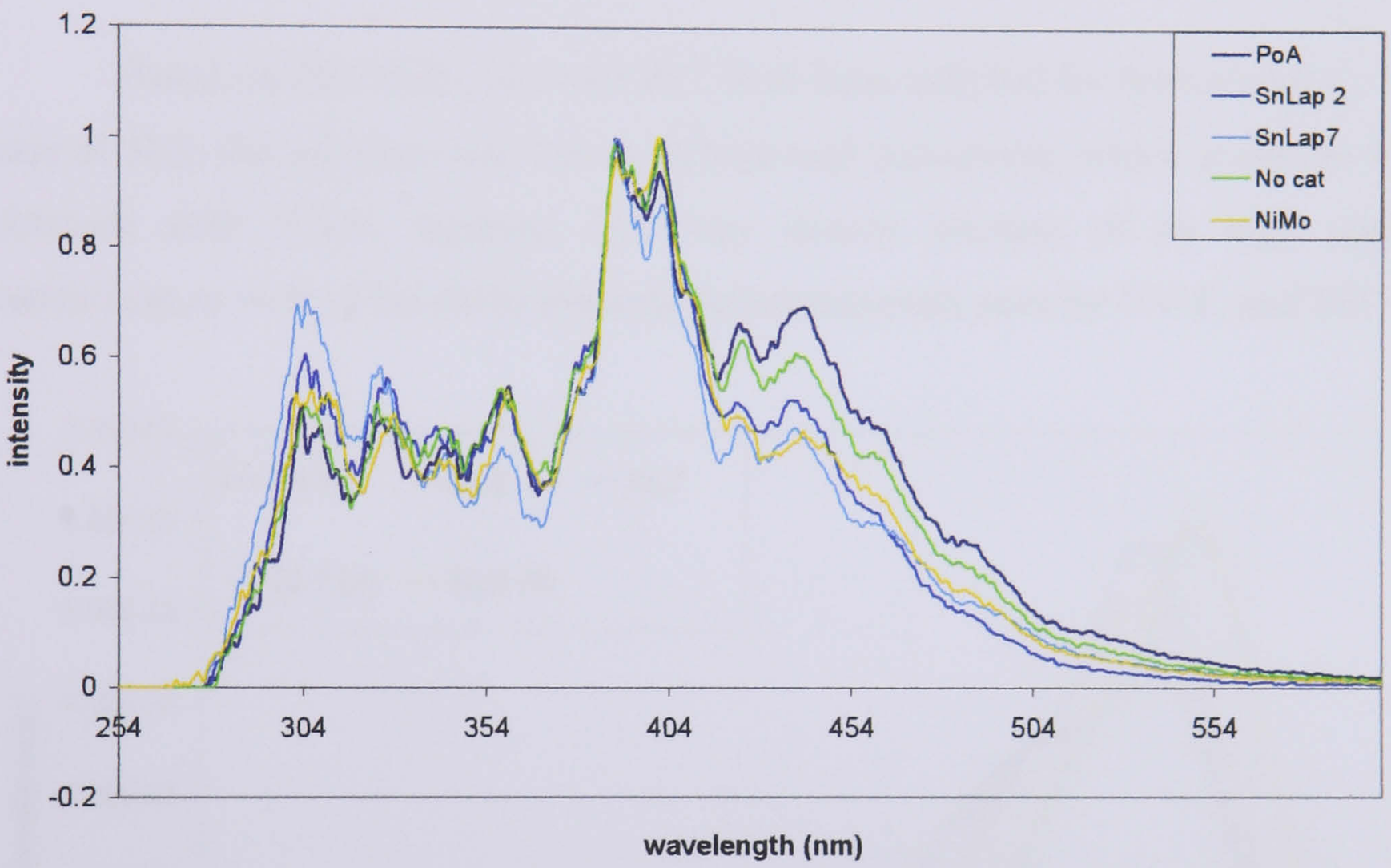


Figure 6.10. Synchronous UV-F spectra of hydrocracking products obtained with tin laponites. All spectra have been peak normalised.

The synthesis of these two catalysts was carried out a second time to check the repeatability of the procedure. The Sn laponites were analysed by XPS at Aston University. The results showed lack of repeatability in the amount of tin in the pillared clays. The catalytic performance of these new preparations was also different as Table 6.4 shows. The two newly prepared Sn laponites also showed different SEC chromatograms (Figure 6.11), shifted towards longer retention times than those of the initial preparations. At this stage of their development, this lack of repeatability is a major obstacle to the utilisation of Sn laponites as hydrocracking catalysts.

Table 6.4. Conversions and carbonaceous deposition on the catalyst for two preparations of Sn laponites 2 and 7. The Sn content in the fresh catalyst measured by XPS has been provided by our partner group at Aston University.

Catalyst	Sn content (% fresh catalyst weight)	Apparent conversion (%)	Carbonaceous Deposits (as % of the recovered solids)	Real conversion (%)
SL2	0.319	55	21	37
SL2 (II)	0.551	45	27	21
SL7	0.419	59	43	18
SL7 (II)	0.450	54	32	23

Based on this study, SL2 and SL7 have been selected for further testing. In the case of SL2, the selection was due to its high real conversion, which is similar to that obtained with NiMo, whereas SL7 was chosen because of its high apparent conversion as well as the shifts towards lighter materials seen by UV-F, and SEC.

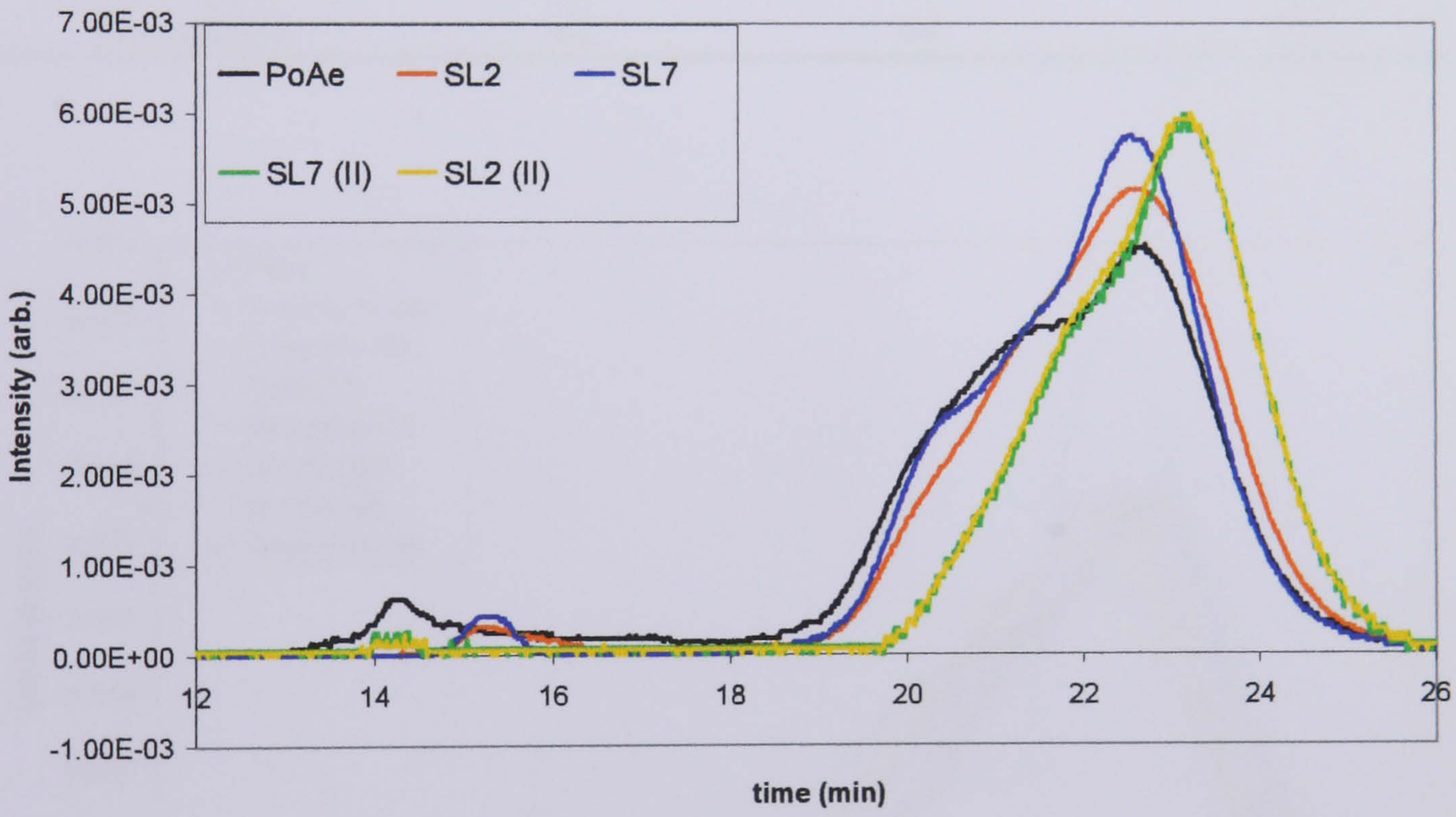


Figure 6.11. Mixed-A column SEC chromatograms of hydrocracking products obtained using two different preparations of SL2 and SL7. All chromatograms have been area normalised.

6.3.3 Evaluation of other catalysts

The other catalysts tested were Eu montmorillonite, Ce montmorillonite, Ce-Cr montmorillonite and Cr laponite. The three montmorillonites are novel catalysts

which had not been tested by Begon while some preparations of Cr laponite were tested within that project (Begon et. al. [70, 71]). All catalysts showed conversions significantly higher than the no-catalyst run. In particular, Eu montmorillonite and Ce montmorillonite exhibited high real conversions, near that of the reference catalyst, NiMo (see Table 6.5).

Table 6.5. Apparent and real conversions and deposition on the catalysts for several pillared clays.

Catalyst	Apparent conversion (%)	Carbonaceous solids (as % of the filter cake)	Real conversion (%)
$NiMo/Al_2O_3$	55	26	36
Eu montmorillonite	51	23	33
Untreated laponite	52	22	32
Ce montmorillonite	47	23	30
Cr laponite CL1a	54	29	28
Ce-Cr montmorillonite	50	28	25
Na montmorillonite	47	28	24
Cr laponite CL B61	48	31	23
No catalyst	41	64	21

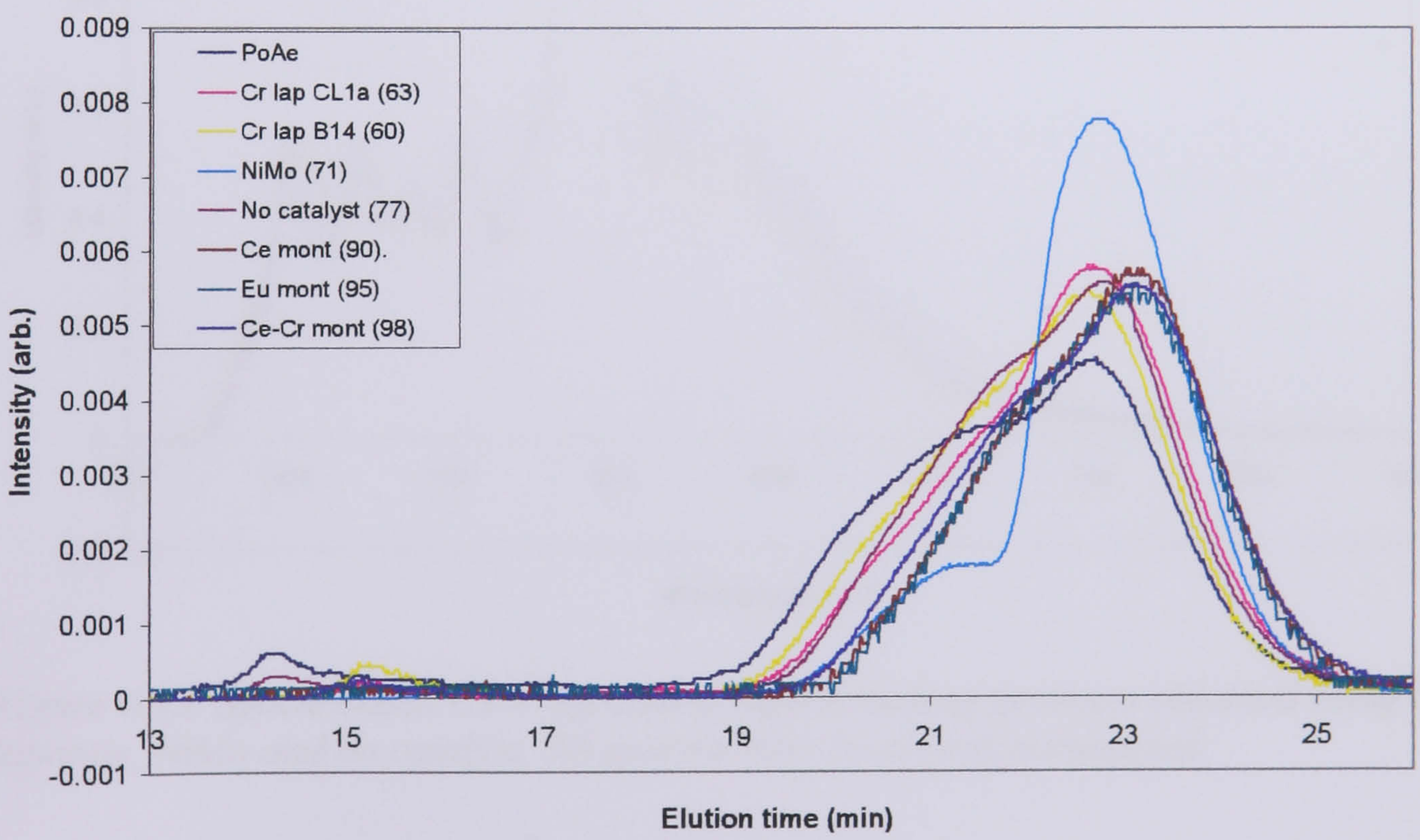


Figure 6.12. Mixed-A column SEC chromatogram of hydrocracking products obtained with several pillared clays. All chromatograms have been area normalised.

The relatively higher apparent conversions of the Ce and Eu montmorillonites parallel the SEC results. The three montmorillonites showed large shifts of the SEC chromatogram towards longer elution times (Figure 6.12). Those shifts are comparable to the product distribution obtained with the $NiMo/Al_2O_3$ catalyst. The retained peaks appeared at slightly longer times than in the distribution obtained with NiMo and the excluded peak has almost completely disappeared. On the other hand, the Cr laponites did not perform substantially better than the no-catalyst run, although they were able to shift the excluded peak towards longer retention times.

The UV-fluorescence spectra of the two Cr laponites shown in Figure 6.13 exhibited intermediate shifts between that obtained with NiMo at shorter wavelengths and those of the feed and of the no-catalyst run at longer wavelengths. The Cr laponite CL1a showed a better performance than the Cr laponite B14, which is in agreement with observations from SEC.

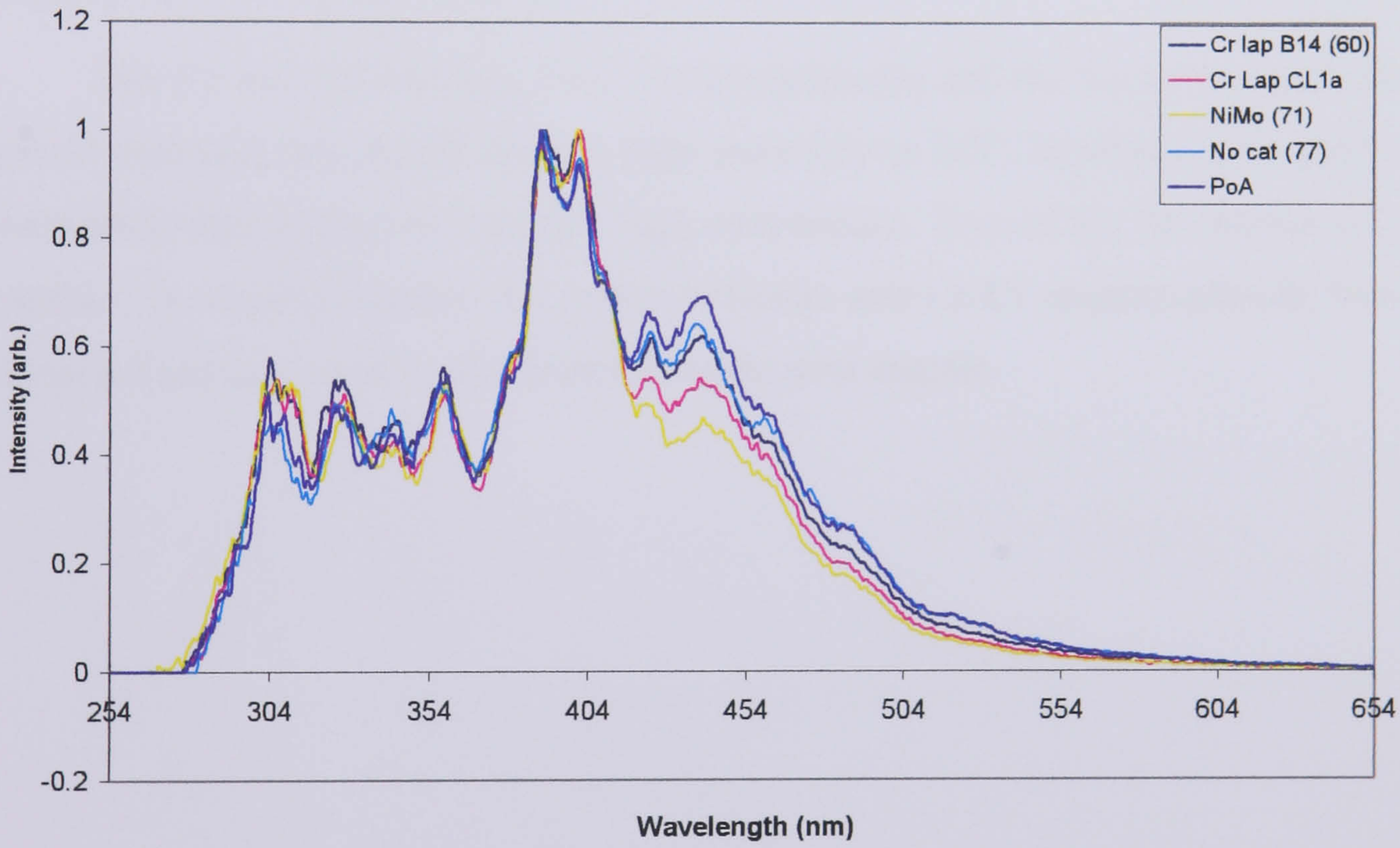


Figure 6.13. Synchronous UV-F spectra of hydrocracking products obtained using Cr laponite, NiMo and no catalyst. All spectra have been peak normalised.

6.4 CONCLUSIONS

A number of pillared clays have been tested as catalysts to hydrocrack a coal extract from the Point of Ayr pilot plant. The catalysts tested consisted of several Cr montmorillonites and Sn laponites, a Cr laponite, and Eu, Ce, and Ce-Cr

montmorillonites. The Cr montmorillonites and Sn laponites exhibited different activities depending on the method followed in their preparation. CM3, a Cr montmorillonite synthesised from Na montmorillonite by a conventional method, showed higher apparent and real conversions and lighter products by SEC and UV-F than the rest of Cr montmorillonites. It was selected for further studies along with CM6a, which performed better than the other Cr montmorillonite synthesised from Wyoming Bentonite.

The lack of repeatability in the synthesis of the Sn laponites was a major difficulty faced in their study. The conversions achieved with them as catalysts spanned a large range. Some formulations showed an activity similar to that of the $NiMo/Al_2O_3$ while the conversions obtained with others were lower than that of the non-catalysed run. To date, no straightforward relation between catalytic activity and catalyst properties has been found.

The Ce montmorillonite, Ce-Cr montmorillonite and the Eu montmorillonite showed relatively large shifts towards light materials by SEC. In addition, Ce and Eu montmorillonites exhibited relatively high conversions. Two of the Sn laponites, Cr laponite, Ce montmorillonite, Eu montmorillonite and Ce-Cr montmorillonite were also tested at longer time scales described in the next chapter.

7 PILLARED CLAYS AS HYDROCRACKING CATALYSTS: TESTS WITH REUSED CATALYSTS

7.1 INTRODUCTION

The previous chapter described a series of screening tests on pillared clay catalysts. They included chromium laponite, cerium, cerium-chromium and europium montmorillonite and several chromium montmorillonites and tin laponites prepared by diverse methods. Those tests involved two-hour experiments where fresh catalysts were used in every case to hydrocrack the Point of Ayr coal extract. Two among the Cr-montmorillonites and two among the Sn laponites have been identified as the most promising catalysts and have been selected for further testing together with the Cr laponite and the Eu, Ce and Ce-Cr montmorillonites. The catalysts coated with carbonaceous material recovered from the first series of runs have been reused in another set of two-hour long experiments.

7.2 EXPERIMENTAL

The filter cake obtained in the first series of runs containing the catalysts and its deposits was washed with a 4:1 mixture of $CHCl_3$ and CH_3OH and dried in a vacuum oven for 3 hours at 60°C. In the second series of runs, 250 mg of the coated catalysts were used to hydrocrack 1 gram of Point of Ayr extract, the same feed used in the previous experiments.

The reaction conditions and procedures applied were the same as those followed in earlier experiments and described in Chapter 3. Briefly, the hydrocracking reaction was carried out at 190 bar hydrogen pressure and 440°C. The products were collected with the chloroform methanol mixture and filtered. The liquid was dried in a rotary evaporator to remove the solvent. SEC, UV-F and TGA analyses were carried out on the liquid products. The carbonaceous content of the "coated" solids was determined by TGA. The amount of new deposits was calculated applying equation 3.4.

7.3 RESULTS AND DISCUSSION

7.3.1 Evaluation of the Cr montmorillonites

The CM3 and CM6a catalysts coated with carbonaceous material recovered from the runs described in the previous chapter have been reused. The reference catalyst, $NiMo/Al_2O_3$, and the two raw clays, Na montmorillonite and Wyoming Bentonite have also been reused.

Table 7.1 shows the conversions achieved in experiments using the coated catalysts. Results from the experiments with fresh catalysts described in the previous chapter have also been included for comparison. Some general patterns in the catalyst behaviour can be distinguished from these experiments. First, the real conversion has always increased in the second use of the catalysts. In some cases this increase has been remarkable as for CM3 and the two raw clays, whereas it has been smaller but noticeable in CM6a and $NiMo/Al_2O_3$. Second, all catalysts have shown a sharp drop in the amount of new carbonaceous solids deposited during the second run compared to the first one. All catalysts had exhibited a high level of carbonaceous deposition after the first use, which ranged between 26 and 35% of the filter cake. It was expected that some sort of saturation of the adsorbing positions would take place leading to a drop in the amount of new material depositing during the second run. Both Cr montmorillonites, but mainly CM3 exhibited very low increases in the amount of deposits, 4% of the solids recovered after the experiment in the case of the CM3. This increase was relatively higher for the rest of the catalysts (above 10%).

On the other hand, the catalysts presented differences in the trends followed by the apparent conversion. It decreased in the second use of the CM3 and CM6a and remained almost constant for the rest of the catalysts. This is probably linked to the lower deposition on the two Cr montmorillonites. This lower deposition makes a larger part of the "$>450°C$" fraction remain in the liquid and, therefore, to decrease the value of the apparent conversion even though the real conversion increases.

The CM3 catalyst showed the same real conversion as the $NiMo/Al_2O_3$ (45%). This supports the results from the first run showing a relatively high catalytic activity towards the hydrocracking of coal derived materials. The two raw clays also showed certain catalytic activity after 4 hours, although it was lower than that of CM3. Na montmorillonite and Wyoming Bentonite presented similar performances in terms of

conversions, and both of them hydrocracked a larger fraction of the ">450°C" material than the CM6a.

Table 7.1. Apparent and real conversions and recovered solids for various reused catalysts.

Catalyst	Use	Apparent conversion (%)	Solids (as % of the filter cake)	Real conversion (%)
CM3	1st	64	35	29
	2nd	48	4	45
CM6a	1st	50	27	27
	2nd	39	9	33
$NiMo/Al_2O_3$	1st	55	26	36
	2nd	59	16	45
Wyoming Bentonite	1st	44	26	23
	2nd	48	14	38
Na montmorillonite	1st	47	28	24
	2nd	45	10	40
No catalyst	---	41	64	21

Figure 7.1 and Figure 7.2 show the SEC chromatograms of liquid products from the reactions catalysed by the reused CM3, $NiMo/Al_2O_3$ and Na montmorillonite. Chromatograms of the Point of Ayr extract and its hydrocracking products obtained using no catalyst are also shown for comparison. The excluded peak has been removed and the retained peak has shifted towards longer elution times (smaller sizes) than those of the feed and the non-catalysed reaction for all products, regardless of the catalyst employed. The opposite happened when reusing CM3 and Na montmorillonite. In these cases the reused catalyst produced smaller shifts towards larger sizes than the fresh one.

The SEC behaviour of CM6a is illustrated in Figure 7.3. Products from the first and second runs showed very similar chromatograms. The excluded peak was shifted towards longer retention times and it was smaller than that of the feed, although it did not completely disappear as happened when using CM3 or the $NiMo/Al_2O_3$. The product distribution using Wyoming Bentonite also appeared at larger sizes than that of the other raw clay, the Na montmorillonite.

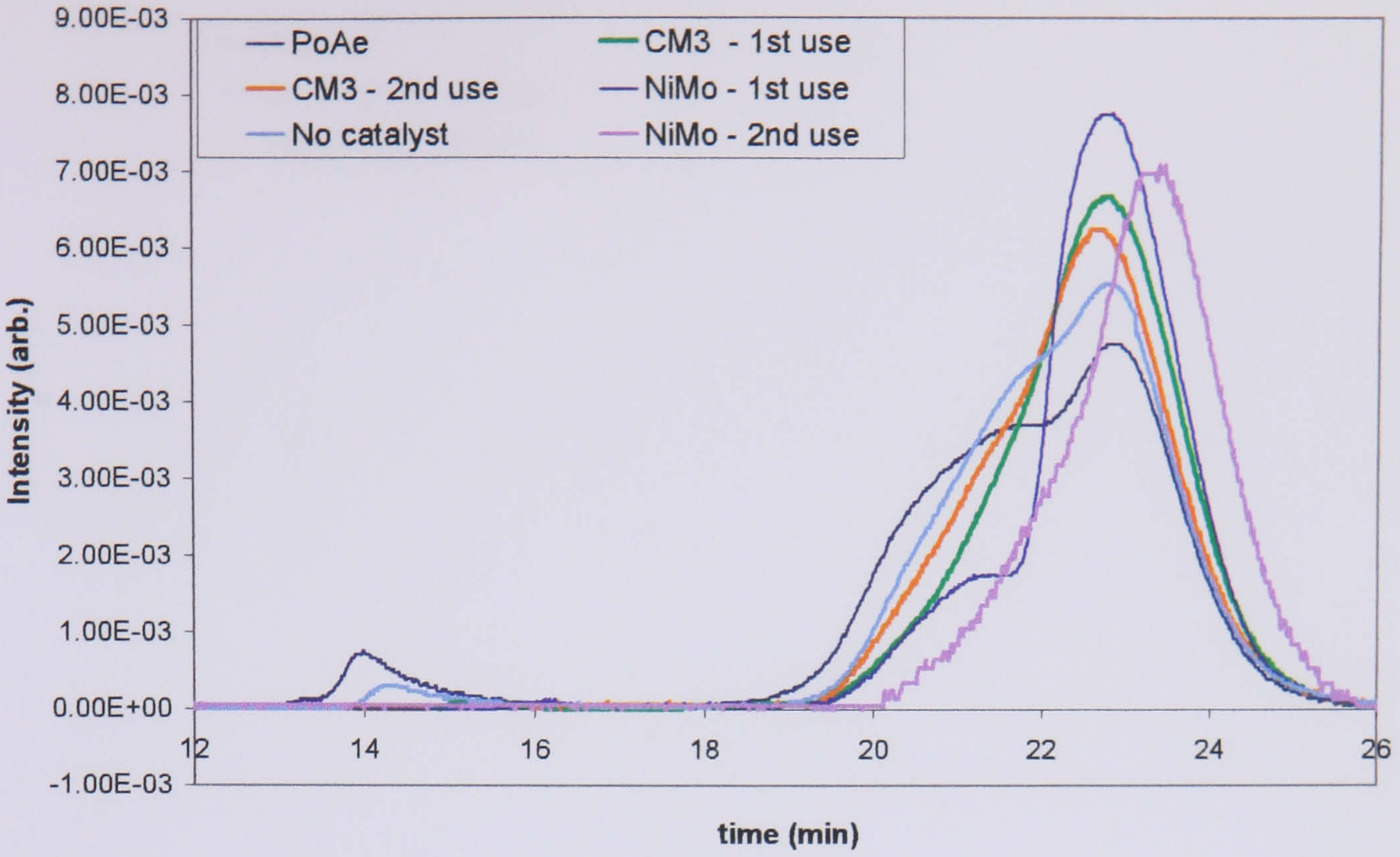


Figure 7.1. Mixed-A column SEC chromatogram of the hydrocracking products obtained using CM3, no catalyst and NiMo. All chromatograms have been area normalised.

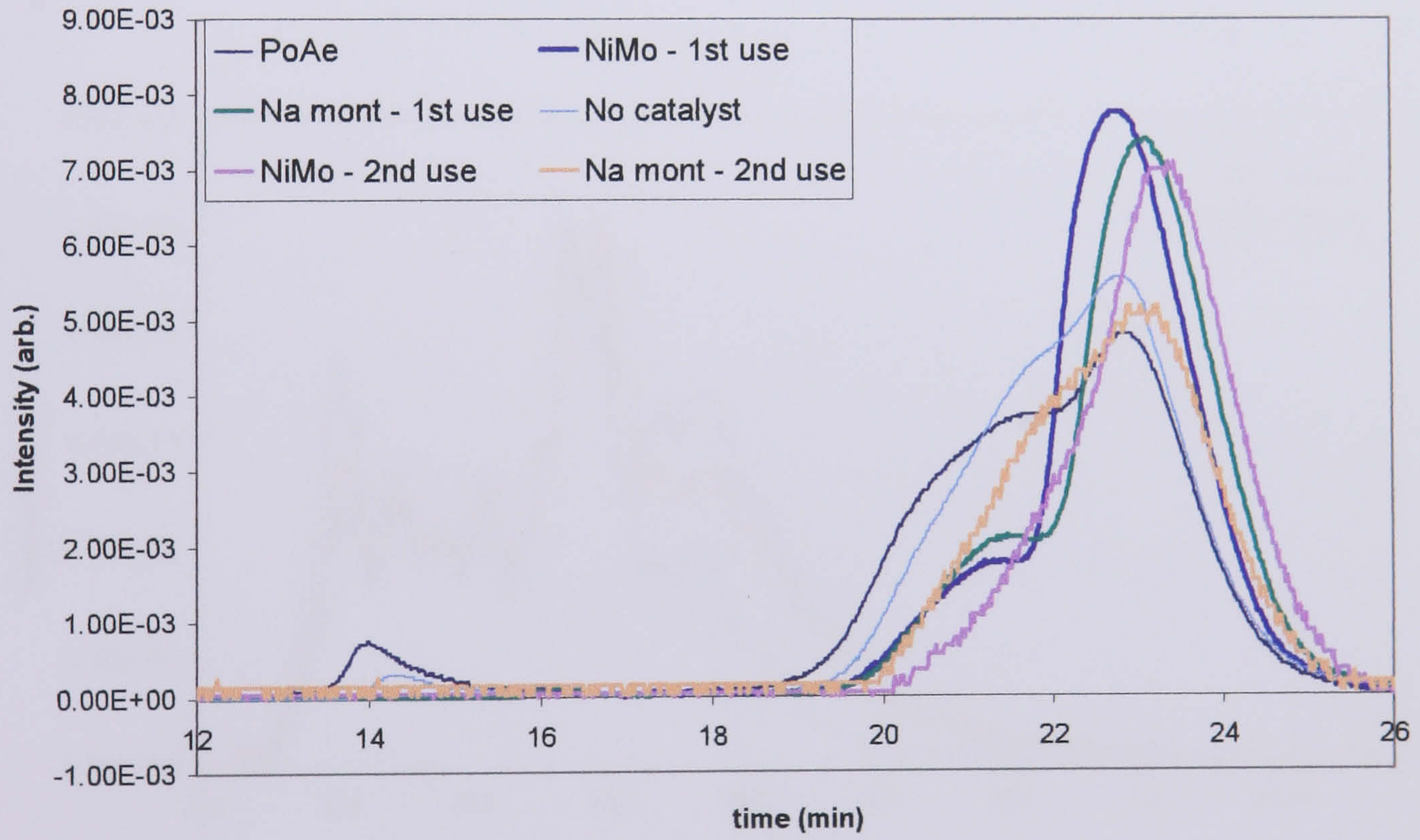


Figure 7.2. Mixed-A column SEC chromatogram of the hydrocracking products obtained using Na montmorillonite and NiMo. All chromatograms have been area normalised.

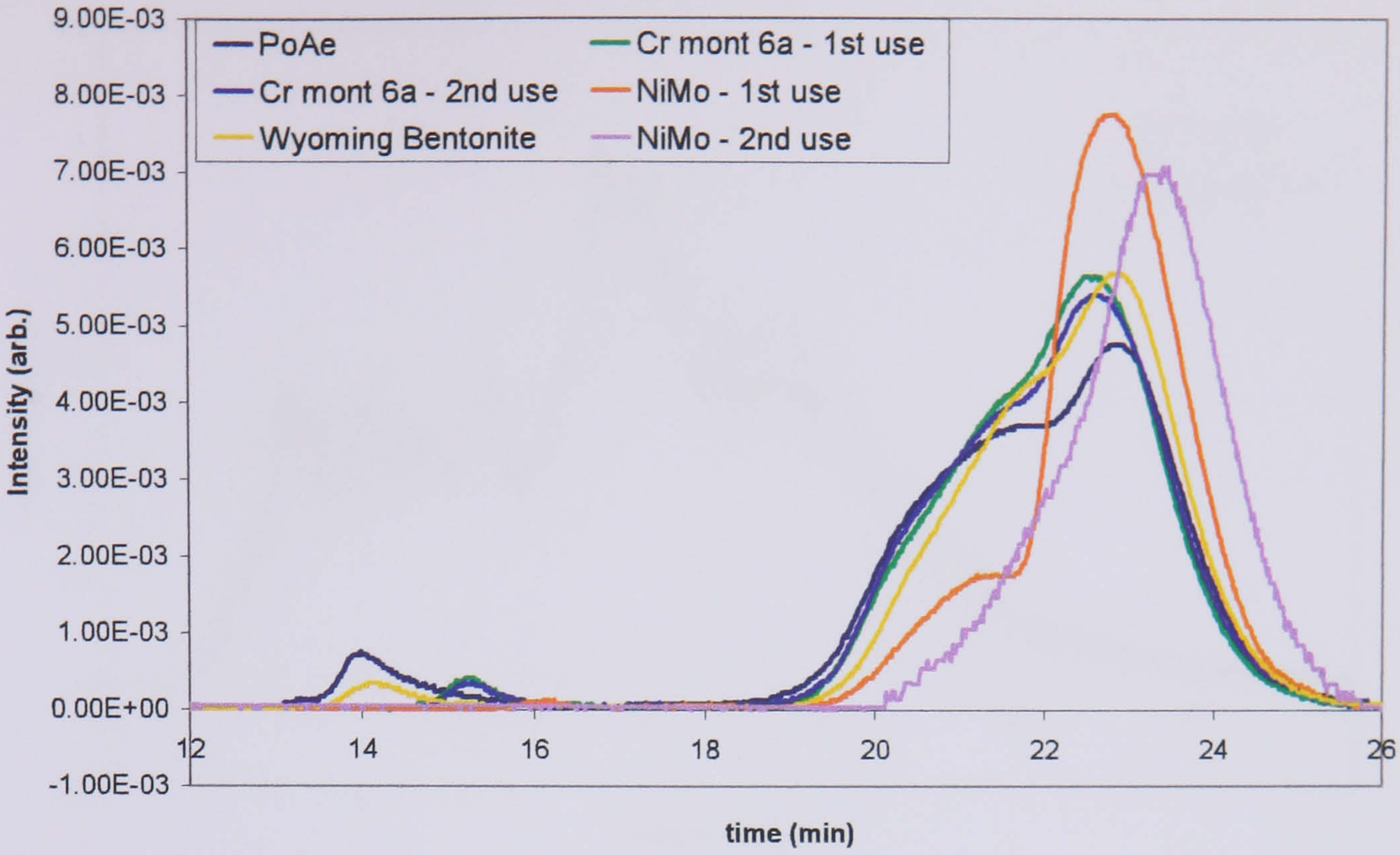


Figure 7.3. Mixed-A column SEC chromatogram of the hydrocracking products obtained using CM6a, Wyoming Bentonite and NiMo. All chromatograms have been area normalised.

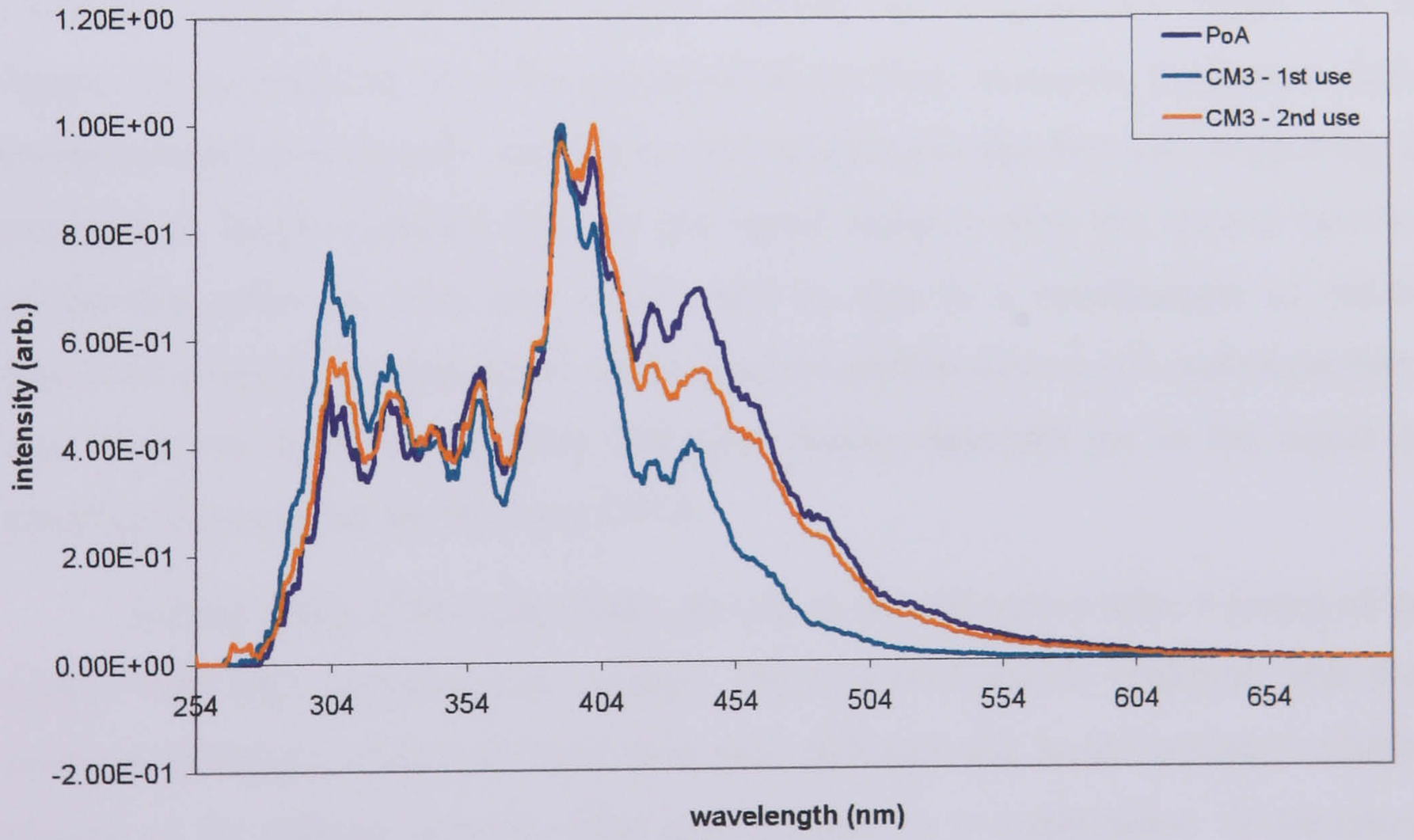


Figure 7.4. Synchronous UV-F spectra of hydrocracking products obtained with fresh and reused CM3 as catalysts. All spectra have been peak normalised.

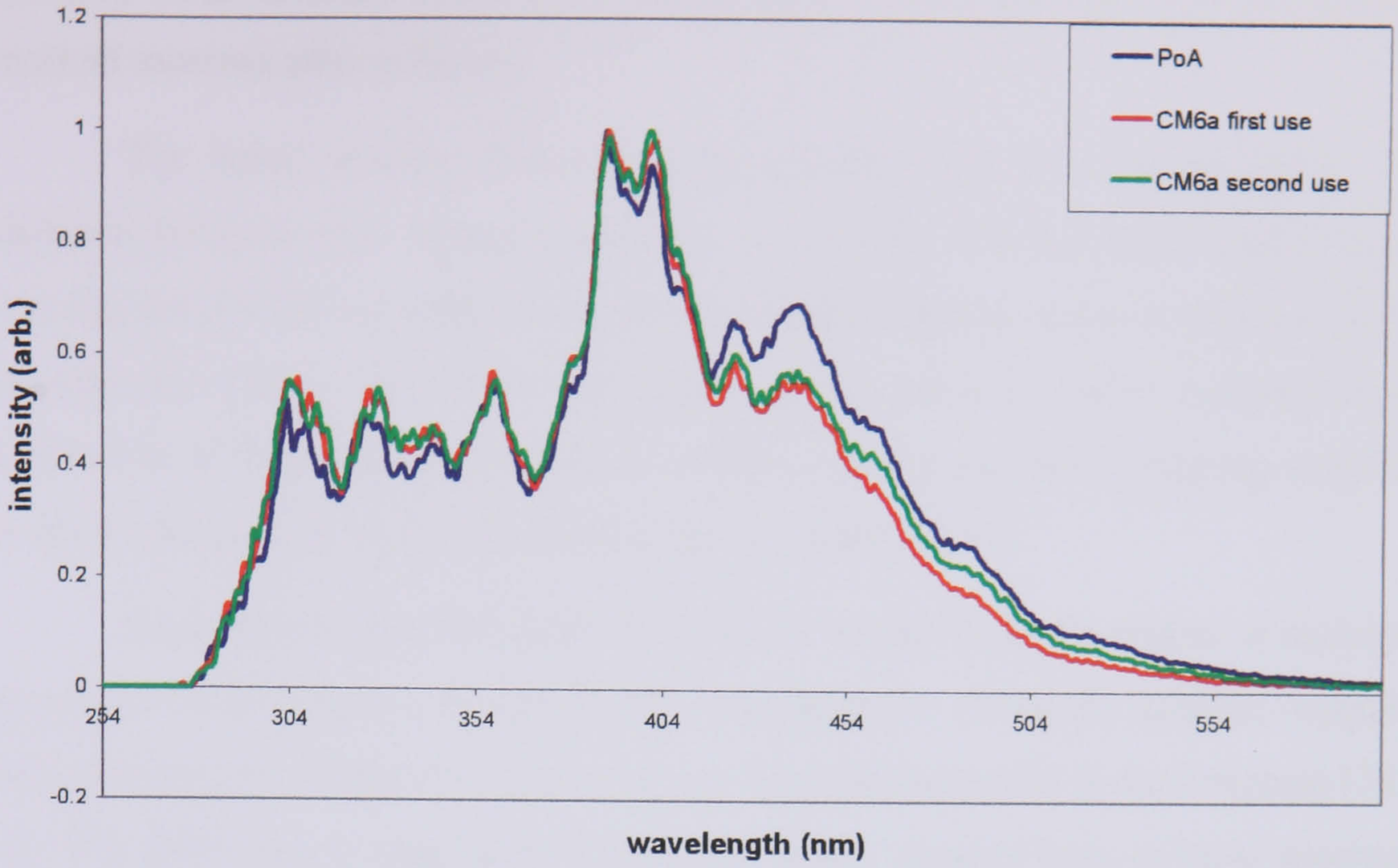


Figure 7.5. Synchronous UV-F spectra of hydrocracking products obtained with fresh and reused CM6a as catalysts. All spectra have been peak normalised.

The synchronous UV-Fluorescence spectra of the products from the reused CM3 and CM6a showed shifts towards shorter wavelengths (see Figure 7.4 and Figure 7.5 respectively) than the spectrum of the feed. However, both were shifted towards longer wavelengths than those corresponding to the first use, suggesting the presence of larger aromatic rings in the liquid samples after the second two-hour period than after the first use. This could be due to a combination of catalyst deactivation and lower deposition on the catalyst surface when a pre-coated catalyst is used. A lower deposition implies that more heavy materials are in the liquid and therefore are analysed by SEC and UV-F.

Summarising, CM3 and CM6a proved to be still active after 4 hours of use, despite their high carbonaceous content. The real conversions achieved with these catalysts increased relative to their first use, although the liquid products obtained seemed to be slightly heavier. This may be due to a combination of decreasing catalytic activity and lower deposition levels which leave a larger part of the ">450°C" fraction in solution.

No correlation between catalytic activity and catalyst properties has been found. Despite exhibiting a lower surface area, smaller basal spacing and lower ion

content, CM3 seemed to be more active than CM6a. The surface area showed a marked increase after pillaring.

The basal spacing shown by the pillared clays is a measurement of the distance between two consecutive layers in the clay. On the other hand, the basal spacing did not change when Na in the Na montmorillonite was exchanged with Cr to produce the CM3. The CM6a basal spacings measured by X-ray diffraction at the University of Birmingham seemed to collapse during the hydrocracking experiment to give a mixture of shorter basal spacings, 16.3 and 19.9 Å.

Basal spacings of the order of 15-25 Å, would be in the region of micropores or small mesopores according to IUPAC classification. These are small in comparison with the pore size values of hydrocracking catalysts described in the literature [13, 20, 31, 37]. However, it must be noted that the values reported here as basal spacing are not equivalent to pore diameter. They only measured the separation between clay layers, whereas the pore diameters are also affected by the distance between pillars. The pore diameter distribution of CM3 obtained by surface area measurement will be presented in the next chapter, along with results from scanning electron microscopy.

Table 7.2. Characteristics of fresh catalysts. Values supplied by the project partners at Aston University.

Compound	Raw Clay	BET Surface area (m^2/g)	Basal Spacing (Å)	Cr content (%)
CM3	Na montmorillonite	174	15.9	2.61
CM6a	Wyoming Bentonite	253	22.4	4.52
Na montmorillonite	---	51	15.9	---
Wyoming Bentonite	---	39	15.2	---

7.3.2 Evaluation of the Sn laponites

The catalysts SL2 and SL7 have also been reused and their conversions are shown in Table 7.3. They showed opposite trends. SL2 had achieved a high conversion in the first series of runs, but it completely lost its activity in the second use. The amount of new solids generated reusing this catalyst (in addition to the deposition during the first use) was very high: 37% of the filter cake. The low real

conversion achieved with the reused catalyst also provided evidence on the deactivation suffered by SL2.

Table 7.3. Apparent and real conversions and recovered solids for various reused catalysts.

Catalyst	Use	Apparent conversion	Solids	Real conversion
SL2	1st	55	21	37
	2nd	51	37	20
SL7	1st	59	43	18
	2nd	40	3	38
$NiMo/Al_2O_3$	1st	55	26	36
	2nd	59	16	45
Untreated laponite	1st	52	22	32
	2nd	53	19	38
No catalyst	---	41	64	21

By contrast, SL7 exhibited a marked decrease in the amount of carbonaceous solids deposited on the catalyst during the second run. The conversion of the ">450°C" material increased from 18% in the first run to 38% in the second.

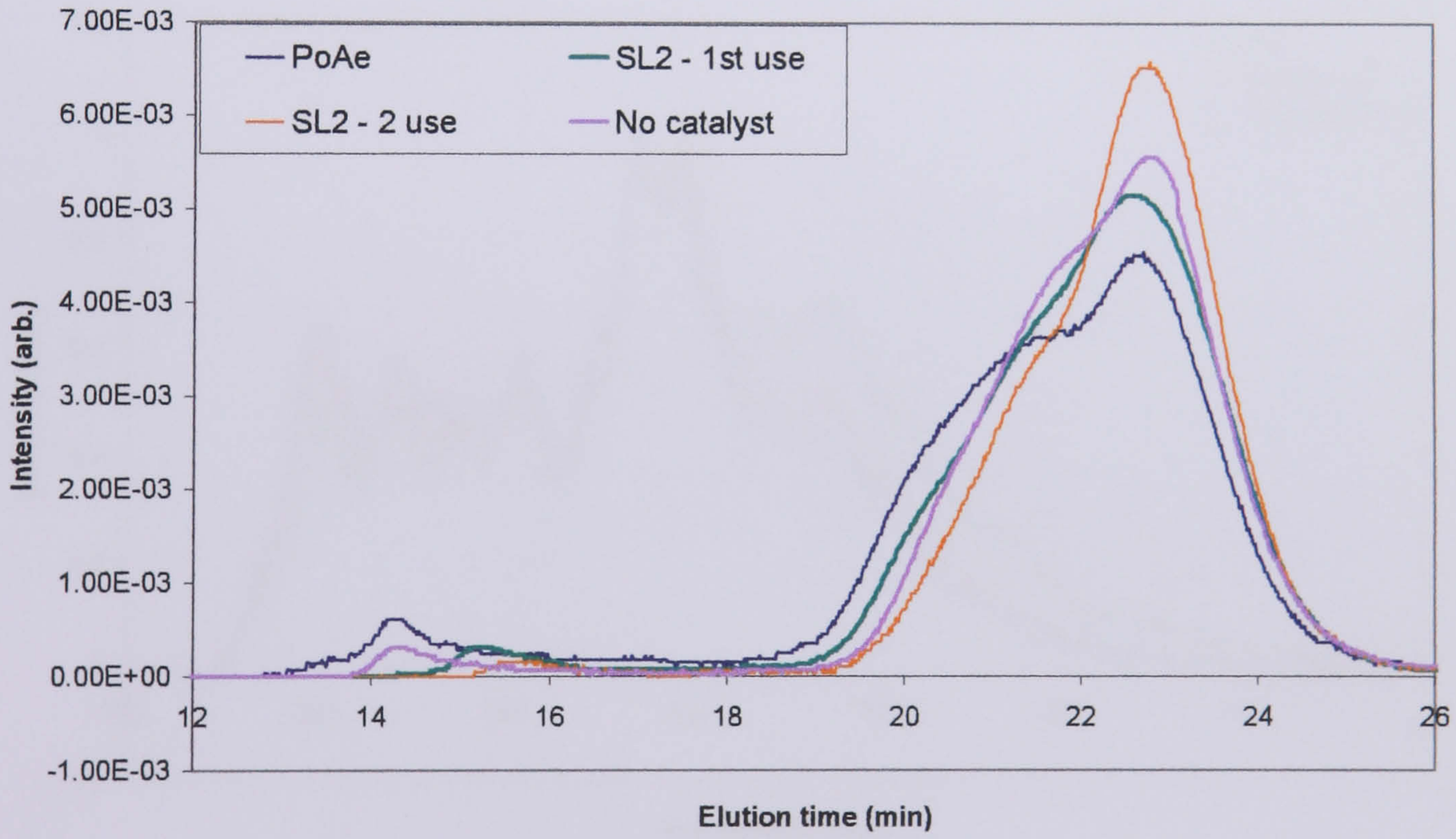


Figure 7.6. Mixed-A column SEC chromatogram of hydrocracking products obtained with SL2 (fresh and reused) as catalyst. All chromatograms have been area normalised.

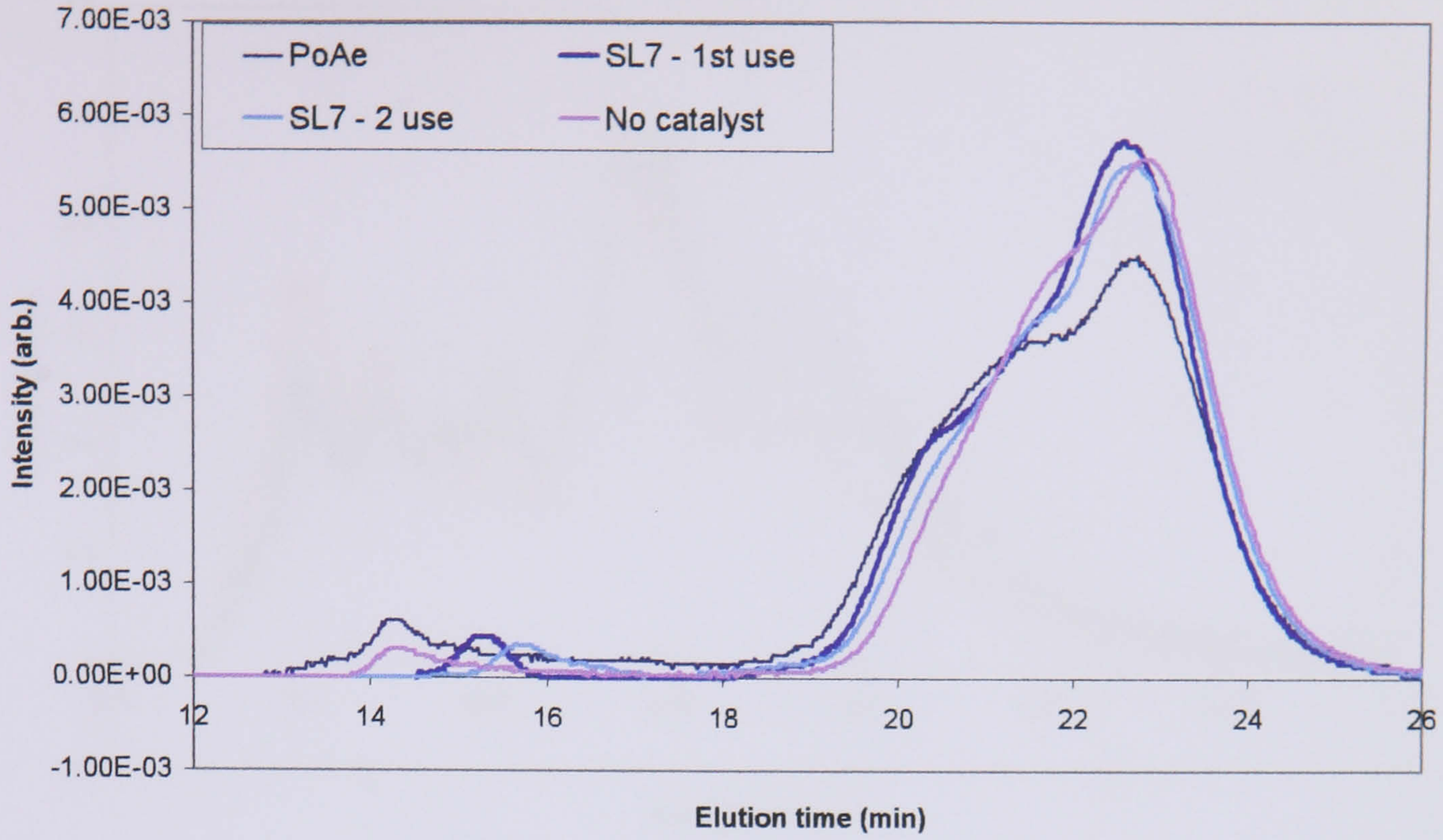


Figure 7.7. Mixed-A column SEC chromatogram of hydrocracking products obtained with SL7 (fresh and reused) as catalyst. All chromatograms have been area normalised.

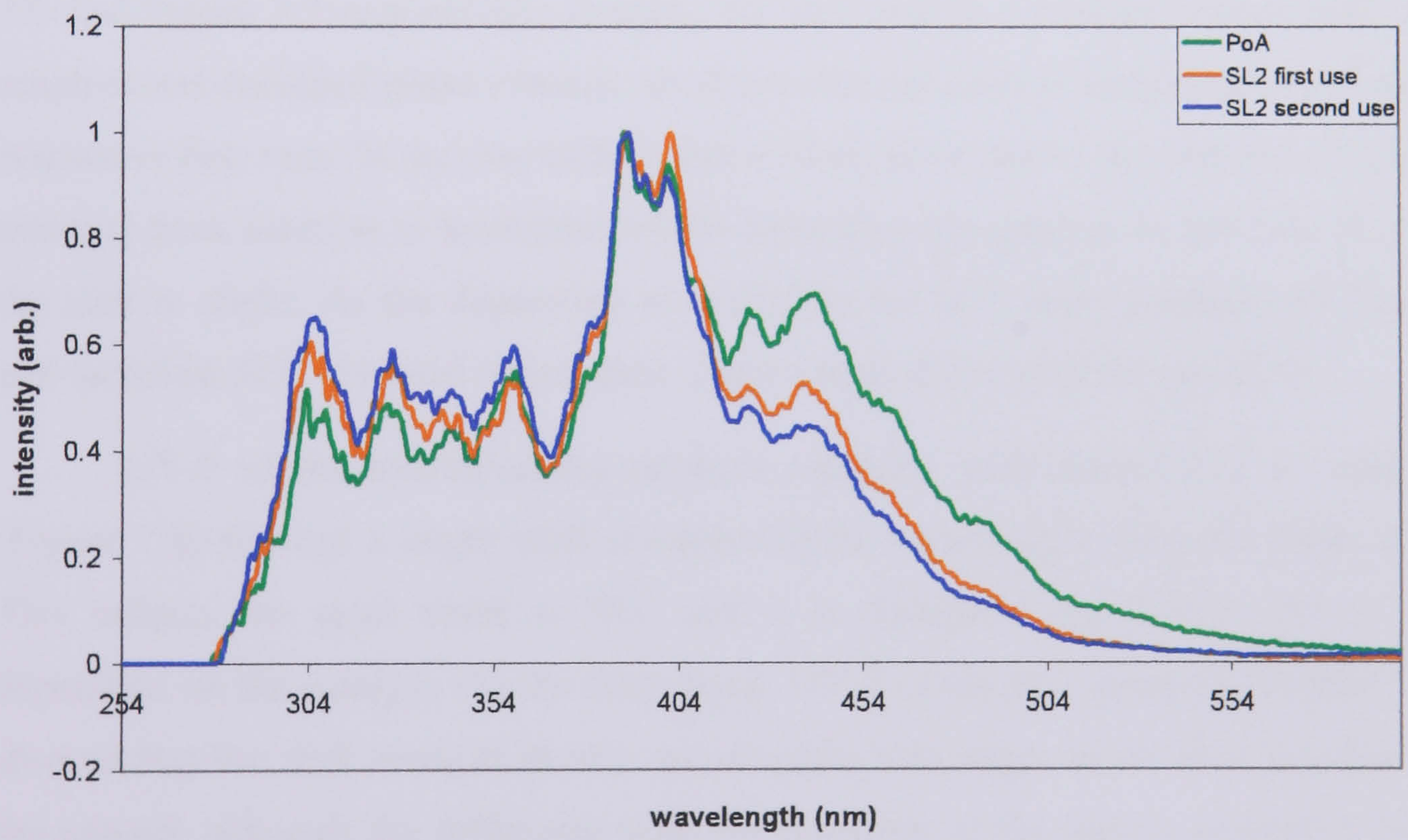


Figure 7.8. Synchronous UV-F spectra of hydrocracking products obtained using fresh and reused SL2. All spectra have been peak normalised.

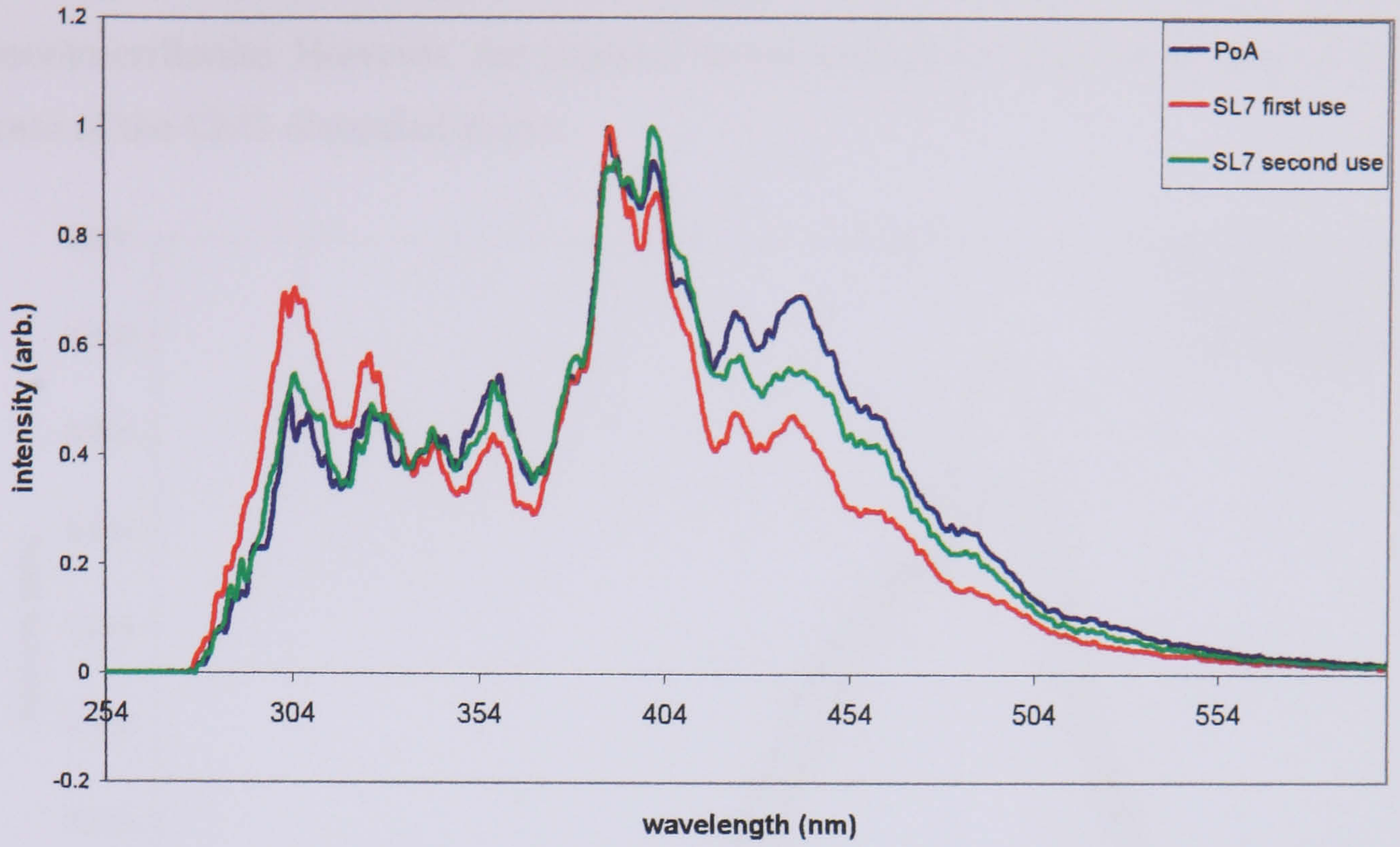


Figure 7.9. Synchronous UV-F spectra of hydrocracking products obtained using fresh and reused SL7. All spectra have been peak normalised.

The SEC chromatograms of products from SL2 and SL7 are shown in Figure 7.6 and Figure 7.7 respectively. Reusing the SL2 and SL7 catalyst shifted both the retained and excluded peaks towards smaller molecular sizes in comparison with their respective first runs. In the case of SL2 this is likely to be due to the removal of heavy material from solution as insolubles which deposit on the catalyst. In the case of SL7 the shift is slight. As the deposition is negligible for SL7, most products are liquid and therefore SEC revealed information about a large fraction of the products.

UV-F of the hydrocracking products obtained with reused SL2 as catalyst (Figure 7.8) showed a larger shift towards shorter wavelengths than the fresh SL2. This reflects the same trend as SEC and it is thought to be mainly due to the deposition on the catalyst. On the other hand, UV-F of the SL7 products (Figure 7.9) showed that the shift towards shorter wavelengths was larger in the first use than in the second, although the difference with the spectrum of the feed is evident in both runs.

7.3.3 Evaluation of other catalysts

The conversions achieved reusing Cr laponite CL1a, Eu-montmorillonite, Ce montmorillonite and Ce-Cr montmorillonite are shown in Table 7.4. All catalysts

showed an increase in real conversions after second use with the exception of Eu montmorillonite. However, the increase in real conversion was not as large as in the case of the CM3 discussed above.

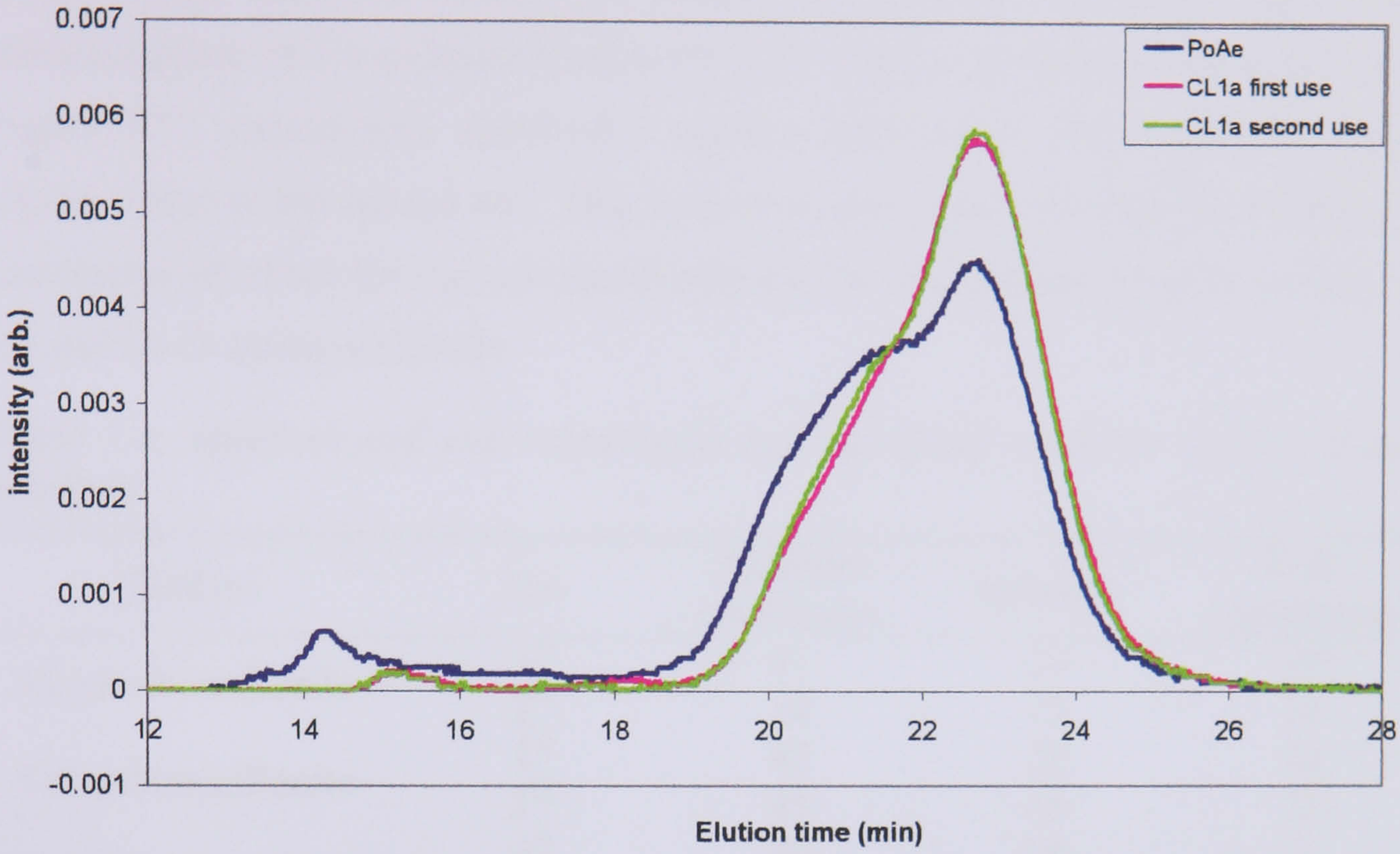


Figure 7.10. Mixed-A column SEC chromatogram of hydrocracking products obtained using fresh and reused CL1a. All chromatograms have been area normalised

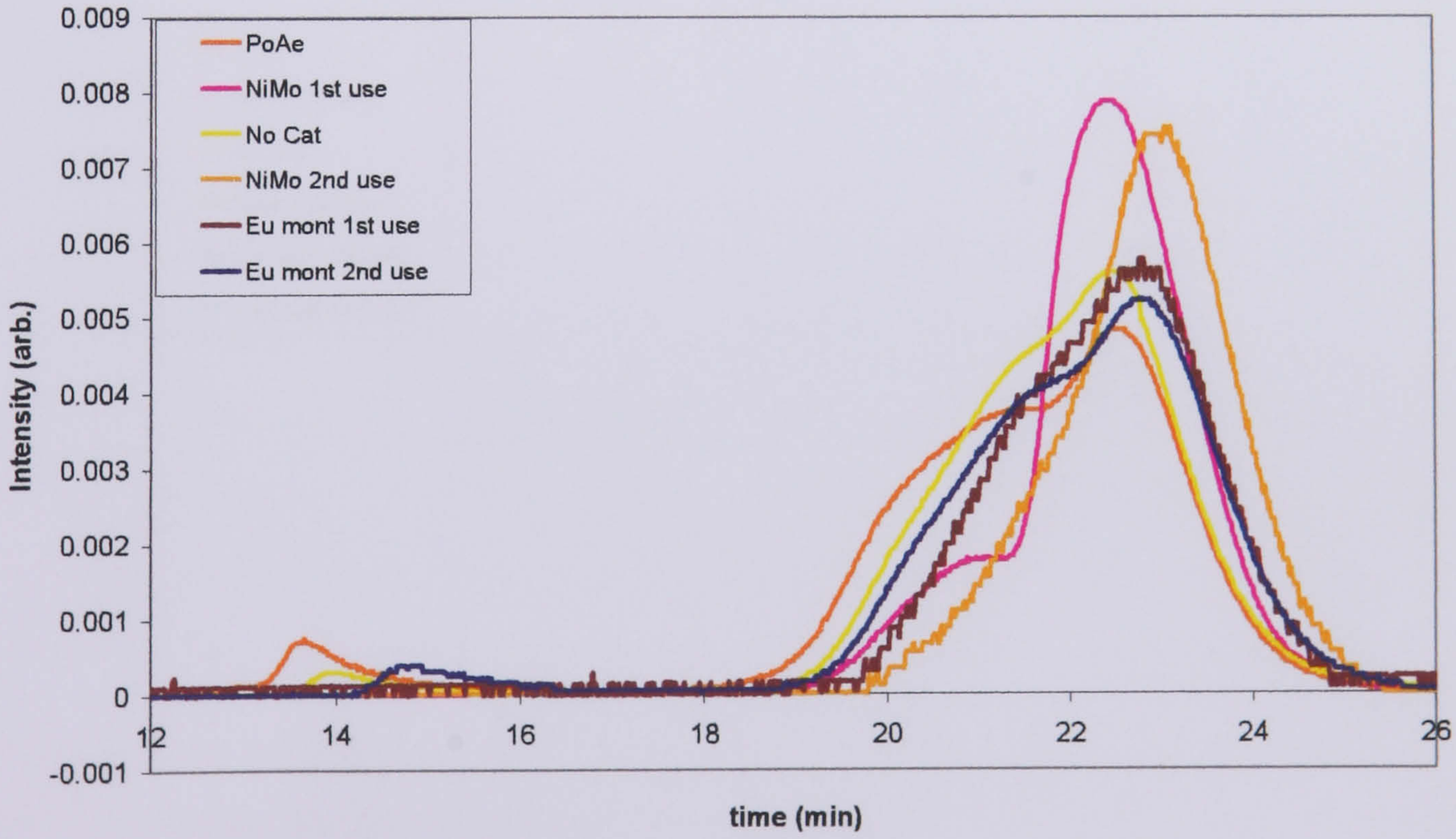


Figure 7.11. Mixed-A column SEC chromatogram of hydrocracking products obtained using fresh and reused Eu montmorillonite. All chromatograms have been area normalised

As can be seen in Figure 7.10, the SEC chromatograms of products from fresh and reused CL1a were almost undistinguishable. The SEC chromatograms of the Eu montmorillonite products (Figure 7.11) showed a shift towards shorter elution times (larger sizes) after the second use relative to the first use. By contrast, SEC chromatograms of Ce montmorillonite and Ce-Cr montmorillonite (Figure 7.12 and Figure 7.13 respectively) exhibited a product distribution shifted towards longer elution times in the second use. This behaviour was consistent with the decrease in conversion observed for Eu montmorillonite and the increase observed in the case of Ce and Ce-Cr montmorillonite.

Table 7.4. Apparent and real conversions and recovered solids for various reused catalysts.

Catalyst	Use	Apparent conversion	Deposits	Real conversion
Eu montmorillonite	1st	51	23	33
	2nd	34	13	24
Ce montmorillonite	1st	47	23	30
	2nd	43	14	32
Ce-Cr montmorillonite	1st	50	28	25
	2nd	47	13	37
Cr laponite CL1a	1st	54	29	28
	2nd	45	19	34

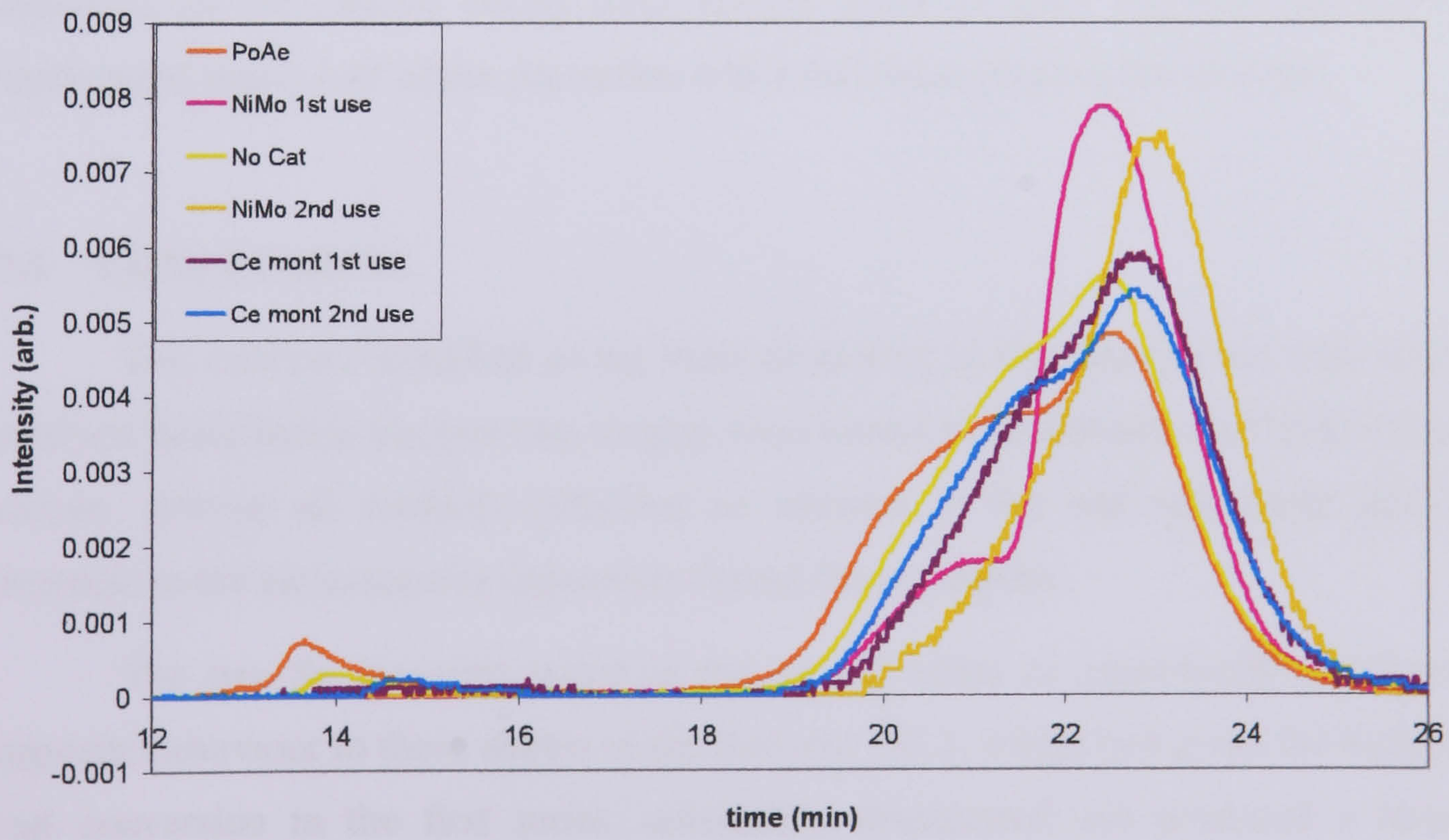


Figure 7.12. Mixed-A column SEC chromatogram of hydrocracking products obtained using fresh and reused Ce montmorillonite. All chromatograms have been area normalised.

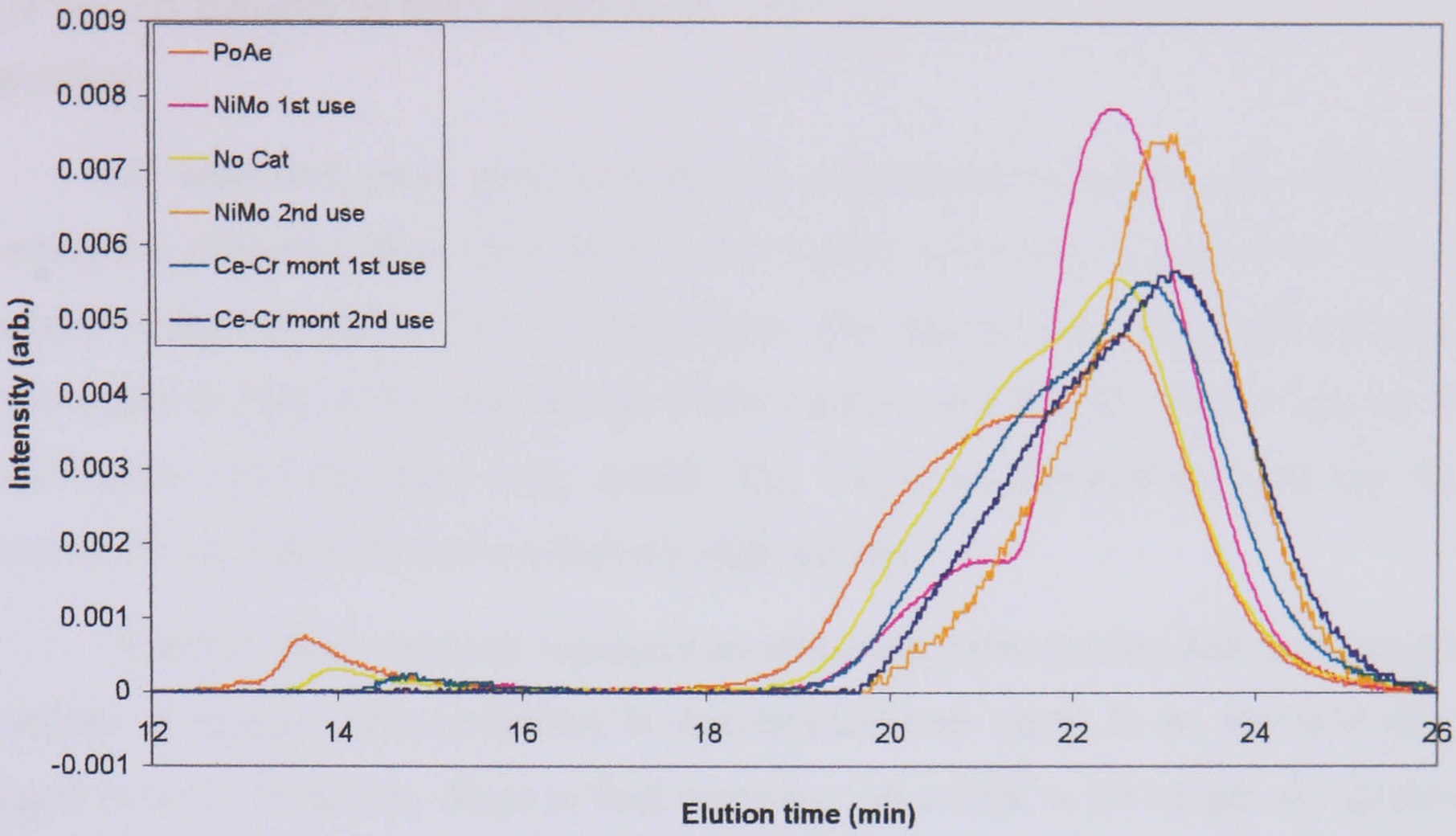


Figure 7.13. Mixed-A column SEC chromatograms of hydrocracking products obtained using fresh and reused Ce-Cr montmorillonte. All chromatograms have beeen area normalised.

All catalysts showed a decrease in the amount of carbonaceous solids deposited on the catalyst during these second series of runs. The new deposition represented nearly half of the deposition which had taken place in the first run.

7.4 CONCLUSIONS

The catalysts identified as the most promising in the experiments with fresh catalysts described in the previous chapter were reused to hydrocrack the Point of Ayr extract. Almost all catalysts exhibited an increase in the real conversion and a decrease in the carbonaceous deposition during the second use.

The two Sn laponites tested in the second series of experiments exhibited opposite behaviour to those shown in the first test. SL2, which had given the highest real conversion in the first series, completely deactivated and produced a large amount of solids deposited in the catalyst leading to a very low conversion. On the other hand, the conversion achieved with SL7 markedly increased. Given the

difficulties in repeatability in synthesis, which needs to be clarified, of these catalysts, it is not yet possible to draw conclusions about the best synthesis procedure for tin laponites.

All untreated clays gave increases in conversions relative to the first run. Among the pillared clays, CM3 showed the highest real conversion and the lowest amount of deposits added to the coating layer. This catalyst has shown effectiveness comparable to that of the commercial NiMo catalyst and did not show evidence of deactivation over the time scale tested. The Ce-Cr montmorillonite and the Ce montmorillonite also showed a relatively high activity.

Whether these catalysts represent an advantage over present day commercial catalysts in terms of the resistance to deactivation now needs to be assessed over longer periods. However, drops in feed reactivity set a limit in the length of reaction time for meaningful batch reactor runs. In addition, it is not possible to achieve long reaction times by reusing the catalyst with fresh feed, since a fraction of the catalyst is always lost and therefore the amount of catalyst recovered after several uses would be insufficient. The use of a continuous reactor would be therefore desirable compared to the batch process used in this work to expand the study on the most promising catalysts, namely CM3, and Ce and Ce-Cr montmorillonites, over longer time scales.

8 CATALYST CHARACTERISATION

8.1 INTRODUCTION

In the last three chapters, the results from experiments using pillared clays and a commercial $NiMo/Al_2O_3$ as hydrocracking catalyst were presented. The latter, the Sn laponite 7 (SL7) and the Cr montmorillonite 3 (CM3) were selected to carry out surface area measurements. The catalysts recovered after the hydrocracking experiments were also examined.

Scanning electron microscopy was applied to fresh CM3, to CM3 recovered from the first and second runs, and to the catalyst recovered after the carbonaceous deposits were removed. The catalyst characteristics and how they are affected by the hydrocracking process will be discussed briefly in this chapter.

8.2 EXPERIMENTAL

8.2.1 Surface area measurements

This technique has been applied to the fresh and reused CM3 and SL7, as well as to the fresh $NiMo/Al_2O_3$ and the coated catalyst recovered from the time series experiments described in Chapter 5. The equipment and procedure have been detailed in the experimental chapter (section 3.2.6).

8.2.2 Scanning electron microscopy and X-ray microanalysis

A JEOL JSM 840 scanning electron microscope has been employed. Its maximum resolution is 10 nm and it is capable of quantifying elements present in the sample by X-ray microanalysis to an accuracy of within 0.1%. Elemental data can be presented either as a table showing the composition in a given number of points over the sample or as maps of surface concentration of the elements.

The samples were coated beforehand with a thin layer of carbon to improve electrical conductivity over the surface. This layer was sufficiently thin (150 Å) and uniform to avoid confusion with the carbonaceous deposition during the hydrocracking process.

X-ray microanalysis has been carried out on the catalyst surface to identify the elemental composition of the sample. The X-ray analysis is performed over a 0.8 μm

sided square and it penetrates 3 to 4 μm under its surface. The SEM and X-ray microscopy detectors are located in different positions. As a consequence, some zones of the SEM picture which appear dark may show signal in the elemental distribution and vice versa.

8.3 RESULTS AND DISCUSSION

8.3.1 Surface area measurements

Both fresh pillared clays, SL7 and CM3, showed higher surface area than the fresh $NiMo/Al_2O_3$. In particular, the Sn laponite 7 exhibited a large BET surface area of 350 m^2/g. A sharp drop in surface area was observed for the used pillared clays. After 4 hours in operation, the measured surface areas for SL7 and CM3 were in the order of 1 m^2/g as shown in Table 8.1. The measurement of such a small surface area has high experimental error. However, it is clear that the surface area showed a great reduction as a consequence of the deposition of carbonaceous material during hydrocracking. No reliable total pore volume and average pore diameter were obtained for the used pillared clays since the values were too small.

Table 8.1. BET surface area, total pore volume and average pore diameter of fresh and coated $NiMo/Al_2O_3$, and the catalysts recovered from hydrocracking runs. All values shown were obtained in this laboratory.

Sample	BET Surface Area (m^2/g)	Total Pore Volume (cm^3/g)	Average Pore Diameter (nm)
Fresh CM3	104	0.10	3.7
CM3 used twice	~1	n.a.	n.a.
Fresh SL7	350	0.23	2.6
SL7 used twice	~1	n.a.	n.a.
Fresh $NiMo/Al_2O_3$	78	0.28	14.7
Coated $NiMo/Al_2O_3$	45	0.12	11.0
0 min run Coated $NiMo/Al_2O_3$	51	0.09	7.3
10 min run Coated $NiMo/Al_2O_3$	52	0.13	10.2
30 min run Coated $NiMo/Al_2O_3$	51	0.12	9.4

The coated $NiMo/Al_2O_3$ recovered after the 0, 10 and 30 minute runs were also examined by surface area measurements. As described in Chapter 5, a $NiMo/Al_2O_3$ catalyst previously coated with a coal tar pitch was used in those experiments. The $NiMo/Al_2O_3$ showed a smaller decrease in surface area than the pillared clays. After coating the catalyst with the coal tar pitch, the catalyst experienced a drop in surface area from 78 to 45 m^2/g.

Figure 8.1 shows the pore size distribution of the catalyst before and after coating. Although coating produced a general decrease in the pore volume for all pore diameters, the shape of the distribution remained similar to that of the fresh catalyst. It was possible to observe a sharper drop in pore volume in the region of pore diameters between 4 and 8 nm. The maxima of both distributions were at nearly 10 nm.

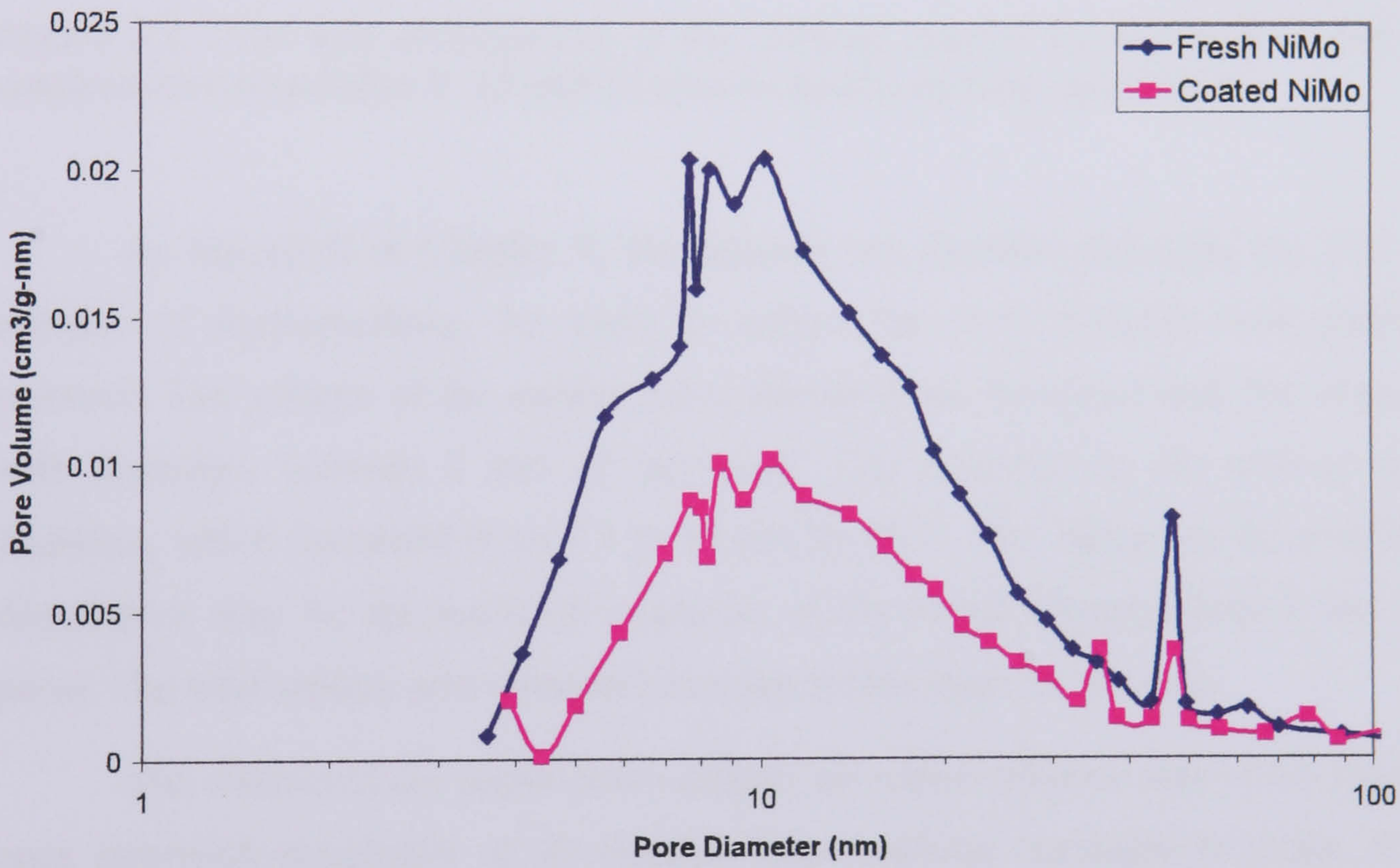


Figure 8.1. Pore size distributions of fresh and coated NiMo.

After the "0 minute" hydrocracking experiment with the Point of Ayr hydrocracker feed, changes in the pore size distribution of the catalyst were clear (Figure 8.2). There was a net decrease in the volume of pores around 10 nm while a remarkable increase in volume was observed for pores of 5 nm in diameter and below. It seems that the initial deposition on the catalyst tended to produce pore mouth constriction and reduce the size of the larger pores.

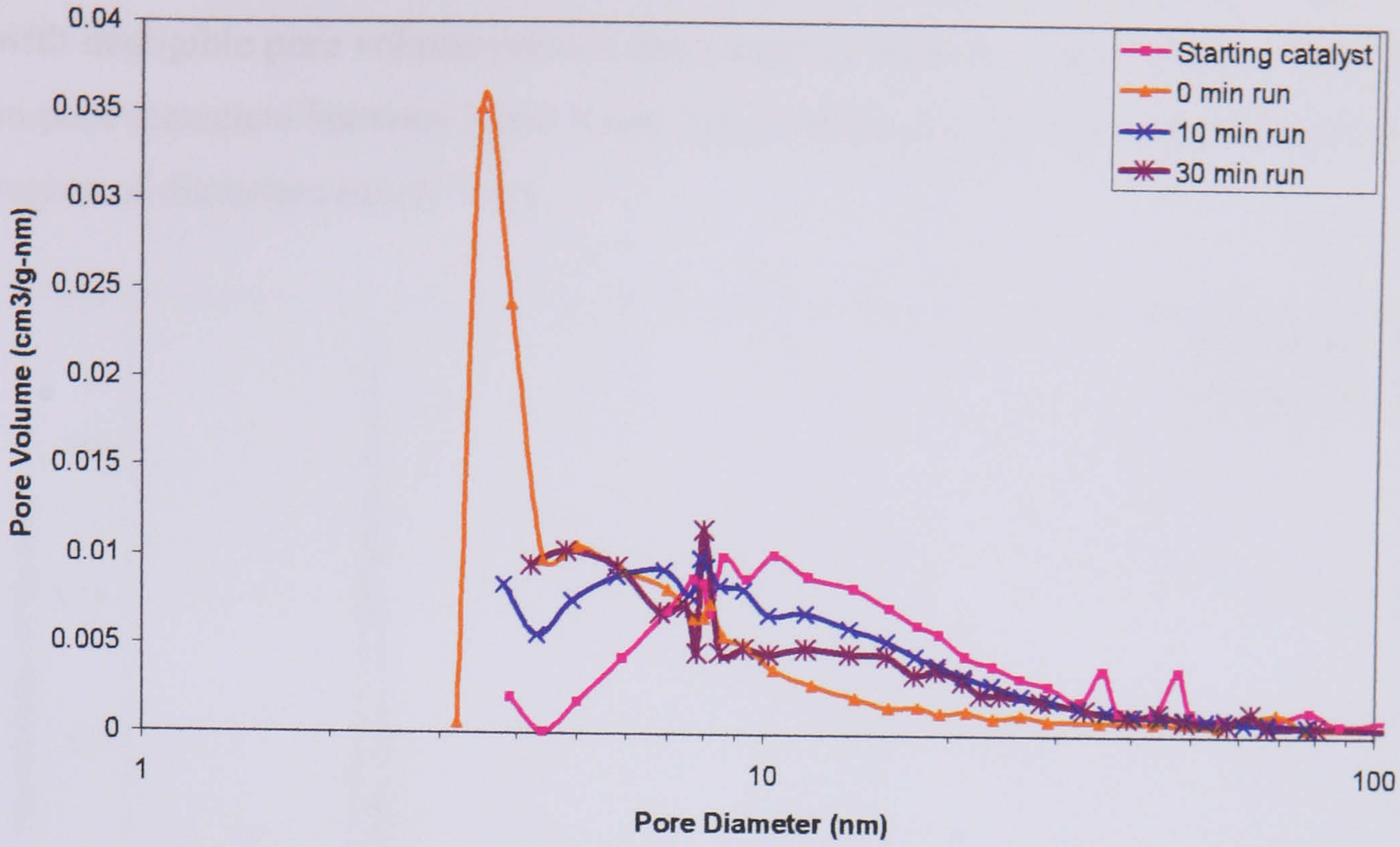


Figure 8.2. Pore size distributions of the starting catalyst (coated NiMo) and the catalysts recovered after 0, 10 and 30 minutes hydrocracking experiments.

As discussed in Chapter 5, the deposits are dynamic and after the first 10 minutes of hydrocracking the trend to reduce the pore diameter was partially reversed. The volume of the smaller pores (below 5nm) decreased and that of pores with diameters between 5 and 20 increased. This reflected on the average pore diameter, which increased from 7.3 to 10 nm by BET. The change in the pore size distribution may be the result of migration of the initial deposits further into the pores. The total surface area remained constant within these 10 minutes.

The volume of the larger pores slightly decreased whereas that of the smaller ones increased marginally at 30 minutes hydrocracking compared to those at 10 minutes. This is in line with observations suggesting a gradual built-up of carbonaceous deposits on the catalyst after the initial deposition [7, 29]. The BET average pore diameter showed a small decrease from 10.2 to 9.4 nm and the surface area showed no changes.

The pore size distribution of the fresh $NiMo/Al_2O_3$ was much broader than those of the pillared clays, which are shown in Figure 8.3. While the $NiMo/Al_2O_3$ showed a distribution centred at 9 nm but expanding up to around 50 nm, the pillared clays exhibited very narrow peaks in the pore diameter distribution, with maxima

between 3 and 4 nm. In the fresh CM3 the pore diameters ranged from 3 to 4.5 nm, with negligible pore volume outside that range. Sn laponite 7 also shows a sharp peak in pore diameters between 3 and 4 nm, but in addition it showed some porosity in the region of diameters below 3 nm.

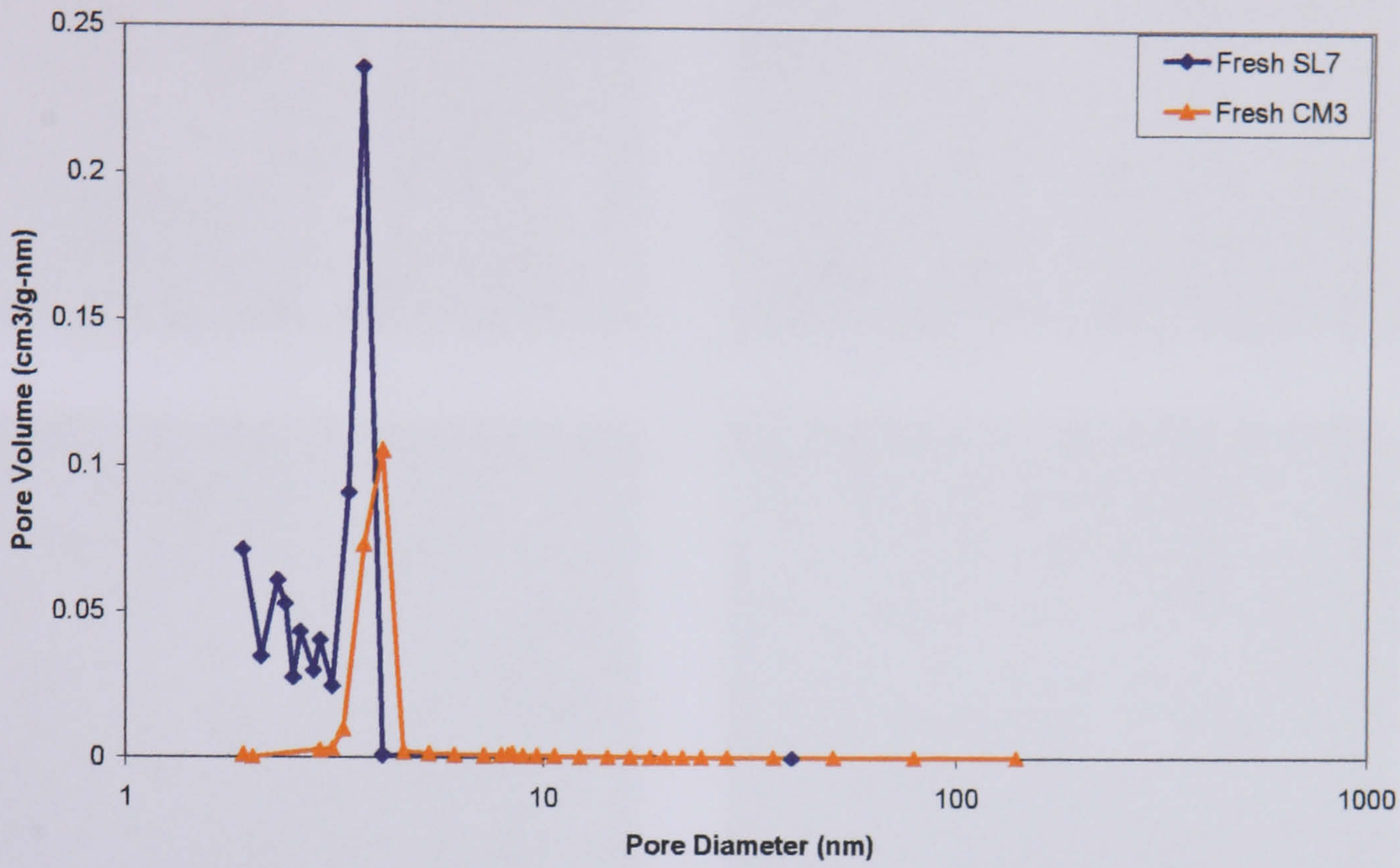


Figure 8.3. Pore size distributions of fresh Sn laponite 7 and Cr montmorillonite 3.

After 4 hours hydrocracking, the porosity of the pillared clays decreased to about a thousandth of that of the fresh catalysts and the volume of the pores below 60 nm in diameter was too small to be measured. The small pores appear to have been blocked by the carbonaceous deposits.

8.3.2 Scanning Electron Microscopy and X-ray microanalysis.

Samples of fresh CM3, and CM3 after first and second uses and after removal of the carbonaceous layer by combustion in a thermogravimetric analyser have been examined by scanning electron microscopy and X-ray microanalysis. The X-ray microanalysis method is presented in Figure 8.4, showing a fresh CM3 catalyst particle of approximate size 20 μm and the corresponding Si, Al, oxygen and carbon profiles. The latter is due to the coating used to enhance conductivity and it showed an even distribution all over the sample, whereas the Si, Al and O profiles were concentrated on the particle surface. As expected, a good correlation between Si, O and Al distribution in the clay structure was observed.

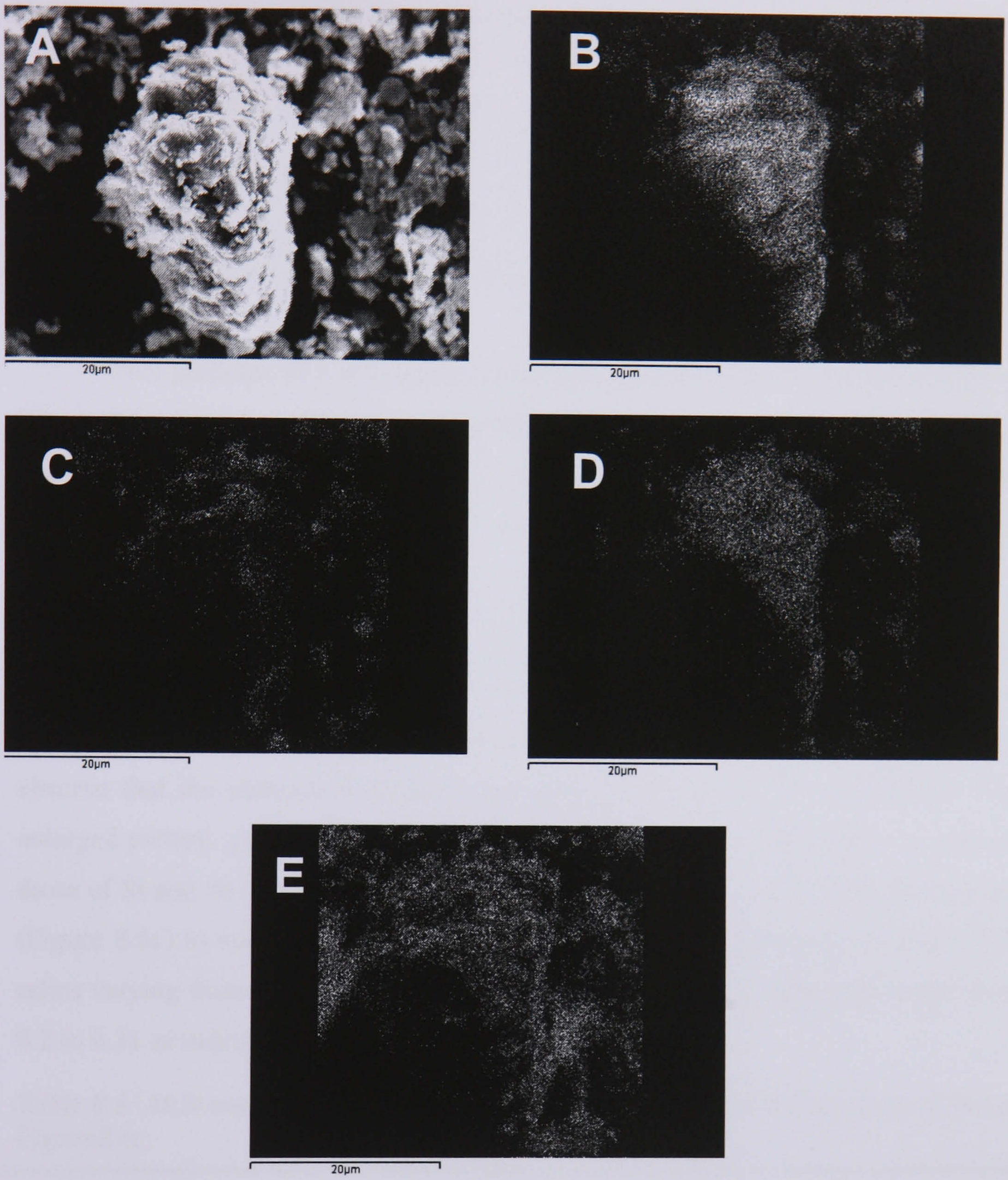


Figure 8.4. SEM of a CM3 catalyst particle (a). Its elemental composition profiles obtained by X-ray microanalysis are also shown: (b) Silicon, (c) Aluminium, (d) Oxygen, (e) Carbon.

The SEM analyses have shown a dispersion in particle sizes (Figure 8.5), which was confirmed by particle size distribution of the fresh Cr-montmorillonite 3 determined by sieving. A sample of fresh CM3 was sieved using the following mesh sizes: 105, 150 and 212 µm. The particle size distribution obtained is shown in Table 8.2.

Table 8.2. Particle size distribution of the fresh CM3 catalyst obtained by sieving

Particle size (μm)	Fraction of the sample
> 212	17 %
150 - 212	23 %
105 - 150	13 %
< 105	47 %

Two particles of $CaCl_2$ appeared as contamination on the top left corner of Figure 8.5a. Fourteen points on the surface were taken to generate the quantitative elemental analysis. These points are shown in Figure 8.5b and the results showed variations in the Al/Si ratio between 0 and 0.74 and in the Cr/Si ratio between 0 to 0.59.

SEM and X ray microscopy of CM3 after 1st use are shown in Figure 8.6. The large scale SEM image (Figure 8.6a) showed large and uniform carbonaceous deposits (in red in the picture). However, when the scale is magnified it is possible to observe that the carbonaceous layer deposited preferentially in some regions. The enlarged picture, presented in Figure 8.6b, shows the carbon distribution in red and those of Si and Al in green and blue respectively. Five points were taken in that zone (Figure 8.6c) to measure elemental composition by X-ray microscopy revealed C:Si ratios varying from 2.7 to 44.7, whereas the variation in Al/Si ratios only varied from 0.2 to 0.31 as indicated in Table 8.3.

Table 8.3. Al:Si and C:Si ratio measured by X-ray microscopy in five points shown in Figure8.6c.

Point No.	Al:Si ratio	C:Si ratio
1	0.31	6.2
2	0.12	23.0
3	0.31	23.5
4	0.20	2.7
5	0.21	44.7



Figure 8.5. (a)Fresh CM3 catalyst. (b) Fourteen points taken for elemental analysis.

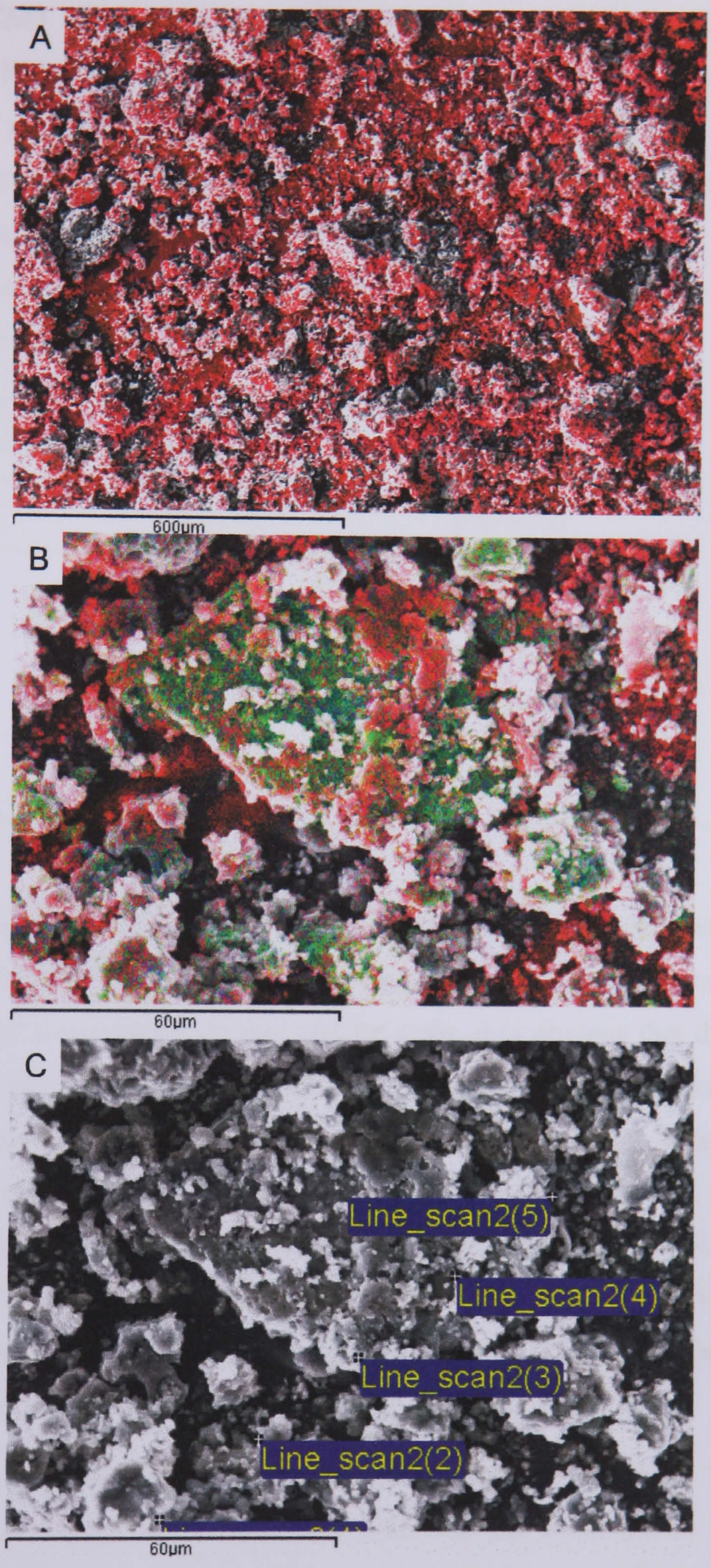


Figure 8.6. SEM micrographs of CM3 used once. (a) shows the carbonaceous deposition in red; (b) shows the carbon distribution (red), silicon (green) and aluminium (blue); (c) five points taken for the determination of elemental composition shown in Table 8.3.

The CM3 was reused and SEM and X-ray microscopy after 2nd use are presented in Figure 8.7. Figure 8.7a shows several catalyst particles and the Cr concentration mapped in red. Cr does not seem evenly distributed; there are some zones with particularly high concentration. The spread in particle sizes is evident. The heavy carbonaceous deposition can be observed in the carbon profile (Figure 8.7b). Si, Al and O showed similar profiles among themselves reflecting the composition of the clay particles (Figure 8.7c, d, and e, respectively).

Table 8.4. Al:Si and C:Si ratio measured by X-ray microscopy in four points shown in Figure8.7g. Points are numbered from left to right.

Point No.	Al:Si ratio	Cr:Si ratio	C:Si ratio
1	0.53	0	484
2	0.76	0	76
3	0.88	8.2	243
4	0.62	25.6	63

A region centred in the zone of higher Cr concentration was magnified. Figure 8.7f shows the carbonaceous deposits (blue), the Cr concentration (red) and the silica in the clay (green). At this smaller scale, it is obvious that the deposits are not uniformly distributed. Four points along the SEM micrograph shown in Figure 8.7f were selected for elemental composition determination by X-ray microscopy. The positions of these points are shown in Figure 8.7g. The results are given in Table 8.4. A larger concentration of carbon is seen on the points on the left in Figure 8.7f and Figure 8.7g decreasing towards the right. The Cr:Si ratio showed large variations from one point on the catalyst surface to another, from 0 to 25.6, whereas the Al:Si ratio exhibited a much narrower range, from 0.52 to 0.88.

The carbonaceous layer seems to be thinner in areas where the Cr concentration is higher. This result is in line with the observations of preferential carbonaceous deposition on the catalyst support discussed in Chapter 2 [42-44]. A model proposed by Diez et al. [25] suggested that the hydrogenation on the active sites clears a surrounding area from deposits. Richardson et al. found that this model successfully fitted the dependence of coke deposition on hydrogen pressure, reaction

time, feed to catalyst ratio and feed composition [36]. The lack of homogeneity in the deposits observed in this work may provide an explanation for persistent catalytic activity observed even though the deposition levels were high.

8.4 CONCLUSIONS

Surface area measurements showed that the pillared clay catalysts had larger surface areas than the commercial $NiMo/Al_2O_3$ used as reference. However, they showed a very narrow pore diameter distribution, concentrated in the region between 3 and 4.5 nm, whereas the $NiMo/Al_2O_3$ exhibited a much larger range.

After 4 hours in operation both the surface area and the porosity of the pillared clays showed a marked decrease, consistent with the large deposition of carbonaceous materials measured by TGA. On the other hand, the $NiMo/Al_2O_3$ catalyst showed more resistance to drops in surface area and pore blockage, likely to be due to its larger pore size distribution.

SEM and X-ray microscopy were applied to fresh CM3 and the spent catalyst after first and second use and after the removal of carbonaceous deposits. The carbonaceous materials seemed to deposit preferentially over some zones of the catalyst, leaving other clay particles still exposed after 4 hours of operation. Some micrographs suggested that regions with higher Cr contents might present lower deposits. This suggests that the presence of hydrogenation activity in the Cr sites clears a surrounding area from deposits. This has been reported previously in the literature in the case of NiMo catalysts [25, 36] and suggests an explanation for the persistent activity of the CM3 catalyst in spite of the high levels of carbonaceous deposits.

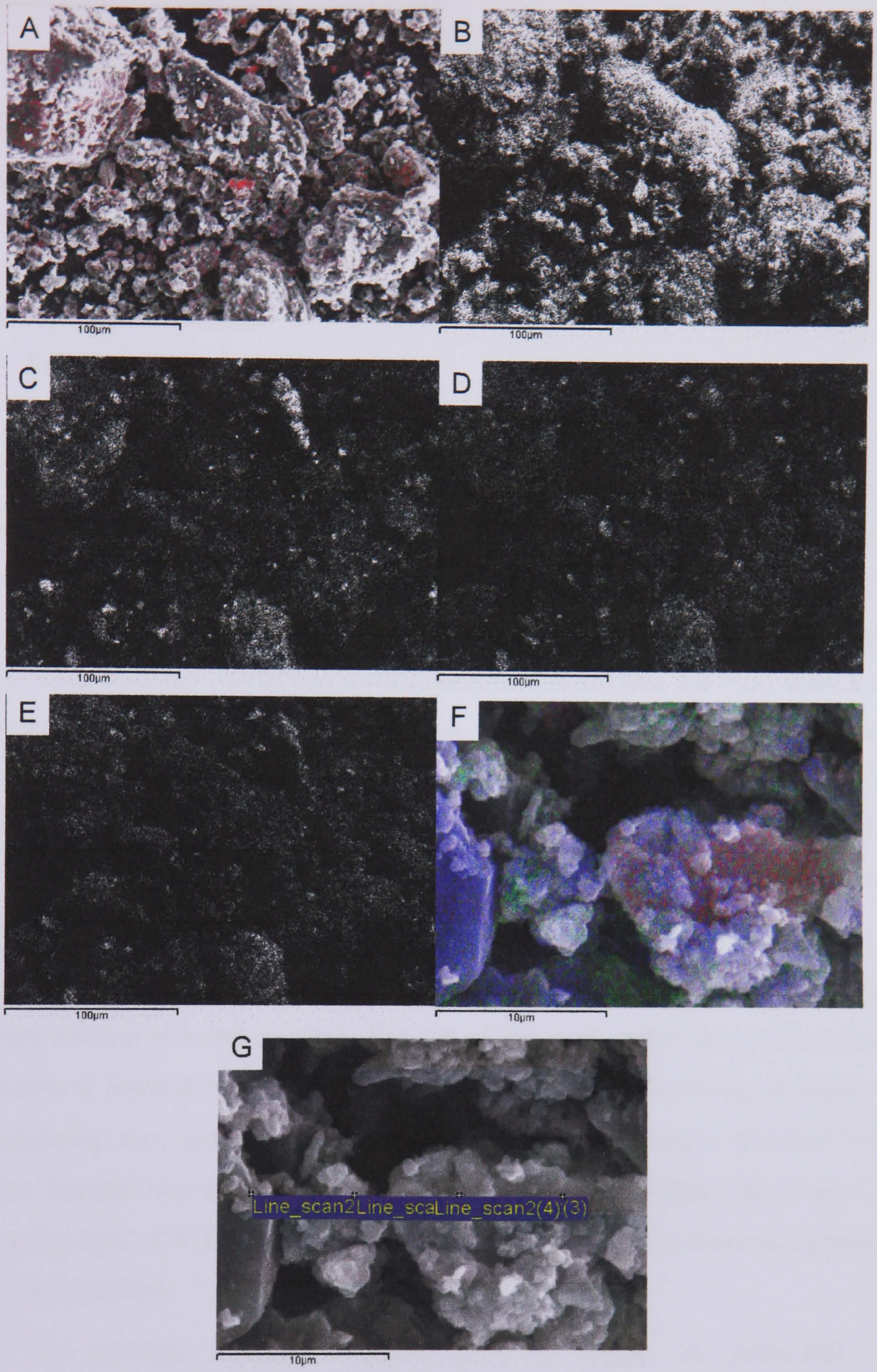


Figure 8.7. (a) SEM of the CM3 used twice; the Cr distribution is shown in red; (b) Carbon X-ray microanalysis profile; (c) Si X-ray microanalysis profile; (d) Aluminium X-ray microanalysis profile; (e) Oxygen X-ray microanalysis profile; (f) The area richer in Cr is magnified; X-ray microanalysis profiles of carbon (blue), silicon (green) and chromium (red) are shown;(g) four points taken for the determination of elemental composition shown in Table 8.4.

9 HYDROCRACKING OF OTHER FEEDS: A VACUUM RESIDUE AND THE PYRIDINE INSOLUBLE FRACTION OF A COAL TAR PITCH

9.1 HYDROCRACKING OF THE PYRIDINE INSOLUBLE FRACTION OF A COAL TAR PITCH

9.1.1 Introduction

The pyridine insoluble fraction of a coal tar pitch has been extensively characterised in this laboratory by several analytical techniques. Size exclusion chromatography has shown that this fraction is significantly heavier than the acetone and pyridine soluble fractions in terms of its molecular size distribution. A larger amount of material elutes under the excluded peak in the pyridine insolubles than in the two other fractions. UV-Fluorescence spectra of these three fractions show a shift of the signal towards longer wavelengths as well as a decrease in the fluorescence intensity in the series acetone solubles, pyridine solubles, pyridine insolubles. This indicates the presence of increasingly larger aromatic rings along the series. MALDI-TOF MS has also been used to characterise this sample. This application will be described in the next chapter.

In earlier work Begon et al. [65] attempted to hydrocrack the pitch pyridine insoluble fraction of a coal tar pitch. The aim of that work was to gain information on the structural features of the sample by analysing its hydrocracking products. The hydrocracking was carried out at 440°C and 190 bar hydrogen pressure for 30 minutes. Tetralin was used as solvent and $NiMo/Al_2O_3$ as catalyst. The product was analysed by SEC, UV-F, probe-MS and its boiling point distribution was determined by the TGA method.

The pyridine insoluble fraction gave no signal by probe-MS. The hydrocracked products did show signal by probe-MS and they also showed a reduction in molecular size distribution by SEC. Several alkyl, alkenyl and aromatic groups were detected by probe-MS in that work. However, the presence of tetralin and tetralin derivatives in the products was an obstacle in the interpretation of the results. It was not possible to determine whether the compounds observed by probe-MS were fragments of the sample generated by hydrocracking or reaction products

from tetralin. Similar attempts to generate fragments of this sample by pyrolysis in a wire mesh reactor have been unsuccessful, resulting in the formation of a char [87].

In the present work the pitch pyridine insoluble fraction of the coal tar pitch has been hydrocracked in the absence of solvent. In addition, a coated catalyst has been used to avoid a large deposition of heavy materials on the catalyst surface during the experiment. It was thought that the use of no solvent and a low deposition would allow a more straightforward interpretation of the results.

9.1.2 Experimental

The procedure usually followed in hydrocracking experiments has been described in the experimental section, as well as the method followed to generate the fractions. Some modifications were made to take into account the more viscous nature of the sample and the especial objective of this experiment: the generation of fragments indicative of the nature of the sample.

In a first experiment 500 mg of sample and 150 mg of coated $NiMo/Al_2O_3$ were kept under 200 bar hydrogen pressure and 375°C for 2h. This temperature is just above the onset of thermal reactions [74] and it was expected to be low enough to minimise further cracking of the fragments generated. The preparation of the coated catalyst has been detailed in Chapter 5.

As discussed below, in a second experiment the hydrocracking time was reduced to 2 minutes in order to minimise char formation. On the other hand, the temperature was increased to 450°C to achieve some extent of hydrocracking given the short time applied. Other experimental conditions remained unchanged.

The pyridine insoluble fraction of a coal tar pitch and its two-minute hydrocracking products have been analysed by heated-probe MS. A Jeol JMS-AX505W double focusing spectrometer was employed. The probe temperature was raised from ambient to 400°C at 64°C/min.

9.1.3 Results and Discussion

120 minute hydrocracking

The product from this run was a compact char-like solid, which stuck to the walls of the reactor. $CHCl_3/CH_3OH$ was able to wash only a small fraction of it. In addition to the low solubility of the sample, the dissolution process in $CHCl_3/CH_3OH$

was found to be very slow. 27 mg of soluble products were recovered in $CHCl_3/CH_3OH$, which represented 5.4% of the original sample. After removal of the $CHCl_3/CH_3OH$ soluble fraction from the products, the reactor was washed with NMP and the product filtered.

The starting material (pitch pyridine insolubles) also contained a small $CHCl_3/CH_3OH$ soluble fraction. Size exclusion chromatograms of the $CHCl_3/CH_3OH$ soluble and insoluble fractions of both pitch pyridine insoluble and hydrocracking products are shown in Figure 9.1. As expected, both $CHCl_3/CH_3OH$ soluble fractions showed shifts towards longer times (smaller molecular sizes) in comparison with the $CHCl_3/CH_3OH$ insolubles. This shift is slightly larger in the case of the products. On the other hand, the $CHCl_3/CH_3OH$ insoluble fraction of the products showed a very large proportion of material eluting under the excluded peak. This fraction did not show a considerable difference with the starting material in terms of molecular size distributions.

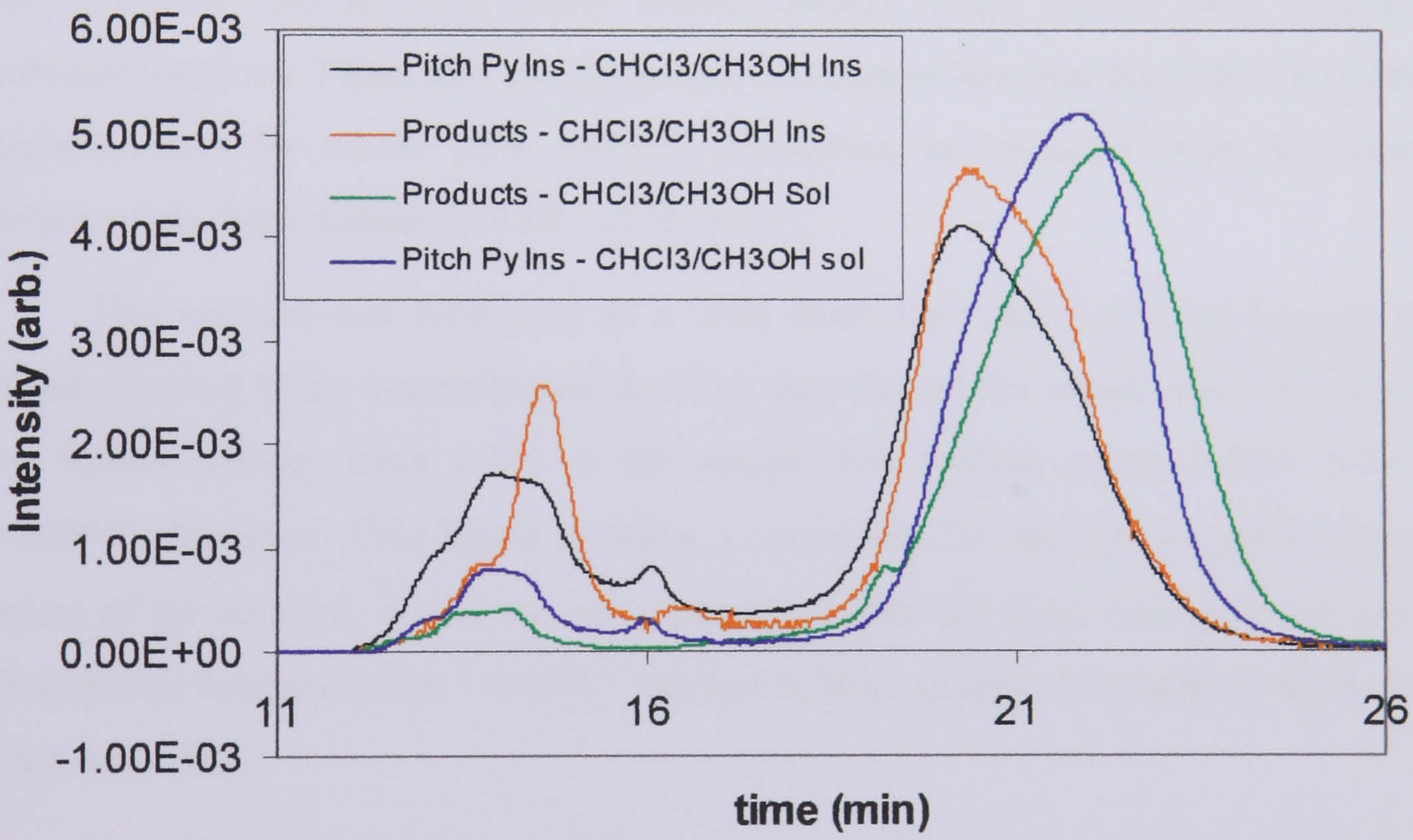


Figure 9.1. Mixed-A column size exclusion chromatograms of the $CHCl_3/CH_3OH$ soluble and insoluble fractions of pitch pyridine insoluble and its hydrocracking products. Area normalisation has been applied to all chromatograms.

A large amount of the products were recovered as carbonaceous solids. TGA analysis on the recovered solids showed an 80% content in carbonaceous material.

The $NiMo/Al_2O_3$ catalyst accounts for the remaining 20%. The initial carbonaceous content of the coated catalyst was 30%. Therefore, the composition of the filter cake can be estimated as 20% inorganic ($NiMo/Al_2O_3$), 9% carbonaceous originally coating the catalyst and 71% sample-derived material.

Data from SEC together with the product characteristics and solids composition suggest that a char was produced instead of lighter materials. It is likely that the condensation of cracking products was predominant rather than the hydrogenation to form lighter products.

2 minute hydrocracking

The pitch pyridine insoluble fraction was washed with $CHCl_3/CH_3OH$ beforehand to remove the small fraction of soluble material. The insoluble portion was used as feed in this second experiment. SEC chromatograms of the whole pitch pyridine insolubles and its two $CHCl_3/CH_3OH$ fractions are shown in Figure 9.2. The $CHCl_3/CH_3OH$ solubles were clearly shifted towards longer elution times than the two other fractions. There were no significant differences between the $CHCl_3/CH_3OH$ insolubles and the whole pitch pyridine insolubles, as expected from the small fraction of the latter soluble in $CHCl_3/CH_3OH$.

The product was recovered as a solid from the reactor without the use of solvent. Boiling point determination by TGA was run on the whole solid recovered after hydrocracking. Only 2.2% of the sample had boiling points below 450°C ("<450°C" fraction). This figure includes a correction for the initial carbonaceous content of the catalyst, which was not separated before the TGA measurement. This represents an increase in the "<450°C" fraction relative to that of the starting material, which was 1.6%.

The SEC chromatograms of the starting material and the products are shown in Figure 9.3. Both the excluded and retained peaks shifted to longer elution times after 2 minute hydrocracking. An increase in the retained to excluded peak ratio was observed in the products.

Figure 9.4 shows the SEC chromatograms of the whole products and its $CHCl_3/CH_3OH$ soluble and insoluble fractions. A discernible shift towards longer retention times appeared along the series $CHCl_3/CH_3OH$ insolubles, whole products, $CHCl_3/CH_3OH$ soluble. However, the $CHCl_3/CH_3OH$ soluble products still contained

a significant amount of excluded material. The presence of $CHCl_3/CH_3OH$ soluble fraction and the shift of the whole products towards longer elution times in comparison with the feed shows that the experiment has effectively hydrocracked a fraction of the sample. As can be seen in Figure 9.4, the signal from the $CHCl_3/CH_3OH$ soluble fraction is very weak due to the low concentration of soluble material recovered.

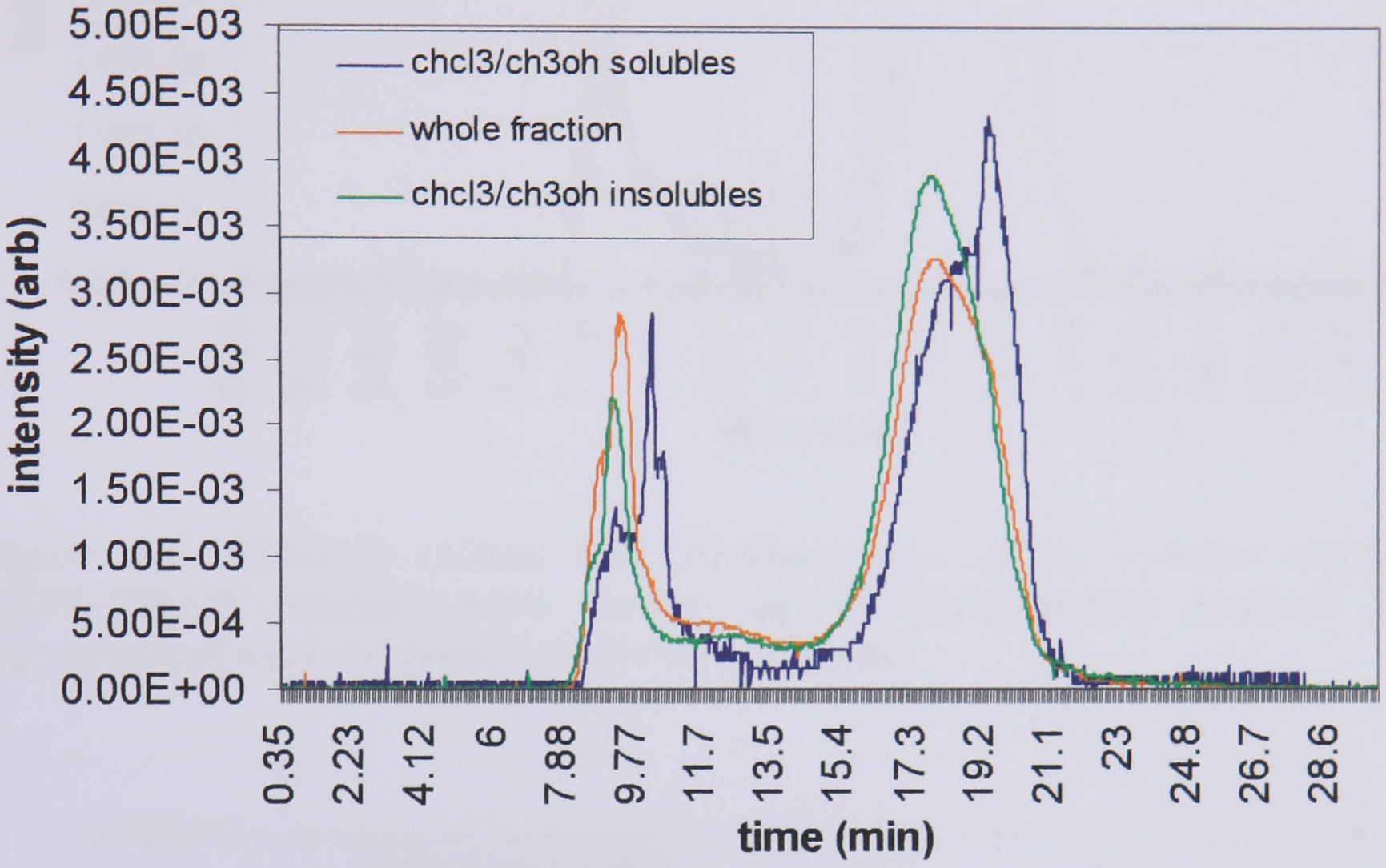


Figure 9.2. Mixed-D column SEC chromatograms of the pyridine insoluble pitch fraction and its $CHCl_3/CH_3OH$ soluble and insoluble sub-fractions. Area normalisation has been applied to all chromatograms.

Probe-MS has been run on the starting material and its $CHCl_3/CH_3OH$ soluble and insoluble fractions. Only some remaining pyridine has been detected in the pitch pyridine insoluble fraction. By contrast, its $CHCl_3/CH_3OH$ soluble fraction has shown some low intensity signal which can be identified as compounds present in coal. Peaks at m/z 202 (fluoranthene, pyrene), 228 (benzanthracene, chrysene, benzophenanthrene), 252 (benzofluoranthene, perylene, benzopyrene), 276 (benzoperylene), 302 (dibenzopyrene) and 326 (rubicene) have been the main compounds identified. It is likely that these compounds did not appear in the spectrum of the whole pitch pyridine insoluble because they were only present in small quantities in that sample. Most material in the pyridine insoluble fraction of the pitch has higher molecular masses than the limit of the technique.

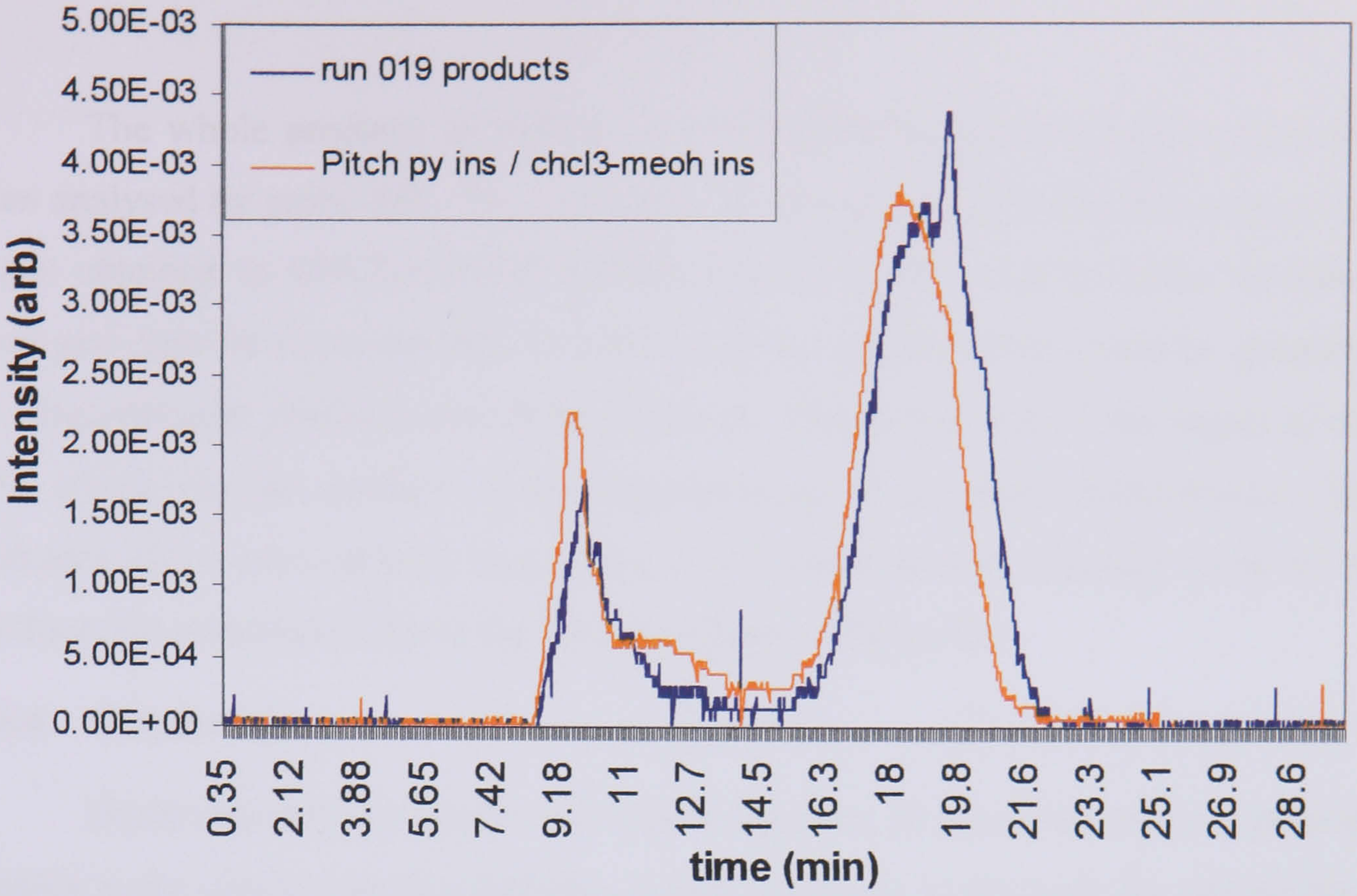


Figure 9.3. Mixed D column SEC chromatograms of the pyridine insoluble, $CHCl_3/CH_3OH$ insoluble pitch fraction and its hydrocracking products. Area normalisation has been applied to all chromatograms.

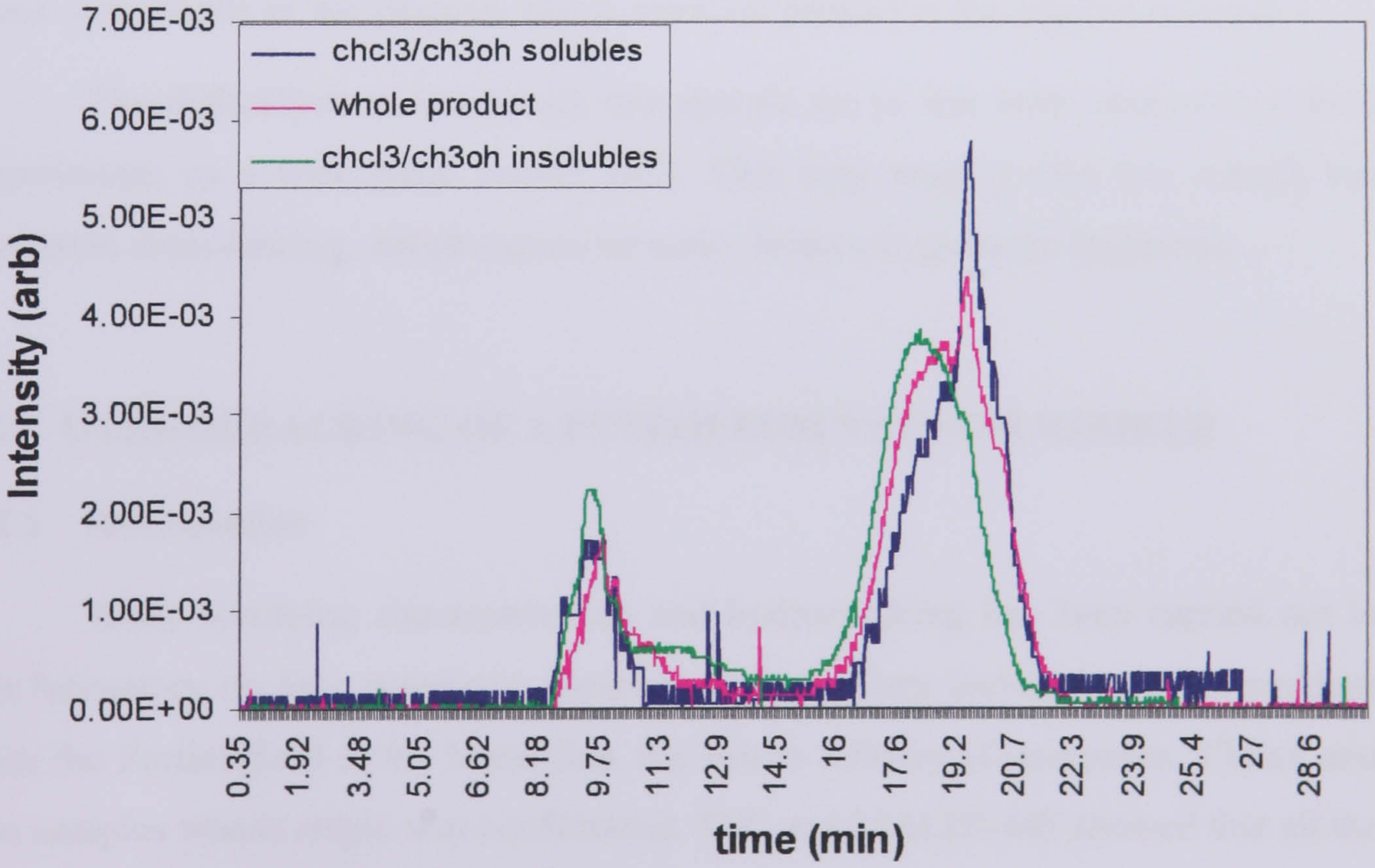


Figure 9.4. Comparison between the mixed-D column SEC chromatograms of the whole hydrocracking products and its $CHCl_3/CH_3OH$ soluble and insoluble fractions. Area normalisation has been applied to all chromatograms.

The whole products as well as its $CHCl_3/CH_3OH$ soluble fraction have also been analysed by probe-MS. The intensities of both spectra were low but some of the peaks obtained in $CHCl_3/CH_3OH$ soluble fraction of the pitch pyridine insolubles were also seen in these samples. In addition some signals which could be generated by fragmentation products have been observed. This is the case of the signal at m/z 191, which can be product of the fragmentation of an alkyl phenanthrene. This indicates that hydrocracking took place to a limited extent, although most of the products have remained above the detection limit of Probe-MS.

9.1.4 Conclusions

Hydrocracking the pyridine insoluble fractions of a coal tar pitch to generate smaller molecules has proven difficult. A first attempt to hydrocrack the sample for 2 hours at 375°C and 200 bar hydrogen pressure led to the formation of a char. A second hydrocracking experiment in which the sample was hydrocracked at a higher temperature, 450°C, for a short time, 2 minutes, was carried out. A slight shift towards lighter product was observed in the products by SEC. Probe-MS showed some compounds in the products which were not present in the original material.

The difficulties to hydrocrack this sample are in line with observations from experiments in a wire mesh reactor [87]. This may suggest that this sample has extensive cross-linking, which cannot be easily broken to generate fragments.

9.2 HYDROCRACKING OF A PETROLEUM VACUUM RESIDUE

9.2.1 Introduction

Work involving characterisation and hydrocracking has been carried out in this laboratory on four petroleum vacuum residues. They included vacuum residues from the Forties field in the North Sea, the Petrox refinery (Concepción, Chile), and two samples whose origin was confidential. SEC and MALDI-MS showed that all the vacuum residues had similar mass ranges [46, 47].

The Petrox residue was hydrocracked under 190 bar hydrogen pressure in the presence of tetralin as solvent in previous work [71]. These experiments were carried out using two pillared clay catalysts [71], a Cr montmorillonite calcined at 500 °C

and a tin laponite, as well as a standard NiMo on silica PBC 90D catalyst. A run without catalyst was also performed. Higher conversions were generally achieved in the hydrocracking of this sample than in coal-derived materials under the same conditions. The products also showed a reduction in the excluded peak and a large shift towards smaller materials by SEC. The largest reductions in sizes were achieved when the pillared clays were used as catalysts.

However, as in the hydrocracking of the pyridine insoluble fraction of the coal tar pitch described above, the presence of tetralin complicated the analysis of products due to the generation of its own reaction products.

As described in Chapter 4, problems derived from the use of tetralin have been overcome in this work where coal liquids were hydrocracked in the absence of a solvent [98]. In the present work, a vacuum residue has been hydrocracked for 2 hours at 440°C in the absence of catalyst and in the presence of an aluminium montmorillonite and the commercial $NiMo/Al_2O_3$ catalyst. The objective of this work has been to determine if the experimental set up implying the use of no catalyst, which was successfully applied to coal derived materials, can also be used in the hydrocracking of petroleum feeds.

9.2.2 Experimental

Three vacuum residues, named as A, B and C, have been received from Shell. The precise origin of the samples is not known due to commercial confidentiality. They have been analysed in this laboratory by SEC and UV-F. The heavier of these vacuum residues according to those analyses, "sample C", has been used as feed in these hydrocracking experiments.

The microbomb reactor and the procedure followed in hydrocracking runs have been described in the experimental section. Briefly, 1 g of sample and 250 mg of catalyst, if used, were charged into the microbomb reactor. It was then pressurised with hydrogen and placed in a fluidised sand bath heater where it reached the operation temperature and pressure, 440°C and 190 bar respectively. Hydrocracking runs were 2 hours long and the products were recovered and analysed. SEC chromatograms of the feed and hydrocracking products were run in a mixed-A column.

9.2.3 Results and Discussion

The boiling point distribution of the vacuum residue C was obtained with the TGA method. 62% of the sample was found to have boiling points above 450°C. Although the ">450°C" fraction is greater than that of the Point of Ayr coal extract and hydrocracker feed (46.5 and 38%, respectively), its reactivity is much higher. The conversion of ">450°C" material in the non-catalytic hydrocracking experiment was almost total, as Table 9.1 shows. However, a large part of the feed was converted into gas products. The fraction of the feed recovered as either solids or $CHCl_3/CH_3OH$ solution was low, only 57%.

Table 9.1. Table of conversions for experiments using Vacuum Residue C as feed. Experiments were performed at 440°C and 190 bar hydrogen pressure. The reaction time was 2 hours.

Catalyst	Apparent conversion (%)	Carbonaceous solids (as % of the filter cake)	Real conversion (%)	Liquid product recovered (as % of the feed)	Total Product recovered (as % of the feed)
No catalyst	98	100	98	57	57
$NiMo/Al_2O_3$	96	12	92	72	75
Al mont.	99	15	76	35	50
Reused Al mont	96	6	94	64	66

As the conversion in the run without catalyst was nearly 100%, no improvements were expected to occur when a catalyst was used. By using $NiMo/Al_2O_3$ or aluminium pillared montmorillonite the conversion actually decreased. The reason for this drop was the presence of carbonaceous deposits on the catalysts, which are included in the ">450°C" fraction. The higher deposition on a fresh Al montmorillonite led to significantly lower conversions, whereas both the $NiMo/Al_2O_3$ and the coated Al montmorillonite showed conversions above 90%.

The low product weights recovered from these experiments reflected the high amounts of gas formed. The formation of gas was higher in the run using fresh Al montmorillonite than in the non-catalysed run. On the other hand, $NiMo/Al_2O_3$ and

the reused Al montmorillonite improved the hydrocracking performance compared to non-catalytic conditions, generating a larger amount of liquid products rather than gases.

Figure 9.5 shows the SEC chromatograms of the vacuum bottoms C and hydrocracking products obtained using the pillared clay catalyst, fresh and reused. It was observed that the small excluded peak eluting at about 14 minutes in the SEC of the feed was completely removed from the chromatogram of the products. Moreover, the retained peak shifted towards smaller masses relative to that of the feed in both runs. However, the shift of the retained peak is smaller in the run when an already coated catalyst is used. There are two factors that may contribute to the retained peak eluting at earlier times in the second run. Firstly, the catalyst deactivation is expected to be larger during the second use of the catalyst. Secondly, the deposition of heavy ends on the catalyst surface decreases when an already coated catalyst is employed. The amount of heavier materials in the liquid products tended therefore to increase. These results showed a clear reduction in molecular sizes after hydrocracking.

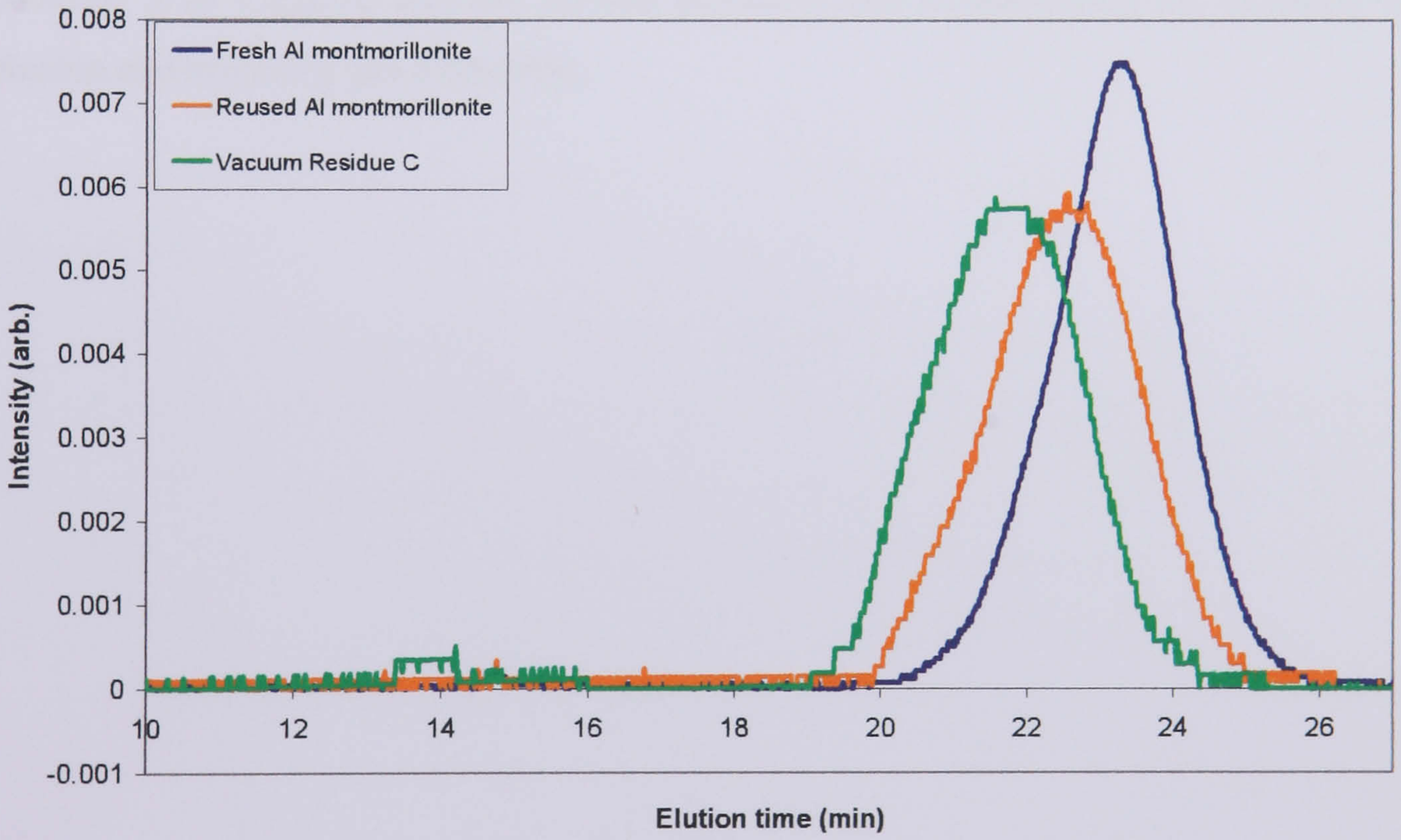


Figure 9.5. Mixed-A column SEC chromatograms of the vacuum residue C and its 2-hour hydrocracking products using fresh and reused Al montmorillonite. All chromatograms have been area normalised.

9.2.4 Conclusions

The hydrocracking of the vacuum residue was very effective. Only the fresh Al montmorillonite showed a real conversion below 90%, and this was mainly due to the relatively large deposition on the catalyst. However, all runs showed a considerable amount of gas products, likely to be of the order of 20 to 45% of the weight of the feed. The use of a catalyst decreased the gas yield in comparison with the run without catalyst. These experiments have shown that even though the residue bottoms C are heavier than the coal derived liquids in terms of boiling point distributions, they were hydrocracked to a larger extent. A combination of lower temperature and hydrogen pressure may improve the amount of liquid products obtained, minimising the gas formation.

It has been observed in previous work that petroleum residues were more easily hydrocracked than coal extracts [71]. However, the results markedly differed from those obtained using tetralin as solvent [71] in the large proportion of gas products. This suggests that the solvent played a role in stabilising the products in solution and reducing gas formation.

10 CHARACTERISATION OF COAL DERIVED SAMPLES BY LASER DESORPTION AND MALDI-TOF MS

10.1 INTRODUCTION

10.1.1 The fundamentals of MALDI-TOF

Matrix Assisted Laser Desorption Ionisation MS (MALDI-MS) is a widely used technique for the characterisation of polymers and biomolecules. Its application to the analysis of hydrocarbons derived from coal and petroleum is at the stage of development. The main advantage of the technique for characterising these samples is that it can cover mass ranges far beyond the limits of conventional mass spectrometry techniques such as GC-MS and Probe-MS. MALDI is a soft ionisation method, which is usually coupled to a time of flight (TOF) mass analyser. This analyser measures the time between the ion generation and detection. The time of flight can be related to the ion m/z ratio by the equation:

$$\frac{m}{z} = \frac{2Ut^2}{s^2}$$

where m is the ion mass, z its charge, U the acceleration voltage, s the flight distance and t the time of flight.

The technique involves mixing a matrix, usually an organic acid of low volatility and molecular weight, with the analyte. The matrix must be a compound capable of absorbing energy at the laser frequency and transferring it to the sample. It also plays a role in sample ionisation by protonating or deprotonating the material. In addition, it behaves as diluting agent, diminishing the interactions among molecules of analyte and reducing in that way the energy required to volatilise the sample. The presence of the matrix provides soft ionisation and volatilisation mechanisms, to minimise fragmentation and allow the determination of high MWs, up to above 100,000 Da. The fundamental processes involved in sample volatilisation by this technique are still the subject of research [99-102].

In the present study, a Bruker Reflex IV model MALDI-TOF spectrometer (Figure 10.1) was used. The excitation of the sample is achieved by irradiation in the UV range (337 nm) with a nitrogen laser. The metallic target is held at a high voltage, typically 20 kV. The ions are accelerated by an electric field towards a field free

region. The spectrometer is equipped with two detectors and can operate in either reflector or linear mode. In reflector mode, the ions are deflected towards the reflector detector (see Figure 10.1) by a voltage situated in the proximity of the linear detector. Ions with higher kinetic energy will penetrate further into the reflector voltage zone than slower ions with the same mass. The resulting longer path will compensate their higher velocity, improving resolution. Hence, the reflector detector provides better resolution for molecules smaller than 20,000 Da. Above that mass range the molecules are too large to be deflected towards the reflector detector.

The linear detector is more suitable for the analyses of these higher masses. It can also be useful in the range below 20,000 Da, although providing lower resolution than the reflector detector. A high mass detector, which is used in the linear mode, provides special sensitivity for high masses, which arrive at the detector with low velocities.

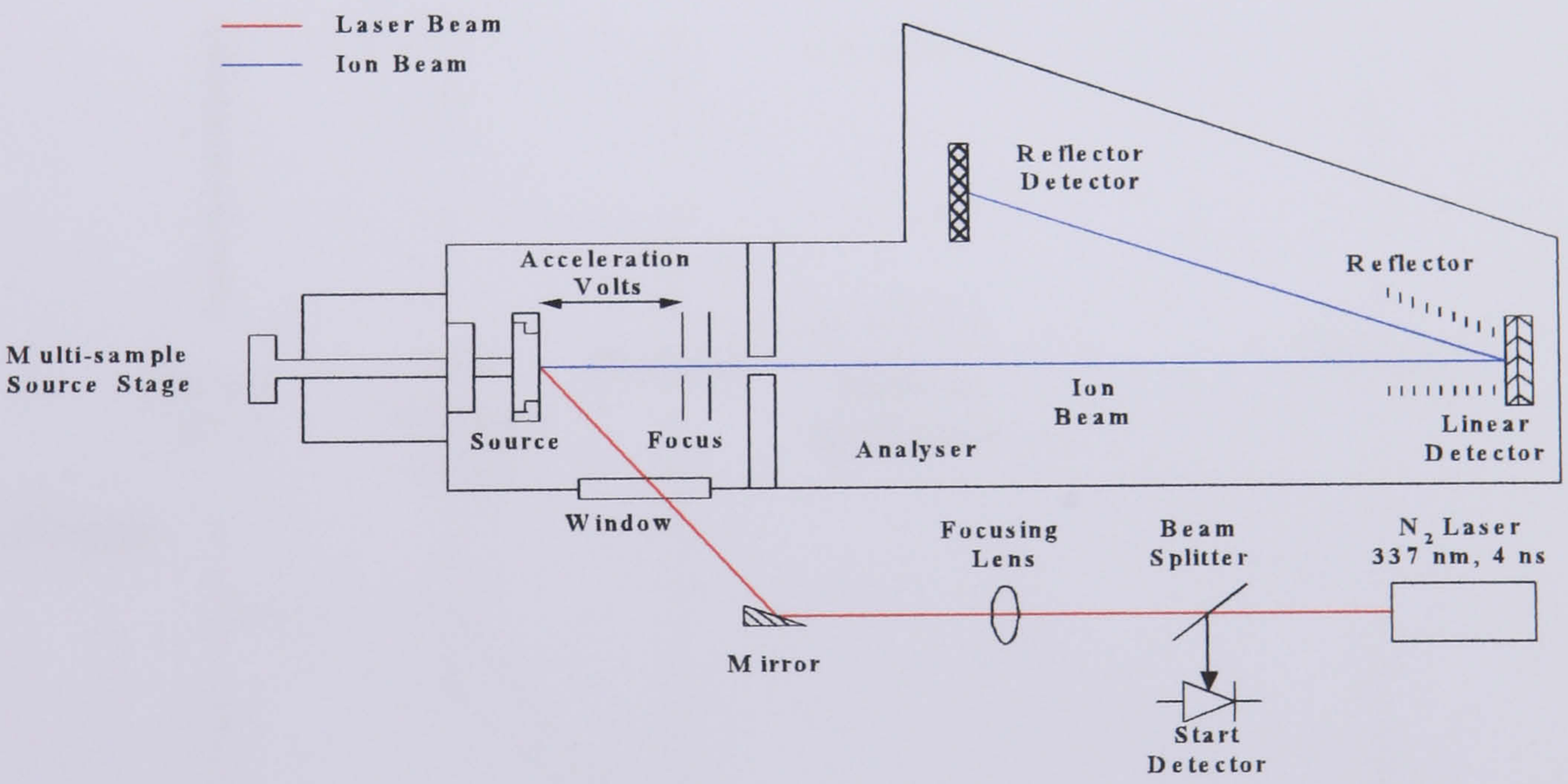


Figure 10.1. Diagram of the MALDI spectrometer.

Two methods are available to minimise the signals produced by the matrix on the spectrum: matrix deflection and matrix suppression. Matrix deflection consists in the application of a voltage perpendicular to the ion trajectory. This voltage is switched on for a short time, of the order of nanoseconds, to deflect ions below a specified mass range. Then it is switched off again to allow the passage of higher

masses. The second method, matrix suppression operates by decreasing sensitivity at the detector for times corresponding to the smaller masses.

A pulsed ion extraction (PIE) system enables dispersion in the initial velocities to be corrected and the signals in the region of interest to be focused. PIE works by means of varying the PIE voltage (P2 in Figure 10.2) situated in front of the sample plate. This voltage is kept at the same value as that of the target, P1, for a certain time following the irradiation of the sample. After that time, whose length in this spectrometer can be set at 200, 400 or 600 ns, it is switched to a lower value. During the time that P1 and P2 are equal the ions experience no electric field. By the time the P2 voltage is switched to a lower value, ions with higher velocities will have travelled a longer distance. When P2 is at the lower value, there exists a field in that region and therefore the ions are accelerated in that region. Therefore, ions which were behind are accelerated for a longer path. As the slower ions are accelerated more than the faster ones, the spread in velocities is narrowed.

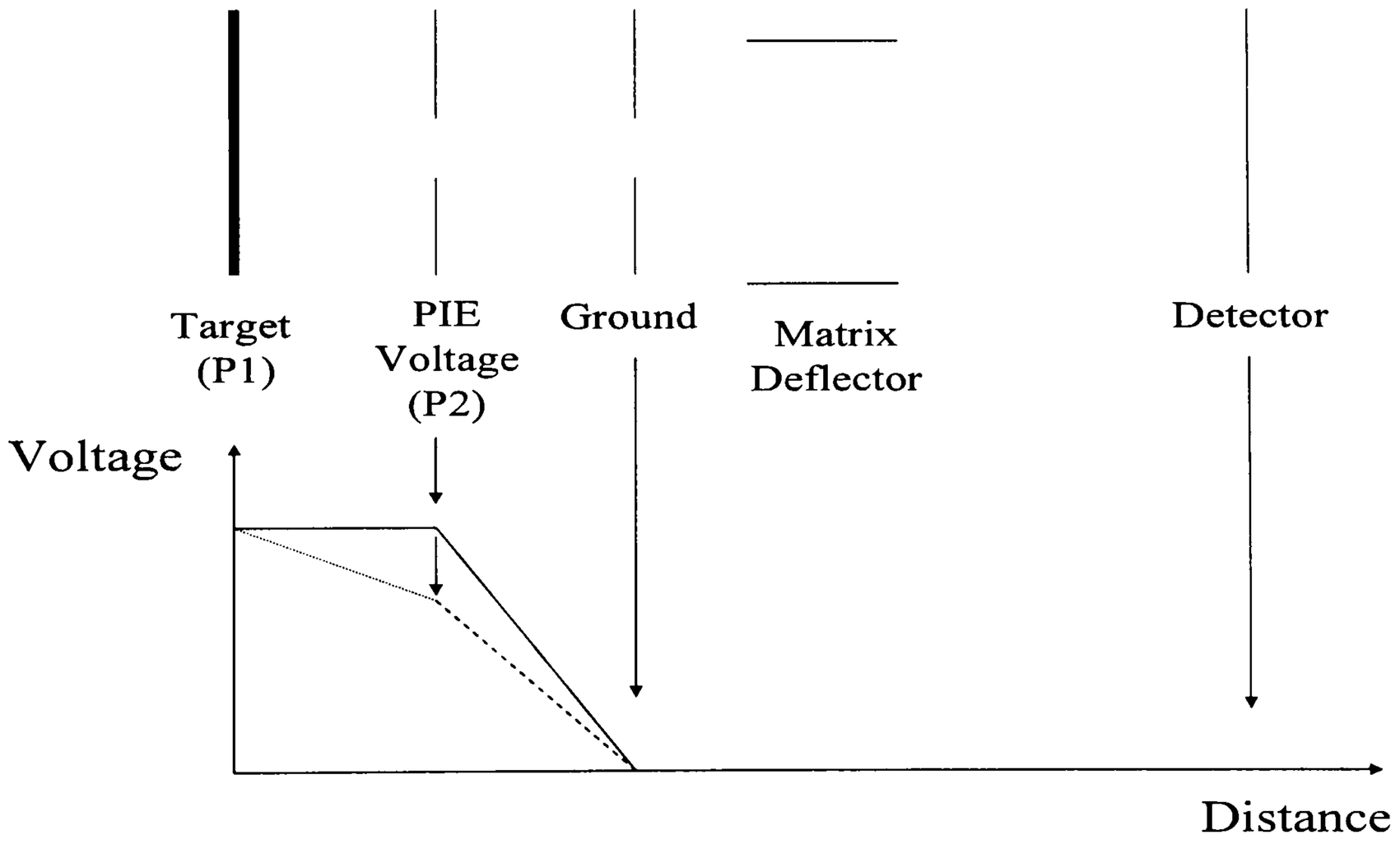


Figure 10.2. Diagram showing pulsed ion extraction (PIE) in the MALDI-TOF spectrometer used in these experiments.

10.1.2 Applications of MALDI-TOF to heavy hydrocarbons

The application of MALDI-TOF to complex samples such as petroleum and coal derived materials has involved considerable method development. The influence

of the ion extraction voltage and matrix composition on the MALDI-MS spectra of a coal tar pitch were investigated by Domin et al. [103] and Lazaro et al. [104]. The intensity of the signal at high masses was observed when raising the extraction voltages from 10kV to 30kV.

Sinapinic acid and 2,5 dihydroxybenzoic acid (DHB) were regarded as the best matrices from a set of compounds that also included 2-(4-hydroxyphenylazo)-benzoic acid (HABA), α-cyano-3-hydroxycinnamic acid (α-cyano), and 9-anthracenecarboxylic acid (9-A). The first two matrices enabled the maximum in the mass distribution to be shifted towards higher values. However, equally good results were obtained by laser desorption alone, although requiring higher sample loading on the MALDI target [103].

The analysis of petroleum and coal-derived materials by MALDI-TOF MS presents complexities derived from the high polydispersity of the samples. The effect of polydispersity on the MALDI spectrum has been analysed in previous work in this laboratory [108]. Mixtures of polystyrene standards were used to simulate samples with high polydispersity [108]. That work showed that the amount of the higher MWs in the sample is underestimated in the presence of smaller material. On the other hand, in petroleum and coal derived samples, it is thought that the small MW materials act as matrix. This allows the application of LD-MS to this kind of sample.

The necessity to obtain more quantitative data on the high mass limit of coal-derived samples led to consideration of different criteria for determining a cut off point for the spectra. A conservative mass limit of about 95,000 Da was thus identified for the coal tar pitch by fractionation of the sample by solubility and application of MALDI-MS on its pyridine insolubles, the heaviest fraction [105].

As described above, a MALDI-TOF mass spectrometer equipped with a high mass detector has been employed in the present work. The influence of the different operational parameters has been re-evaluated for this new spectrometer. The main objective of the present work has been the development of a method to obtain reliable molecular mass distributions of heavy hydrocarbon materials by MALDI-TOF MS. Comparison has been made with results obtained from other techniques, especially SEC. A coal tar pitch was selected for these experiments due to both its greater availability and its previous extensive characterisation by several methods.

As this work focuses on the elucidation of the high mass limit present in coal derived materials, fractionation of the samples has always been carried out beforehand. Coal tar pitch fractions were analysed in order to observe the high mass material in isolation from the more abundant lighter fractions. Two different methods, SEC fractionation and solvent separation, have been used to prepare fractions with narrower polydispersity than the starting material.

10.2 EXPERIMENTAL

The fractionation of the coal tar pitch has been described in the experimental section.

Both MALDI and laser desorption (no matrix) have been applied to the analysis of samples. A Bruker Reflex IV model MALDI-TOF spectrometer was used. The sample was applied on the target as a solution in NMP and dried in a vacuum oven at 100°C, usually for 30 minutes. In cases where a matrix was used, the procedure was similar. Two separate solutions, one of sample and another of matrix, were prepared and successively applied on the target.

Dithranol in combination with the silver salt of trifluoroacetic acid was the matrix of choice used in the work on polystyrenes. Sinapinic acid was preferentially used as matrix for coal samples although some other compounds such as MBTA and dithranol have also been employed.

Typically 100 spectra were added to increase the signal:noise ratio. They were acquired as series of 20 shots. The point of application of the laser on the target was changed between series to avoid local depletion of the sample. Experimental conditions relative to the optimisation of the signal at high masses are discussed below.

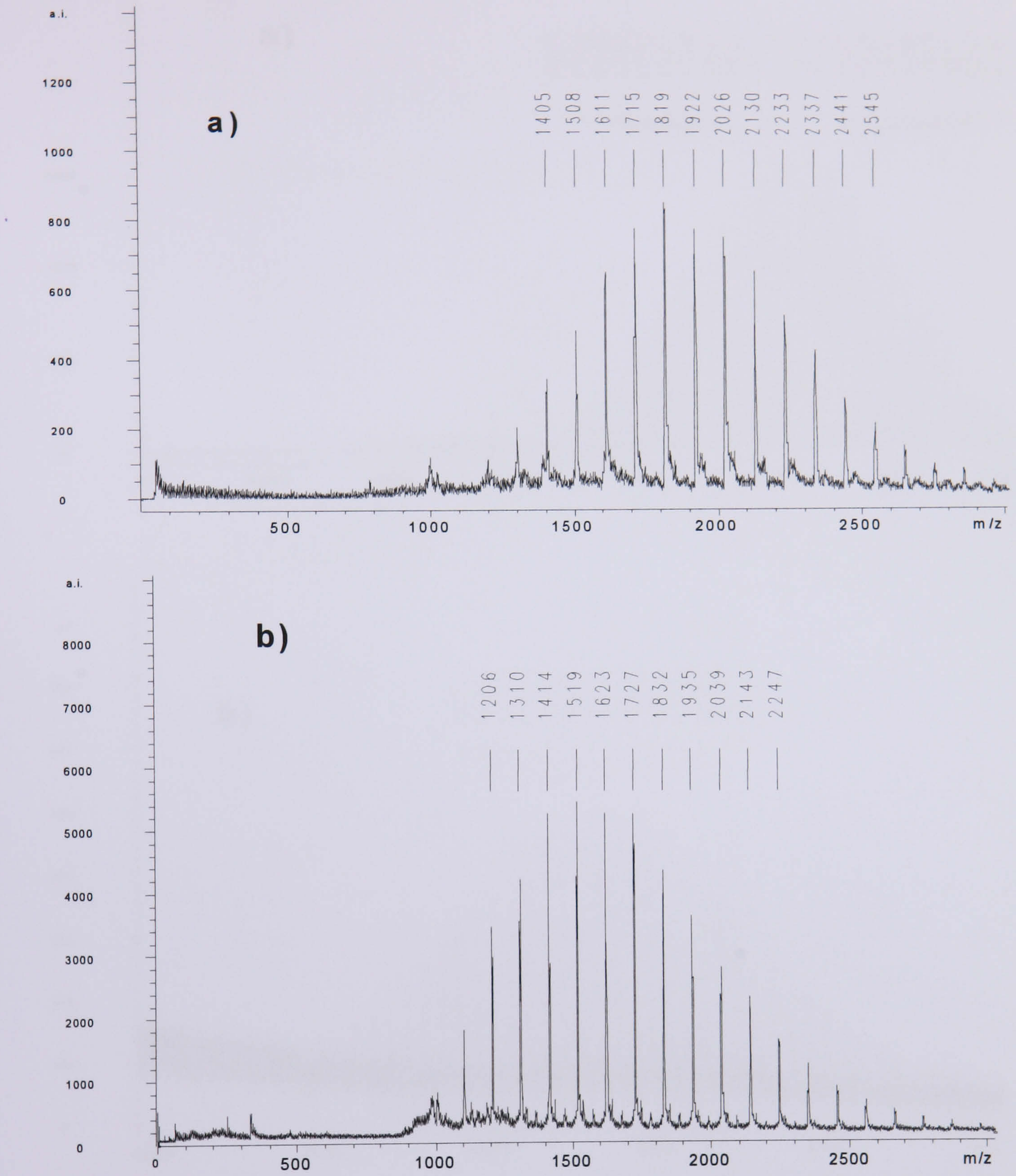
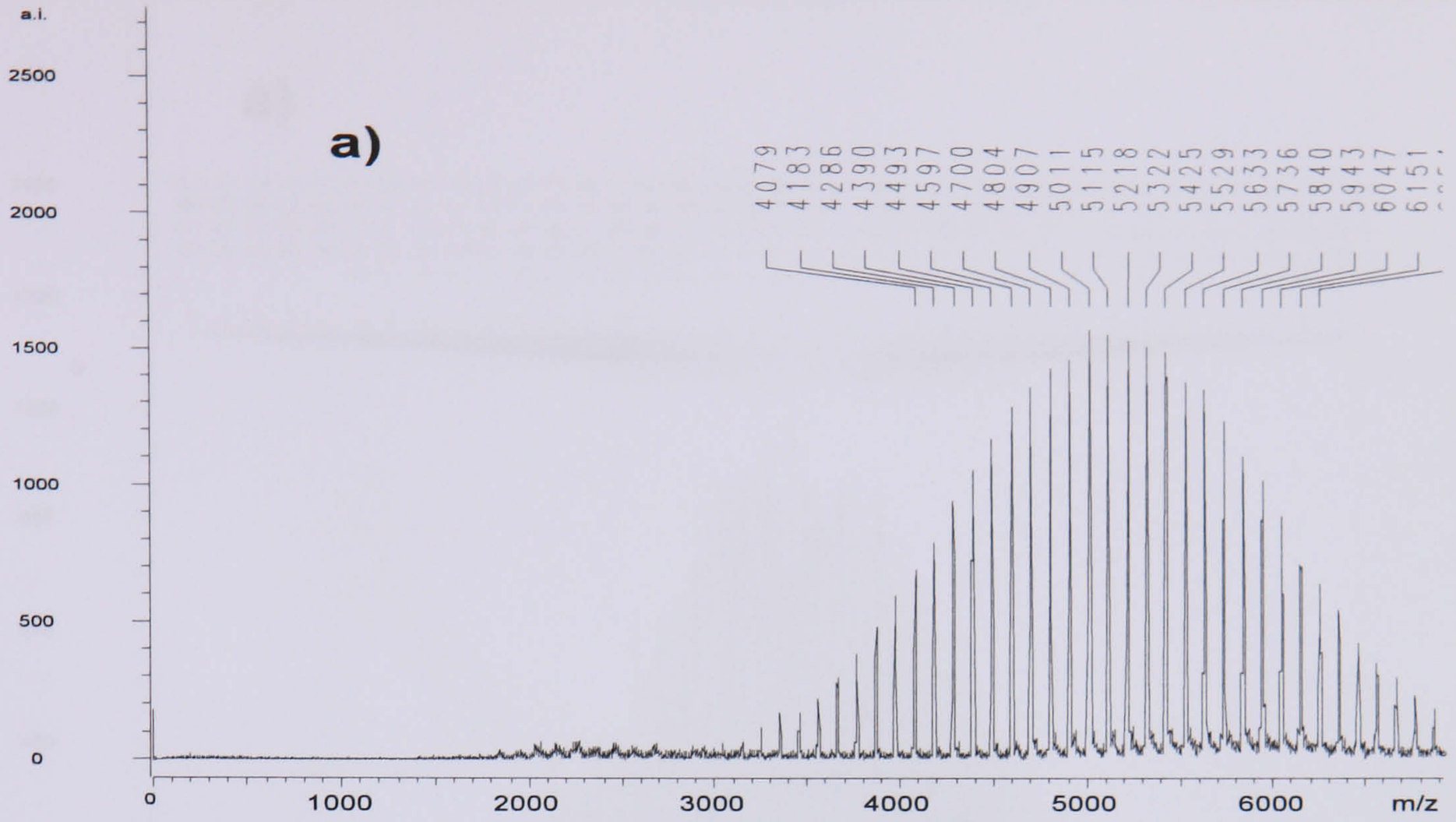


Figure 10.3. MALDI-MS spectra of polystyrene standard 1700 Da recorded by a) reflector b) linear mode.



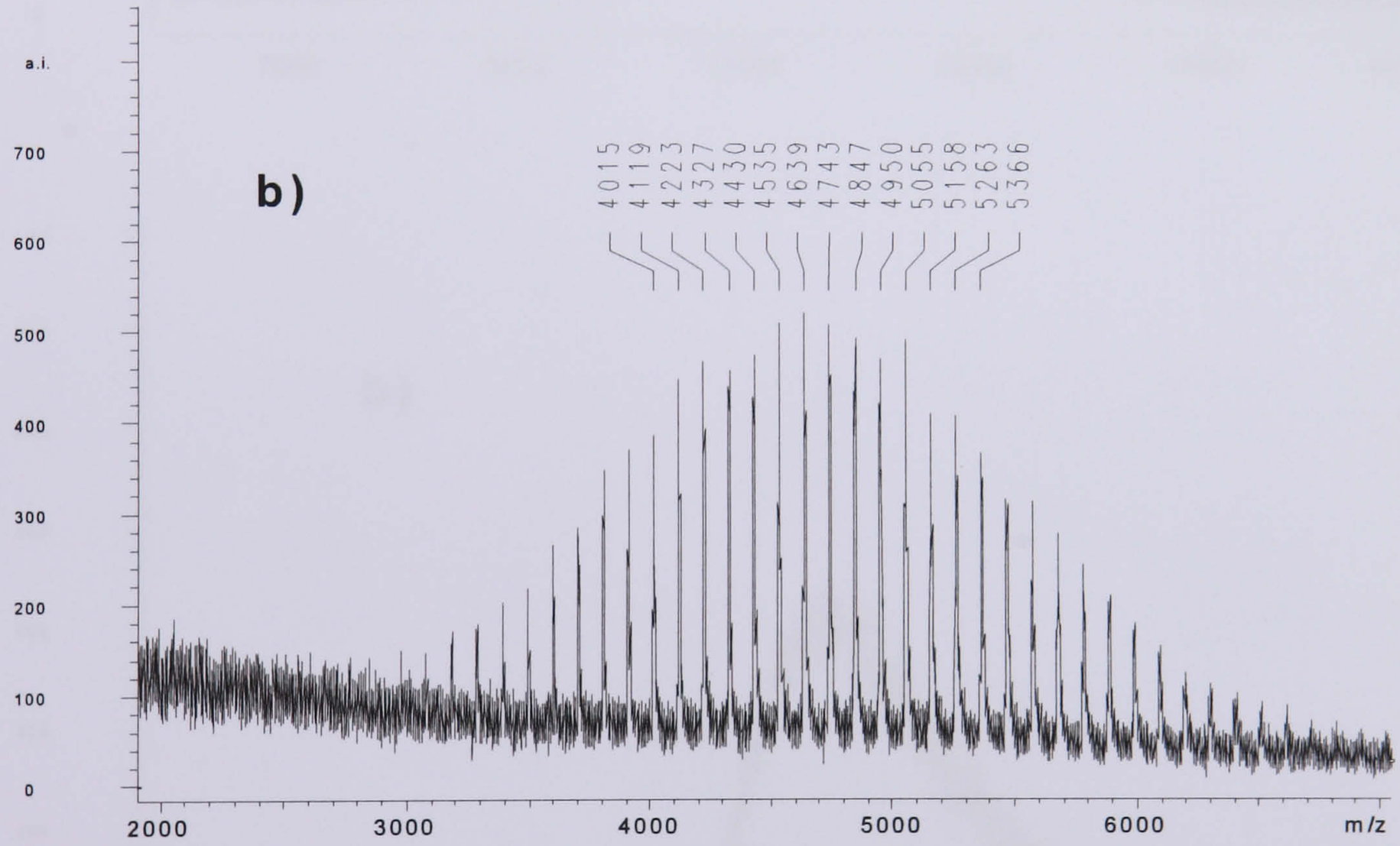


Figure 10.4. MALDI-MS spectra of polystyrene standard 5050 Da recorded by a) reflector b) linear mode.

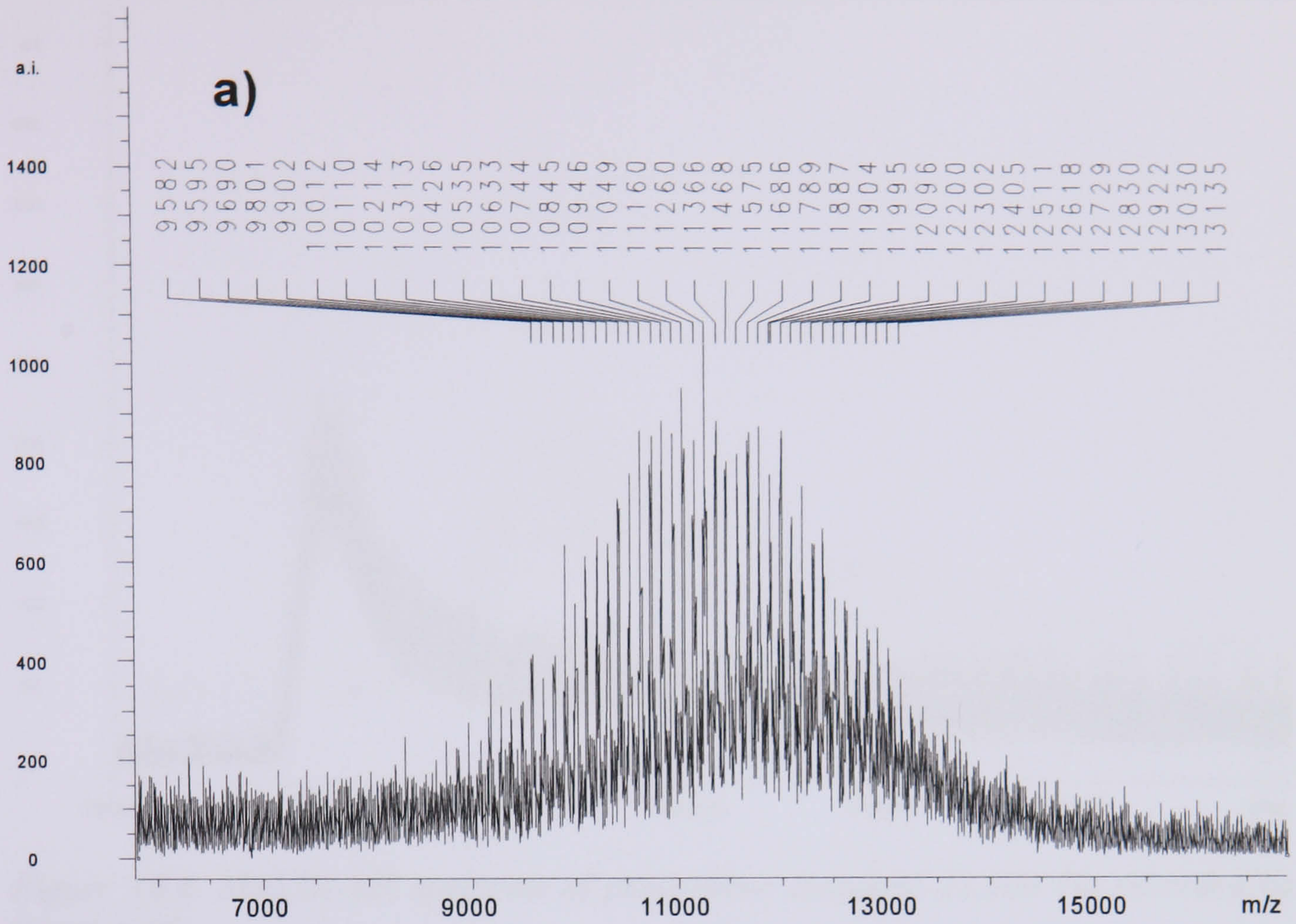


Figure 10.5. MALDI-MS spectra of polystyrene standard 11,600 Da recorded by a) reflector b) linear mode.

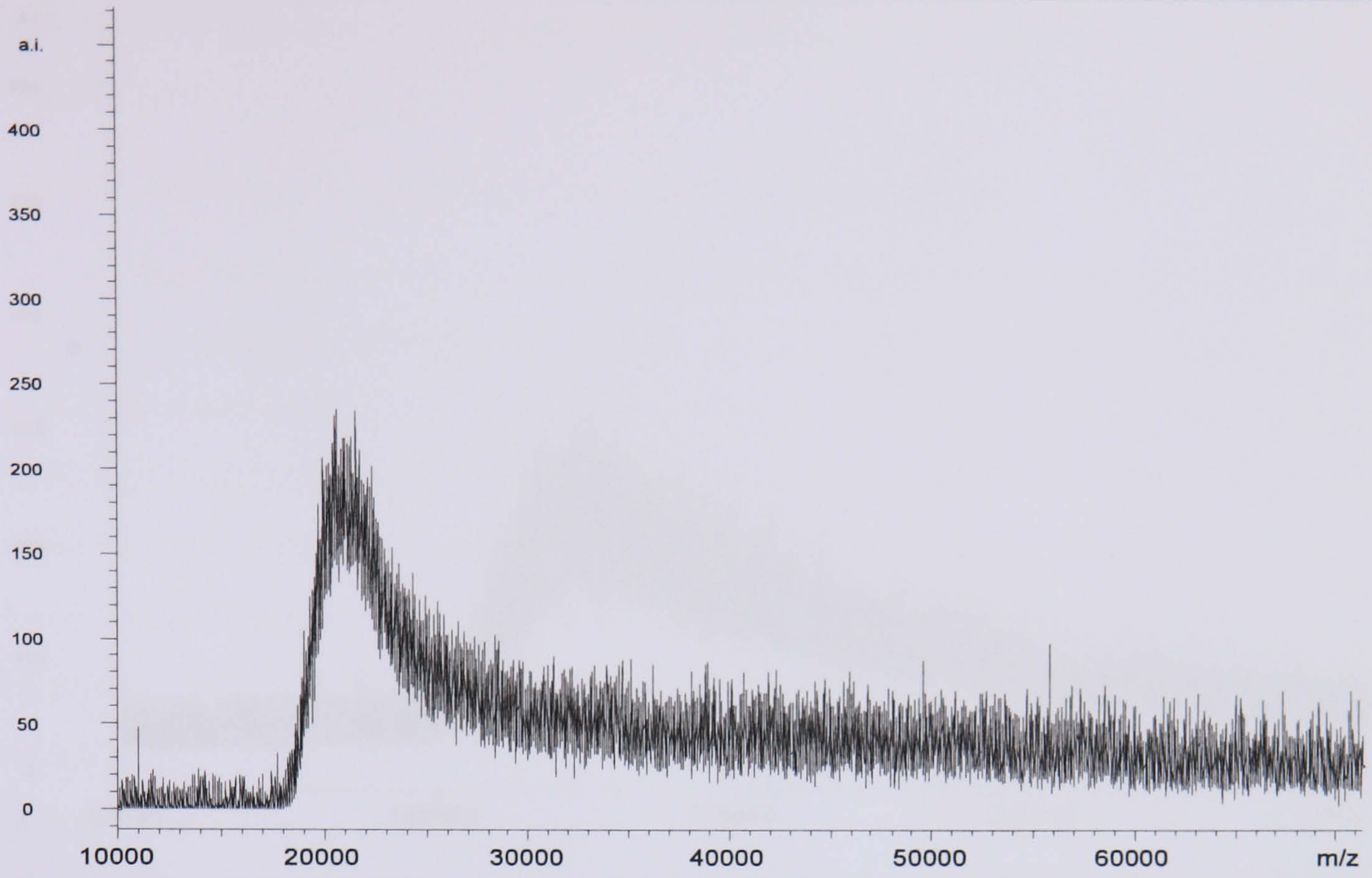


Figure 10.6. MALDI-MS spectrum of polystyrene standard 22,000 Da recorded by linear mode.

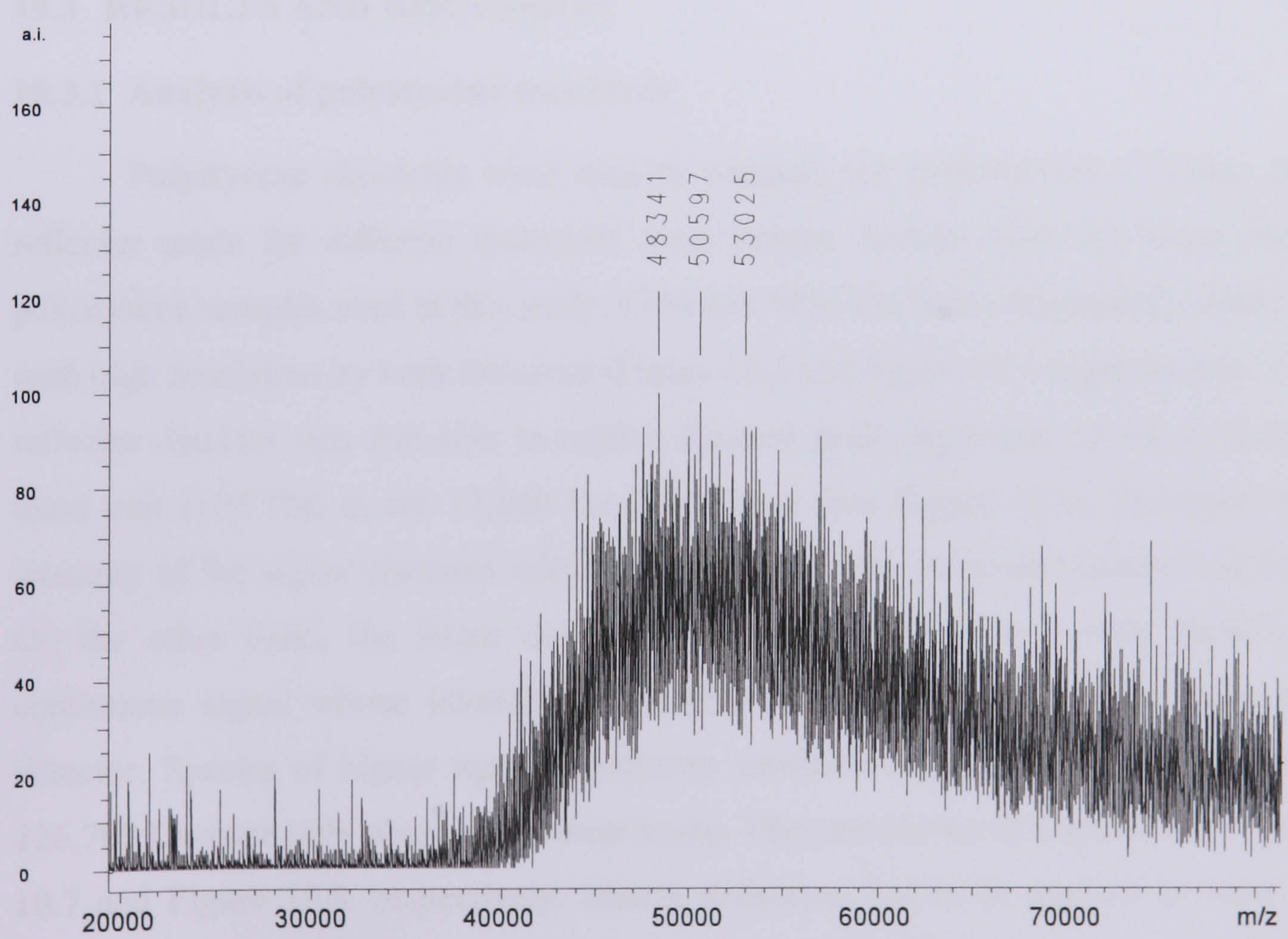


Figure 10.7. MALDI-MS spectrum of polystyrene standard 50,000 Da recorded by linear mode.

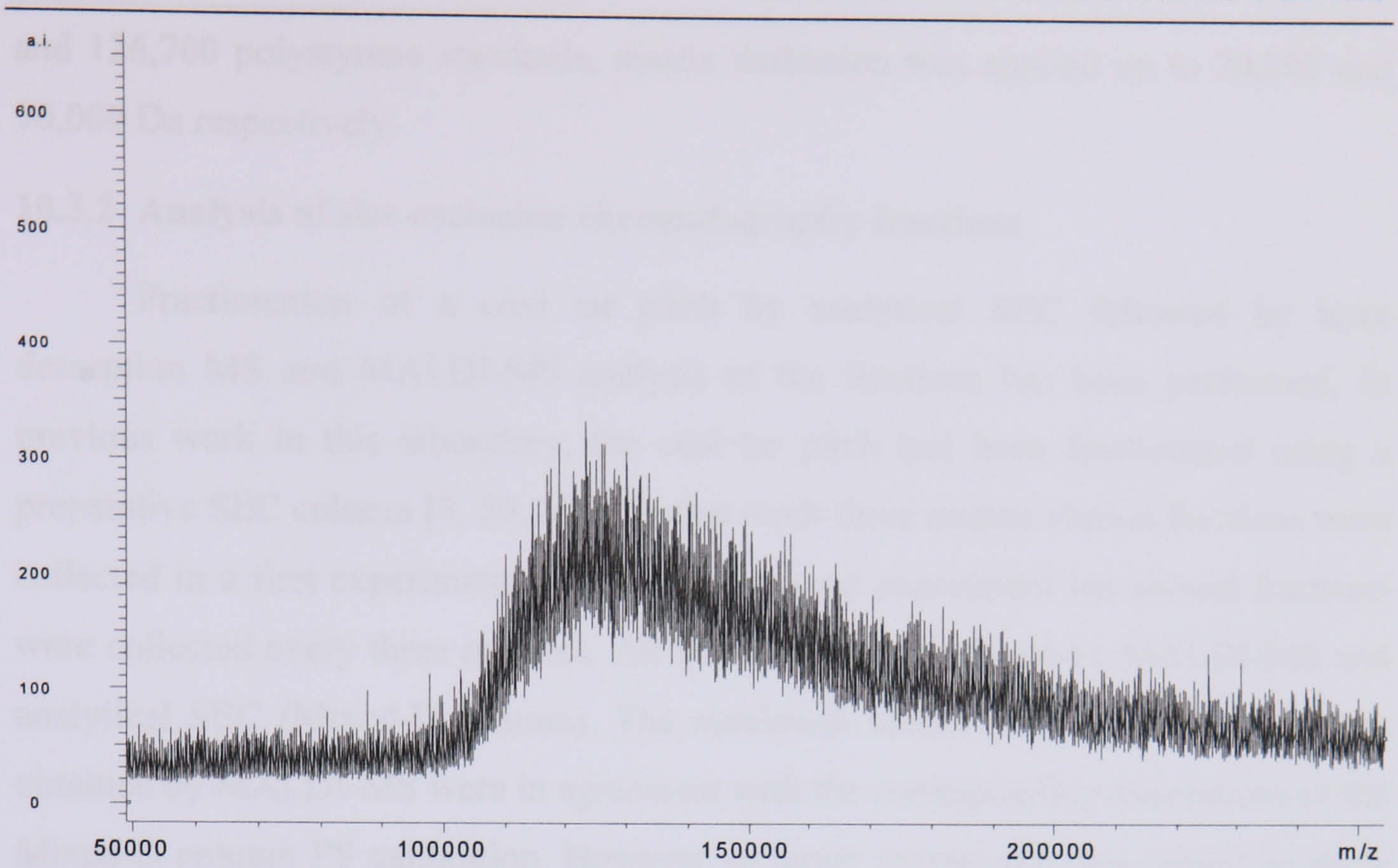


Figure 10.8. MALDI-MS spectrum of polystyrene standard 126,700 Da recorded by linear mode

10.3 RESULTS AND DISCUSSION

10.3.1 Analysis of polystyrene standards

Polystyrene standards were used to compare the performance of linear and reflector mode for different molecular mass ranges. Spectra from the lower mass polystyrene samples used in this study, 1700 and 5050 Da, were successfully obtained with high resolution by both detectors (Figure 10.3 and Figure 10.4 respectively). The reflector detector was still able to resolve discrete peaks separated by the monomer mass unit (104 Da) in the 11,600 Da polystyrene (see Figure 10.5). However, the intensity of the signal obtained with this detector for this particular sample was low. On the other hand, the linear detector gave lower resolution; it only showed a continuous signal whose intensity was higher than that obtained by the reflector detector. Spectra of higher mass polystyrene standards such as 22,000, 50,000 and 126,700 Da were only obtained in linear mode. They are shown in Figure 10.6, Figure 10.7 and Figure 10.8, respectively. Matrix deflection had to be applied in order to obtain signal from the high mass polystyrene standards. Deflection up to 10,000 Da was applied to measure the 22,000 Da polystyrene. To obtain spectra from the 50,000

and 126,700 polystyrene standards, matrix deflection was applied up to 20,000 and 70,000 Da respectively.

10.3.2 Analysis of size exclusion chromatography fractions

Fractionation of a coal tar pitch by analytical SEC followed by laser desorption MS and MALDI-MS analysis of the fractions has been performed. In previous work in this laboratory, the coal tar pitch had been fractionated using a preparative SEC column [3, 59, 106]. In that work three minute elution fractions were collected in a first experiment, whereas in a second experiment ten second fractions were collected every three minutes. All fractions were analysed by MALDI-MS and analytical SEC (Mixed-D column). The maximum values of the mass distributions obtained by MALDI-MS were in agreement with the corresponding estimations of the Mixed-D column PS calibration. However, at larger masses the data tended to show greater dispersion around the calibration line [106].

This work aimed to produce narrower SEC fractions of the coal tar pitch covering the whole chromatogram. An analytical column (Mixed-D) was employed to generate a third set of fractions. The SEC chromatogram of the coal tar pitch used in the fractionation is shown in Figure 10.9. 15 fractions were collected, each of them containing the material eluting from the column for 30 seconds. Four samples were recovered from material showing under the excluded peak, nine under the retained peak, and two in the gap between the retained and excluded peaks. These fractions were subsequently analysed by LD-MS and MALDI-MS with sinapinic acid as matrix. All fractions were run under similar conditions in linear mode and at relatively high laser power (90% of the maximum available in the spectrometer). No matrix deflection was applied in LD-MS experiments, while signal under 300 Da was suppressed by using matrix deflection in MALDI-MS.

The seven earliest eluting fractions, corresponding to elution times between 8.5 and 17 minutes, gave no signal by LD-MS apart from some ions and fragments at the low mass end of the spectrum. This range covers fractions appearing under the excluded peak, the gap between retained and excluded and one sample at the high mass end of the retained peak. The lack of signal may be due to a combination of excessive dilution of the fractions collected from the SEC at those elution times and the low volatility of these materials.

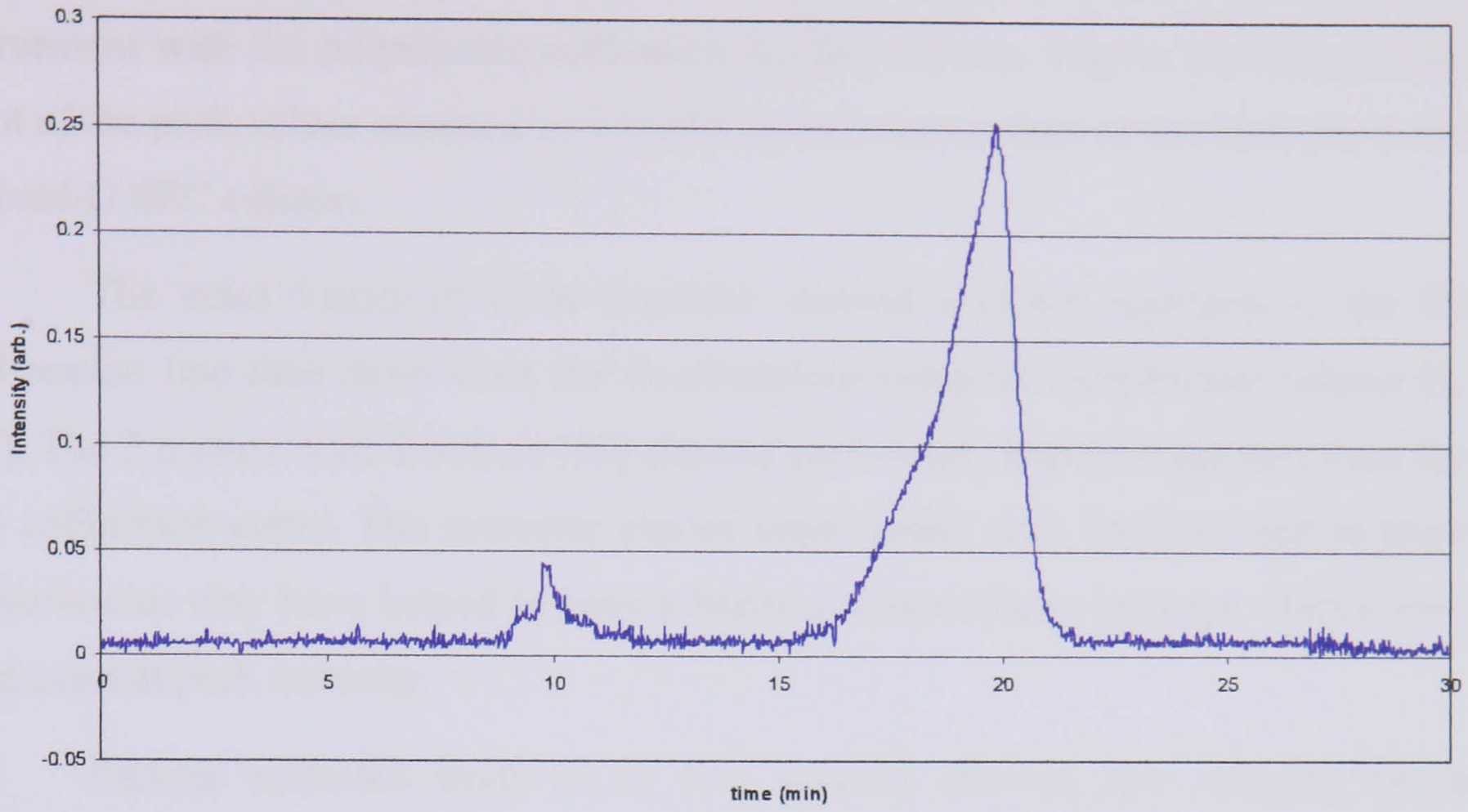


Figure 10.9. Mixed-D column SEC chromatogram of the coal tar pitch. Detection by UVA at 300 nm was employed.

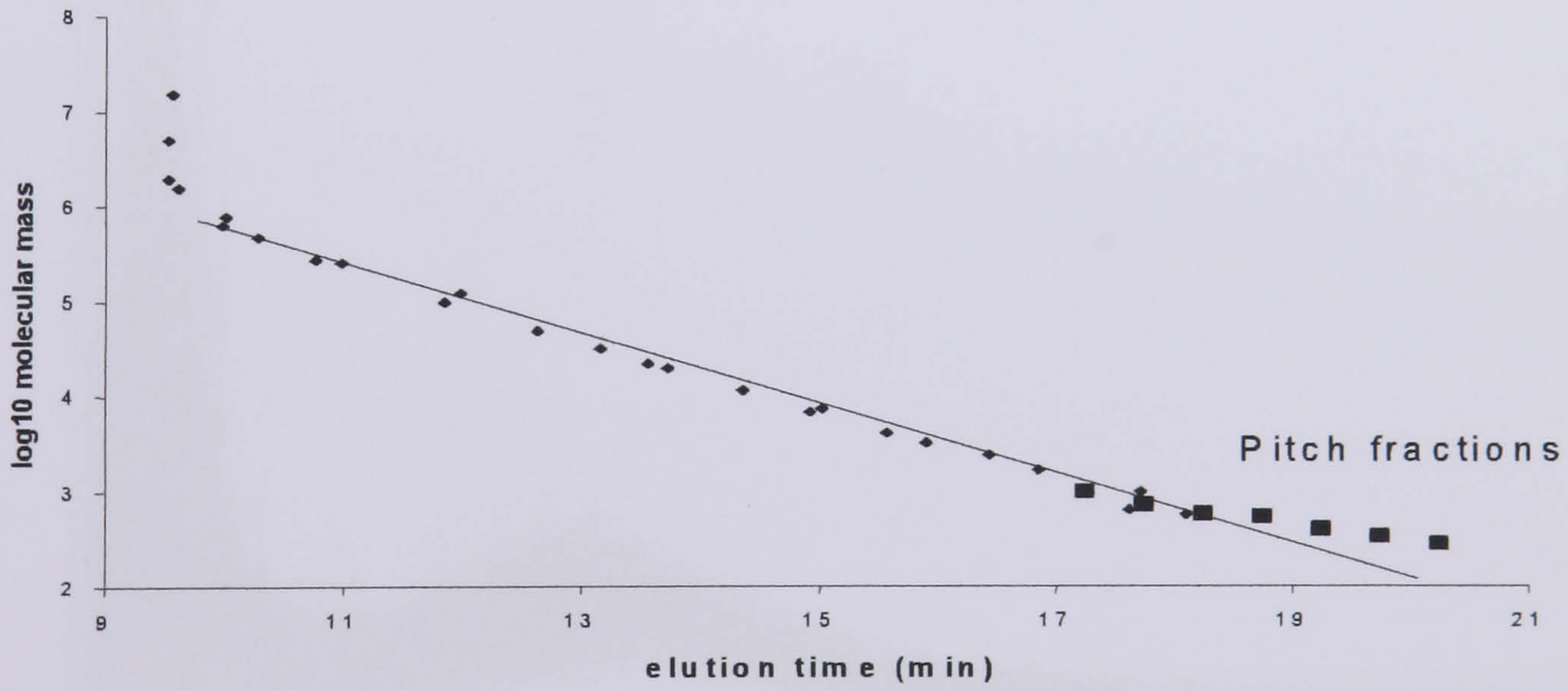


Figure 10.10. Peak-mass of SEC fractions obtained by LD-MS compared with the PS calibration of the Mixed-D column.

Signals were observed in the retained peak fractions. They showed the expected shifts in the mass distribution towards lower values when increasing the

elution time of the sample. Moreover, the peak maximal values were in close agreement with the polystyrene calibration for this column. Figure 10.10 shows the plot of the peak values obtained by LD-MS against elution time of the fractions in the Mixed-D SEC column.

The mass values of these fractions showed a closer approach to the PS calibration line than those from the fractionations using the preparative column [3, 59]. The 3 minute wide fractions [59] showed particularly higher dispersion from the PS calibration curve. The narrower elution times under each fraction used in these experiments may have helped to have a better correspondence between elution time and mass at peak intensity.

Sample collected from 17 to 17.5 minutes showed low intensity but a distribution centred on 1,000 Da was discernible (see Figure 10.11). The intensity of the signal by LD-MS tended to increase towards longer elution times, particularly in the region of masses below 400 Da. Although in this region the signal from the sample was barely distinguished from the signal generated by ions and fragments, a value for the maximum of the distribution can still be obtained.

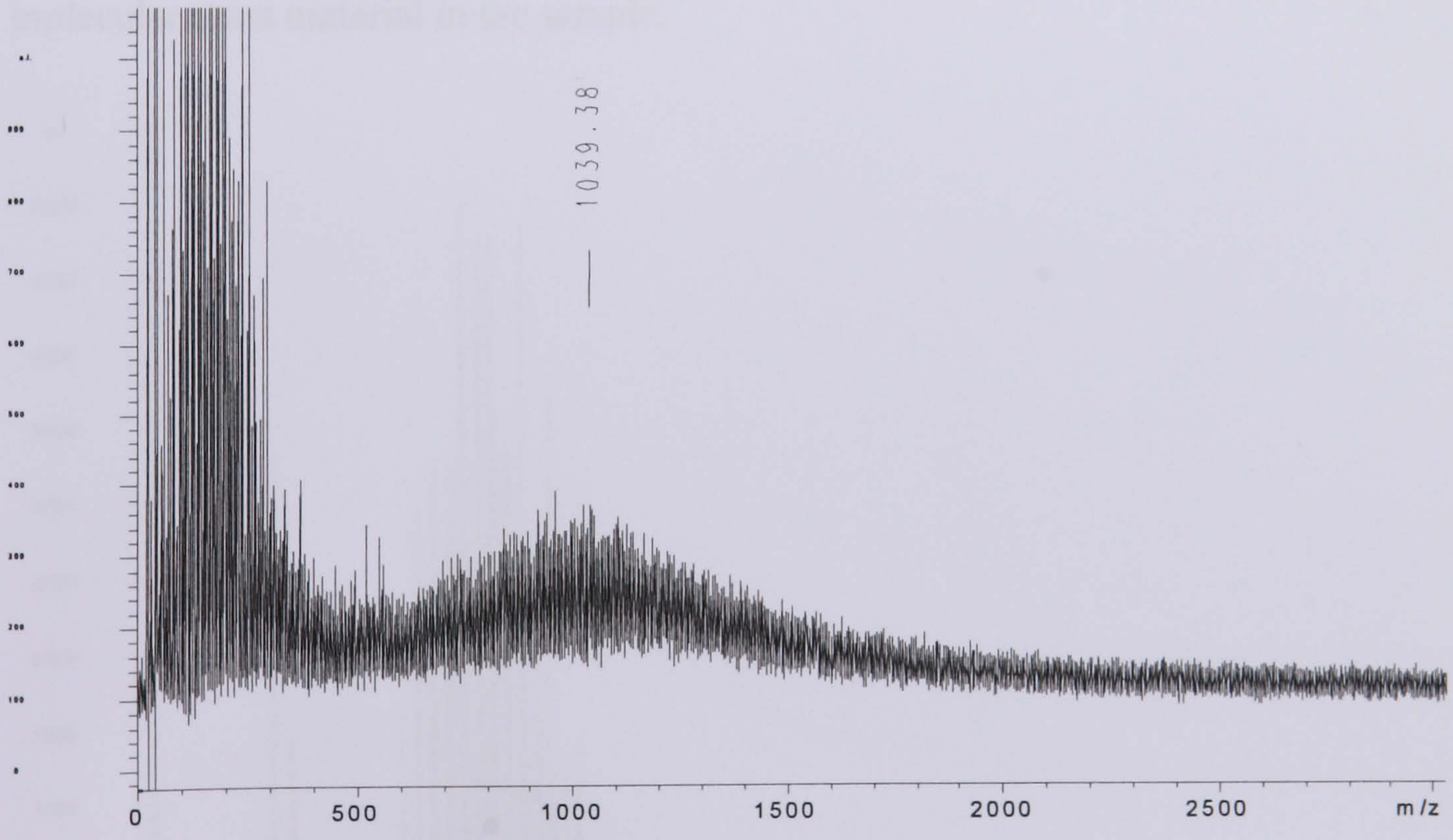


Figure 10.11. LD-MS spectrum of the SEC fraction collected at elution time between 17 and 17.5 min. Spectrum obtained by linear mode.

As mentioned above, although LD-MS gave signal for the lighter fractions, no spectrum could be generated from the heavier ones. It was thought that the aid of a matrix could improve those spectra. Therefore MALDI-TOF MS with sinapinic acid as matrix was run on the whole set of fractions. However, the spectra of all fractions only showed intense matrix-derived signals. It is likely that the lack of results in MALDI-MS experiments is due to the low concentration of material in the fractions collected. In fact, similar spectra have been observed from sinapinic acid on its own when high laser powers and matrix deflection was applied in the experiment, as it was the case in this study.

10.3.3 Analysis of solvent solubility fractions

The coal tar pitch was also fractionated by solubility separation in acetone and pyridine to isolate the heavy material prior to its characterisation by MALDI-MS. Three fractions were produced: acetone soluble, pyridine soluble and pyridine insoluble. In this study, all three samples have been extensively analysed by MALDI-MS and LD-MS to determine the differences between themselves. Most of the work has been focused on the pyridine insoluble fraction since it concentrates the highest molecular mass material in the sample.

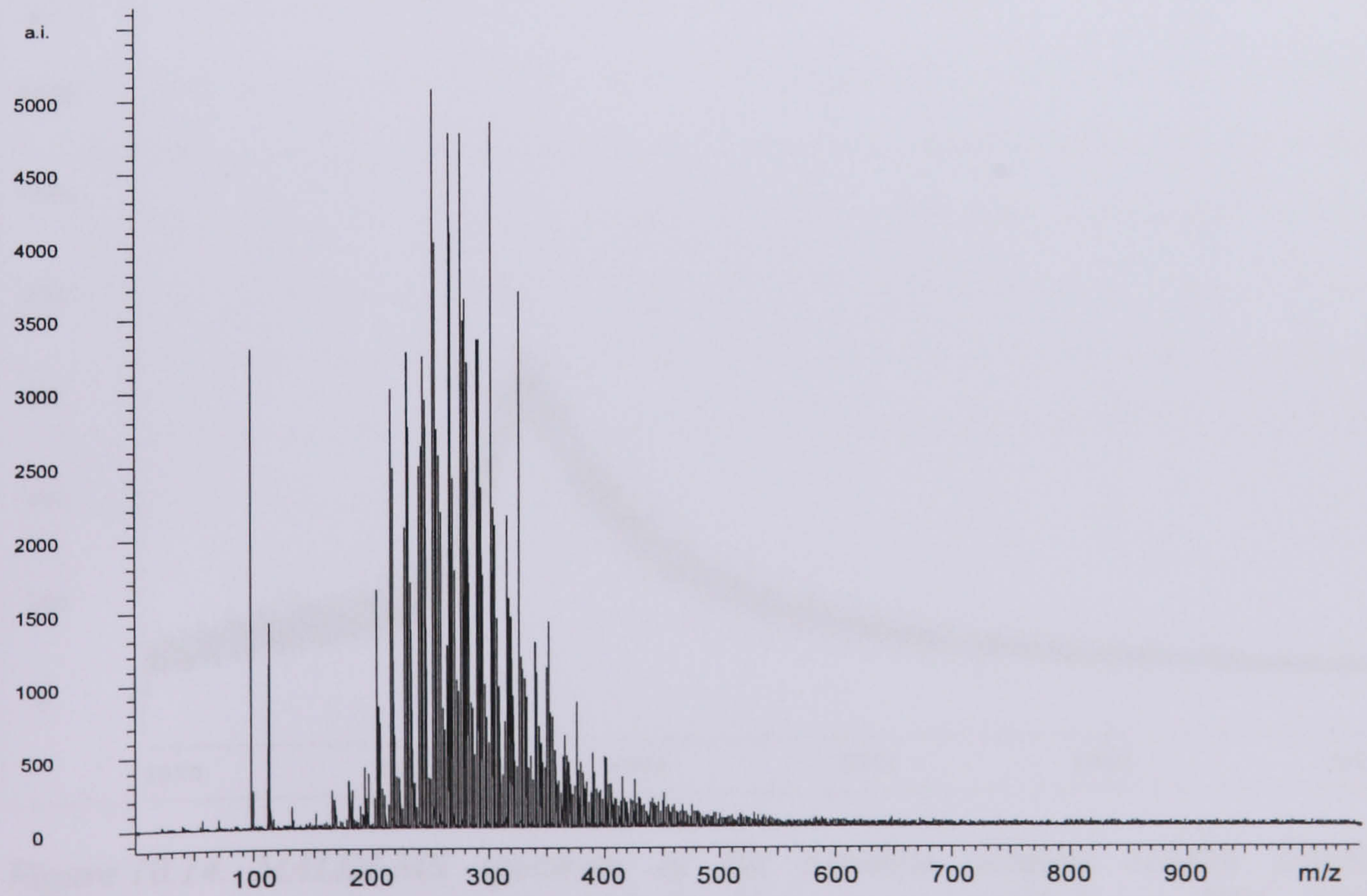


Figure 10.12. Acetone soluble pitch fraction by laser desorption-MS. Reflector mode.

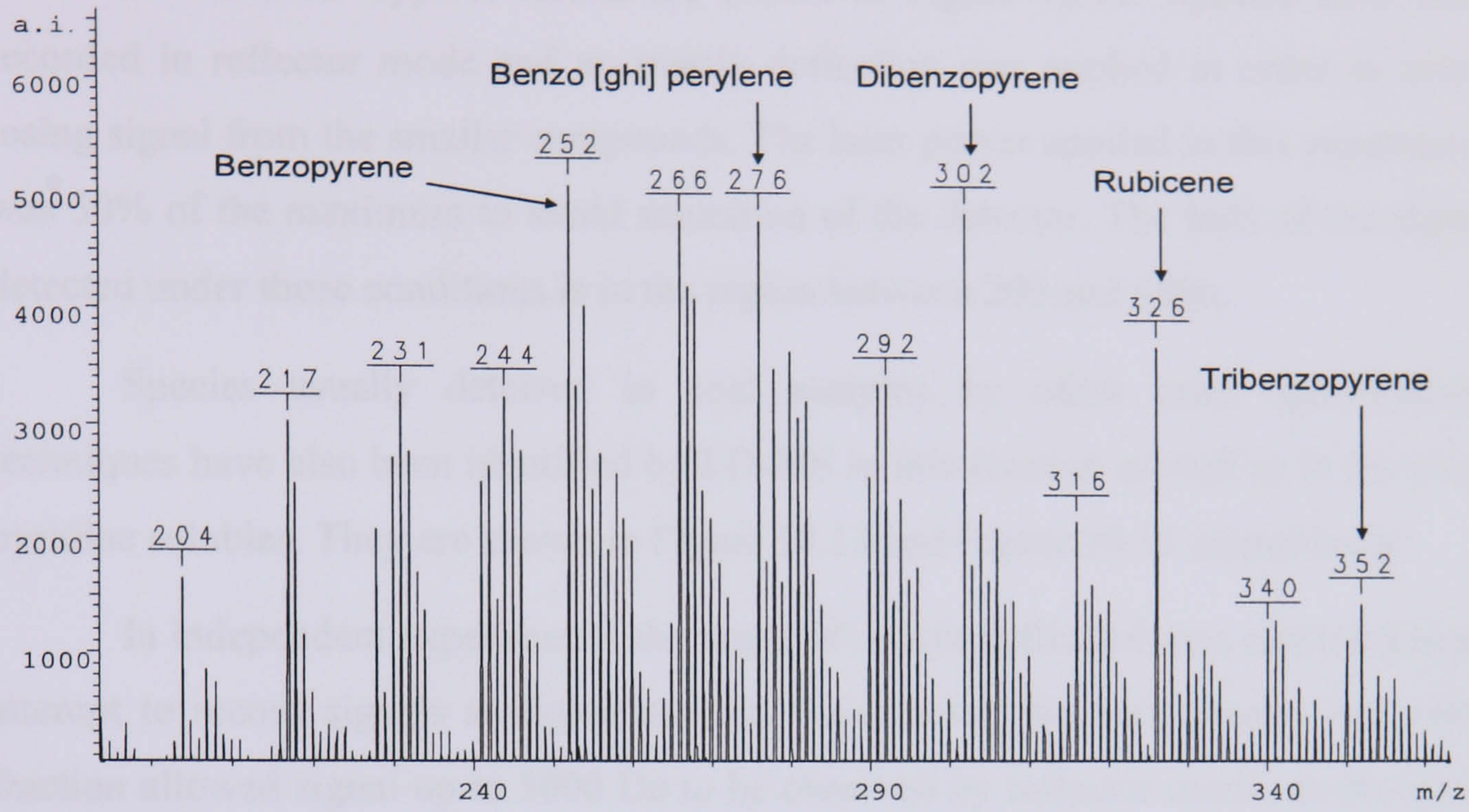


Figure 10.13. Compounds identified in the acetone soluble fraction of the coal tar pitch identified by LD-MS.

Figure 10.14. MALDI-MS spectrum of the pyridine acetone soluble fraction. Dithranol was used as matrix and the laser power applied was 70%. Matrix deflection was applied

The acetone soluble pitch fraction was analysed by MALDI-MS and LD-MS. Both techniques gave very similar results, proving that the acetone soluble material is effective as matrix. Typical results are shown in Figure 10.12. Spectra have been recorded in reflector mode and no matrix deflection was applied in order to avoid losing signal from the smaller compounds. The laser power applied in this experiment was 30% of the maximum to avoid saturation of the detector. The bulk of the signal detected under those conditions is in the region between 200 and 400u.

Species usually detected in coal samples by other mass spectroscopy techniques have also been identified by LD-MS in this fraction as well as in the pitch pyridine solubles. They are shown in Figure 10.13 and Figure 10.16 respectively.

In independent experiments, the range of matrix deflection was extended in an attempt to record signals at higher masses. Suppressing the very intense low mass fraction allowed signal up to 5000 Da to be observed by reflector mode, as shown in Figure 10.14. However, the intensity of these signals decreased continuously at higher masses. Hence increasing laser power levels were applied to the sample. These results were reproducible in experiments run with dithranol as matrix and without matrix.

The pyridine soluble pitch fraction (Figure 10.15) showed a slightly higher molecular mass range than the acetone soluble. It generated strong signals in the range 200 to 500 Da by reflector mode without deflection of the smaller materials. The application of linear mode to this sample led to the observation of the same range of molecular masses as seen by reflector. A higher mass range was observed when deflection was applied in order to suppress signal from the lighter material in this fraction. As in the case of acetone solubles, a higher laser power had to be applied to generate signals at higher masses. Molecular masses up to nearly 3000 Da have been observed in this fraction by this procedure.

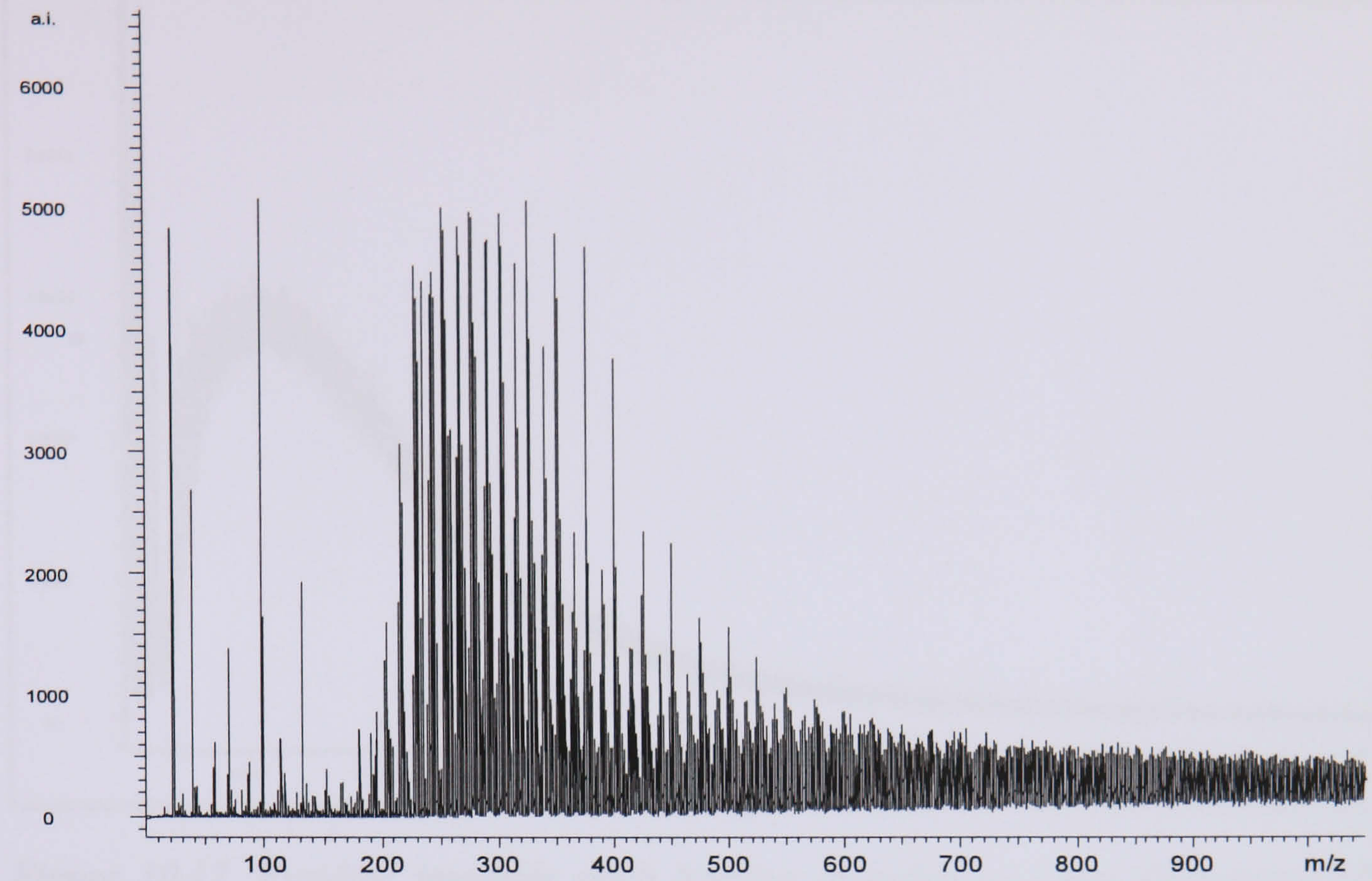


Figure 10.15. Pyridine soluble pitch fraction by laser desorption-MS. Reflector mode.

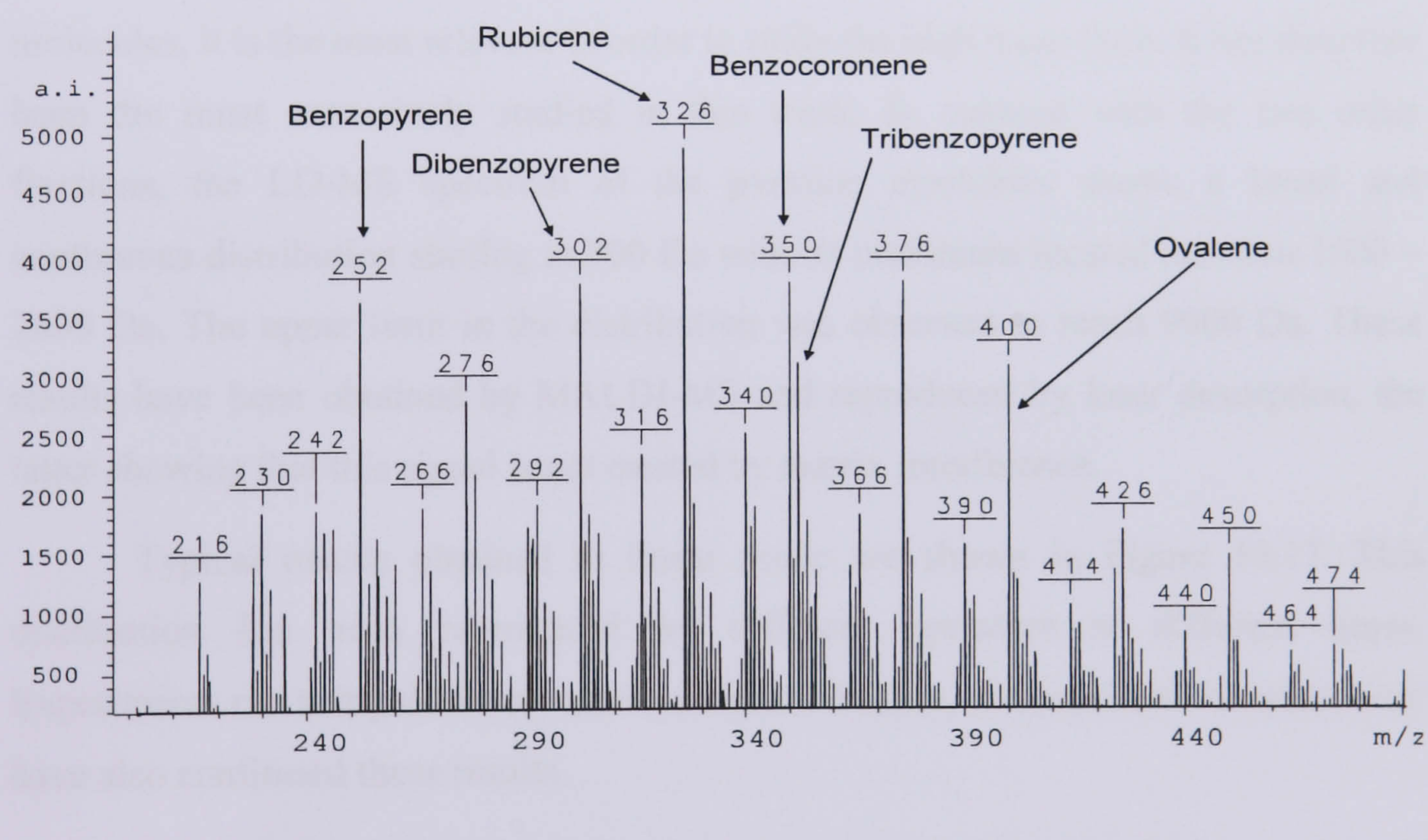


Figure 10.16. Compounds identified in the pyridine soluble fraction of the coal tar pitch by LD-MS.

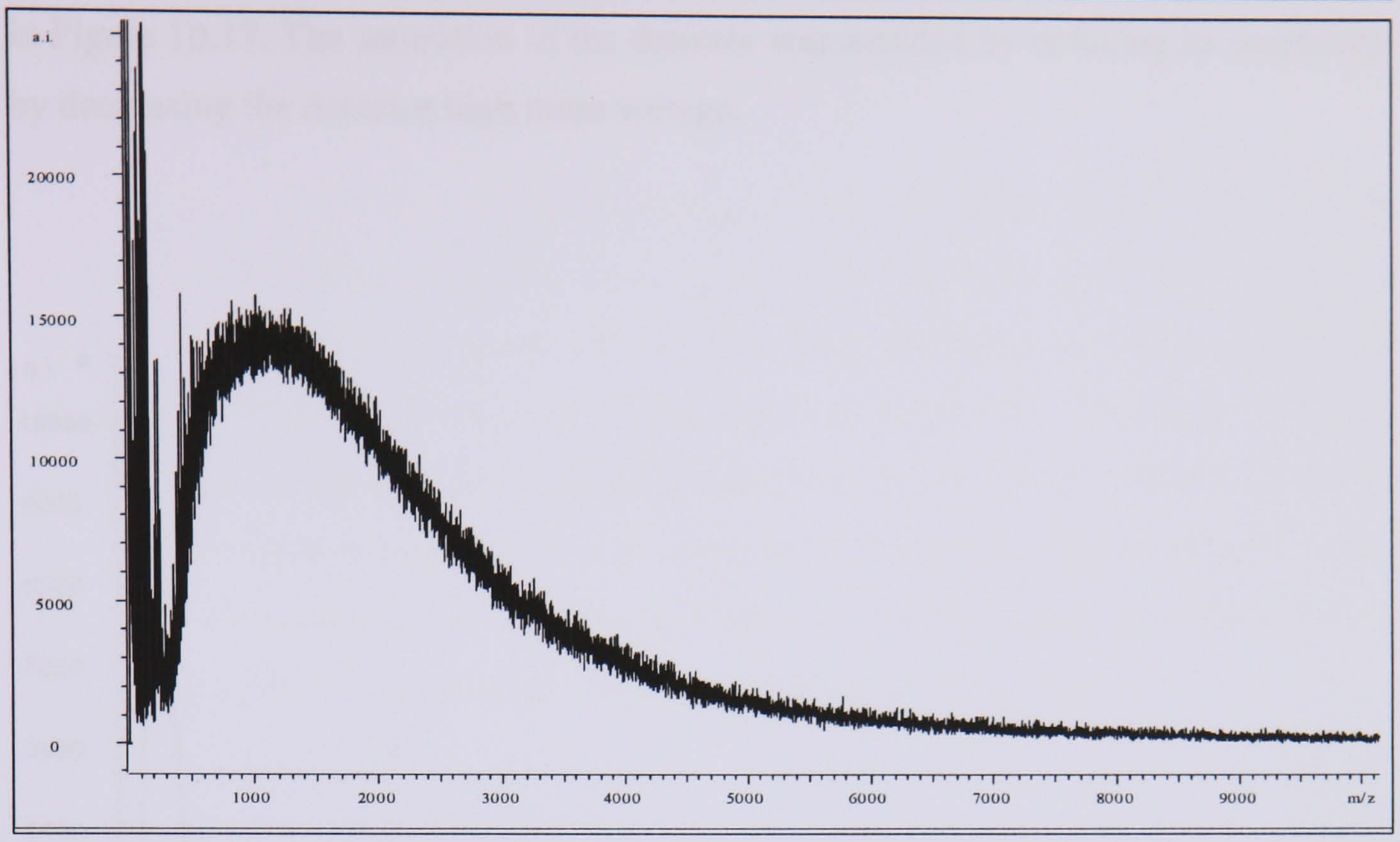


Figure 10.17. Pyridine insoluble pitch fraction recorded by Laser Desorption MS using linear mode.

Since the pyridine insoluble fraction of the coal tar pitch contains the largest molecules, it is the most relevant in order to study the high mass limit. It has therefore been the most extensively studied in this work. In contrast with the two other fractions, the LD-MS spectrum of the pyridine insolubles shows a broad and continuous distribution starting at 500 Da with its maximum located between 1000 – 2000 Da. The upper limit in the distribution was observed to reach 9000 Da. These results have been obtained by MALDI-MS and reproduced by laser desorption, the latter showing that this signal is not caused by matrix interference.

Typical results obtained in linear mode are shown in Figure 10.17. This distribution has been reproduced by different operators at different times. Experiments run using different matrices such as MBTA, dithranol and sinapinic acid have also confirmed these results.

Further work carried out by other researchers in this laboratory showed a second peak in the mass distribution centred at masses nearly 30,000 in addition to the distribution shown above [107]. The spectrum, which was reproduced by several operators, is shown in Figure 10.18. The signal at higher masses was generated by working with higher laser powers than those used to produce the distribution shown

in Figure 10.17. The saturation of the detector was avoided by reducing its sensitivity by decreasing the detector high mass voltage.

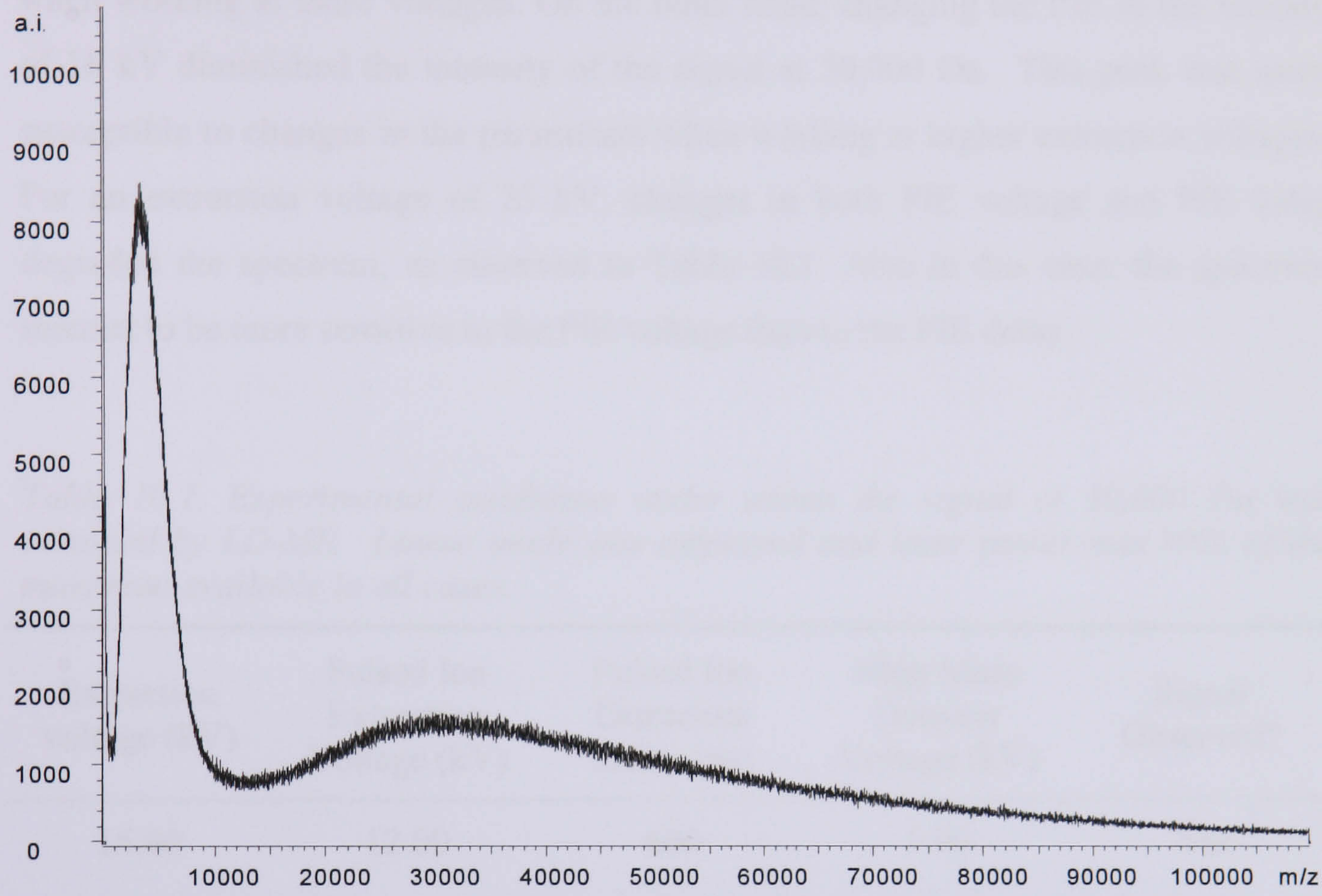


Figure 10.18. MALDI-MS of the pitch pyridine insolubles. Distribution showing a second peak around 30,000 Da. MBTA was used as matrix.

The signal at 30,000 was first obtained employing an extraction voltage of 15 kV opposed to the 20 kV normally used. There was no apparent reason why this signal could be obtained at 15 rather and at 20 kV. Actually higher rather than lower extraction voltages generated signal at larger masses in previous work, as discussed above. Subsequent experiments were therefore focused at reproducing that signal for other extraction voltages. Parameters affecting the pulsed ion extraction system were modified. The ratio between the voltages P1 and P2 applied in the work at 15 kV was applied to the 20 and 25 kV experiments. The extraction delay was also changed. The peak was reproduced working with the conditions detailed in Table 10.1. No differences between spectra generated at different extraction voltages could be appreciated once the parameters shown in Table 10.1 were optimised. The extraction voltage is less a critical parameter in this spectrometer than in those used in previous

works. It is thought that the presence of a detector especially suitable to measure high masses makes unnecessary the application of high extraction voltages to increase the velocity of large mass ions.

Using 20 kV as extraction voltage, a PIE voltage of 16 kV optimised the response to the 30,000 Da peak. No changes in the PIE delay seemed to play a role when working at these voltages. On the other hand, changing the PIE in the vicinity of 16 kV diminished the intensity of the signal at 30,000 Da. This peak was more susceptible to changes in the parameters when working at higher extraction voltages. For an extraction voltage of 25 kV, changes in both PIE voltage and PIE delay degraded the spectrum, as observed in Table 10.1. Also in this case, the spectrum seemed to be more sensitive to the PIE voltage than to the PIE delay.

Table 10.1. Experimental conditions under which the signal at 30,000 Da was obtained by LD-MS. Linear mode was employed and laser power was 80% of the maximum available in all cases.

Extraction voltage (kV)	Pulsed Ion Extraction Voltage (kV)	Pulsed Ion Extraction Delay (ns)	High Mass Detector Voltage (kV)	Signal Observed?
15.00	12.00	600	5.00	Yes
15.00	12.00	200	5.00	Yes
20.00	16.50	200	5.00	Yes*
20.00	16.25	200	5.00	Yes*
20.00	16.00	200	5.00	Yes
20.00	16.00	400	5.00	Yes
20.00	15.75	200	5.00	Yes*
20.00	15.50	200	5.00	Yes*
25.00	20.00	400	4.50	Yes
25.00	20.00	200	4.50	Yes*
25.00	20.50	200	4.50	No

* The signal was observed with low intensity.

The distribution obtained by LD-MS and MALDI-MS of the pitch pyridine insoluble fraction resembles the also bimodal SEC chromatogram of that fraction. Mixed-D column SEC chromatogram of the pitch pyridine insolubles showed a retained peak with a mass range up to 8,000 Da according to the PS calibration (see Figure 10.19). This range is coincident with the distribution at lower masses observed by LD-MS and MALDI-MS.

On the other hand, the SEC excluded peak and the LD-MS and MALDI-MS distribution at higher masses did not show quantitative agreement. It may be speculated that the PS calibration is overestimating the molecular weight of materials eluting under the excluded peak. It has been suggested that a change of molecular shape from a planar to a three-dimensional configuration could make the excluded material to appear at much earlier times than its mass would indicate.

However, the masses predicted by the PS calibration would go up to several million Da. Such molecules would be difficult to volatilise and observe in a MALDI-MS experiment. The lack of signal at the masses predicted can also be due to MALDI-MS limitations.

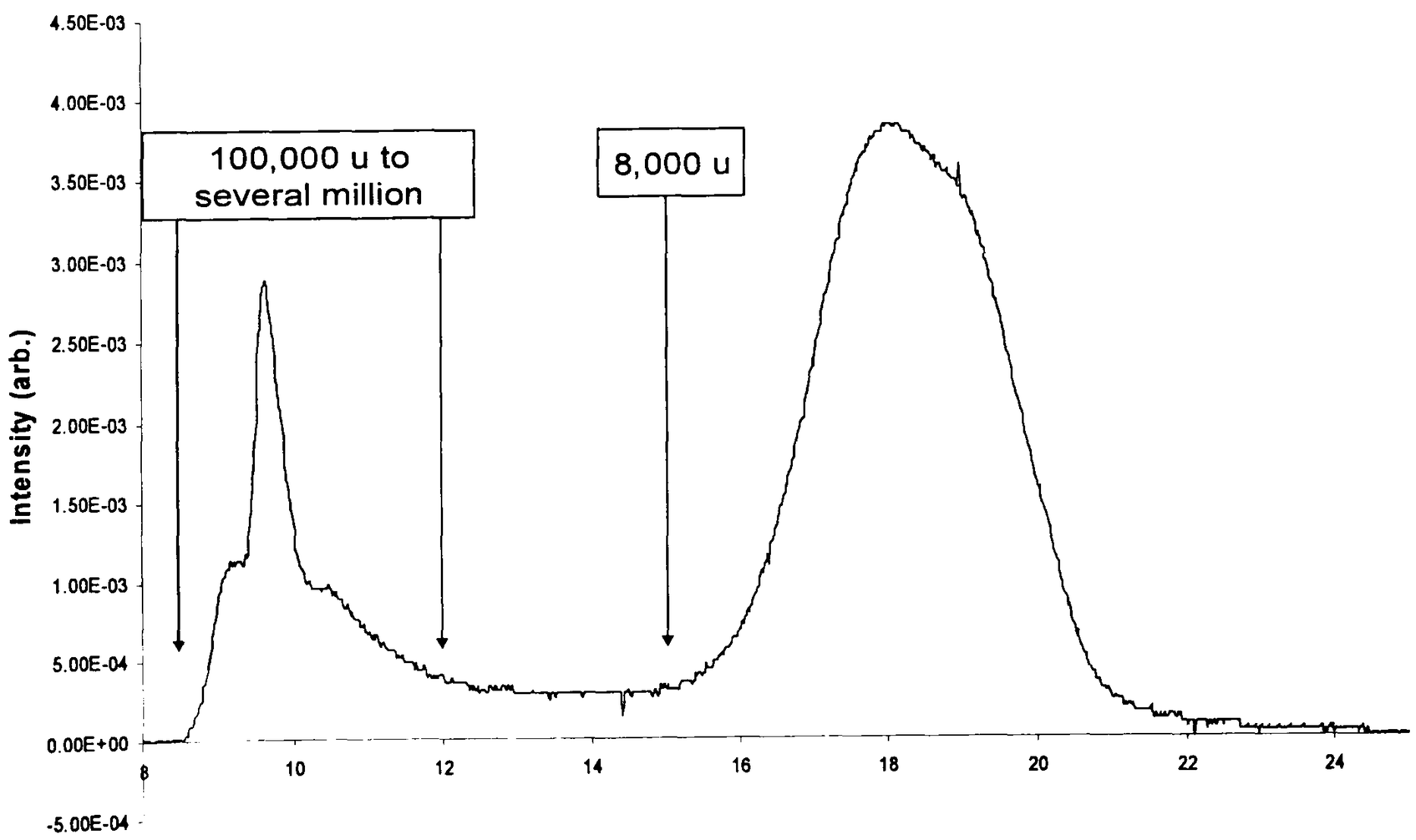


Figure 10.19. Mixed-D column SEC chromatogram of the pyridine insoluble pitch fraction. Mass ranges according to the PS calibration are shown.

10.4 CONCLUSIONS

A MALDI-TOF spectrometer equipped with a detector especially suitable for measurement of high masses has been employed in the determination of molecular mass distributions of heavy hydrocarbons. Significant progress in the application of to the analysis of heavy hydrocarbon fractions has been made. The effect of experimental conditions on the LD-MS and MALDI-MS spectra recorded have been discussed. Using high laser power while lowering the detector sensitivity led to the generation of MALDI-MS and LD-MS of higher mass ranges.

A good correlation between SEC elution times and mass distribution measured by LD-MS and MALDI-MS has been established. Analysis by LD-MS of SEC fractions obtained with an analytical column found the mass of maximum intensity peak in agreement with the predictions of the polystyrene calibration of the SEC column.

LD-MS and MALDI-MS showed a bimodal distribution of the pyridine insoluble fraction of the coal tar pitch. This distribution was first observed by other researchers in this laboratory when using 15kV extraction voltage. This work extended that observation to higher extraction voltages. The reproduction of the spectrum at higher extraction voltage is consistent with the fact that higher extraction voltages should increase rather than decrease the mass range observable, if having any effect at all. This ability to reproduce the spectrum at different extraction voltages indicates that the peak at 30,000 Da is actually generated by the sample rather than by an artefact of the technique.

The lower mass range of the MALDI-MS bimodal distribution coincides with the predictions of the PS calibration for the retained peak of that fraction observed by SEC. The correlation could not be extended to the excluded peak observed in the SEC chromatograms and the higher mass peak in MALDI-MS. The PS calibration could overestimate the mass values eluting under the excluded peak due to a "fullerene-like" effect.

11 CONCLUSIONS AND RECOMMENDATIONS FOR FUTURE WORK

11.1 CONCLUSIONS

Pillared clays synthesised at Aston University were tested. The conditions used for catalyst evaluation differed from previous work in that no solvent was used in hydrocracking a coal extract. This avoided interference from tetralin derived materials in the characterisation of products.

A Cr montmorillonite synthesised by ion exchange from a Na montmorillonite showed activity similar to a commercial $NiMo/Al_2O_3$ catalyst used as reference in this work in terms of conversions of the fraction of the feedstock with boiling points above 450ºC (">450ºC" fraction). This pillared clay catalyst did not show deactivation over the period tested.

In addition to the Cr montmorillonite, one of the Sn laponite (SL7) samples, the Ce montmorillonite, the Ce-Cr montmorillonite and the raw clays, have also shown comparable effectiveness to that of the commercial catalyst and did not show deactivation over the time scale tested.

In addition to the relatively high conversions of the ">450ºC" fraction, these catalysts produced a shift of the SEC chromatograms and UV-F spectra towards smaller molecular sizes relative to those of the feedstock.

Although pillaring increased the basal spacing in the pillared clays, these catalysts showed smaller pore sizes and a narrower pore size distribution than the reference catalyst. A sharp reduction in surface area due to pore blocking was observed after two hours of use. It may be conjectured that the activity shown by the pillared clays is mainly due to reaction on the external surface of the catalyst.

The deposition of carbonaceous material on the Cr montmorillonite pillared clay was not uniform. Thinner deposits were observed in zones of the catalyst richer in chromium. The hydrogenation activity of the chromium pillars may be responsible for clearing an area surrounding the active sites, as it has been observed in NiMo catalysts.

The initial deposition of carbonaceous material on the catalyst surface is large, even when a previously coated catalyst is employed. The initial deposits produced a

reduction in the pore size distribution of a $NiMo/Al_2O_3$ catalyst. These changes in pore size distribution were reversible and the pore size increased as the deposits re-dissolved in the liquid. It has been observed that the deposits are dynamic and material is exchanged with the solution.

Progress has been made in the application of LD-MS and MALDI-MS to the analysis of heavy hydrocarbons. Work done on a coal tar pitch fractions showed a good correlation between SEC elution times and mass distributions measured by LD-MS and MALDI-MS.

LD-MS and MALDI-MS showed a bimodal distribution of the pyridine insoluble fraction of the coal tar pitch. This observation has been confirmed in the present work by reproducing that signal using other sets of parameters, particularly higher extraction voltages. The lower mass range of the MALDI-MS bimodal distribution coincided with the predictions of the PS calibration for the retained peak of that fraction observed by SEC. The correlation could not be extended to the excluded peak observed in the SEC chromatograms and the higher mass peak in MALDI-MS. The PS calibration could be overestimating the mass values eluting under the excluded peak due to a "fullerene-like" effect.

11.2 RECOMMENDATIONS FOR FUTURE WORK

Whether the most active pillared clays represent an advantage over the commercial catalysts in terms of the resistance to deactivation should be assessed over longer periods. However, drops in feed reactivity set a limit in the length of reaction time of every batch which is meaningful. In addition, it is not possible to achieve long reaction times by reusing the catalyst with fresh feed, since a fraction of the catalyst is always lost and therefore the amount of catalyst recovered would be very low after several uses. Therefore it would be desirable to use a continuous reactor rather than a batch process in this next stage of the work.

Lower temperatures and hydrogen pressures should be applied to testing catalysts in the hydrocracking of vacuum residue, in order to avoid the formation of large amounts of gas.

The nature of the material eluting under the SEC excluded peak should be further investigated. Collection of samples at short elution times followed by analysis

by MALDI-MS could provide evidence on whether these materials are large or they have different structures producing a "fullerene-like" effect. However, the preparation of the sample for MALDI-MS is not straightforward since the eluent of the SEC column in the excluded region may be extremely diluted. Optimisation of the matrix to sample ratio will also be required in order to generate a reliable spectrum from these materials.

12 REFERENCES

[1] Kimber, G.M., "Energy for the future – coal liquefaction for the European Environment", Department of Trade and Industry, United Kingdom, Report No. Coal R078, 1997.

[2] "Coal liquefaction: technology status report 010" prepared by the Cleaner Coal Technology Programme" Department of Trade and Industry, United Kingdom, October 1999.

[3] Islas, C.A., PhD thesis, Imperial College, University of London, 2001.

[4] Li, W., Suelves, I., Lazaro, M.J., Zhang, S.F., Morgan, T.J., Herod, A.A., and Kandiyoti, R. "Solvent degradation during coal liquefaction in a flowing-solvent reactor" Fuel 83, 2004 157-179.

[5] Zhang, Sheng-fu., Xu, Bin., Herod, A.A. and Kandiyoti, R., "Hydrocracking reactivities of primary coal extracts prepared in a flowing-solvent reactor", Energy & Fuels 10, 1996, 733-742.

[6] Zhang, Sheng-fu., Shearman, J., Domin, M., Lazaro, M.J., Herod, A.A. and Kandiyoti, R., "Catalytic activity of fullerenes for hydrocracking coal extracts", Fuel 76, 1997, 207-214.

[7] Begon, V., Megaritis, A., Lazaro, M.J., Herod, A.A., Dugwell, D.R., and Kandiyoti, R., "Changes in sample reactivity and catalyst deactivation during early stages of the hydrocracking of a coal extract", Fuel 77, 1998, 1261-1272.

[8] Zhang, Sheng-fu., Xu, Bin, Moore, S.A., Herod, A.A. and Kandiyoti, R., "Comparison of hydrocracking reactivities of coal extracts from a flowing-solvent reactor, a mini-bomb and a pilot plant", Fuel 75, 1996, 597-605.

[9] Begon, V., Suelves, I., Herod, A.A., Dugwell, D.R., and Kandiyoti, R., "Structural effects of sample ageing in hydrocracked coal liquefaction extracts", Fuel 79, 2000, 1423-1429.

[10] Zhang, Sheng-fu., Herod, A.A. and Kandiyoti, R., "Effectiveness of dispersed catalysts in hydrocracking a coal liquefaction extract: a screening study", Fuel 76, 1997, 39-49.

[11] Bridge, A.G., in "Modern Petroleum Technology, Vol. 2 Downstream". Edited by Alan G. Lucas, John Wiley & Sons Ltd. 2000.

[12] Khan, M.R., and Patmore, D.J, in "Petroleum Chemistry and Refining" Edited by James G. Speight, Taylor and Francis, 1998.

[13] Furimsky, E. "Selection of catalysts and reactors for hydroprocessing". Applied Catalysis A: General 171, 1998, 177-206.

[14] Derbyshire, F. "Role of catalysis in coal liquefaction research and development", Energy & Fuels 3, 1989, 273-277.

[15] McMillen, D.F., Malhotra, R., Hum, G.P., and Chang, S-J. "Hydrogen-Transfer-Promoted Bond Scission Initiated by Coal Fragments". Energy & Fuels 1, 1987, 193-198.

[16] Cusumano, J., Dalla Betta, R.A., and Levy, R.B., "Catalysis in coal conversion", Academic Press, Inc 1978.

[17] Mangold, E.C., Muradaz, M.A., Ouellette, R.P., Farah, O.G. and Cheremisinoff, P.N. "Coal liquefaction and gasification technologies", Ann Arbour Science Publishers Inc. 1982.

[18] Absi-Halabi, M., Stanislaus, A., and Trimm, D.L., "Coke formation on catalysts during the hydroprocessing of heavy oils", Applied Catalysis 72, 1991, 193-215.

[19] Furimsky, E., and Massoth, F.E., "Deactivation of hydroprocessing catalysts", Catalysis Today 52, 1999, 381-495.

[20] Song, C., Hanaoka, K., and Nomura, M., "Influence of Pore Structure and Chemical Properties of Supported Mo Catalysts on Their Performance in Upgrading Heavy Liquids" Energy & Fuels 6, 1992, 619-628.

[21] Ancheyta, J., Betancourt, G., Centeno, G., Marroquin, G., Alonso, F., and Garciafigueroa, E., "Catalyst Deactivation during Hydroprocessing of Maya Heavy Crude Oil. 1. Evaluation at Constant Operating Conditions". Energy & Fuels 16, 2002, 1438-1443.

[22] Ancheyta, J., Betancourt, G., Centeno, G., and Marroquin, G., "Catalyst Deactivation during Hydroprocessing of Maya Heavy Crude Oil. II. Effect of Temperature during Time-on-Stream". Energy & Fuels 17, 2003, 462-467.

[23] Cable, T.L., Massoth, F.E., and Thomas, M.G., "Studies on an aged H-coal catalyst", Fuel Process. Technol. 4, 1981, 265-275.

[24] Yamamoto, Y., Kumata, F., and Massot, F.E., "Hydrotreating catalyst deactivation by coke from SRC-II oil", Fuel Process. Technol. 19, 1988, 253-263.

[25] Diez, F., Gates, B.C., Miller, J.T., Sajkowski, D.J., Kukes, S.G., "Deactivation of a NiMo-γ-Al_2O_3 catalyst: Influence of coke on the hydroprocessing activity", Ind. Eng. Chem. Res. 29, 1990, 1999-2004.

[26] de Jong, K.P., Reinalda, D., and Emeis, C.A., in "Catalyst Deactivation", Edited by Delmon, B., and Froment, F.G. Elsevier, Amsterdam, 1994.

[27] Plumail, J.C., Marseu, R., Martino, G., and Toulhoat, H., "Catalytic Upgrading of Heavy Oils – Design of the Hydrotreating Catalysts to Maximise the Conversion into Distillates" Proceedings of the Symposium on Recent Developments in Hydrot. Catal., 6-10 June 1988, Toronto.

[28] Gray, M.R., Zhao, Y., McKnight, C.M., Komar, D.A., and Carruthers, J.D., "Coking of Hydroprocessing Catalyst by Residue Fraction of Bitumen". Energy & Fuels 13, 1999, 1037-1045.

[29] Yoshimura, Y., Sato, T., Shimada, H., and Nishijima, A., Fuel Sci. Technol. Int. 4, 1986, 621.

[30] Reddy, K.M., Wei, B., and Song, C., "Mesoporous molecular sieve MCM-41 supported Co-Mo catalyst for hydrodesulfurisation of petroleum resides" Catalysis Today 1998, 261-272.

[31] Song, C., Nihonmatsu, T., and Nomura, M., "Effect of Pore Structure of Ni-Mo/Al_2O_3 Catalysts in Hydrocracking of Coal Derived and Oil Sand Derived Asphaltenes", Ind. Eng. Chem. Res. 30, 1991, 1726-1734.

[32] Banerjee, D.K., Laidler, K.J., Nandi, B.N., and Patmore, D.J., "Kinetic studies of coke formation in hydrocarbon fractions of heavy crudes", Fuel 65, 1986, 480.

[33] Curtis, C.W., Guin, J.A., Nalitham, R., Mohain, A., and Tarrer, A.R., Am.Chem. Soc. Div. Fuel Chem. (Preprints) 26, 1981, 164.

[34] Suelves, I., Lazaro, M.J., Begon, V., Morgan, T.J., Herod, A.A., and Kandiyoti, R., "Fractionation of coal extracts prior to hydrocracking: an attempt to link sample structure to conversion levels and catalyst fouling", Energy & Fuels 15, 2001, 1153-1165.

[35] Gualda, G., and Kasztelan, S., "Initial deactivation of residue hydrodemetalation catalysts", J. Catal. 161, 1996, 319-337.

[36] Richardson, S. M., Nagaishi, H. and Gray, M. R., "Initial Coke Deposition on a NiMo/γ-Al_2O_3 Bitumen Hydroprocessing Catalyst", Ind. Eng. Chem. Res. 35, 1996, 3940-3950.

[37] Marafi, A., Al-Bazzaz, H., Al-Marri, M., Maruyama, F., Absi-Halabi, M., and Stanislaus, A., "Residual-oil hydrotreating kinetics for graded catalyst systems: effect of original and treated feedstocks", Energy & Fuels 17, 2003, 1191-1197.

[38] Benito, A.M., and Martinez, M.T., "Catalytic hydrocracking of an asphaltenic coal residue" Energy & Fuels 10, 1996, 1235-1240.

[39] Matsushita, K., Hauser, A., Marafi, A., Koide, R., and Stanislaus, A., "Initial coke deposition on hydrotreating catalysts. Part 1. Changes in coke properties as a function of time on stream", Fuel 83, 2004, 1031-1038.

[40] Chu, K.S., Dong, D., Hanson, F.V., and Massoth, F.E., "Comparison of in-situ to ex-situ activities of bitumen-deactivated catalysts", Ind. Eng. Chem. Res. 35, 1996, 4012-4019.

[41] de John, K.P., "Effects of vapour-liquid equilibria on coke deposition in trickle-bed reactors during heavy oil hydroprocessing. 1. Experimental results". Ind. Eng. Chem. Res. 33, 1994, 821-824.

[42] Fleisch, T.H., Meyers, B.L., Hall, J.B., and Ott, G.L., "Multitechnique analysis of a deactivated resid demetallation catalyst", J Catal 86, 1984, 147-157.

[43] van Doorn, J., and Moulijn, J.A., "A Model of Coke on Hydrotreating Catalysts under Reaction Conditions" Fuel Process. Technol. 35, 1993, 275-287.

[44] van Doorn, J., Moulijn, J.A., and Djega-Mariadassou, G., "High-resolution Electron Microscopy of Spent Ni-Mo/Al203 Hydrotreating Catalysts", Applied Catalysis 63, 1990, 77-90.

[45] Muegge, B.D., and Massoth, F.E., "Basic studies of deactivation of hydrotreating catalysts with anthracene", Fuel Process. Technol. 29, 1991, 19-30.

[46] Suelves, I., Islas, C.A., Herod, A.A., and Kandiyoti, R., "Comparison of fractionation methods for the structural characterization of petroleum asphaltenes", Energy & Fuels 15, 2001, 429-437.

[47] Suelves, I., Islas, C.A., Millan, M., Galmes, C., Carter, J.F., Herod, A.A., and Kandiyoti, R., "Chromatographic separations enabling the structural characterisation of heavy petroleum residues", Fuel 82, 2003, 1-14.

[48] Herod, A.A., Lazaro M.J., Domin, M., Islas, C.A., and Kandiyoti, R., "Molecular mass distribution and structural characterisation of coal derived liquids", Fuel 79, 2000, 323-337.

[49] Islas, C.A., Suelves, I., Carter, J.F., Herod, A.A., and Kandiyoti, R., "Pyrolysis-gas chromatography/mass spectrometry of pitch fractions recovered from preparative size exclusion chromatography: structural differences with increasing molecular size", Rapid Communications in Mass Spectrometry 16, 2002, 481-495.

[50] Islas, C.A., Suelves, I., Apicella, B., Herod, A.A., and Kandiyoti, R., "Structure and composition of coal tars: an attempt to correlate molecular structure with increasing molecular mass", Combustion Science and Technology 175, 2003, 775-791.

[51] Herod, A.A., Lazaro, M.J., Suelves, I., Dubau, C., Richaud, R., Shearman, J., Card, J., Jones, A.R., Domin, M., and Kandiyoti, R., "Size exclusion chromatography of soots and coal-derived materials with 1-methyl-2-

pyrrolidinone as eluent: observations on high molecular mass material", Energy & Fuels 14, 2000, 1009-1020.

[52] Herod, A.A., Shearman, J., Lazaro, M.J., Johnson, B.R., Bartle, K.D., and Kandiyoti, R., "Effect of LiBr addition to 1-methyl-2-pyrrolidinone in the size-exclusion chromatography of coal-derived materials" Energy & Fuels 12, 1998, 174-182.

[53] Lazaro, M.J., Herod, A.A., and Kandiyoti, R., "Comparison of the fractionation of a coal tar pitch by solvent solubility and by planar chromatography", Fuel 78, 1999, 795-801.

[54] Herod, A.A., Zhuo, Y. and Kandiyoti, R., "Size-exclusion chromatography of large molecules from coal liquids, petroleum residues, soots, biomass tars and humic substances", J. Biochemical and Biophysical Methods 56, 2003, 335-361.

[55] Islas, C.A., Suelves, I., Li, W., Morgan, T.J., Herod, A.A., and Kandiyoti, R., "The unusual properties of high mass materials from coal-derived liquids", Fuel 82, 2003, 1813-1823.

[56] Li, W., Morgan, T.J., Herod, A.A., and Kandiyoti, R., "Thin-layer chromatography of pitch and a petroleum vacuum residue. Relation between mobility and molecular size shown by size-exclusion chromatography", Journal of Chromatography A 1024, 2004, 227-243.

[57] Lafleur, A.L., and Nakagawa, Y., "Multimode size exclusion chromatography with poly(divinylbenzene)/N-methylpyrrolidinone for the characterization of coal-derived mixtures", Fuel 68, 1989, 741.

[58] Lazaro, M.J., Islas, C.A., Herod, A.A., and Kandiyoti, R., "Calibration of Size Exclusion Chromatography in 1-Methyl-2-Pyrrolidinone for Coal-Derived Materials Using Standards and Mass Spectrometry". Energy & Fuels 13, 1999, 1212-1222.

[59] Karaca, F., Islas, C.A., Millan, M, Behrouzi, M., Morgan, T.J., Herod, A.A. and Kandiyoti, R., "The calibration of size exclusion chromatography columns: Molecular mass distributions of heavy hydrocarbon liquids", Energy & Fuels 18, 2004, 778-788.

[60] Herod, A. A., Islas, C.A., Lazaro, M.J., Dubau, C., Carter, J. F., and Kandiyoti, R., "Correlation of pyrolysis-gas chromatography mass spectra and nuclear magnetic resonance spectra of pitch fraction separated by planar chromatography", Rapid Communications in Mass Spectrometry 13, 1999, 201-210.

[61] Zhuo, Y., Herod A.A., and Kandiyoti, R., "The thermochemical reactions of middle rank coals" in Natural and Laboratory-Simulated Thermal Geochemical Processes. Ikan, R.; Kluwer Academic Publishers: Dordrecht, 2003; Chapter 3, pp 53-151.

[62] Masuda, K., Okuma, O., Kanaji, M., and Matsumara, T., "Chromatographic characterization of preasphaltenes in liquefied products from Victorian brown coal", Fuel 75, 1996, 1065-1070.

[63] Herod, A.A., Stokes, B.J., and Schulten, H., "Coal tar analysis by mass spectrometry – a comparison of methods", Fuel 72, 1993, 31-43.

[64] Herod, A.A., and Kandiyoti, R., "Fractionation by planar chromatography of a coal tar pitch for characterisation by size-exclusion chromatography, UV fluorescence and direct-probe mass spectrometry", Journal of Chromatography A 708, 1995, 143-160.

[65] Begon, V., Islas, C.A., Lazaro, M.J., Suelves, I., Herod, A.A., Dugwell, D.R., and Kandiyoti, R., "Structural features of large molecular mass material in coal-derived liquids: catalytic hydrocracking of the pyridine-insoluble fraction of a coal-tar pitch" Eur. J. Mass Spectrom. 6, 2000, 39-48.

[66] Islas, C.A., Suelves, I., Carter, J.F., Herod, A.A., and Kandiyoti, R., "Pyrolysis gas chromatography/mass spectrometry of a coal extract and its fractions separated by planar chromatography: correlation of structural features with molecular mass", Rapid Communications in Mass Spectrometry, 14, 2000, 1766-1782.

[67] Islas, C.A., Suelves, I., Carter, J.F., Li, W., Morgan, T.J., Herod, A.A., and Kandiyoti, R., "Pyrolysis gas chromatography/mass spectrometry of fractions separated from a low-temperature coal tar: an attempt to develop a general method for characterising structures and compositions of heavy hydrocarbon liquids", Rapid Communications in Mass Spectrometry, 16, 2002, 774-784.

[68] Parker, J.E., Johnson, C.A.F., John, P., Smith. G.P., Herod, A.A., Stokes, B.J., and Kandiyoti, R., "Identification of large molecular mass material in high temperature coal tars and pitches by laser desorption mass spectroscopy", Fuel 72, 1993, 1381-1391.

[69] Li, C., Wu, F., Cai, H.Y., and Kandiyoti, R., "UV-Fluorescence spectroscopy of coal pyrolysis tars", Energy & Fuels 8, 1994, 1039-1048.

[70] Bodman, S.D., Mc Whinnie, W.R., Begon, V., Suelves, I., Lazaro, M.J., Morgan, T.J., Herod, A.A., and Kandiyoti, R., "Metal-ion pillared clays as hydrocracking catalysts (I): Catalyst preparation and assessment of performance at short contact times", Fuel 81, 2002, 449-459.

[71] Bodman, S.D., Mc Whinnie, W.R., Begon, V., Millan, M., Suelves, I., Lazaro, M.J., Herod, A.A., and Kandiyoti, R., "Metal-ion pillared clays as hydrocracking catalysts (II): effect of contact time on products from coal extracts and petroleum distillation residues", Fuel 82, 2003, 2309-2321.

[72] Zhang, Sheng-fu., Xu, Bin., Herod, A.A., Kimber, G.M., Dugwell, D.R., and Kandiyoti, R., "Effect of coal rank on hydrocracking reactivities of primary coal extracts prepared in a flowing-solvent reactor", Fuel 75, 1996, 1557-1567.

[73] Begon, V., Suelves, I., Li, W., Lazaro, M.J., Herod, A.A., and Kandiyoti, R., "Catalytic hydrocracking of primary maceral concentrate extracts prepared in a flowing solvent reactor", Fuel 81, 2002, 185-202.

[74] Li, Chun-Zhu., Madrali, E.S., Wu, F., Xu, B., Cai, H.Y., Guell, A.J., and Kandiyoti, R., "Comparison of thermal breakdown in coal pyrolysis and liquefaction", Fuel 73, 1996, 851-865.

[75] Morgan, T.J., Millan, M, Behrouzi, M., Herod, A.A. and Kandiyoti, R., "On the limitations of UV-Fluorescence Spectroscopy in the Detection of High-Mass Hydrocarbon Molecules" Energy&Fuels 19, 2005, 164-169.

[76] Winans, R.E., and Hunt, J.E. "An overview of resid characterisation by mass spectrometry and small angle scattering techniques", Preprints of Symposia, Volume 44, No. 4, pp 725-727, 218th ACS National Meeting. August 22-26, 1999. New Orleans, LA.

[77] Strausz, O.P., Peng, P., and Murgich, J., "About the colloidal nature of asphaltenes and the MW of covalent monomeric units", Energy & Fuels 16, 2002, 809-822.

[78] Groenzin, H., and Mullins, O.C., "Molecular size and structure of asphaltenes from various sources", Energy & Fuels 14, 2000, 677-684.

[79] Sheu E.Y., De Tar, M.M., and Storm, D.A., "Surface activity and dynamics of asphaltenes" in "Asphaltene Particles in Fossil Fuel Exploration, Recovery, Refining, and Production Processes", pp115-121. Edited by Mahendra K. Sharma and Teh Fu Yen. Plenum Press, 1994.

[80] Sheu E.Y., De Tar, M.M., and Storm, D.A., "Structure and interaction of asphaltene colloids in organic solvents" in "Asphaltene Particles in Fossil Fuel Exploration, Recovery, Refining, and Production Processes" pp155-165 Edited by Mahendra K. Sharma and The Fu Yen. Plenum Press, 1994.

[81] Espinat, D., Rosenberg, E., Scarsella, M., Barre, L., Fenistein, D., and Broseta, D., "Colloidal structural evolution from stable to flocculated state of asphaltene solutions and heavy crudes", in "Structures and Dynamics of the Asphaltenes" pp145-201 Mullins and Sheu. Plenum Press, 1998.

[82] Storm D.A., and Sheu E.Y., "Characterization of colloidal asphaltenic particles in heavy oil", Fuel 74, 1995, 1140-1145.

[83] Pfeiffer, J.P., and Saal, R., "Asphaltic Bitumen as Colloid System" J. Phys. Colloid Chem. 44, 1940, 139-149.

[84] Gutierrez L.B., Ranaudo, M.A., Mendez, B., and Acevedo, S., "Fractionation of asphaltene by complex formation with p-nitrophenol. A method for structural studies and stability of asphaltene colloids", Energy & Fuels 15, 2001, 624-628.

[85] Zhang, Sheng-fu, PhD thesis, Imperial College, University of London, 1995.

[86] McDonnell, M.E., and Walsh, E.K, p257-261 in "A guide to materials characterization and chemical analysis". Edited by John P. Sibila, VCH Publishers 1988.

[87] Islas, C.A., Peralta, D., Millan, M., Morgan, T.J., Herod, A.A., Kazarian, S., Diez, M.A., Lee, A., Bismarck, A., and Kandiyoti, R., "Structural features of a coal tar pitch and its fractions", paper in preparation.

[88] Begon, V., PhD thesis, Imperial College, University of London, 1998.

[89] Olson, E.S., and Sharma, R.K., "Naphthene Upgrading with Pillared Synthetic Clay Catalysts", Energy & Fuels 10, 1996, 587-590.

[90] De Stefanis, A., Perez, G., Lilla, E., Ursini, O., and Tomlinson, A.A.G., "Conversions of resins and asphaltenes in porous catalysts", J. Anal. Appl. Pyrolysis 57, 2001, 37-44.

[91] Occelli, M.L., Schweizer, A.E., Fild, C., Schwering, G., Eckert, H., and Auroux, A., "Gallioaluminosilicate Molecular Sieves with the Faujasite Structure", Journal of Catalysis 192, 2000, 119 -127.

[92] Manos, G., Yusof, I.Y., Gangas, N.H., and Papayannakos, N., "Tertiary Recycling of Polyethylene to Hydrocarbon Fuel by Catalytic Cracking over Aluminium Pillared Clays" Energy & Fuels 16, 2002, 485-489.

[93] Grzybek, T., Klinik, J., Olszewska, D., Papp, H., and Smarzowski, "The influence of montmorillonite treatment on structure, sorption properties and catalytic behaviour: Part I. Zirconia pillared clays modified with manganese as denox catalysts", J., Pol. J. Chem. 75, 2001, 857-868.

[94] Meier, L.P., Nueesch, R., and Madsen, F.T., "Organic pillared clays", Journal of Colloid Interface Science 238, 2001, 24-32.

[95] Gultek, A., Seckin, T., Onal, Y., and Icduygu, M.G., "Preparation and phenol captivating properties of polyvinylpyrrolidinone-montmorillonite hybrid materials", Journal of Applied Polymer Science 81, 2001, 512-519.

[96] Lacey, A.L., Hayes, M.H.B., and Vaidyanathan, L.V., "Preparation of iron pillared clays and their applications for sorption of humic substances", in "Humic Substances in Soils, Peats and Waters", Hayes and Wilson. RSC, pp219-225 1997.

[97] Bodman, S.D., PhD thesis, Aston University, 1999.

[98] Gyftopoulou, M.E., Millan, M., Bridgwater, A.V., Dugwell, D., Kandiyoti, R., and Hriljac J.A., "Pillared clays as catalysts for hydrocracking of heavy liquid fuels". Applied Catalysis A,General 282, 2005, 205-214.

[99] Karas, M., and Kruger, R., "Ion formation in MALDI: the cluster ionization mechanism" Chem. Rev. 103, 2003, 427-439.

[100] Zhigilei, L.V., Leveugle, E., Garrison, B.J., Yingling, Y.G., and Zeifman, M.I., "Computer simulations of laser ablation of molecular substrates", Chem. Rev. 103 (2): 321-347, Feb 2003.

[101] Dreisewerd, K., "The desorption process in MALDI" Chem. Rev. 103, 2003, 395-425.

[102] Knochenmuss, R., "A quantitative model of ultraviolet matrix-assisted laser desorption/ionisation including analyte ion generation", Analytical Chemistry 75, 2003, 2199-2207.

[103] Domin, M., Moreea, R., Lazaro, M.J., Herod, A.A., and Kandiyoti, R., "Choice of extraction voltage and matrix in the matrix-assisted laser desorption-ionization time-of-flight mass spectrometry of coal tar pitch – pyridine insolubles", Rapid Communications in Mass Spectrometry 11, 1997, 638-645.

[104] Lazaro, M.J., Herod, A.A., Cocksedge, M., Domin, M., and Kandiyoti, R., "Molecular mass determination in coal-derived liquids by MALDI mass spectrometry and size-exclusion chromatography", Fuel 76, 1997, 1225-1233.

[105] Lazaro, M.J., Herod, A.A., Domin, M., Zhuo, Y., Islas, C.A., and Kandiyoti, R., "Determining a "safe" high-mass limit in matrix-assisted laser desorption/ionisation time-of-flight mass spectra of coal derived materials with reference to instrument noise", Rapid Communications in Mass Spectrometry 13, 1999, 1401-1412.

[106] Islas, C.A., Suelves, I., Millan, M., Apicella B., Lazaro, M.J., Herod, A.A., and Kandiyoti, R., "Matching average masses of pitch fractions of narrow polydispersity, derived from matrix-assisted laser desorption/ionisation time-of-flight mass spectrometry, with the polystyrene calibration of SEC", Journal of Separation Science 26, 2003, 1422-1428.

[107] Millan, M, Morgan, T.J., Behrouzi, M., Karaca, F., Galmes, C., Herod, A.A. and Kandiyoti, R., "The high mass component (>m/z 10,000) of coal tar pitch by matrix-assisted laser desorption/ionisation mass spectrometry and size-exclusion chromatography" Rapid Communications in Mass Spectrometry 19, 2005, 1867-1873.

[108] Domin, M., Moreea, R., Lazaro, M.J., Herod, A.A., and Kandiyoti, R., "Effect of polydispersity on the characterisation of coal-derived liquids by matrix-assisted laser desorption/ionisation time-of-flight mass spectrometry: inferences from results for mixtures of polystyrene molecular mass standards" Rapid Communications in Mass Spectrometry 11, 1997, 1845-1852.

APPENDIX I: LIST OF PUBLICATIONS RELATED TO THE PRESENT WORK

1. Millan, M, Behrouzi, M., Karaca, F., Morgan, T.J., Herod, A.A. and Kandiyoti, R., "Large molecular mass materials in asphaltenes by size exclusion chromatography and MALDI-mass spectrometry", Accepted for publication in Catalysis Today.

2. Millan, M, Morgan, T.J., Behrouzi, M., Karaca, F., Galmes, C., Herod, A.A. and Kandiyoti, R., "The high mass component (>10,000) of coal tar pitch by MALDI-MS and size exclusion chromatography", Rapid Communications in Mass Spectrometry 19, 2005, 1867-1873.

3. Karaca, F., Millan, M, Behrouzi, M., Herod, A.A. and Kandiyoti, R., "The size exclusion chromatography calibration of 'Mixed-A' and 'Mixed-D' columns using various polymers and compounds: an application to coal derived materials", Accepted for publication in Analytica Chimica Acta.

4. Gyftopoulou, M.E., Millan, M., Bridgwater, A.V., Dugwell, D., Kandiyoti, R., and Hriljac J.A., "Pillared clays as catalysts for hydrocracking of heavy liquid fuels", Applied Catalysis A, General 282, 2005, 205-214.

5. Morgan, T.J., Millan, M, Behrouzi, M., Herod, A.A. and Kandiyoti, R., "On the limitations of UV-Fluorescence Spectroscopy in the Detection of High-Mass Hydrocarbon Molecules", Energy & Fuels 19, 2005, 164-169.

6. Karaca, F., Islas, C.A., Millan, M, Behrouzi, M., Morgan, T.J., Herod, A.A. and Kandiyoti, R., "The calibration of size exclusion chromatography columns: Molecular mass distributions of heavy hydrocarbon liquids", Energy & Fuels 18, 2004, 778-788.

7. Apicella, B., Ciajolo, A., Millan, M., Galmes, C., Herod, A.A., and Kandiyoti, R., "Oligomeric carbon and siloxane series observed by matrix-assisted laser desorption/ionisation mass spectrometry during the analysis of soot formed in fuel-rich flames", Rapid Communications in Mass Spectrometry 18, 2004, 331-338.

8. Begon, V., Suelves, I., Islas, C.A., Millan, M., Dubau, C., Lazaro, M.J., Law, R.V., Herod, A.A., Dugwell, D., and Kandiyoti, R., "Comparison of the quaternary aromatic carbon contents of a coal, a coal extract and its hydrocracking products by NMR methods", Energy & Fuels 17, 2003, 1616-1629.

9. Islas, C.A., Suelves, I., Millan, M., Apicella B., Lazaro, M.J., Herod, A.A., and Kandiyoti, R., "Matching average masses of pitch fractions of narrow polydispersity, derived from matrix-assisted laser desorption ionisation time-of-flight mass spectrometry, with the polystyrene calibration of SEC" J Sep Sci 26, 2003, 1422-1428.

10. Bodman, S.D., Mc Whinnie, W.R., Begon, V., Millan, M., Suelves, I., Lazaro, M.J., Herod, A.A., and Kandiyoti, R., "Metal-ion pillared clays as hydrocracking catalysts (II): effect of contact time on products from coal extracts and petroleum distillation residues" Fuel 82, 2003, 2309-2321.

11. Suelves, I., Islas, C.A., Millan, M., Galmes, C., Carter, J.F., Herod, A.A., and Kandiyoti, R., "Chromatographic separations enabling the structural characterisation of heavy petroleum residues" Fuel 82, 2003, 1-14.